ABSTRACT

Title of Document:	TOWARDS PARTIAL OXIDATION OF METHANE TO METHANOL: OXIDATION OF MONOMETHYL M^{II}-CH_3 (M=Pt, Pd) COMPLEXES WITH O_2 IN WATER
	Anna V. Sberegaeva, Doctor of Philosophy, 2014
Directed By:	Professor Andrei N. Vedernikov, Department of Chemistry and Biochemistry

C-H Functionalization of methane, catalyzed by Pt^{II} compounds with H_2PtCl_6 as stoichiometric oxidant, has been reported by Shilov *et al*. in the 1970's. Since then a number of attempts have been made to utilize atmospheric oxygen instead of expensive H_2PtCl_6. The key to a success is to achieve fast and selective $Pt^{II}Me$ – to – $Pt^{IV}Me$ oxidation with O_2. Previously our group has reported di(2-pyridyl)methanesulfonate (dpms) ligand – enabled aerobic oxidation of $Pt^{II}Me$ to produce $Pt^{IV}Me$ intermediates and methanol.

In this work, factors affecting the rate and selectivity of aerobic oxidation of aqueous (dpms)$M^{II}Me(OH_2)$ complexes (M = Pt, Pd) are studied in detail with special attention paid to the effect of additives and the solution pH. We found that oxidation of (dpms)$Pt^{II}Me(OH_2)$ is fastest at pH 8.0 and formation of a Pt-to-Pt methyl group transfer product, a C_1 – symmetric (dpms)$Pt^{IV}Me_2(OH)$ complex, occurs at pH > 10.

The latter becomes the major product at pH 14. Results of a kinetics study, isotopic labeling experiments and DFT calculations (collaboration with Prof. W.A. Goddard) are reported and the mechanism of the oxidation reactions is discussed. Compared to (dpms)$Pt^{II}Me(OH_2)$, (dpms)$Pt^{II}Me(OAc)^-$ complex is less reactive towards O_2, whereas (dpms)$Pt^{II}Me(I)^-$ complex reacts at a faster rate than (dpms)$Pt^{II}Me(OH_2)$ at pH 6.5; chloro- and bromo-analogs are unreactive.

Reactivity of Pd^{II} complexes containing the same auxiliary dpms ligand is more diverse compared to the Pt^{II} analogs. For example, neutral (dpms)$Pt^{II}Ph(DMSO)$ is inert towards O_2, while (dpms)$Pd^{II}Me(SMe_2)$ undergoes aerobic functionalization to form methanol, among other products, already at room temperature. Oxidation of (dpms)$Pd^{II}Me(X)^-$, X = I, OH with O_2 in water results in formation of methanol and ethane under milder conditions compared to (dpms)$Pt^{II}Me(OH_2)$. Palladium complexes have been submitted to oxidation with I_2 and peroxides in aqueous solution, kinetics studies, and model reacions. Results show that when O_2 is used as the oxidant, photochemical oxidation leads to both ethane and methanol in high combined yield under ambient light and temperature. Reaction selectivity towards MeOH can be modulated by adjusting the reaction pH. The mechanism of these oxidation reactions is proposed, and is different from the mechanism of oxidation of analogous Pt complexes.

TOWARDS PARTIAL OXIDATION OF METHANE TO METHANOL: OXIDATION OF MONOMETHYL M^{II}-CH_3 (M=Pt, Pd) COMPLEXES WITH O_2 IN WATER

By

Anna Vladimirovna Sberegaeva

Dissertation submitted to the Faculty of the Graduate School of the
University of Maryland, College Park, in partial fulfillment
of the requirements for the degree of
Doctor of Philosophy
2014

Advisory Committee:
Professor Andrei N. Vedernikov, Chair
Professor Michael P. Doyle
Professor Philip R. DeShong
Professor Bryan W. Eichhorn
Professor William F. McDonough

Dedication

To my entire wonderful family

Acknowledgements

My sincere thanks go to my mentor Professor Andrei Vedernikov. He taught me a great deal about the research process and was always supportive and kind.

Throughout the four years at UMD I had the pleasure of working along with Will Oloo, Shrin Pal, Dave Jenkins, Daoyong Wang and David Watts. I'm very grateful for their advice and friendship. Special thanks to my former desk and lab bench neighbor Will, and my undergraduate students Yearin Byun, Poorna Sreekumar, and high school student Pranish Katwal.

I'd like to thank Wei-Guang Liu and Smith Nielsen from Professor W. A. Goddard group at the California Institute of Technology for doing calculations on the platinum system. This collaboration would not be possible without Center for Catalytic Hydrocarbon Functionalization and its director Professor Brent Gunnoe at the University of Virginia.

Our department enjoys the services of the X-ray crystallographer Peter Y. Zavalij, NMR staff Yiu-Fai Lam and Yinde Wang and mass spectroscopist Yue Li. I have been assisted on numerous occasions by XRD, NMR and MS staff and I appreciate their competence and enthusiasm.

I'm very grateful for my dear friends Kaitlyn Crawford, Soumya Rastogi, Romina Heymann, Dina Jaber and Dmitri Sabasovs. I'd like to mention my kitties Nochka and Miyuki, and our new puppy Buddy. Buddy was more of a trouble than help so far though.

The best gift a family can give is love, and I'll be always grateful for the love of my parents Galina and Vladimir Sberegaev, my babika Antonina Tatarinova and

my late grandfather Evgeniy Tatarinov. I will always try to make you proud. I feel very lucky to be loved by my second family Leonza and Teresa Johnson. Most of all, I'm grateful for the love of my husband Travis L. F. Johnson. I'm looking forward to our life together.

Table of Contents

List of Schemes

List of Tables

List of Figures

List of Abbreviations

Ac	acetyl
Alk	alkyl
Ar	aryl
aq.	aqueous
atm	atmosphere
bpy	2,2’-bipyridyl
bpym	2,2’-bipyrimidine
calcd	calculated
CH	carbon-hydrogen bond
CHD	1,4-cyclohexadiene
Cp	cyclopentadienyl
Cp*	pentamethylcyclopentadienyl
Cy	cyclohexyl
DCE	1,2-dichloroethane
DFT	Density Functional Theory
DMF	*N*,*N*-dimethylformamide
DMSO	dimethylsulfoxide
dpk	di-2-pyridyl ketone
dpm	di-2-pyridylmethane
dpms	di-2-pyridylmethanesulfonate
equiv.	equivalent(s)
ESI-MS	electrospray ionization mass spectrometry
g	grams
h	hour(s)
HOMO	Highest Occupied Molecular Orbital
Hz	Hertz
i-Pr	isopropyl
J	NMR coupling constant
kcal/mol	kilocalorie(s) per mole
M	moles per liter
*m*CPBA	*meta*-chloroperoxybenzoic acid
Me	methyl
Medpms	6-methyl-2-pyridyl 2-pyridyl methanesulfonate
MeOH	methanol
m	meta
mg	milligrams
MHz	megahertz
min	minute(s)
mL	milliliter(s)
mM	millimoles per liter
mmol	millimole(s)
mol	mole(s)
MMO	methane monooxygenase

m/z	mass-to-charge ratio
NADH	nicotinamide adenine dinucleotide
NHC	N-heterocyclic carbene
NMR	nuclear magnetic resonance
NOE	Nuclear Overhauser Effect
o	ortho
OAc	acetate
ORTEP	Oak Ridge Thermal Ellipsoid Plot
p	para
Ph	phenyl
py	pyridine
rt	room temperature
s	second(s)
$t_{1/2}$	half-life
tach	1,3,5-triaminocyclohexane
tacn	1,4,7-triazacyclononane
t-Bu	tertiary butyl
t-Bu-dpms	4-tert-2-butyl-pyridyl 2-pyridyl methanesulfonate
TFE	2,2,2-trifluoroethanol
THF	tetrahydrofuran
TMEDA	*N*,*N*,*N′*,*N′*-tetramethylethylenediamine
Tol	tolyl
Tp	hydridotrispyrazolylborate
XRD	X-ray diffraction
μL	microliter(s)
μM	micromoles per liter
μmol	micromole(s)

Chapter 1 : Mechanistic Approaches to Selective Alkane Functionalization

1.1 Importance of Catalytic Methane to Methanol Conversion

Methane, the main component of natural gas, is a valuable chemical feedstock, but it has not been utilized to its full potential due to difficulties associated with its selective partial oxidation. Currently conversion of methane to useful products occurs via generation of carbon monoxide and hydrogen (syn-gas). Syn-gas can be used in a number of ways, e.g. in the Fisher-Tropsh process to convert syn-gas into higher alkanes[1], or into methanol by selective CO hydrogenation over Cu/ZnO catalyst. Formation of syn-gas is a highly energy-consuming process, requiring high temperatures (850 ° C). For this reason, partial oxidation of methane under milder conditions is a very attractive goal for the scientific and engineering community (Eq. 1.1).

$$CH_4 + 0.5\,O_2 \longrightarrow CH_3OH$$

Equation 1.1

1.2 Non-Organometallic Approach to Functionalization of Alkanes

Examples of hydrocarbon functionalization using heterogeneous catalysts include reaction of oxidative coupling of methane on basic oxides[2], transition metal oxides[3], and iron complexes encapsulated in zeolites[4]. These catalysts require temperatures exceeding 250 ºC, and they produce MeOH in low yield and poor selectivity due to overoxidation.

$$CH_4 + O_2 + NADH + H^+ \xrightarrow{MMO} CH_3OH + H_2O + NAD^+$$

Equation 1.2

In nature the metabolism of methanotroph bacteria utilizes methane monoxygenase enzyme (MMO) to efficiently convert methane to methanol under physiological conditions (Eq. 1.2). Monooxygenases utilize one equivalent of NADH to partially reduce one dioxygen molecule to form one molecule of H_2O and convert CH_4 to CH_3OH.[5] Between the two enzyme classes, soluble MMO (sMMO) and particulate MMO (pMMO), sMMO is well understood and well-studied, while structure and reactivity of pMMO is mostly unknown. However, it has been established that diiron cluster in sMMO binds and activates dioxygen, while copper ion was implicated as a key cofactor.[5,6,7] Attempts to develop Cu-based system for C–H bond functionalization using dioxygen yielded anisole-containing polypyridylamine peroxodicopper(II) complex, which is capable to hydroxylate toluene and ethylbenzene.[8] There are numerous works, targeting development of iron[9] and some other 3-d block metal[10] complexes-based systems that mimic function of natural enzymes. In particular, a biochemistry-inspired approach has been developed in Groves's lab using manganese porphyrin Mn(TPP)Cl. A reaction between Mn(TPP)Cl, sodium hypochlorite and unactivated alkanes afforded alkyl chlorides and trace amounts of oxygenation products.[11]

1.3 Organometallic Approach to Functionalization of Alkanes

Homogeneous catalysis offers flexibility for tuning the catalyst for desired selectivity. Catalysts for methane functionalization should be compatible with products (e.g. methanol or methyl halide), and must be tolerant of the oxidant. In addition, the catalyst must be more reactive towards alkane than functionalization product. Given that bond dissociation energy of CH_4 is ~104 kcal/mol *vs.* MeOH ~94

kcal/mol, this requirement could be challenging. The discussion related to various approaches to functionalization of primary alkanes is presented below.

1.3.1 Advances of the Shilov System

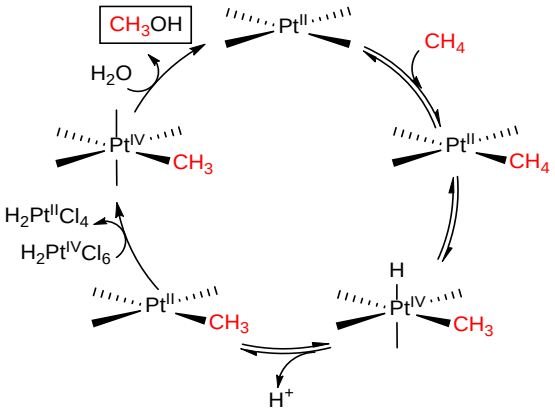

Scheme 1.1 Proposed mechanism for Pt^{II}-catalyzed oxidation of methane in aqueous solution.

Catalytic functionalization of methane has been known since early 1970's.[12] It has been demonstrated that MeOH and MeCl can be generated using $[Pt^{II}Cl_4]^{2-}$ as a catalyst and $H_2Pt^{IV}Cl_6$ as oxidant at 120 °C.[13] Mechanistic studies on the Shilov system revealed that the process involves three steps: 1) C–H bond activation, 2) Pt^{II} to Pt^{IV} oxidation, and 3) reductive elimination of CH_3-X (Scheme 1.1).[14] The reaction begins with C-H bond activation, resulting in a $[CH_3Pt^{II}Cl_n(H_2O)_{3-n}]^{(n-1)-}$ complex, which is oxidized to $[CH_3Pt^{IV}Cl_n(H_2O)_{5-n}]^{(n-3)-}$ by $H_2Pt^{IV}Cl_6$. The catalytic cycle is complete when CH_3 group of the $[CH_3Pt^{IV}Cl_n(H_2O)_{5-n}]^{(n-3)-}$ complex undergoes nucleophilic attack by H_2O or Cl^-,[15] to form functionalized product MeOH or MeCl and regenerate Pt^{II} catalyst. The success of the Shilov system is due to two features: first, the rate of $CH_3^{\delta-}$-Pt^{II} to $CH_3^{\delta+}$-Pt^{IV} oxidation is considerably faster than the rate of protonolysis of CH_3-Pt^{II}, and second, $CH_3^{\delta+}$-Pt^{IV} is not susceptible to protonation, but rather to the nucleophilic functionalization of the methyl ligand.[16]

Another important feature of the Shilov system, is unusual selectivity in C-H bond activation: CH_4 > 1° > 2° > 3°,[13] and H-CH_2CH_3 > H-CH_2CH_2OH > H-$CH(OH)CH_3$[17,18]. The latter trend was established when oxidation of CH_3CH_3 and $CH_3{}^{13}CH_2OH$ as substrates, showed formation of *unlabeled* ethanol and ethylene glycol as predominant products.[17] A mechanism that leads to formation of ethylene glycol includes four steps: 1) formation of Pt^{II}-C_2H_6 species via electrophilic C-H activation, 2) β-H abstraction to form $[Cl_3Pt^{II}(CH_2CH_2)]^-$, 3) oxidation of the Pt^{II}-olefin complex ($[Cl_3Pt^{II}(CH_2CH_2)]^-$) to Pt^{IV}-β-hydroxyalkyl ($[Cl_5Pt^{IV}(CH_2CH_2OH)]^{2-}$), and 4) hydrolysis of Pt^{IV} via nucleophilic S_N2 mechanism to form 1,2-diol.[17,19] Labeling experiments indicate that ($[Cl_5Pt^{IV}(CH_2CH_2OH)]^{2-}$ does not arise by direct oxidation of $[Cl_3Pt^{II}(CH_2CH_2OH)]^{2-}$, in other words, equilibrium in Eq. 1.3 lies far to the left.[17]

$$[Cl_3Pt^{II}(CH_2 = CH_2)]^- + H_2O \underset{}{\overset{\text{slow}}{\rightleftharpoons}} [Cl_3Pt^{II}(CH_2CH_2OH)]^{2-} + H^+$$

Equation 1.3

When ethanol alone was exposed to the reaction conditions of the Shilov system, ethylene glycol was formed via the same Pt^{II}-ethylene ($[Cl_3Pt^{II}(CH_2CH_2)]^-$) intermediate[17], however, other products have also been observed.[20] Among other products were chloro- and hydroxyacetaldehyde, acetaldehyde hydrate ($CH_3CH(OH)_2$)[17], glycolic acid, acetic acid and CO_2[20].

Sen *et al*. proposed that acetaldehyde was formed via $[Cl_5Pt^{IV}(CH_2CH(O)]^{2-}$ intermediate,[17] while labeling studies, performed by Bercaw *et al*. showed that glycolic acid formed via oxidation of ethylene glycol, rather than hydroxylation of acetic acid.[20]

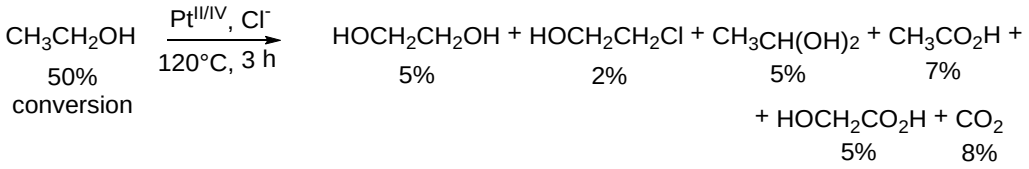

Equation 1.4

Formation of acetaldehyde hydrate was proposed to occur through an independent pathway, that did not involve a symmetrical $[Cl_3Pt^{II}(CH_2CH_2)]^-$ species, based on distribution of ^{13}C label in $^{13}CH_3CH(OH)_2$, when starting from $^{13}CH_3CH_2OH$. The likely pathway is heterogeneous oxidation of ethanol, catalyzed by trace amount of metallic platinum.[17]

As mentioned above, Pt^{II} is not indefinitely stable under the reaction conditions of Shilov system, and eventually precipitates as metallic platinum,[17,20,21] which can lead to further oxidation of methanol to overoxidation products, and therefore, the loss of selectivity.[22] Another obvious drawback of Shilov system is the requirement for Pt^{IV} as stoichiometric oxidant.

The mechanism of $R^{\delta-}$-Pt^{II} to $R^{\delta+}$-Pt^{IV} oxidation step has been evaluated in more detail. Specifically, the question was whether oxidation occurs via an electron transfer mechanism or an alkyl-ligand exchange mechanism. The question was resolved by performing reaction between a $[RPt^{II}Cl_n(H_2O)_{3-n}]^{(n-1)-}$ (R = C_2H_6) and isotopically labeled $[^{195}Pt^{IV}Cl_6]$ as an oxidant (Scheme 1.2).[23] Results showed that isotopically labeled ^{195}Pt did not appear in the $[RPt^{IV}Cl_n(H_2O)_{5-n}]^{(n-3)-}$, meaning that oxidation involves an electron transfer mechanism.

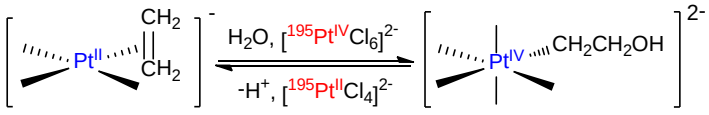

Scheme 1.2 Oxidation of Zeise's salt by $^{195}Pt^{IV}$.

An electron transfer mechanism suggests that expensive Pt^{IV} could be replaced with another oxidant, if two requirements are satisfied: 1) the rate of oxidation of $[RPt^{II}Cl_n(H_2O)_{3-n}]^{(n-1)-}$ should be several orders of magnitude faster than the rate of protonolysis, and 2) the oxidant should be mild enough as to oxidize only Pt^{II}-R and not inorganic $[Pt^{II}Cl_4]^{2-}$.[16]

One of the reports demonstrates the use of Cl_2 (gas) as an oxidant. When a sapphire NMR tube was charged with an aqueous solution of $Na_2Pt^{II}Cl_4$ and $Na_2Pt^{IV}Cl_6$, 72 psi of Cl_2, and 400 psi of CH_4 and heated in the dark at 125 °C for 1 h, selective formation of methyl chloride and methanol (formed via hydrolysis of methyl chloride) were observed.[24] The equilibrium (Eq. 1.5) was proposed where Cl_2 regenerates Pt^{IV} oxidant. Such equilibrium would inevitably shut down the catalytic cycle, because no Pt^{II} would be available for C-H activation of methane. In addition, although the reaction was performed in the dark, the involvement of Cl radicals could not be excluded. Overall, turnover rates of 0.24 h^{-1} were observed. When accounted for decrease in $[Pt^{II}]$, turnover rate of at least 24 h^{-1} was reported.[24]

$$Na_2Pt^{II}Cl_4 + Cl_2 \rightleftharpoons Na_2Pt^{IV}Cl_6$$

Equation 1.5

When H_2O_2 was used as the stoichiometric oxidant, turnover rates of 0.09 h^{-1} were observed at 92 °C.[25] The reaction was performed in strongly acidic media (1 M trifluoromethanesulfonic acid), and $Na_2Pt^{IV}Cl_6$ was replaced with $Pt^{IV}Cl_4$. Reoxidation of Pt^{II} to Pt^{IV} occurred via Eq. 1.6

$$Pt^{II} + 2H^+ + H_2O_2 \rightleftharpoons Pt^{IV} + 2H_2O$$

Equation 1.6

Under these conditions, formation of metallic Pt was not observed, however, the rate of the reaction is too slow for practical application.

From a practical perspective, the most efficient catalytic conversion of methane to methanol derivative was performed in sulfuric acid, catalyzed by Hg^{II} at 180 °C (Scheme 1.3, **A**).[26]

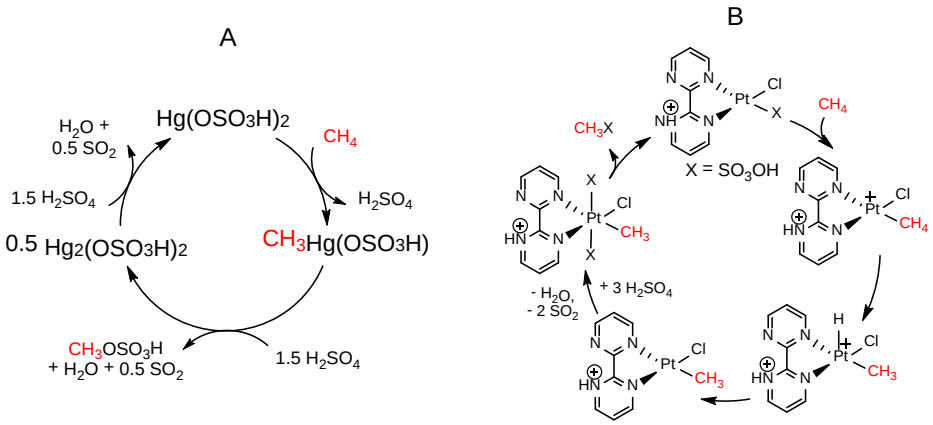

Scheme 1.3 A: proposed mechanism for functionalization of methane with $Hg(OSO_3H)_2$ in H_2SO_4. B: proposed mechanism for functionalization of methane in Catalytica system.

Methyl bisulfate was generated in 43% yield at 50% conversion of methane, with a turnover frequency of 10^{-3} s^{-1} (3.6 h^{-1}).[26] The reaction was proposed to occur via electrophilic activation of methane, followed by simultaneous formation of CH_3OSO_3H and Hg^{I}. Sulfuric acid acts as a solvent and as an oxidant for Hg^{I} to regenerate the catalyst $Hg^{II}(OSO_3H)_2$. Although, high selectivity for monofunctionalized product indicates a non-radical mechanism, it is possible that a radical pathway occurs concurrently since Hg^{II} is a one electron oxidant.[27]

Catalytic conversion of CH_4 to CH_3OSO_3H was even more efficient with bipyrimidyl-supported Pt^{II} complex $(bpym)Pt^{II}(X)_2$ (X = Cl, SO_4). Methyl bisulfate was generated in 72% yield at 90% conversion of methane, with a turnover frequency of 10^{-2} s^{-1} (0.36 h^{-1}).[28] Similar to the Hg^{II} system, this reaction follows electrophilic

mechanism with oxidation being the rate determining step (Scheme 1.3, **B**). In addition, the system is very stable; neither oxidation of the ligand nor formation of Pt^0 is observed. Similar systems based on Au[29] and Pd[30] have been reported for catalytic conversion of methane to methanol and acetic acid respectively.

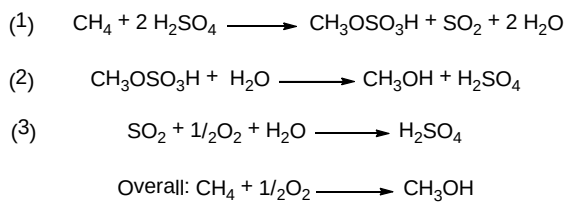

Scheme 1.4 A possible three-step sequence for methane conversion, consisting of (1) oxidation of methane to methyl bisulfate as in a; (2) hydrolysis of methyl bisulfate to methanol and sulfuric acid; (3) oxidation of SO_2 produced in step (1) to sulfuric acid.

High selectivity of Hg^{II} and $(bpym)Pt^{II}(X)_2$ (X = Cl, SO_4) systems is due to the formation of the methane derivative with bisulfate acting as a protective group. In order to convert CH_3OSO_3H to methanol, additional steps are required. At present, the overall process (Scheme 1.4) is not competitive with the industrial indirect conversion of methane to methanol via synthesis gas.[21] In order to be practically viable, the system needs to be compatible with a cheap oxidant, preferably O_2.

1.3.2 Pd-catalyzed Methane to Methanol Conversion

Due to its versatile reactivity, palladium is an attractive metal for methane to methanol conversion. Unlike Pt^{IV}, Pd^{IV} oxidation state is not as easily accessible, therefore, an alternative strategy to Shilov's Pt^{II}/Pt^{IV} system would be Pd^0/Pd^{II} redox couple. The hypothetical catalytic cycle would involve three steps: 1) C-H bond activation, 2) reductive elimination of hydroxylated product and formation of Pd^0, and 3) reoxidation of Pd^0 to Pd^{II} with O_2 (Scheme 1.5).[31]

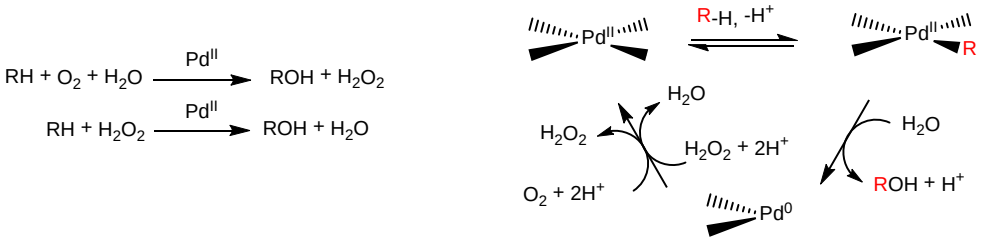

Scheme 1.5 Hypothetic mechanism of functionalization of hydrocarbons via Pd^{II}/Pd^{0} couple.

Efficient reoxidation of the catalyst is crucial for the success of the catalytic cycle. Oxygen is thermodynamically capable of oxidizing Pd^{0} to Pd^{II}, but often cannot be involved directly in this oxidation. Direct oxidation of Pd^{0} by O_2 was observed, but under very specific conditions. The first example of such transformation was reported in case of $(Ph_3P)_4Pd^{0}$ complexes in benzene. The η^2-peroxo complex $(Ph_3P)_2Pd^{II}(\eta^2\text{-}O_2)$ was observed as a product.[32]

More recently, Stahl and co-workers prepared the bathocuproine coordinaned Pd^{0} complex (Scheme 1.6), which reacts readily with oxygen at room temperature to produce η^2-peroxo Pd^{II}.[33] The role of the electronic spin state of singlet d^{10} Pd^{0} and triplet O_2 was investigated be DFT calculations. Electron transfer from Pd^{0} center occurs by forming a triplet diradical with one spin delocalized on Pd and the other one on O_2.[34]

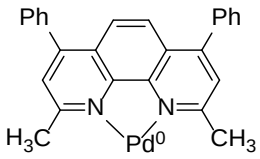

Scheme 1.6 Bathocuproine-coordinated Pd^{0}.

Electron transfer mediators can help overcome the unfavorable kinetics of oxidation of Pd^{0} with O_2. In 1987 Sen and co-workers reported stoichiometric functionalization of methane to methyl trifluoroacetate in CF_3COOH at 80 °C according to Eq 1.7. In this process Pd^{II} was deactivated via formation of Pd^{0}, and

methyl ester was obtained in >60% yield based on Pd^{II}.[35] This problem was resolved by combining three redox couples: Pd^{II}/Pd^0, *p*-benzoquinone/hydrobenzoquinone (Q/H_2Q), and NO_2/NO in trifluoroacetic acid (Scheme 1.7). Selective oxidation of methane to methyl trifluoroacetate was achieved at 80 °C in 690% yield based on Pd^{II} (TOF ~0.7 h^{-1}).[36]

$$CH_4 + CF_3COOH + Pd^{2+} \longrightarrow CF_3COOCH_3 + Pd^0 + 2H^+$$

Equation 1.7

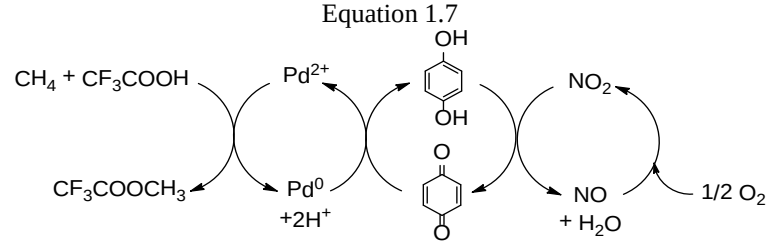

Scheme 1.7. Catalytic oxidation by O_2 through an electron transfer chain via Pd^{II}/Pd^0 couple.

Benzoquinone is an effective oxidant for Pd^0, but the reaction comes to a standstill once all Q is reduced to H_2Q. Addition of O_2 regenerates *p*-benzoquinone, but Pd^0 to Pd^{II} reoxidation is not sufficiently fast to prevent precipitation of Pd^0. This can be resolved by addition of large excess of Q, or addition of a catalyst for aerobic regeneration of *p*-benzoquinone (NO_2). The oxidation process is described in Scheme 1.7 where Pd^{II} is the active catalyst which oxidizes methane to CF_3COOCH_3. Reduced Pd^0 is regenerated by Q, forming Pd^{II} and H_2Q. Then NO_2 oxidizes H_2Q to Q, and NO is finally reoxidized to NO_2 by O_2.[36]

Significantly more efficient conversion of CH_4 to CF_3COOCH_3 was achieved with *p*-tetrachlorobenzoquinone (TCQ) in combination with Pd/C, 1.0 MPa CO and 0.5 MPa O_2 at 140 °C. The catalytic activity was improved with TOF as high as 120 h^{-1}.[37] Based on the studies by Park *et al*., the first step in the proposed mechanism is formation of H_2 via Pd/C catalyzed water gas shift reaction (WGS) between CO and H_2O. Dihydrogen reacts readily with an intermediate complex Pd^0-TCQ, forming

reduced TCHQ. TCHQ is oxidized by O_2, releasing H_2O_2. The *in situ* generated H_2O_2 oxidizes the surface of Pd^0 to Pd^{II}, which reacts stoichiometrically with CH_4 to form CF_3COOCH_3.[37,38]

Heterogeneous Pd/C catalyst can also catalyze methane oxidation when $CuCl_2$ is used as a cocatalyst. The reaction was performed at 85-95 °C in the presence of CO and O_2 and resulted in rapid accumulation of product (TOF = 71 min^{-1}). Similar to the oxidation in the presence of TCQ, reaction is facilitated by *in situ* formation of H_2O_2. The overall transformation is summarized in Scheme 1.8 where three catalytic steps occur in tandem. The first step is the WGS reaction, leading to oxidation of CO to CO_2 and formation of H_2. The second step involves catalytic reaction to generate H_2O_2. The third step is oxidation of alkane by H_2O_2.[39] This system is also effective for hydroxylation of 1° C-H bonds of organic substrates, such as aliphatic acids.[40]

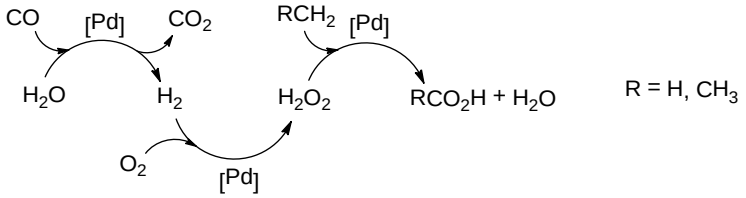

Scheme 1.8 Pd-mediated oxidation of methane and ethane by O_2 in aqueous medium at 70-110 ºC in the presence of CO.

Another example of aerobic functionalization of CH_4 involves $K_2PdCl_4/H_5PMo_{10}V_2O_{40}$ system. The major product of this oxidation is CH_3COOH, which is proposed to form via a radical mechanism, where polyoxoacid abstracts H• from methane to form a methyl radical (CH_3•). Methyl radical is oxidized by $H_5PMo_{10}V_2O_{40}$ to a methyl cation CH_3^+, to form subsequently CH_3COOH and CF_3COOCH_3.[41]

Although electron-transfer mediators (ETM) allow catalytic conversion of methane to functionalized products, reactions involving ETM lead to undesirable biproducts. Selectivity becomes problematic in some cases, and O_2 is not directly involved in reoxidation of reduced palladium. Utilization of multidentate ligands might facilitate oxidation of palladium by O_2 without the need for electron transfer mediators.

1.3.3 Oxy-Insertion Catalytic Cycle

An alternative to the Shilov system, could be the "Oxy-insertion" mechanism.[42] This mechanism includes insertion of an oxygen atom of a YO reagent into M-R bond, generating M-OR. The 1,2-addition of the C-H bond of a hydrocarbon across a M-OR bond regenerates M-hydrocarbyl and releases the product ROH. Reoxidation of Y to YO with O_2 completes the catalytic cycle.[43] Although much less studied, this mechanism offers utilization of more electropositive metals, such as Ir and Re, where M- $R^{\delta-}$ bond polarization is opposite compared to the more electronegative transition metals M-$R^{\delta+}$ complexes.[43]

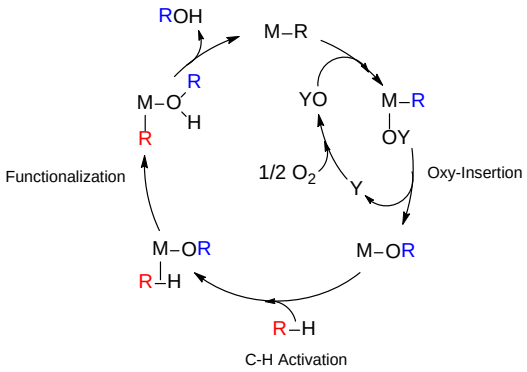

Scheme 1.9 Possible pathways for C-H functionalization involving the 1,2-addition of C-H bonds across metal–heteroatom bonds.

C-H addition across a metal-oxygen bond is a crucial step in the pathway in Scheme 1.9. According to the catalytic cycle, formation of an oxy-functionalized

product occurs concurrently with C-H activation of a hydrocarbon. Such C-H activation/oxy-functionalization reaction was demonstrated in case of (acac-O,O)$_2$Ir^{III}(OCH$_3$)(L), (L = MeOH, pyridine) (Scheme 1.10). C-H activation of benzene occurred cleanly in high yield, with generation of MeOH. Reaction with benzene-d$_6$, resulted in the formation of labeled CH$_3$OD in >95% yield, confirming the pathway shown in Scheme 1.10. C-H activation is initiated by dissociation of MeOH or the pyridine ligand, followed by rearrangement of acac ligands to place methoxo *cis* to the open coordination cite, coordination of benzene, and 1,2-addition of C-H bond via σ-bond metathesis.[44]

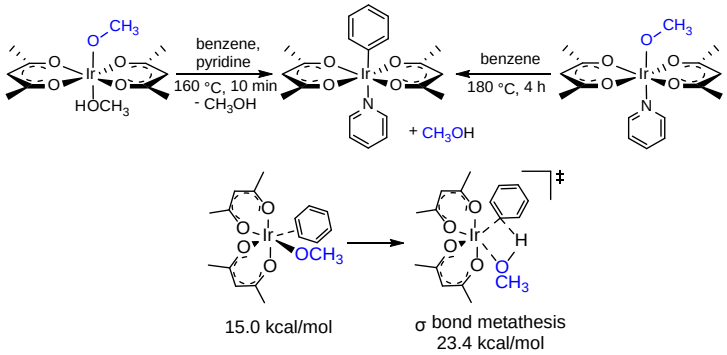

Scheme 1.10 Proposed mechanism of benzene C-H activation by (κ^2-*O*,*O*-acac)$_2$Ir(OMe)(MeOH).

Of course, for a catalytic system, the identity of the hydrocarbyl group in the substrate and in the product should be the same; nevertheless, this reaction demonstrates one of the few examples of 1,2-addition across M-OR bond.

Goldberg *et al.* have demonstrated that Rh^I-OR (R = H, CH$_2$CF$_3$, C$_6$H$_5$) complexes activate C-H bonds of benzene at elevated temperatures. In case of the phenoxide ligand, the presence of water was necessary to initiate the H/D exchange reaction, and approximately 15 turnovers were observed after 100 h.[45] Mechanistic studies indicated that Rh^I-OH/D$_2$ is the active catalyst, formed by heterolytic

dissociation of OR group (R = CH_2CF_3, C_6H_5). The rate determining step is the displacement of solvent by benzene or C-H oxidative addition Scheme 1.11).[46]

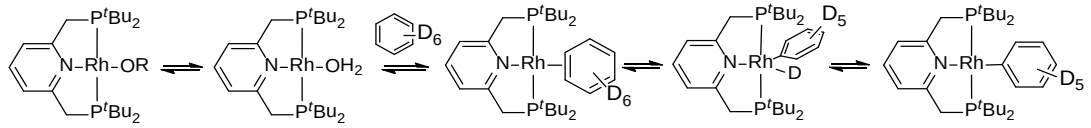

R = H, CH_2CF_3, C_6H_5

Scheme 1.11 Proposed mechanism for C-H bond activation of arenes using (PNP)Rh(OR).

The second important step in the catalytic cycle in Scheme 1.9, is M-R bond functionalization. One of the few examples of the insertion of oxygen into M-R bond have been reported by Periana *et al*. in case of methyltrioxorhenium (CH_3ReO_3) complex.

Methyltrioxorhenium (CH_3ReO_3), known as an olefin epoxidation catalyst,[47] was shown to decompose with formation of MeOH in water when treated with H_2O_2, as an oxidant.[48] Further, it was discovered that non-peroxo oxidants, such as PhIO, pyridine-N-oxide and periodates, led to selective formation of methanol via oxy insertion pathway. The mechanism of O atom insertion was proposed to occur via a Baeyer-Villiger intermediate, where the oxidant coordinates to the metal, followed by methyl group migration without the change in metal oxidation state (Scheme 1.12).[43] Aryl derivatives of rhenium trioxide were also shown to undergo quantitative oxy-insertion in the presence of H_2O_2, and $NaIO_4$.[49] Calculated Baeyer-Villiger reaction transition state was reported to be 10.7 kcal/mol, which is 6.3 kcal/mol lower than in case of methyltrioxorhenium (CH_3ReO_3).[43,49]

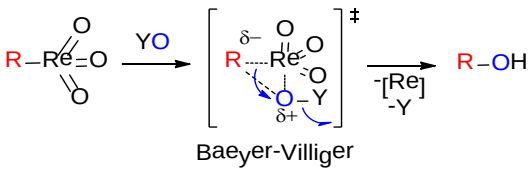

Scheme 1.12 Baeyer–Villiger-type transition state for O-insertion into Re-CH_3 bond.

Theoretical calculations were performed in order to identify the activation barriers for Baeyer-Villiger O-atom insertion pathway for various metals. Results showed that insertions of this type are favored by earlier transition metal complexes,[50] thus, it is important to discover new methods that would lower activation barriers for oxy-insertion into M-R bonds for late transitions metals, typically used for C-H activation. Groves *et al.* reported a flavin-based catalyst that facilitates organometallic Baeyer-Villiger reaction. The addition of a 12 mol % loading based on methyltrioxorhenium (CH_3ReO_3) complex provided a two orders of magnitude rate enhancement over uncatalyzed reaction in the unbuffered solution and more than five orders of magnitude rate enhancement in the buffered solution at *pD* = 3.4. The proposed mechanism is shown in Scheme 1.13.[51]

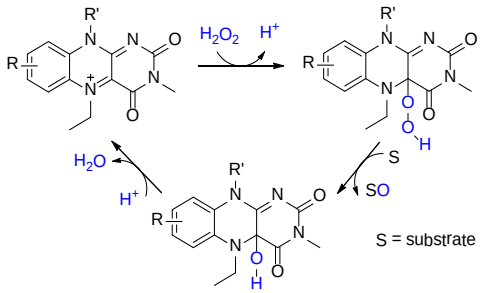

Scheme 1.13 Mechanism for Flavin-Catalyzed Oxidations (S =Substrate).

Although 1,2-addition across the M-OR bond, and oxy-insertion into M-R bond have been demonstrated, little is known about either reaction and experimental precedent is limited. In addition, oxy-insertion has been observed with high valent Re^{VII} d^0 metal, which is incapable of C-H activation.[42]

1.3.4 Metal-Oxo Catalytic Cycle

Another alternative for C-H bond functionalization is related to enzymatic systems, containing a metal-oxo functionality. Scheme 1.14 shows three steps: 1)

abstraction of H-atom of hydrocarbon by M^{n+2}=O to form M^{n+1}-OH and alkyl radical, 2) rebound step, where R• recombines with OH ligand and alcohol is eliminated, and 3) reoxidation of M^n to generate M^{n+2}=O.[52]

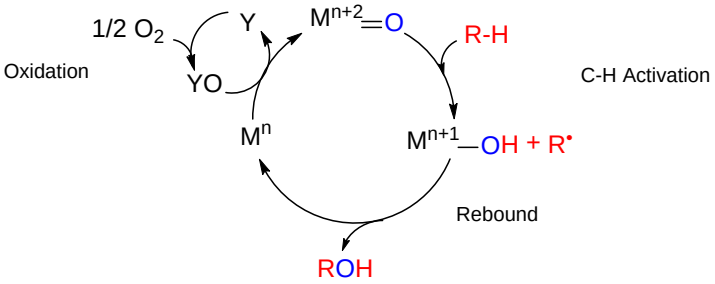

Scheme 1.14 C–H functionalization via metal oxo pathway.

Very facile C-H bond hydroxylation via rebound mechanism has been demonstrated in case of model active site of cytochrome P450, a cationic oxoiron(IV)-porphyrin. When *m*CPBA was added to a solution of hydrocarbon and Fe^{III} catalyst, the corresponding alcohol was formed in 90% yield based on the oxidant. Reaction rates were very fast, on the order of $k_3 \sim 10^3 - 10^6$ M^{-1} s^{-1}, depending on the hydrocarbon and correlated well with C-H bond dissociation energy. An radical-rebound reaction scenario was confirmed by $H_2{}^{18}O$ labeling experiment and a moderate kinetic isotope effect of k_H/k_D = 2.1 was reported (Scheme 1.15).[53]

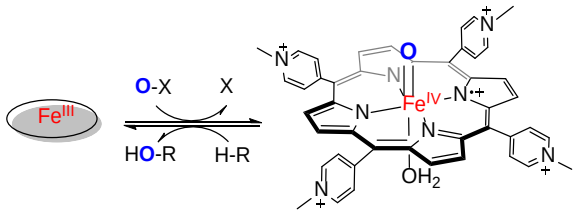

Scheme 1.15 Substrate oxygenation mediated by oxoiron(IV)-porphyrin π radical cation.

High selectivity in catalytic chlorination of aliphatic C-H bonds has been reported with a Mn-porphyrin catalyst, tetrabutylammonium chloride, $(^tBu)_4NCl$, as a phase transfer catalyst and sodium hypochlorite, NaClO, as a chlorine source

(Scheme 1.16). The yield of chlorinated products for simple and complex substrates ranged between 12-74%. Substrates with strong C-H bonds (BDE ~ 100 kcal/mol) have also been chlorinated with moderate yield. Regarding the mechanism, it is expected that basic NaClO will oxidize the starting Mn^{III} porphyrin to a dioxo- or oxohydroxoMn^{V} complex. High valent Mn^{V}-oxo will initiate hydrogen atom abstraction from the substrate and will generate an alkyl radical and a Mn^{IV}-OH complex.[11] Since NaClO is present in great excess, product forming step occurs via a chlorine atom transfer from the Mn^{IV}-OCl complex to the R•. Subsequently Mn^{IV} is reoxidized to Mn^{V}=O.[11]

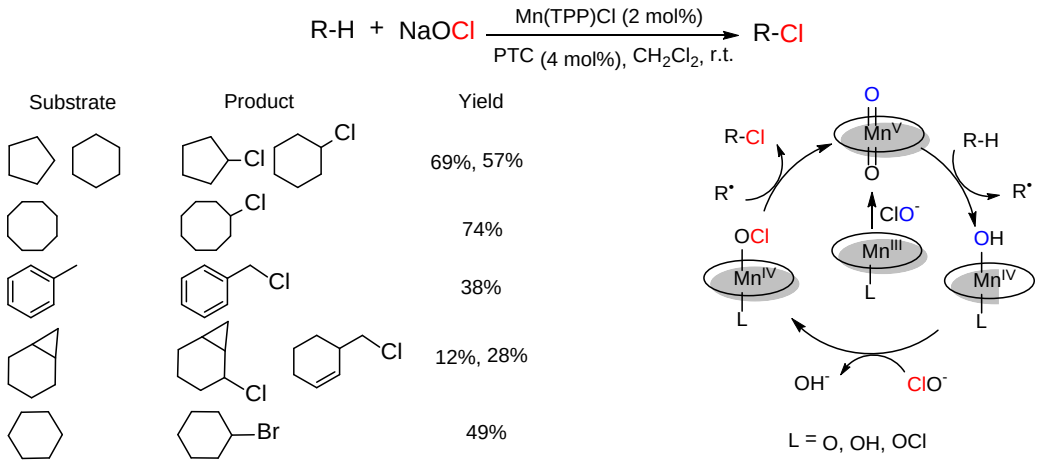

Scheme 1.16 Proposed C-H chlorination mechanism via trans-dioxo Mn(V) porphyrins.

Such high (95% for methylene-chlorinated) selectivity is unusual for radical based reactions. Groves *et al.* postulate that the nature of porphyrin meso-substituent was affecting C-H selectivity – when pyridines were used as axial ligands, loss of selectivity was observed.[11]

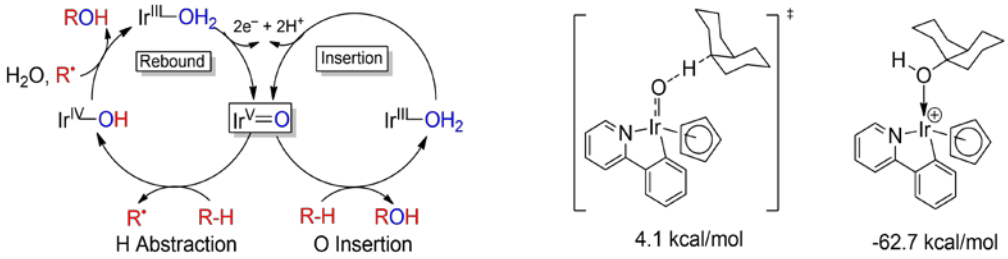

Scheme 1.17. Alternative reaction mechanism postulated for Ir-catalyzed C-H activation.

Crabtree *et al*. proposed that C-H oxidation of alkanes by Cp*Ir complexes occurs via direct oxygen insertion rather than radical rebound route. The authors argue that high level of stereoretention is inconsistent with rebound mechanism. Theoretical calculations also suggest that oxygen insertion is a lower energy pathway, with transition states (TS) of 4.1 kcal/mol (Scheme 1.17).[54] High-valent metal-oxo active species are generated *in situ* when Cp*Ir complexes react with an oxidant, such as ceric ammonium nitrate ($[NH_4]_2[Ce^{IV}(NO_3)_6]$, CAN)[54,55] or sodium periodate ($NaIO_4$)[56]. Hydroxylation of secondary alkane C-H bonds with CAN occurred with moderate to good yields. Substrate scope and selected catalysts are shown in Scheme 1.18. In all of the cases the active catalyst was proposed to be $[Cp^*Ir^{V}(O)(N\text{-}X)]^+$ (X = C, O).[55]

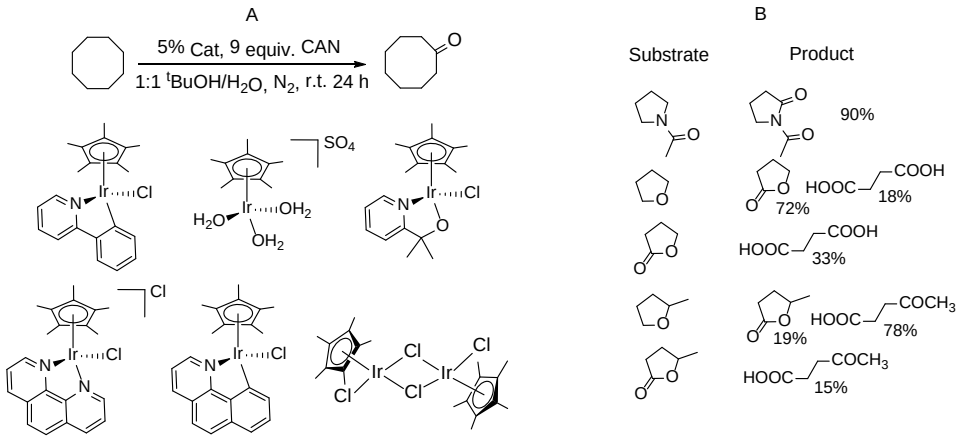

Scheme 1.18 A: screening of the catalysts for cyclooctane oxidation. B: C-H oxidation of heterocycles with $[Cp^*Ir(H_2O)_3][SO4]$, conditions: 1% 2, 8 equiv CAN, 50 µL substrate, in 10 mL D_2O solvent under N_2, r.t., dark, 30 min.

When sodium periodate was used as an oxidant, a more efficient oxidation of alkanes was observed; however, methane was overoxidized to CO_2 in 39% yield, and ethane was transformed to acetic acid in up to 25% yield.[56]

So far, there is no experimental evidence that partial oxidation of methane can be achieved by either enzymatic model compounds[11,53] or by organometallic M=O species[54-56]. In addition, strong oxidants are required for these systems in order to regenerate high energy metal-oxo species. Another drawback is that involvement of free radicals can lead to undesirable side reactions.

1.3.5 Additional Examples of C-H bond Functionalization

Sen *et al*. reported formation of methane bisulfate CH_3OSO_3H not only in the presence of $HgSO_4$, compare with Periana's Hg^{II}/H_2SO_4[26] methane functionalization system, but also in the presence of other oxidants: $K_2S_2O_8$ (39%), $Ce(SO_4)_2$ (38%), $PbSO_4$ (95%),[57] and H_2O_2, *m*CPBA, AIBN, $PbEt_4$[58]. The authors postulated that an additional pathway where C-H activation does not occur must be operational. Instead, the role of the oxidant in sulfuric acid is to generate a methane cation-radical from methane by outer-sphere electron transfer, followed by proton loss, and conversion of methyl radical to CH_3OSO_3H (Scheme 1.19, **A**). This pathway was supported by observation that when ethane was subject to the reaction conditions, formation of CH_3OSO_3H was still observed (up to 25%) (Scheme 1.19, **A**).[57] When oleum was used in combination with $K_2S_2O_8$, conversion of methane to CH_3OSO_3H was observed (Scheme 1.19, **B**).[27]

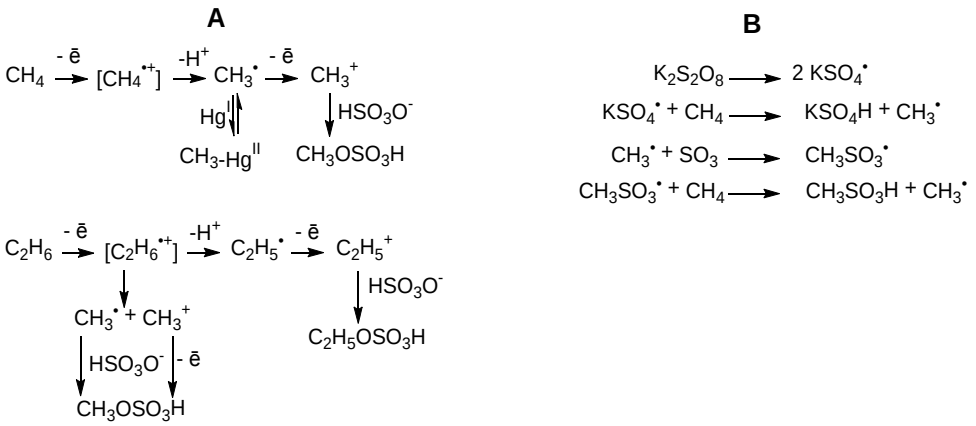

Scheme 1.19 A: formation of alkyl radical by outer sphere electron transfer, followed by proton loss, in sulfuric acid. B: plausible mechanism for the $K_2S_2O_8$-initiated conversion of methane to CH_3SO_3H by fuming sulfuric acid.

The high selectivity towards monofunctionalized product in a radical mechanism was explained in terms of reduced susceptibility of the H-CH_2OSO_3H bond to both electrophilic attack and H-atom abstraction, due to the destabilizing inductive effect of -OSO_3H group on the electron-deficient carbon.[57]

N-heterocyclic carbene Pd^{II} complexes have shown very efficient transformation of methane to the methyl trifluoroacetate. The reaction was performed in the presence of $K_2S_2O_8$ as an oxidant in trifluoroacetic acid (TFA), and resulted in 3000% yield (TON = 30) of functionalized product (based on the Pd), Scheme 1.20.[59]

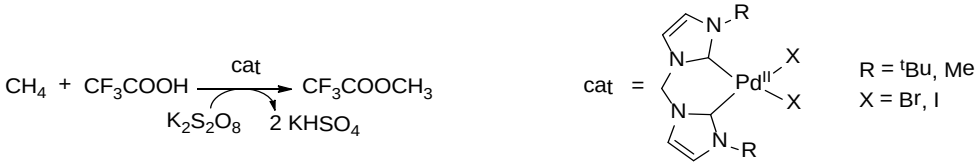

Scheme 1.20 (NHC)Pd^{II}-mediated catalytic conversion of methane into the corresponding methyl esters. Conditions 14 h at 90 ºC, p(CH_4) 30 bar.

Although the authors did not discuss the mechanism of this transformation, previous reports by Sen *et al.* for reactions under similar conditions indicate a radical mechanism. Conversion of methane to methyl trifluoroacetate (400% yield, TON = 4)

was also catalyzed by $Co^{III}(OCOCF_3)_3/O_2$ (1-5 atm). Co^{III} is presumably deactivated via formation of CoF_2.[60]

$$CH_4 + CO + 1/2O_2 \xrightarrow[KI,\ H_2O,\ 100\ °C]{RhCl_3} CH_3COOH$$

Equation 1.8

Conversion of methane and CO to acetic acid has been demonstrated with aqueous rhodium trichloride as catalyst. Reaction occurred only in the presence of CO and O_2, and the yield of acetic acid was substantially increased in the presence of I^- ions. Competition between CH_4 and $^{13}CH_3OH$ as substrates indicated that formation of a Rh-CH_3 species occurs from methane. Since methanol was not carbonylated under the reaction conditions, the function of I^- in this system is not the same as in Monsanto acetic acid process (Eq. 1.8).[61]

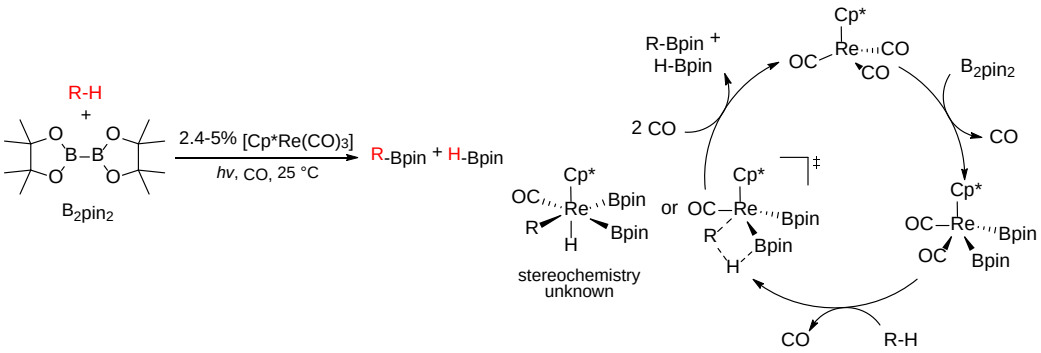

Scheme 1.21 Proposed mechanism for the photochemical reaction of B2pin2 with alkenes, catalyzed by $Cp^*Re(CO)_3$.

Catalytic borylation of alkanes was reported with Re[62] and Rh[63] complexes. Irradiation of B_2pin_2 in hydrocarbon under 2 atm of CO in the presence of 2.4 - 5.0 mol% of catalyst, afforded corresponding alkylborane in 75-100% yield. Interestingly, no secondary boronate esters were generated, indicating regiospecific reaction of rhenium bis-boryl complex with the alkane primary C-H bond. The mechanism involves initial oxidative addition of the diboron compound, followed by

C-H activation (via oxidative addition or σ-bond metathesis), and CO assisted reductive elimination of alkyl borane (Scheme 1.21).[62]

Development of the process in which Pt^{IV} is replaced by a more practical oxidant will be facilitated if we better understood how oxidants function in the actual oxidation step. Such information is difficult to glean from a catalytic system. In the following chapters we will discuss in detail the mechanism of oxidation of Pt^{II} and Pd^{II} complexes with O_2.

Chapter 2 : Effect of pH on the Aerobic Oxidation of (dpms)$Pt^{II}Me(OH_2)$ and (dpms)$Pt^{II}Me(OH)^-$ complexes: Pt^{II}-to-Pt^{IV} Oxidation and Methyl Group Transfer Reactivity

2.1 Aerobic Oxidation of Pt^{II} to Pt^{IV}: Examples and Mechanisms

The Shilov system appears to be one of the most promising for catalytic conversion of methane to methanol. All three steps have been realized, expensive Pt^{IV} can be replaced with another oxidant[16], and deposition of metallic platinum can be avoided with the proper choice of ligand[28]. Despite these advances, the direct use of O_2 as an oxidant has not been realized. Attempts to address this issue have been made since the discovery of Shilov's system, however, success in this area has been limited.[64,65]

Dioxygen is the most compelling oxidant for Shilov-type system. It is environmentally friendly and inexpensive, lacks toxic byproducts, and sometimes can be replaced by air. The difficulty in implementing O_2 in the Shilov system is due to the low energy of platinum valence orbitals,[66] and the high energy barrier for electron transfer to O_2. Although dioxygen is potentially a thermodynamically strong oxidant with $E^0 = 1.23$ V[66], examples of its reactions with Pt^{II} are very limited. Even singlet oxygen maybe unreactive with Pt^{II} unless strong σ-donor is present.[67]

The unfavorable kinetics of aerobic oxidation of Pt^{II} to Pt^{IV} can be circumvented by an electron-transfer mediator (ETM), which would carry electrons from the metal to the oxidant via a low energy pathway.[68] Electron transfer mediators have several advantages: 1) the oxidation potential of ETM is sufficient for oxidation

of Pt^{II} to Pt^{IV} ($E^0_{Pt^{2+}/Pt^{4+}}$ = -0.68 V)[17] or Pt^{III} and 2) the reduced form of the ETM can be readily reoxidized by O_2.[64,65] The second alternative is to employ a strong σ-donor or potentially tridentate ligands which will raise the energy of HOMO (σ-antibonding d_z^2 orbital) of the platinum complex.

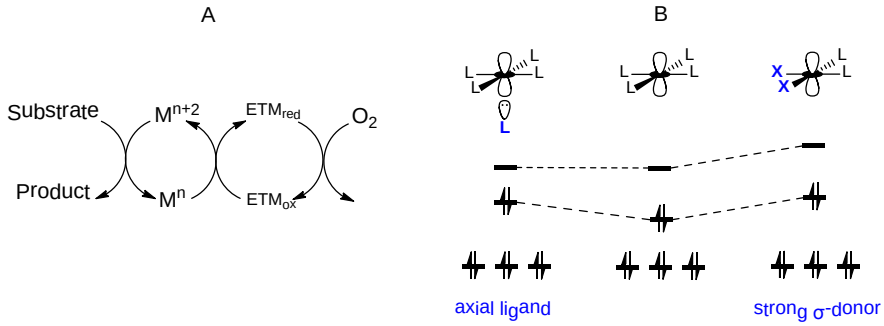

Scheme 2.1 A: Substrate oxidation via electron transfer facilitated by an electron-transfer mediator. B: qualitative MO diagram of a square-planar platinum(II) complex. Effects of axial ligands and strong σ-donors on HOMO energy.

2.2 Oxidation with Electron Transfer Mediators

Shilov *et al*. reported that methane can be oxidized by O_2 with Pt^{II} as a catalyst in the presence of heteropolyacid ($Na_8HPMo_6V_6O_{40}$). Under the reaction conditions (120°C, $p(CH_4)$ = 60 atm, $p(O_2)$ = 10 atm, $[K_2PtCl_4]$ = 3.3 x 10^{-2} M, $[Na_8HPMo_6V_6O_{40}]$ = 1.4-9.5 x 10^{-3} M), the maximum methanol concentration was between 2-3 x 10^{-2} M. At $[Na_8HPMo_6V_6O_{40}]$ =1.4 x 10^{-3} M, the rate of oxidation increases. However, at higher concentrations the rate of methane overoxidation increases too. The system is not stable, and metallic platinum appears over time.[65]

Deposition of Pt metal can be avoided with the use of a proper ligand. A bipyrimidyl-polyoxometalate Pt^{II} hybrid complex, impregnated on a silica matrix, $[(Mebpym)PtCl_2]^+[H_4PV_2Mo_{10}O_{40}]^-/SiO_2$, was shown to oxidize methane to methanol, ethane and acetaldehyde under considerably milder conditions than Shilov's heteropoly acid system. Reactions were performed at 50-60°C, $p(CH_4)$ ~ 30

atm, p(O_2) ~ 1-2 atm. System showed ~33 turnovers/4 h. No formation of Pt aggregates or leaching of Pt into the solution was observed. Reaction is proposed to occur via the Shilov-type catalytic cycle (Scheme 2.2), and a S_N2 pathway for product formation was confirmed by labeling studies with $H_2{}^{18}O$.[64]

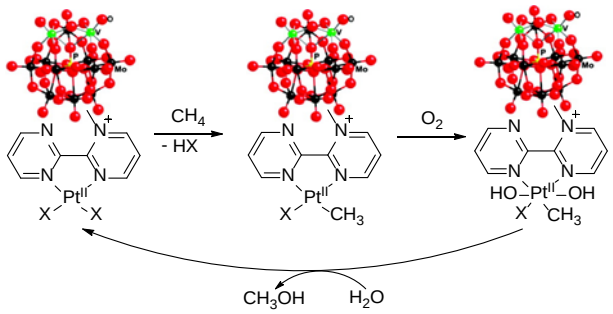

Scheme 2.2 Aerobic oxidation of methane catalyzed by $[Pt(Mebipym)Cl_2]^+[H_4PV_2Mo_{10}O_{40}]^-/SiO_2$.

Sen *et al*. demonstrated catalytic hydroxylation of ethanesulfonate by $[PtCl_4]^{2-}$ with $CuCl_2$ as a cocatalyst in the presence of acid at elevated temperature (160 °C) and O_2 pressure. Higher turnovers are observed in the presence of chloride and copper ions and low pH is necessary for catalysis. In 4 h 42 turnovers were observed. When ethane was used as a substrate, formation of ethanol, ethylene glycol and acetic acid was observed in 34, 45 and 19 % yield respectively (Scheme 2.3), and a S_N2 pathway for product formation was confirmed by labeling studies with $H_2{}^{18}O$.[64,69]

This catalytic system does not deactivate via precipitation of Pt metal, instead all Pt^{II} is eventually converted to Pt^{IV}. Since Cu^{II} is not capable of oxidizing Pt^{II} to Pt^{IV}, a stronger oxidant such as H_2O_2 is generated by the combination of Cu and O_2.[70] Additional studies are needed to elucidate this mechanism.[16]

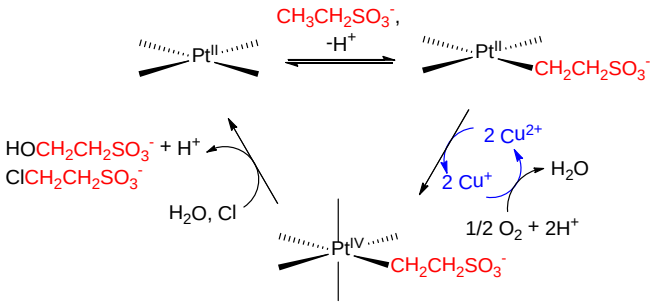

Scheme 2.3 Catalytic hydroxylation of ethanesulfonate by $[PtCl_4]^{2-}$ with $CuCl_2$ as a cocatalyst.

Bercaw *et al*. compared a variety of oxidants in a competitive oxidation *vs.* protonation reaction of $[Pt^{II}(CH_3)Cl_3]^{2-}$. The ratio (k_{ox}/k_H^+) for Cu^{II}, Fe^{III} and $Na_3[H_3PV_3Mo_9O_{40}]$, as well as $Pt^{IV}Cl_4^{2-}$ is shown in Table 2.1. Other one-electron oxidants such as $Na_2Ir^{IV}Cl_6$, and $[NH_4]_2[Ce^{IV}(NO_3)_6]$ lead to oxidation of $[Pt^{II}(CH_3)Cl_3]^{2-}$ to form $[Pt^{IV}(CH_3)Cl_5]^{2-}$.[70]

Entry	Oxidant	k_{OX}/k_H^+
1	$Na_2Pt^{IV}Cl_6$	20 ± 4
2	$Cu^{II}Cl_2$	191 ± 24
3	$O_2/Cu^{II}Cl_2$[b]	173 ± 35
4	$Fe^{III}Cl_3$	14 ± 3
5	$Na_3[H_3PMo_9V_3O_{40}]$[c]	15 ± 3

Table 2.1 k_{OX}/k_H^+ for a variety of oxidants reacting with $[Pt^{II}(CH_3)Cl_3]^{2-}$ (1) at constant $[H^+]$.

2.3 Effect of Semi-Tripodal and σ-Donor Ligands on Aerobic Oxidation of Pt^{II}

The first example of an aerobic oxidation of Pt^{II} to Pt^{IV} under mild conditions was reported by Sarneski *et al*. The reaction of dichloro-2,2'-bipyridyl $Pt^{II}(bipy)Pt^{II}Cl_2$ with cis,cis-1,3,5-triaminocyclohexane (tach) under air resulted in stoichiometric formation of $[(bipy)Pt^{IV}(k^3\text{-tach})]^{2+}$ (Scheme 2.4).[71]

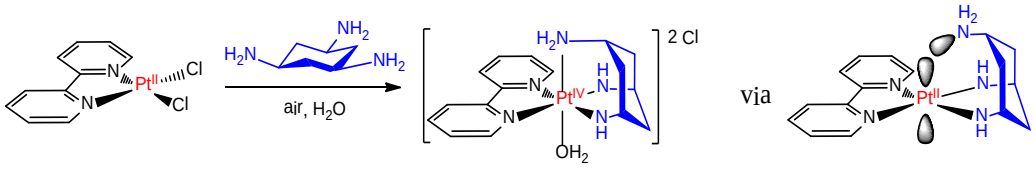

Scheme 2.4 Reaction of $(bipy)Pt^{II}Cl_2$ with *cis,cis*-1,3,5-triaminocyclohexane. Oxidation of Pt^{II} to Pt^{IV} under air.

Formation of $[(bipy)Pt^{IV}(k^3\text{-tach})]^{2+}$ occurs via a precursor Pt^{II} complex with a squire planar configuration, containing a bidentate tach ligand. The steric proximity of the non-coordinated NH_2 group to the filled d_z^2 orbital of Pt^{II} metal center, facilitates oxidation of Pt^{II} to Pt^{IV}. Similarly, when $[(k^2\text{-tacn})_2Pt]^{2+}$ (1,4,7-triazacyclononane, tacn) is exposed to air at 90 °C for 20 h, formation of $[(k^3\text{-tacn})_2Pt]^{4+}$ (Scheme 2.5) is observed.[72]

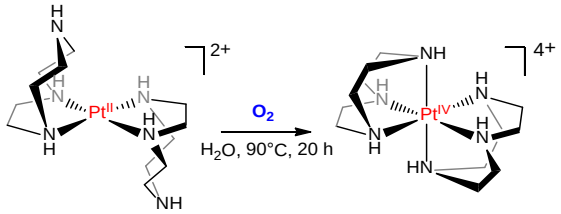

Scheme 2.5 1,4,7-triazacyclononane-ligand supported oxidation of Pt^{II} to Pt^{IV} under O_2.

Involvement of peroxo- or superoxo- intermediates in oxidation of Pt^{II} to Pt^{IV} with O_2 was proposed when a platinum(IV) dimer, bridged by two peroxo ligands, was isolated from the reaction of $[(k^2\text{-tacn})PtCl(DMSO)]^+$ with O_2. Authors postulate that coordination of O_2 is followed by displacement of DMSO ligands by peroxo ligands, to give a stable peroxo Pt^{IV} dimer (Scheme 2.6).[73] The oxidation is facilitated by the tridentate ligand, which promotes octahedral coordination to the metal center, and removal of two electrons from the metal's valence orbitals.

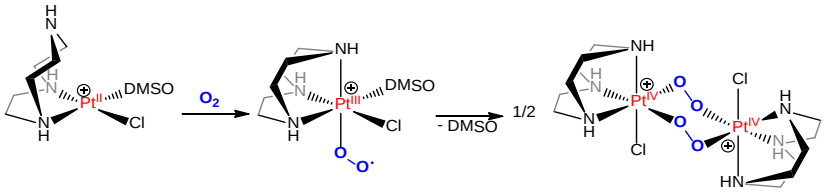

Scheme 2.6 Formation of bis(μ_2-peroxo)platinum(IV).

The effect of σ-donors on reactivity of Pt^{II} complexes was first demonstrated with $(k^2\text{-tacn})Pt(CH_3)_2$, which was oxidized to $[(k^3\text{-tacn})_2Pt(CH_3)_2OH]^+$ under air at ambient temperature. The proposed mechanism for this transformation is shown in

Scheme 2.7, where short-lived superoxoplatinum(III) intermediate is protonated by H_2O to give a hydroperoxo Pt^{IV}. Hydroperoxide would then oxidize a second equivalent of (k^2-tacn)$Pt(CH_3)_2$.[74]

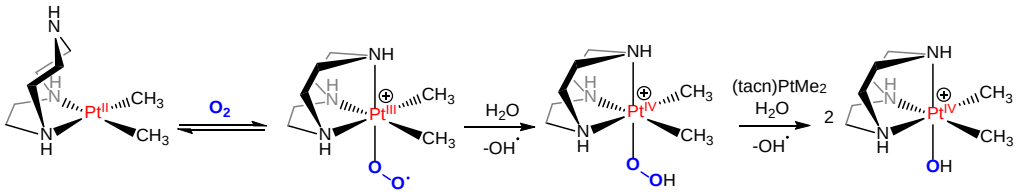

Scheme 2.7 Proposed mechanism of oxidation of (κ^2-tacn)$Pt(CH_3)_2$ is oxidized to $[(\kappa^3\text{-tacn})Pt(CH_3)_2(OH)]^+$ with O_2.

Aerobic oxidation of Pt^{II} can be achieved in the *absence* of semi-labile tridentate ligands when strong σ-donor ligands, such as methyl groups, are present. A variety of dimethylplatinum(II) complexes, supported by bidentate N-donor ligands were shown to undergo aerobic oxidation to Pt^{IV} (Scheme 2.8).[75,76] However, when methyl groups on Pt^{II} are replaced with a Cl or Ph ligand ((tmeda)Pt^{II}MeCl, (tmeda)$Pt^{II}Cl_2$, (tmeda)$Pt^{II}Ph_2$), no oxidation takes place.[75,77]

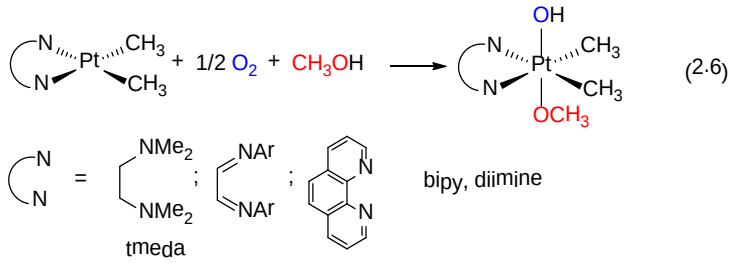

Scheme 2.8 Oxidation of (N-N)$Pt^{II}Me_2$ with O_2 in methanol.

Based on the previous reports,[73,74] the reaction was proposed to occur in two consecutive steps. In the first step, (N-N)$Pt^{II}Me_2$ reacts with dioxygen to form (N-N)Pt^{IV}(OOH)(OMe)$(Me)_2$. In the second step, this complex oxidizes a second equivalent of (N-N)$Pt^{II}Me_2$. Disproportionation of (N-N)Pt^{IV}(OOH)(OMe)$(Me)_2$ (Scheme 2.9, **B**) which was isolated and characterized, occurs at a slower rate than oxidation of (N-N)$Pt^{II}Me_2$.[75]

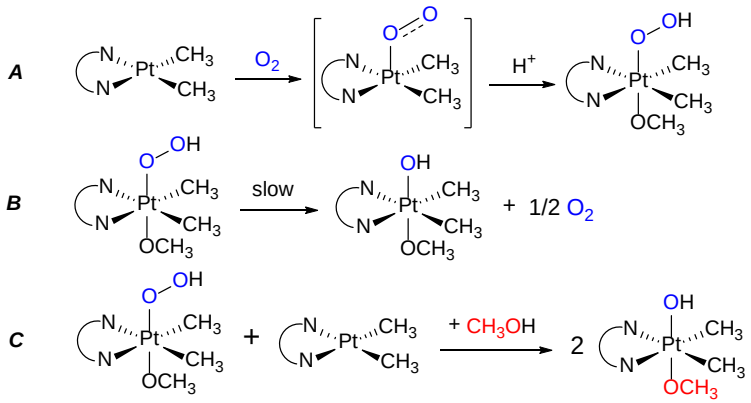

Scheme 2.9 Proposed mechanism of oxidation of (N-N)$Pt^{II}Me_2$ with O_2 in methanol.

Recently, the intermediacy of superoxide was proposed in the spin trap studies of reaction between ($^tBuN_4$)$Pd^{II}Me_2$ and O_2. Oxidation in the presence of 5,5-dimethyl-1-pyrroline-N-oxide (DMPO), a commonly used spin trap for O-centered radicals, showed formation of an unstable DMPO spin adduct (Scheme 2.10) by EPR.[78]

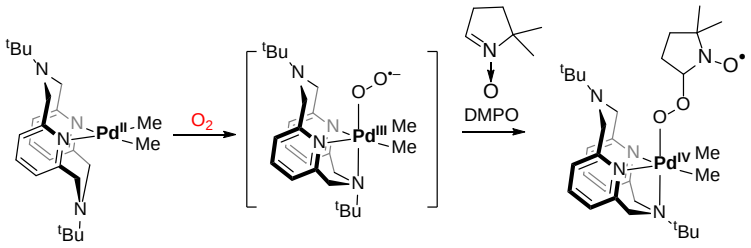

Scheme 2.10 Proposed mechanism of oxidation of (N4)$Pd^{II}Me_2$ by O_2 and formation of a DMPO radical adduct.

Overall, aerobic oxidation of Pt^{II} to Pt^{IV} can be achieved using electron transfer mediators, semilabile tridentate facially chelating ligands, and strong electron releasing groups. The use of electron transfer mediators is undesirable due to potential overoxidation of the organic substrates, low selectivity, and accumulation of peroxointermediates.[70]

Implementation of strong σ-donors allows for oxidation of Pt^{II} to Pt^{IV} with O_2 and in the absence of ETM. High reactivity of Pt^{II}-dimethyl complexes is due to

stabilization of Pt^{IV} center by electron donation of the Me groups. The limitation of the resulting $Pt^{IV}Me_2$ complexes is their inability to promote formation of C-O functionalized products.

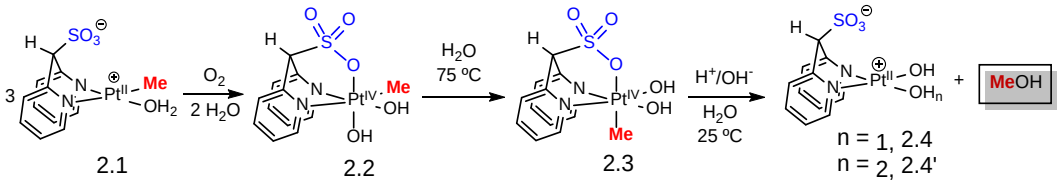

Scheme 2.11 Oxidation of $(dpms)Pt^{II}Me(OH_2)$ to $(dpms)Pt^{IV}Me(OH)_2$ with O_2 and formation of methanol.

Previously, our group demonstrated that di(2-pyridyl)methanesulfonate (dpms, Scheme 2.11), enables selective conversion of Pt^{II} monomethyl complex $(dpms)Pt^{II}Me(OH_2)$ to its monomethyl Pt^{IV} hydroxo counterpart, C_1-symmetric $(dpms)Pt^{IV}Me(OH)_2$. Moreover, formation of methanol from the C_1-symmetric $(dpms)Pt^{IV}Me(OH)_2$ complex via its mirror-symmetric (C_s) isomer **2.3** has also been demonstrated.[79] The effect of the pendant sulfonate group on the enthalpy and entropy of oxidation has been evaluated using DFT calculations (Scheme 2.12) by Wei-Guang Liu from California Institute of Technology (W. A. Goddard III group).

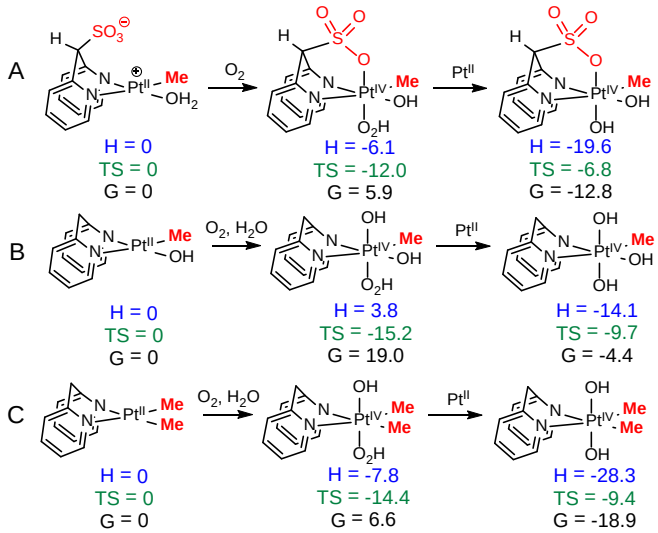

Scheme 2.12 Enthalpy, entropy and Gibbs free energies for oxidation of Pt^{II} at 273.15 K, $p(O_2)$ = 1 atm, pH 7. A: $(dpms)Pt^{II}Me(OH_2)$. B: $(dpm)Pt^{II}Me(OH)$. C: $(dpm)Pt^{II}Me_2$.

Formation of Pt^{IV}-OOH intermediate in endergonic for reactions **A**, **B** and **C** in (Scheme 2.12) mostly due to positive entropy contribution to the reaction Gibbs energy. The sulfonate group (Scheme 2.12, **A**) lowers the reaction entropy by 3.2 kcal/mol, compared to the (dpm)$Pt^{II}Me_2$ analog **B** and by 2.4 kcal/mol compared to the (dpm)Pt^{II}Me(OH) **C** (12.0, 15.2, and 14.4 kcal/mol respectively). The enthalpy of reaction leading to (dpms)Pt^{IV}Me(OH)(OOH) was calculated to be -6.1 kcal/mol, which is 9.9 kcal/mol lower than **B**. Enthalpic stabilization by sulfonate group is comparable to the stabilization by electron donating methyl ligands. Formation of (dpm)$Pt^{IV}Me_2$(OH)(OOH) is 11.6 kcal/mol more favorable than (dpm)$Pt^{IV}Me(OH)_2$(OOH).

Formation of (dpms)$Pt^{IV}Me(OH)_2$ is also entropically more favorable than dpm monomethyl and dimethyl analogue (3.1 and 2.6 kcal/mol respectively). The gain in enthalpy, however, is most substantial for the formation (dpm)$Pt^{IV}Me_2(OH)_2$, followed by (dpms)$Pt^{IV}Me(OH)_2$ and (dpm)$Pt^{IV}Me(OH)_3$, (28.3, 19.6 and 14.1 kcal/mol).

This analysis, for the first time, elucidates the ability of the dpms ligand to enable oxidation of monomethyl Pt^{II} complexes. Its success is due to the lower ΔH and $T\Delta S$ of this reaction, compared to the analogous complex without sulfonate ligand. Reaction parameters are comparable to the dimethyl complexes, which are unable to perform C-O functionalization.

2.4 Experimental and Computation Study

In the original Shilov system Pt^{II} complexes exhibit both electrophilic and nucleophilic properties: Pt^{II} acts as an electrophile in the C-H activation step and as a

nucleophile in Pt^{II} to Pt^{IV} oxidation step. Thus, the presence of electron releasing groups (CH_3) will facilitate oxidation, but will prohibit C-H activation, necessary for the catalytic turnover. Facially chelating ligands such as tacn can promote aerobic oxidation even of cationic complexes[73], however, the C-O reductive elimination from $Pt^{IV}Me$ has not been demonstrated with those ligands[75-77]. Weakly coordinating SO_3 group of the $dpms^-$ ligand allows for oxidation of Pt^{II} to Pt^{IV} and C-O reductive elimination from $Pt^{IV}Me$. It has been previously reported that oxidation of $(dpms)Pt^{II}Me(OH_2)$ complexes in water has a half-life of $t_{1/2}$ = 15 min at 20 °C.[79] The reaction was proposed to occur via mechanism, similar to the one proposed by Puddephatt[74] and later by Bercaw[75] (Scheme 2.13).

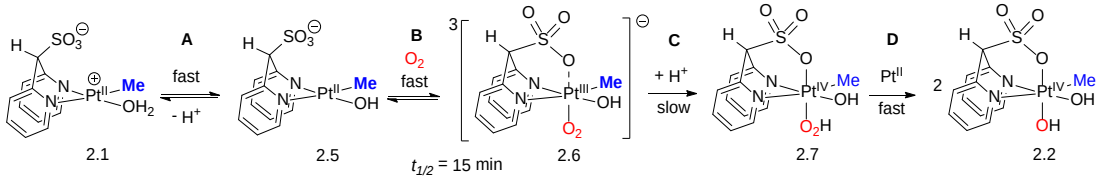

Scheme 2.13 Proposed mechanism of oxidation of $(L)Pt^{II}Me(OH_2)$ to $(L)Pt^{IV}Me(OH)_2$ with O_2.

The first step in Scheme 2.13 is formation of anionic $[(dpms)Pt^{II}Me(OH)]^-$ via deprotonation of $(dpms)Pt^{II}Me(OH_2)$. This step is followed by axial attack of O_2 to generate transient superoxoplatinum(III) $^3[(dpms)Pt^{III}(Me)(\eta^1\text{-}O_2)(OH)]^-$. Protonation of the superoxo intermediate is the rate-limiting step due to a spin forbidden interconversion. This step is proposed to occur via a proton-coupled electron transfer to give $(dpms)Pt^{IV}Me(OH)(OOH)$, followed by the O-O bond cleavage and the formation of the final product $(dpms)Pt^{IV}Me(OH)_2$.[80] Since this mechanism involves two steps, which depend on the concentration of H^+, pH might have a substantial effect on the reactivity of monomethyl Pt^{II} complexes.

2.5 Effect of pH on the Aerobic Reactivity of Monomethyl Pt^{II} Complexes

Previously Vedernikov *et al*. demonstrated that aerobic oxidation of unbuffered (dpms)Pt^{II}Me(OH$_2$) complexes in water leads to almost quantitative formation of *C*$_1$-symmetric (dpms)Pt^{IV}Me(OH)$_2$.[79] When oxidation was performed in buffer solutions of pH 4.1 – 10.0, *C*$_1$-*sym*-(dpms)Pt^{IV}Me(OH)$_2$ was formed with ≥ 96 ± 1% selectivity. In addition, a product resulting from Me group transfer, *C*$_1$-*sym*-(dpms)Pt^{IV}Me$_2$(OH)[79], was formed in 1-2% yield (Scheme 2.14, Table 2.2). The latter pathway becomes more pronounced at pH 11.9 and 14.0, where the methyl group transfer product forms in 50 and 70% yield respectively (Scheme 2.14, Table 2.2).

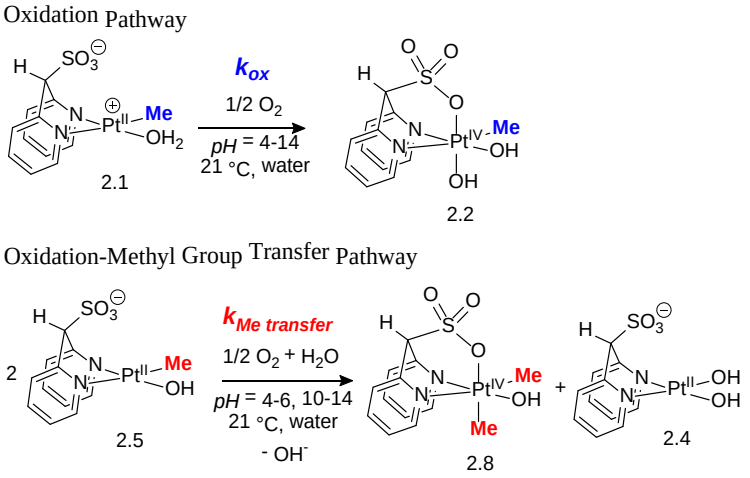

Scheme 2.14 Oxidation pathway, leading to (dpms)Pt^{IV}Me(OH)$_2$, Me group transfer pathway, leading to (dpms)Pt^{IV}Me$_2$(OH).

pH	**2.2** (%)	**2.8** (%)
4.1	96 ± 1	2 ± 1
5.9	97 ± 1	1 ± 1
8.0	99 ± 1	0
10.0	98 ± 1	2 ± 1
11.9	51 ± 2	50 ± 2
14.0	30 ± 1	70 ± 1

Table 2.2 Product distribution in aerobic oxidation of K(dpms)Pt^{II}Me(OH) *vs*. pH.

The mechanism of oxidation of (dpms)Pt^{II}Me(OH$_2$) in a buffer solution at pH 4.1 – 10.0 was studied using the reaction kinetics. Reaction half-lives are shown numerically and graphically in Table 2.3 and Chart 2.1. At pH 4.1, 5.9 and 8.0, the rate of the reaction increases with a shortest half-life at pH 8.0 ($t_{1/2}$ = 3.9 ± 0.2 min). At pH 10.0, reaction rate begins to decrease, $t_{1/2}$ = 13 ± 0.6 min at pH 10.0, and $t_{1/2}$ = 5.6 ± 0.3 h at pH 14.0. This observation can be rationalized in terms of the proposed

mechanism of oxidation. According to Scheme 2.13, pH dependent steps are deprotonation of (dpms)$Pt^{II}Me(OH_2)$ to form anionic $[(dpms)Pt^{II}Me(OH)]^-$, and proton coupled electron transfer to form peroxo-Pt^{IV}, (dpms)Pt^{IV}Me(OH)(OOH). Thus, the increase in the reaction rate in the pH range between 4.1 – 8.0 can be attributed to the increase in the fraction of (dpms)$Pt^{II}Me(OH)^-$. In fact, based on the pK_a = 8.15±0.02 of (dpms)$Pt^{II}Me(OH_2)$, the fraction of (dpms)$Pt^{II}Me(OH)^-$ increases from 0.009% at pH 4.1 to ~0.6% at pH 5.9 to ~40% at pH 8.0. Furthermore, the decrease in the reaction rate at pH ≥ 10.0, is also consistent with the mechanism proposed in Scheme 2.13, where the proton-coupled electron transfer step is inhibited by high $[OH^-]$.

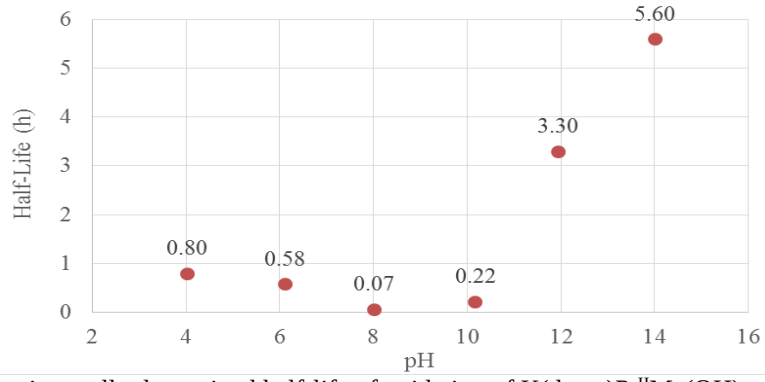

Chart 2.1 Experimentally determined half-life of oxidation of K(dpms)Pt^{II}Me(OH) *vs.* pH, 21.0 ºC, p(O_2) = 1 atm at pH 4.1 – 14.0.

pH	$t_{1/2}$, h	$t_{1/2}$, min	Reaction Order [SM]
4.1	0.80 ± 0.03	48 ± 2	1
5.9	0.58 ± 0.03	34.5 ± 1.5	1
8.0	0.065 ± 0.003	3.9 ± 0.2	1
10.0	0.22 ± 0.01	13 ± 0.6	2
11.9	3.3 ± 0.1	198 ± 6	1-2
14.0	5.6 ± 0.3	336 ± 18	1

Table 2.3 Experimentally determined half-life and reaction order of oxidation of K(dpms)Pt^{II}Me(OH) *vs.* pH, 21.0 ºC, p(O_2) 1 atm.

2.5.1 Reactivity of K(dpms)PtIIMe(OH) at pH 4.1 – 8.0

Since two parallel reactions **Pt^{II}**Me-to-**Pt^{IV}**Me oxidation and Pt^{II}**Me**-to-Pt^{IV}**Me_2** oxidation-methyl group transfer are taking place at pH 4.1, 5.9, the overall first order rate constant can be defined as: $k_{overall} = k_{ox} + k_{Me\ transfer}$. Since the first pathway is predominant at pH 4.1 - 8.0, it is also 1st order in [Pt^{II}], with a pseudo-1st order rate constant k_{ox-1}, Thus, the overall rate constants are:

pH 4.1 and 5.9 $\quad k_{overall} = k_{ox-1} + k_{Me\ transfer}$

pH 8.0 $\quad k_{overall} = k_{ox-1}$

For pH 4.1, 5.9, the rate constant $k_{overall}$ was determined from kinetic plots of $ln([Pt^{II}Me]_0/[Pt^{II}Me])$ *vs.* time, and k_{ox-1} and $k_{Me\ transfer}$ were determined from $k_{overall}$ and the observed product ratio. Reaction rate constants and Gibbs activation energies $\Delta G^{\#}$ for both pathways are summarized in Table 2.4.

At pH 4.1 - 8.0 the value of the pseudo-1st order rate constant k_{ox-1} increases. The increase is 33% between pH 4.1 and 5.9 and 11-fold between pH 4.1 and 8.0. The increase of k_{ox-1} with pH may be related to 1) the greater reactivity of (dpms)Pt^{II}Me$(OH)^-$ toward O_2 compared to (dpms)Pt^{II}Me(OH_2), and 2) the growing

pH	k_{ox-1}, s^{-1}	$\Delta G_{ox-1}^{\#}$	k_{ox-2}, $M^{-1}s^{-1}$	$\Delta G_{ox-2}^{\#}$	$k_{Me\ transfer}$, s^{-1}	$\Delta G_{Me\ transfer}^{\#}$
4.1	$(2.4\pm0.1)\times10^{-4}$	22.1	-	-	$(4.8\pm0.2)\times10^{-6}$	24.3
5.9	$(3.2\pm0.1)\times10^{-4}$	21.9	-	-	$(6.7\pm0.3)\times10^{-6}$	24.1
8.0	$(2.9\pm0.3)\times10^{-3}$	20.6	-	-	-	-
10.0	-	-	0.32±0.03	17.9	$(9.1\pm0.2)\times10^{-6}$	24.0
11.9	-	-	$(7.9\pm0.1)\times10^{-3}$	20.0	$(3.19\pm0.02)\times10^{-5}$	23.2
14.0	-	-	$(1.13\pm0.04)\times10^{-3}$	21.2	$(2.61\pm0.05)\times10^{-5}$	23.4

Table 2.4 First order and second order rate constant and Gibbs activation energies for oxidation of K(dpms)Pt^{II}Me(OH) *vs.* pH.

fraction of the more reactive anionic complex (dpms)Pt^{II}Me$(OH)^-$ in solution. The fraction of **2.5** changes from about 0.009% at pH 4.1 to ~0.6% at pH 5.9 to ~40% at

pH 8.0. Based on this consideration and data in Table 2.4 the reactivity of **2.5** with respect to O_2 is 25 times greater than that of **2.1**; $k_{ox\text{-}1}$(**2.5**) : $k_{ox\text{-}1}$(**2.1**) ~ 25 : 1.

Monitoring the reaction kinetics allows for the determination of the reaction order in the starting [$Pt^{II}Me$] complex. As shown in Table 2.4, reactions at pH 4.1, 5.9 and 8.0 are 1st order in [Pt^{II}]. According to Scheme 2.13, the pseudo first order dependence on [$Pt^{II}Me$] is expected for the steps: ***A*** – deprotonation; ***B*** – O_2 coordination, assuming that [O_2] is constant; and ***C*** – proton coupled electron transfer. Step ***A*** is unlikely to be the rate-limiting under current conditions since proton transfer is usually very fast in aqueous solutions. The interaction of Pt^{II} with O_2 (step ***B***) was studied by Bercaw *et al*. who reported that the rate of oxidation of (phen)$Pt^{II}Me_2$ (Scheme 2.9) was independent of pH. Authors suggested that O_2 coordination was the rate-limiting step.[75] A similar oxidation mechanism was proposed for our system, and since the rate of oxidation of (dpms)$Pt^{II}Me(OH)^-$ is strongly affected by pH, we cannot exclude that step ***B*** is the rate-limiting step in Scheme 2.13. Step ***C*** is a transformation of ^{3}[(dpms)Pt^{III}(Me)(η^1-O_2)(OH)]$^-$ to ^{1}[(dpms)Pt^{IV}Me(OH)(OOH)]. This step is pH dependent and involves triplet to singlet spin interconversion. We propose that at pH 4.1, 5.9 and 8.0, ***C*** is the rate-limiting step (Scheme 2.13).

Reactions of O_2 with (dpms)$Pt^{II}Me(OH)^-$ and (dpms)$Pt^{II}Me(OH_2)$ in water at pH 7 were analyzed computationally by Wei-Guang Liu from Prof. W. A. Goddard III group. The triplet-singlet crossing point **b** (Scheme 2.15) is at 25.4 kcal/mol. Once intermediate **c**, (dpms)Pt^{IV}Me(OH)(OOH), is produced, formation of the final product (dpms)$Pt^{IV}Me(OH)_2$ occurs via transition state **d** or **d′**. The energy of **d** is lower

compared to **d′** due to the presence of the aqua ligand on Pt^{II} metal center. The aqua ligand transfers one of the protons to the O^{-}, which is produced in the O-O bond cleavage step. In the absence of the neighboring proton, the energy of transition state **d′** increases by 1.0 kcal/mol higher.

The pH dependence of the Gibbs energy of the key species in Scheme 2.15 is as follows. For each pH unit the energy of **d′** increases by 1.36 kcal/mol. In its turn, the energy of **d** is increased by 2.72 kcal/mol for each pH unit at pH > 7.

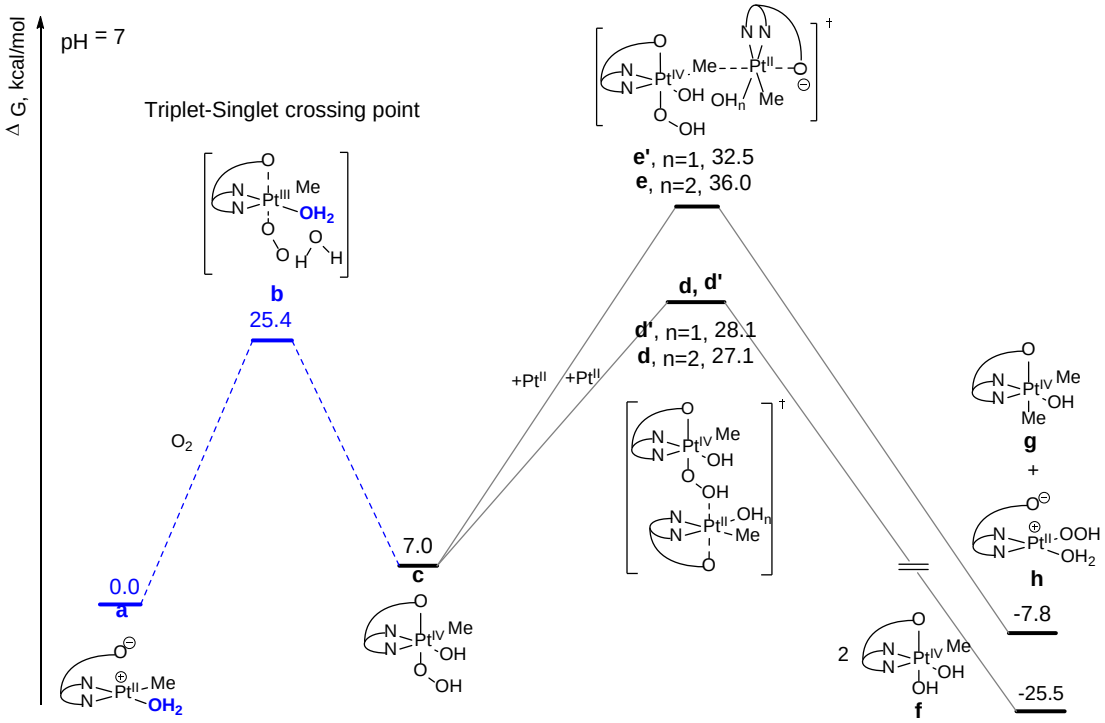

Scheme 2.15 Calculated Gibbs free energy along the potential energy surface of the oxidation of Pt^{II} with O_2 at pH 7 in water.

The energy of the intermediate **c** also increases with pH, consistent with the experimentally found decreasing rate of oxidation at pH > 10.0.

Not consistent with our kinetics experiments is that at pH 7.0 the relative energy of **d** (**d′**) is higher than the energy of **b**. Hence, the DFT predicts that the rate determining step is the O-O bond cleavage **d** (**d′**), and the overall reaction rate is 2nd

order in Pt^{II}. In fact, the reaction becomes 2nd order at a higher pH ≥ 10.0; this will be discussed in the next section. In turn, at pH ≤ 8.0, the overall reaction is 1st order in [Pt^{II}]. Therefore, the energy of **d** is overestimated by ~5 kcal/mol. One possible explanation is the inability of DFT calculations to account for the resonance stabilization between the four lone pairs of two O atoms with the antibonding orbital of the O-O bond being broken.

Also, consistent with experimental observation is a higher energy of transition state **e** and **e′**, which leads to the methyl group transfer product LPt^{IV}**Me**$_2$(OH). As pH increases, the free energy of both **e** and **e′** increases as well. Overall, the reaction mechanism in Scheme 2.15 does not explain high selectivity for LPt^{IV}**Me**$_2$(OH) at high pH.

2.5.2 Oxidation of K(dpms)Pt^{II}Me(OH) at pH 10.0 – 14.0

As pH is increased from 8.0 to 10.0, the overall reaction order changes from 1st to 2nd in [Pt^{II}]. At pH 10.0 (dpms)$Pt^{II}Me(OH)^-$ is the predominant specie (> 99%) in solution. The change in the reaction order from 1st to 2nd without a change in product distribution suggests that the rate-limiting step at pH 10.0 is different from the rate-limiting step at pH 4.1, 5.9 and 8.0. We propose that the RDS is now **d** (Scheme 2.15), which is pH dependent and involves a bimolecular cleavage of the O-O bond (Scheme 2.16). The observed 2nd order rate constant is defined as $k_{ox\text{-}2}$. According to Scheme 2.16, this step is expected to be inhibited at higher pH values, which was observed experimentally.

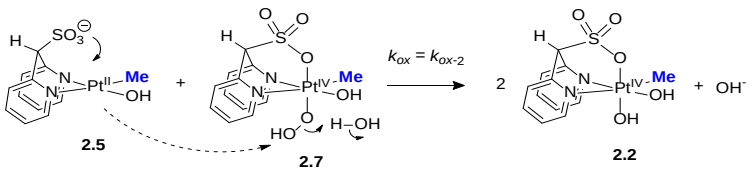

Scheme 2.16 Bimolecular O-O bond cleavage in (dpms)Pt^{IV}Me(OH)(OOH).

At pH 11.9 the competition between oxidation and oxidation-Me-transfer pathway is increased as reflected in the product distribution, LPt^{IV}**Me**$(OH)_2$ and LPt^{IV}**Me**$_2$(OH), formed in 1:1 ratio. The overall reaction order in [Pt^{II}] at pH 11.9 is intermediate between 1st and 2nd due to the oxidation pathway (2nd order) and the Me transfer pathway (1st order) occurring at similar rates.

At pH 14.0 overall oxidation reaction appears to be 1st order in [Pt^{II}] with a pseudo-1st order rate constant $k_{Me\ transfer}$ (Table 2.4). Complex (dpms)Pt^{IV}**Me**$_2$(OH) is a major product (70% yield), and the Me-transfer pathway becomes predominant, however, oxidation of **Pt^{II}**Me-to-**Pt^{IV}**Me still contributes significantly to the overall process. Therefore, the reaction order in [Pt^{II}Me] is also intermediate between 1 and 2 but closer to 1.

For reactions at pH 10.0, 11.9 and 14.0 rate constants $k_{ox\text{-}2}$ and $k_{Me\ transfer}$ were found using a numerical integration and least-square curve fitting of the experimental data, assuming 2nd order in [Pt^{II}] for **Pt^{II}**Me-to-**Pt^{IV}**Me oxidation and 1st order for the Me transfer reaction (Table 2.4). The dramatic change in half-lives (Table 2.3) and product distribution (Table 2.2) at high pH indicates that the reaction direction leading to Pt-to-Pt methyl group transfer operates via an alternate mechanism than the one shown in Scheme 2.13.

Previously Puddephatt *et al*. reported methyl ligand transfer reactions between electron rich tetramethyl Pt^{IV} complexes and electrophilic Pt^{IV} (Scheme 2.17) The

authors proposed that reactions proceed by initial dissociation of the triflate ligand of *fac*-[(N-N)$Pt^{IV}Me_3(SO_3CF_3)$] to form cationic five-coordinate intermediate [(N-N)$Pt^{IV}Me_3]^+$. This intermediate undergoes attack by one of the nucleophilic methylplatinum ligands of (***N-N***)$Pt^{IV}Me_4$ to give (N-N)$Pt^{IV}Me_4$ and (***N-N***)$Pt^{IV}Me_3(SO_3CF_3)$. Methyl group tranfer reactivity was attributed to the presence of a good leaving group (SO_3CF_3) of (***N-N***)$Pt^{IV}Me_3(SO_3CF_3)$ and highly nucleophilic (N-N)$Pt^{IV}Me_4$.[81]

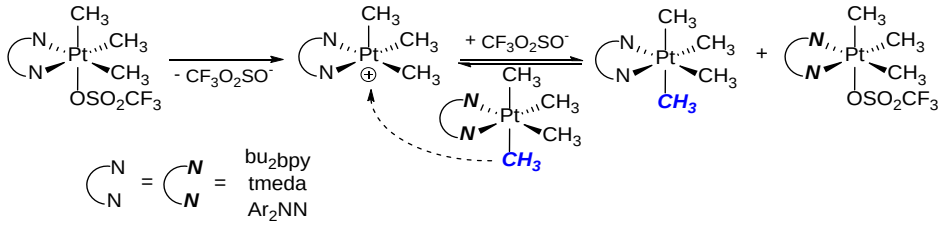

Scheme 2.17 Proposed mechanism of Pt^{IV}-to-Pt^{IV} methyl group transfer.

A disproportionation of C_1-symmetric (dpms)Pt^{IV}**Me**$(OH)_2$ to give C_1-symmetric LPt^{IV}**Me**$_2$(OH) and $LPt^{IV}(OH)_3$ seems to be unlikely under our reaction conditions

In another report Me-transfer occurred via transfer of nucleophilic Me ligand of *cis*-[$Pt^{II}Me_2(PMe_2Ph)_2$] to the electrophilic *cis,cis,trans*-[$Pt^{IV}Me_2(NO_2)_2(PMe_2Ph)_2$)] complex.[82] Alkyl halide transfer has also been demonstrated in mixed metal systems: Pt^{II}-to-Pd^{IV} (Scheme 2.18).[83]

$Pt^{IV}Me_2(NO_2)_2(PMe_2Ph)_2$ + *cis*-$Pt^{II}Me_2(PMe_2Ph)_2$ ⟶ *fac*-$Pt^{IV}Me_3(NO_2)(PMe_2Ph)_2$ + *trans*-$Pt^{II}Me(NO_2)(PMe_2Ph)_2$

Scheme 2.18 Pt^{IV}-to-Pt^{II} methyl group transfer.

More recently, methyl transfer product was observed as a minor product in the oxidative addition of EtI to [(bpy)$Pt^{II}Me_2$]. A likely mechanism is intermolecular Me

transfer between $[(bpy)Pt^{IV}Me_2Et]^+$ and $[(bpy)Pt^{II}Me_2]$.[84] A plausible mechanism of Pt-to-Pt methyl group transfer in our system is discussed below.

2.6 Model Studies of Pt^{IV}-to-Pt^{II} Me Group Transfer via Isomerization of Pt^{IV}

2.6.1 From C_1-symmetric $(dpms)Pt^{IV}(CH_3)(OH)_2$ to $K(dpms)Pt^{II}(CH_3)OH$)

In order to assess the feasibility of Pt^{IV}-to-Pt^{II} Me group transfer in our system, a reaction between C_1-symmetric $(dpms)Pt^{IV}\mathbf{Me}(OH)_2$ and $(dpms)Pt^{II}Me(OH)^-$ was performed at pH 14. Formation of the methyl transfer product **2.8** was observed in 72% yield at 22 days of reaction time (Scheme 2.19, **A**). The reaction showed 1st order dependence in $[Pt^{IV}]$ and the first-order rate constant $k_{2.5\text{-}2.2} = (7.6 \pm 0.1)\times10^{-7}$ s^{-1} was determined. Comparison of $k_{2.5\text{-}2.2}$ with the reaction rate constant $k_{Me\ transfer}$ at pH 14 (Scheme 2.14, Table 2.4) shows that the model reaction **A**

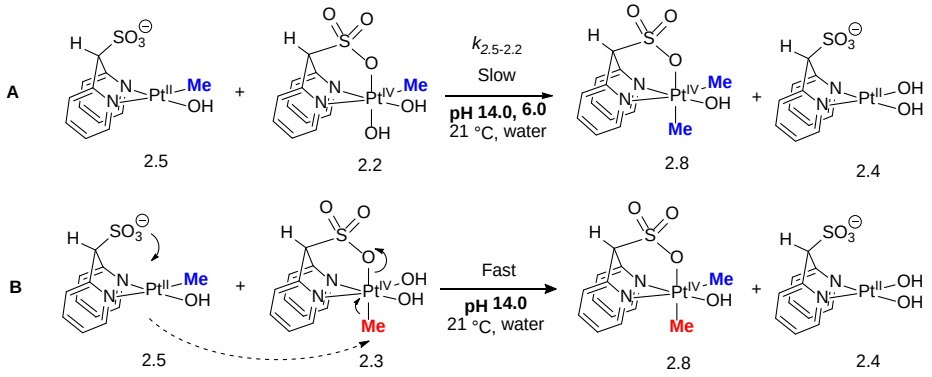

Scheme 2.19 Pt^{IV}-to-Pt^{II} methyl group transfer under argon at pH 14.0. A: C_1-symmetric $(dpms)Pt^{IV}Me(OH)_2$. B: C_s-symmetric $(dpms)Pt^{IV}Me(OH)_2$.

in Scheme 2.19 is 34 times slower. However, when C_s-symmetric complex **2.3**, an isomer of **2.2**, was reacted with $(dpms)Pt^{II}Me(OH)^-$, quantitative and rapid (<5 min) formation of the **2.8** was observed (Scheme 2.19, **B**). Enhanced reactivity of **2.3** can be attributed to the fact that the sulfonate ligand (SO_3) is a much better leaving group compared to the pyridine ligand, therefore, formation five-coordinate Pt^{IV}, required

for methyl group transfer[81,85], occurs more readily in case of isomer **2.3** compared to isomer **2.2**.

The possibility of C_1-symmetric (dpms)Pt^{IV}**Me$_2$**(OH) being formed via Pt^{IV}-to-Pt^{II} Me group transfer at pH 6.0 (Scheme 2.19, **A**) was also explored. Noticeable protonolysis of (dpms)Pt^{II}Me(OH_2) was observed already after one day of reaction time, therefore, kinetic measurements could not be performed. Nonetheless, at 22 days formation of (dpms)Pt^{IV}**Me$_2$**(OH) was observed in 70 ± 1% yield, the remaining 30% mass balance balance is presumed to be due to the formation of methane. After 21 h of reaction time, (dpms)Pt^{IV}**Me$_2$**(OH) was formed in ~1%, whereas the same amount was generated in approximately one hour in reaction with O_2. Overall, direct Me transfer from C_1-symmetric (dpms)Pt^{IV}**Me**$(OH)_2$ to (dpms)Pt^{II}Me is unlikely under pH 6.0 and 14.0.

Previosuly complex **2.3** was shown to produce MeOH under basic and acidic conditions, at room temperature.[79] Interstingly, in reactions **A** and **B** in Scheme 2.19 methanol was not observed. This suggests that complex **2.5** is several orders of magnitude more nucleophilic than OH^-.

Considering very slow reaction **A** (Scheme 2.19), and very fast Me group transfer in reaction **B** (Scheme 2.19), the first step in reaction **A** might be rate limiting isomerization of **2.2** into **2.3** (Scheme 2.20). This assumption is consistent with the experimentally observed first order dependence in [Pt^{IV}], and indicates that the rate constant $k_{2.5\text{-}2.2} = (7.6 \pm 0.1)\times10^{-7}$ s^{-1} may be effectively the rate of isomerization of **2.2** into **2.3**: $k_{2.5\text{-}2.2} = k_{\text{isom (pH 14)}}$ (Scheme 2.20).

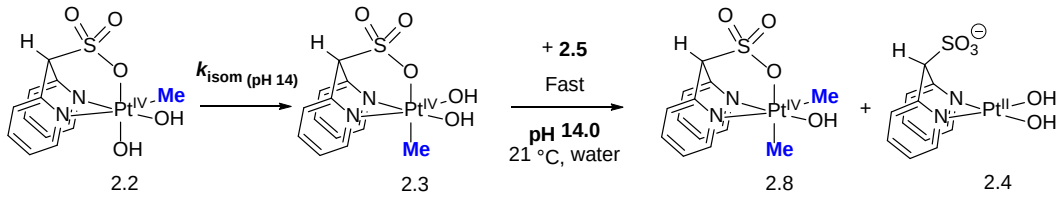

Scheme 2.20 Proposed pathway for formation of (dpms)$Pt^{IV}Me_2(OH)$ via isomerization of C_1-symmetric (dpms)$Pt^{IV}Me(OH)_2$.

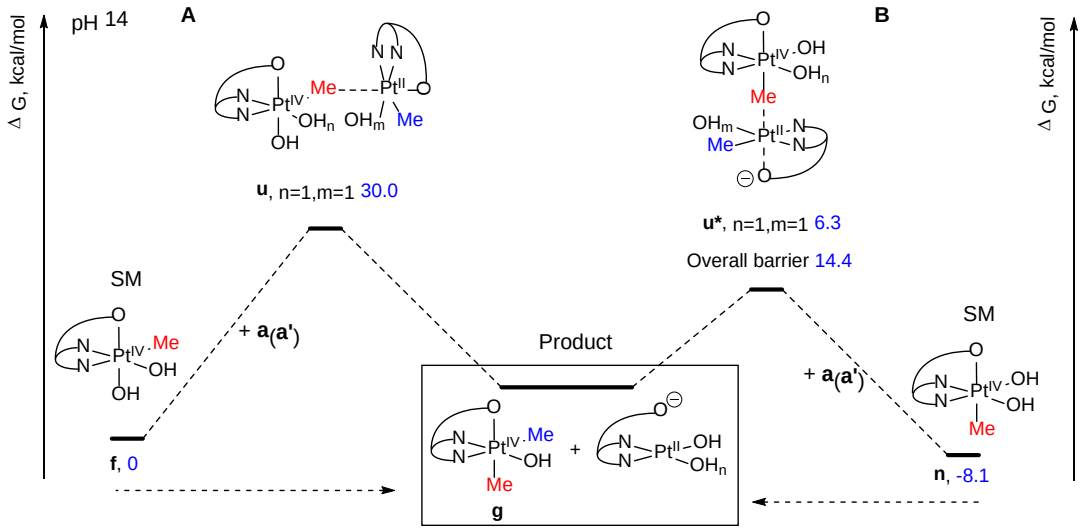

Scheme 2.21 Calculated Gibbs free energies for Pt^{IV}-to-Pt^{II} methyl group transfer at pH 14. A: from C_1-symmetric (dpms)$Pt^{IV}Me(OH)_2$. B: from C_s-symmetric (dpms)$Pt^{IV}Me(OH)_2$.

In order to provide insight into a faster methyl group transfer between **2.3** and **2.5** compared to **2.2** and **2.5** DFT calculations were employed to determine the reaction barriers for two possible pathways (Scheme 2.21, **A** and **B**). At pH 14.0, the barrier to form **g** (**2.8**) from **n** (**2.3**) is 14.4 kcal/mol, much lower than from **f** (**2.2**). The same trend persists over pH 0.0 and 7.0.

The results of a model reaction in Scheme 2.19 **A** show that formation of **2.8** via methyl group transfer from Pt^{IV} to Pt^{II} is thermodynamically accessible but is not kinetically competitive with the process that occurs under oxidation with O_2. Based on the reaction in Scheme 2.19 **B** and Scheme 2.21, **B** complex **2.3** should be produced in the aerobic oxidation reaction prior to the formation of **2.8**.

2.6.2 From (dpms)$Pt^{IV}(CH_3)_2(OH)$ to K(dpms)$Pt^{II}(CD_3)(OH)$

Scheme 2.19 **B** and Scheme 2.21 **B** show that methyl transfer from C_s-symmetric (dpms)Pt^{IV}**Me**$(OH)_2$ is very facile. It cannot be excluded that the axial methyl group in (dpms)Pt^{IV}**Me**$_2$(OH) complex could also undergo migration. Whether

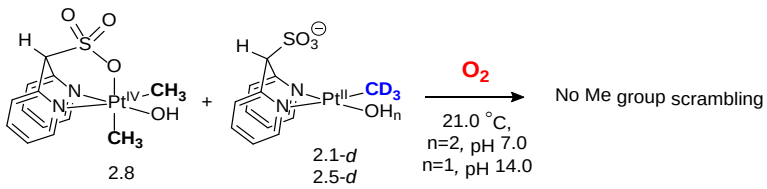

Scheme 2.22 Competition experiment between Pt-to-Pt methyl group transfer and oxidation with O_2.

complex **2.8** is able to participate in the methyl group transfer reactivity on the time scale of the oxidation with O_2, was assessed in the reaction between C_1-symmetric (dpms)Pt^{IV}**(CH$_3$)$_2$**(OH) and (dpms)Pt^{II}(**CD$_3$**)$(OH)^-$ at pH 7.0 and 14.0 under aerobic conditions (Scheme 2.22). In that case, formation of mixed labeled (dpms)Pt^{IV}**(CD$_3$)$_{eq}$**(OH)$(CH_3)_{ax}$ would be expected. When oxidation of (dpms)Pt^{II}(**CD$_3$**)$(OH)^-$ was performed in the presence of C_1-symmetric (dpms)Pt^{IV}**(CH$_3$)$_2$**(OH) at pH 7.0 and 14.0 products of Me scrambling were not observed (Scheme 2.22). However, when an equimolar mixture of **2.8** and **2.5-*d*** was kept under an argon atmosphere complex (dpms)Pt^{IV}**(CD$_3$)$_{eq}$**(OH)(**CH$_3$**)$_{ax}$ was produced in 25% yield after 10 days at pH 14.0.

2.6.3 Mechanism of Isomerization of (dpms)$Pt^{IV}Me(OH)_2$ at pH 14.0

In Section 2.6.1 isomerization of **2.2** to **2.3** at pH 14.0 was proposed to be the first step in reaction **A** Scheme 2.19. Here the mechanism of isomerization of **2.2** to **2.3** was studied in more detail. Theoretical calculations propose the mechanism shown in Scheme 2.23 where coordination of the aqua ligand occurs in a RDS with a

barrier of 28.9 kcal/mol. This leads to intermediate **w**, where sulfonate is no longer coordinated to the Pt^{IV} metal center (7.0 kcal/mol), and then to intermediate **x** (11.6 kcal/mol). In **x** OH is a stronger *trans* effect ligand than H_2O. As a result, H_2O dissociates producing a 5-coordinate intermediate **y**. Isomerization of **y** is accompanied by recoordination of SO_3 giving isomer (dpms)Pt^{IV}**Me**$_{(ax)}(OH)_2$. An alternative mechanism was also considered where OH ligand trans to the SO_3 group dissociates from (dpms)Pt^{IV}**Me**$_{(eq)}(OH)_2$. This pathway has a 44.9 kcal/mol barrier (not shown), which is not viable.

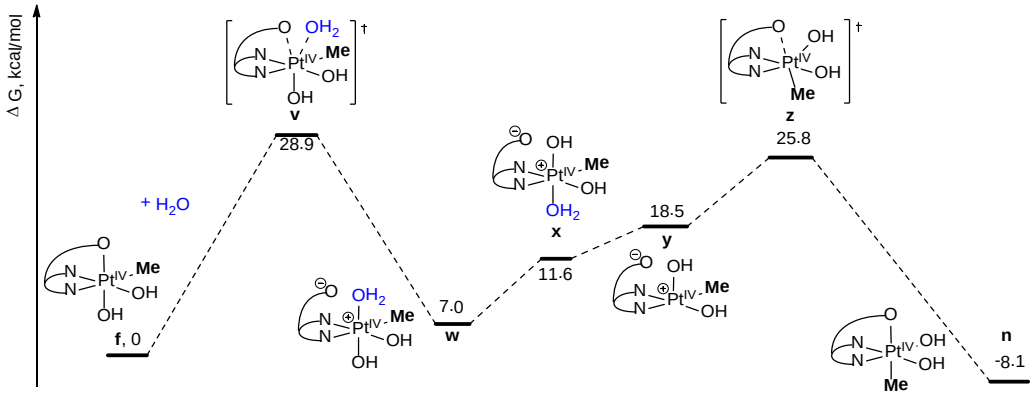

Scheme 2.23 Calculated Gibbs free energy for the isomerization of Pt^{IV} monomethyl complex.

Experimental evidence for the proposed mechanism is discussed below. When complex **2.2** was monitored by ^{1}H NMR spectroscopy at 31.0 ºC under an argon atmosphere at pH 14.0 slow disappearance of **2.2** was observed (Scheme 2.24). It was expected that isomerization of **2.2** to **2.3** under these reaction conditions would lead to quantitative formation of MeOH, as was shown previously[79]. However, analysis of the product distribution at 86% conversion of **2.2** after 19 days showed that MeOH was formed in only 23% yield. Other methyl-containing products included *C*$_1$-symmetric (dpms)Pt^{IV}**Me**$_2$(OH) (42 ± 1%) and a new specie **2.10** which is proposed to be *C*$_1$-symmetric (dpms)Pt^{IV}**Me**$(OH)_3^-$ **2.10** (14 ± 1%) (Scheme 2.24). The reaction

showed 1st-order dependence in [**2.2**] and the 1st order rate constant $k_{(2.2)}$ = (1.21 ± 0.06) × 10^{-6} s^{-1} was determined.

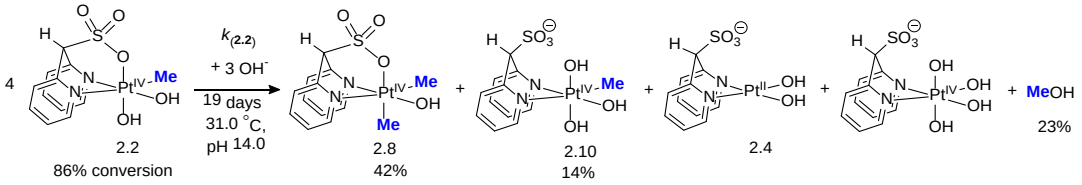

Scheme 2.24 Reactivity C_1-symmetric (dpms)$Pt^{IV}Me(OH)_2$ under argon at pH 14.0.

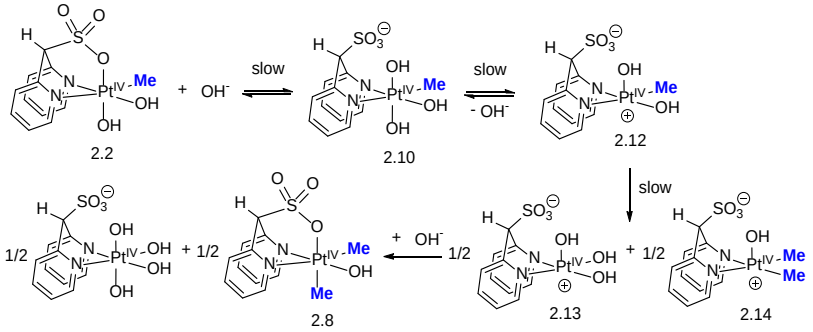

Scheme 2.25 Proposed mechanism for reactivity of 2.2 under argon at pH 14.0.

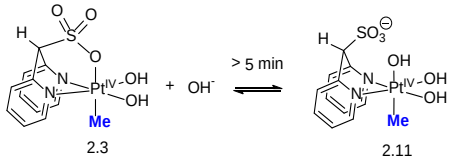

Scheme 2.26 Reactivity C_s-symmetric (dpms)$Pt^{IV}Me(OH)_2$ under argon at pH 14.0.

Presence of complex **2.10** supports the mechanism proposed by DFT calculations, however, presence of **2.8** indicates that Pt-to-Pt methyl group transfer is taking place. In the absence of Pt^{II}, **2.8** could form via methyl ligand disproportionation according to mechanism in Scheme 2.25. More work is needed to elucidate the reaction mechanism. Interestingly, complex **2.11** formed quantitatively in reaction between **2.3** and OH^- in the aqueous solution at pH 14.0 (Scheme 2.26).

2.7 Computational Studies of Pt^{IV}-to-Pt^{II} Methyl Group Transfer via Isomerization of Pt^{II}

The process which can account for the formation of C_1-symmetric (dpms)Pt^{IV}**Me**$_2$(OH) from LPt^{II}Me(OH_2) under aerobic conditions is shown in Scheme 2.19 **B**. In this reaction the Me group is transferred from the axial position in C_s-symmetric LPt^{IV}**Me**$(OH)_2$. Hence, we propose that the monomethyl Pt^{IV} complex **2.3** also forms along with its isomer **2.2** but, in contrast to **2.2**, **2.3** is trapped rapidly with the second mole of Pt^{II}Me. For the dimethyl Pt^{IV} complex to form as a minor product in the pH range of 4.1 – 10.0 the rate of the formation of **2.3** should be slow compared to **2.2.** At pH $\geq$ 11.9, however, **2.3** should form at a comparable rate. Formation of C_1-symmetric LPt^{IV}**Me**$_{(ax)}(OH)_2$ **2.3** via isomerization of **2.2** is too slow under both acidic and basic conditions. Direct pathways from (dpms)Pt^{II}Me$(OH)^-$ to C_1-symmetric LPt^{IV}**Me**$(OH)_2$ at pH 14.0 were considered using DFT calculations.

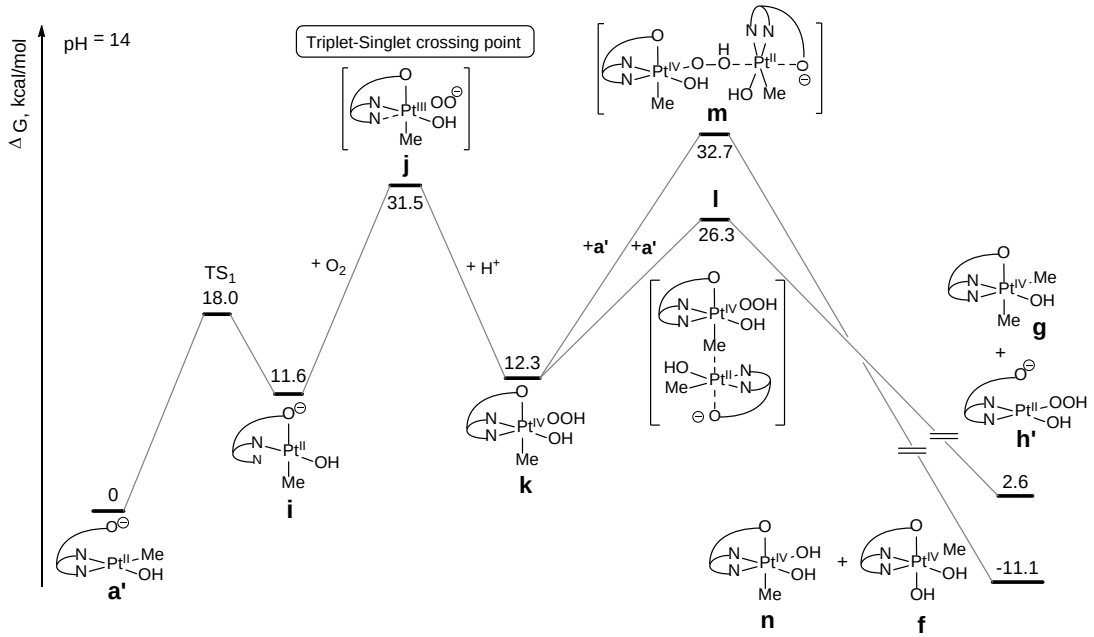

Scheme 2.27 Calculated Gibbs free energy along the potential energy surface for the proposed mechanism of the Pt^{IV}-to-Pt^{II} methyl transfer at pH 14 in water.

The most likely pathway involves isomerization of ($\kappa N,\kappa N$-dpms)$Pt^{II}Me(OH)^-$ to ($\kappa N,\kappa O$-dpms)$Pt^{II}Me(OH)^-$ (complex **i** in Scheme 2.27) prior to its reaction with O_2. Formation of **i** has a free energy barrier of 18.0 kcal/mol. Intramolecular isomerization of Pt complexes with the activation energy of 13.6 kcal/mol have been reported previously.[86,87] This step is followed by activation of O_2 via the triplet-singlet crossing point **j** to produce **k**. Methyl transfer from **k** occurs via transition state **l** and results in the formation of the target complex **n** along with hydroperoxo Pt^{II} complex **h′**. Complex **h′** can oxidize second equivalent of (dpms)$Pt^{II}Me(OH)^-$ with a 20.1 kcal/mol barrier at pH 14. The RDS in this pathway corresponds to the triplet-singlet crossing point **j** (31.5 kcal/mol) whose energy is pH - independent. According to the relative barriers of methyl transfer **l** (26.3 kcal/mol) and the O-O bond cleavage **m** (32.7 kcal/mol), Me transfer is more favorable. This is consistent with experimental observations at pH 14.0.

2.8 Methyl Transfer and Isomerization Paths via Pt^{III}

Dioxygen can act as one or two electron oxidant[66], therefore involvement of one electron oxidation pathway should be considered. Recently mononuclear Pt^{III} complexes have been isolated and fully characterized.[88]

One of the reactions where Pt-to-Pt alkyl group transfer was proposed to involve Pt^{III} intermediates is oxidative addition of PrI or EtI to (bpy)$Pt^{II}Me_2$ in acetone and benzene.[84] In another example Me group transfer occurred in reaction between diimine-$Pt^{II}Me_2$ and Cp_2Fe^+ and produced a ~1:1 mixture of cationic (N-N)$Pt^{II}Me(MeCN)^+$ and (N-N)$Pt^{IV}Me_3(MeCN)^+$ (Scheme 2.28). The reaction was proposed to occur via one electron oxidation leading to a short-lived cation-radical

(N-N)$Pt^{III}Me_2^+$ which was stabilized by a solvent molecule to form a 17 ē pentacoordinate specie, followed by intermolecular methyl transfer. The involvement of a homolytic cleavage of Pt^{II}-Me bond to form methane or reductive elimination pathway to form ethane was ruled out due to only trace amounts of methane or ethane at the end of the reaction.[89]

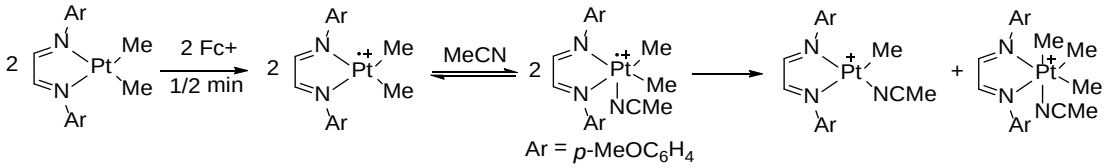

Scheme 2.28 Proposed mechanism of methyl group transfer via Pt^{III} intermediates.

2.8.1 Pt^{III}-to-Pt^{II} Methyl Group Transfer

One can considere one-electron oxidation of (dpms)Pt^{II}Me(OH)$^-$ by O_2 as a means of generating (dpms)Pt^{IV}**Me$_2$**(OH). In this scenario (dpms)Pt^{III}Me(OH) intermediate can transfer its methyl group as a methyl radical to another (dpms)Pt^{II}Me(OH)$^-$. The resulting (dpms)$Pt^{III}Me_2$(OH)$^-$ would undergo an one-electron oxidation to form C_1-symmetric (dpms)Pt^{IV}**Me$_2$**(OH).

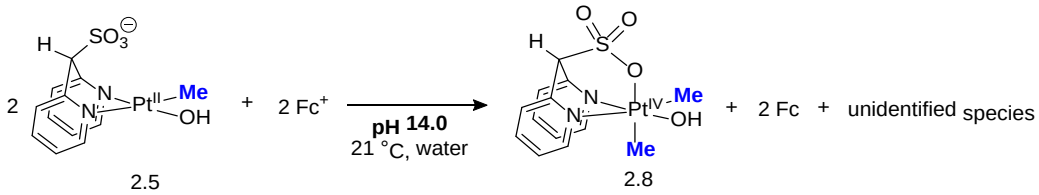

Scheme 2.29 One electron oxidation of K(dpms)Pt^{II}Me(OH) with Cp_2Fe^+.

When (dpms)Pt^{II}Me(OH)$^-$ was combined with a solution of Cp_2Fe^+ in water or methanol, formation of C_1-symmetric (dpms)Pt^{IV}**Me$_2$**(OH) occurred (Scheme 2.29). However, the product was generated in only 23% yield along with unidentified species. Increasing the amount of the oxidant did not affect the product yield. This result suggests that the involvement of Pt^{III} intermediates in oxidation – methyl group

transfer pathway in Scheme 2.14 cannot be excluded though it was not confirmed in aerobic oxidation of (dpms)$Pt^{II}Me(OH)^-$.

2.8.2 Pt^{IV}-to-Pt^{III} Methyl Group Transfer

The pathway in Scheme 2.30 explores computationally a Pt^{IV}-to-Pt^{III} methyl transfer. Formation of **a*'** from **a'** requires 23.3 kcal/mol based on the experimentally found one-electron reduction potential of O_2 (-325 mV *vs.* SHE)[90] though the activation barrier for this reaction remains unknown. Isomerization of **a*'** to form **i*** has a 35.0 kcal/mol barrier (TS_2). Formation of **i*** is followed by methyl radical transfer from Pt^{IV} to **a*'** or **i***. Reaction produces dihydroxo Pt^{III} and C_1-symmetric (dpms)Pt^{IV}**Me2**(OH). Transition states **o** and **p** have free energy 41.7 and 39.1

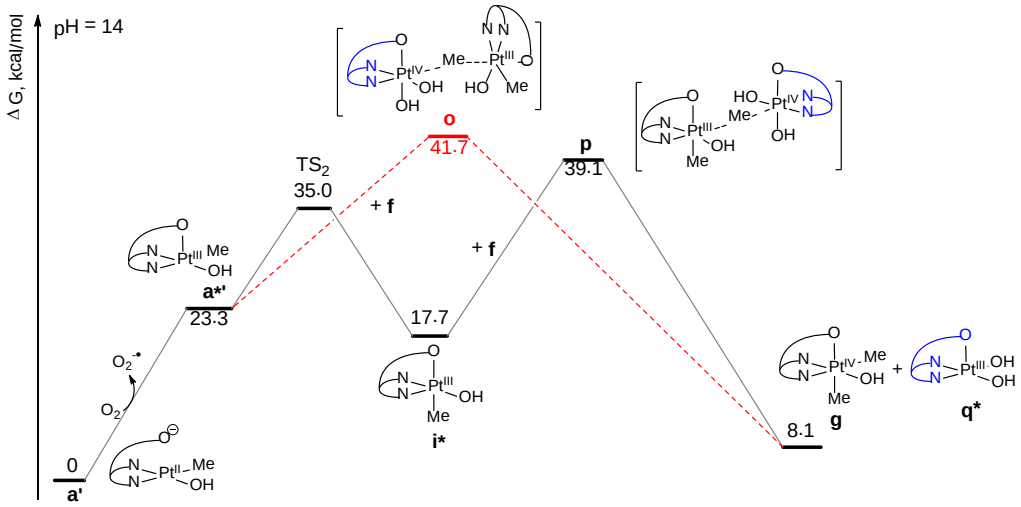

Scheme 2.30 Calculated Gibbs free energy along the potential energy surface for the proposed mechanism of the Pt^{IV}-to-Pt^{III} methyl transfer at pH 14 in water.

kcal/mol respectively (Scheme 2.30), which is considerably higher than pathways in Scheme 2.27. Hence, mechanisms in Scheme 2.30 are not likely to be involved in aerobic oxidation of ((dpms)$Pt^{II}Me(OH)^-$ and formation of C_1-symmetric (dpms)Pt^{IV}**Me2**(OH). A homolytic Pt^{III}-to-Pt^{II} methyl transfer mechanism was the next mechanistic possibility considered for the involvement of Pt^{III} intermediates.

2.8.3 Homolytic Cleavage of Pt^{III}-Me Bond

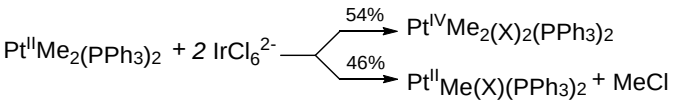

Scheme 2.31 One and two electron oxidation of Pt^{II} by the one-electron oxidant hexachloroiridate(IV).

Homolytic cleavage of Pt^{III}-Me bond has been proposed in the reaction of *cis*-$(Ph_3P)_2Pt^{II}Me_2$ complexes with $IrCl_6^{2-}$. Methyl radical was trapped as MeCl in ~40% yield. A competitive two-electron oxidation occurs concurrently, and leads to $(Ph_3P)_2Pt^{IV}Me_2Cl_2$ (Scheme 2.31).[91]

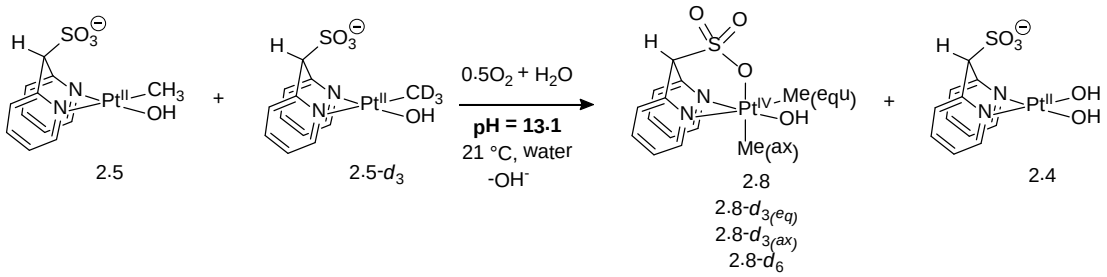

Scheme 2.32 Measurement of the secondary kinetic isotope effect in oxidation of Pt^{II} with O_2 at pH 14.0.

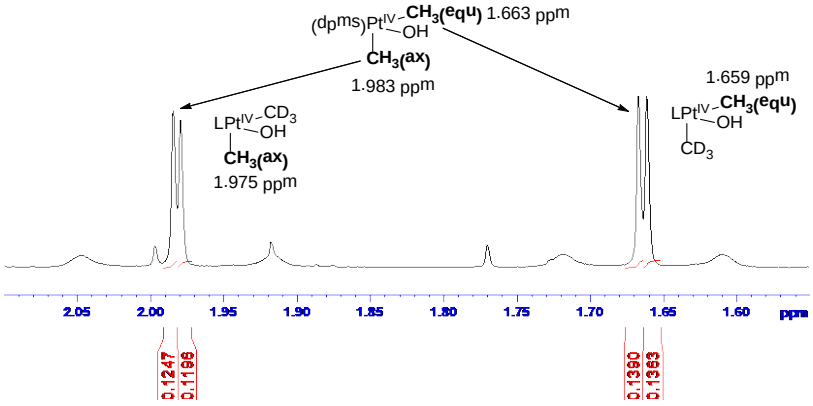

Figure 2.1 Upfield region of ^1H NMR spectrum after oxidation of 1:1 mixture of (dpms)$Pt^{II}CH_3(OH)^-$ and (dpms)$Pt^{II}\boldsymbol{CD_3}(OH)^-$.

To test the likelihood of a homolytic methyl transfer mechanism, we carried out oxidation of an equimolar mixture of (dpms)$Pt^{II}CH_3(OH)^-$ and (dpms)$Pt^{II}\boldsymbol{CD_3}(OH)^-$ (Scheme 2.32). This reaction was performed under identical conditions as in the kinetics studies. Analysis of the product distribution at 100%

conversion by ^{1}H NMR spectroscopy shows formation of four isotopologues of *C*$_1$-symmetric (dpms)Pt^{IV}**Me$_2$**(OH) complex (Scheme 2.32, Figure 2.1). Assignment of the chemical shifts to three out of four Pt^{IV} complexes was confirmed by their independent synthesis. The content of (dpms)Pt^{IV}**(CD$_3$)$_2$**(OH) was estimated by subtraction of integration values of the methyl groups from the aromatic region.

A homolytic mechanism of Me group transfer would be characterized by a noticeable secondary deuterium kinetic isotope effect (SKIE) of 1.1-1.2.[84,92,93,94] If a homolytic cleavage of Pt-Me bond is the rate determining step, the ratio of LPt^{IV}(CH$_3$)(OH)(CH$_3$)/ LPt^{IV}(CH$_3$)(OH)(CD$_3$) should be ≠ 1. However, the observed SKIE = 0.98±0.02, which is close to unity within experimental error. This result suggests that a homolytic methyl radical transfer does not contribute substantially to the oxidation - methyl transfer reaction in Scheme 2.14.

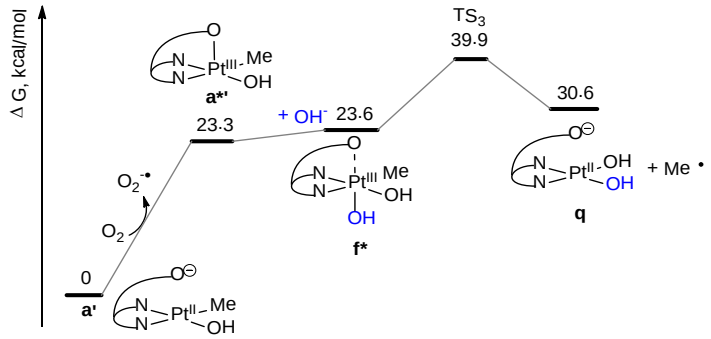

Scheme 2.33 Calculated Gibbs free energy along the potential energy surface for the proposed mechanism of the homolytic cleavage of Pt^{III}–C bond.

Finally, a pathway involving formation of free Me radicals from Pt^{III} has been investigated by DFT calculations (Scheme 2.33). Formation of **a*′** with an unknown activation energy is followed by coordination of OH- to form intermediate **f***; this process is slightly uphill. Homolytic cleavage of Pt^{III}-Me bond, however, has a free

energy barrier of 39.9 kcal/mol, rendering this process inaccessible at room temperature.

Oxygen can serve as a good radical trap for free methyl radicals.[95,96] The absence of MeOH and MeOO-containing products, further supports the conclusion that free radicals are not involved in oxidation - methyl transfer reaction.

2.9 Summary and Conclusions

In the original Shilov system, protonolysis of $Pt^{II}CH_3$ is in competition with oxidation of $Pt^{II}CH_3$ to $Pt^{IV}CH_3$. This system is successful in part due to oxidation being 20 times faster than protonolysis. Therefore, optimization of the oxidation conditions is essential for the advancement of the new methane to methanol system. In this chapter we have shown that the rate and selectivity of oxidation of (dpms)Pt^{II} monomethyl complexes by O_2 can be modulated by simply changing pH of the buffer solution. More importantly, faster rates of oxidation of (dpms)$Pt^{II}Me(OH_2)$ complexes have been achieved ($t_{1/2}$ = 3.9 min, pH 8.0), compared to the previously reported unbuffered system ($t_{1/2}$ = 15 min)[79].

Oxidation – methyl group transfer pathway has been observed at pH $\geq$ 12, where significant formation of Me group transfer product occurred. This new reaction is a useful model in achieving oxidative coupling of methane to ethane.[97] The reaction mechanism has been studied in great detail using kinetics measurements, model studies and theoretical calculations. The proposed reaction mechanism is given in Scheme 2.34.

The experimentally observed 1st order in [Pt^{II}] at pH 4.1 – 8.0 suggests that the rate-limiting step of the oxidation is dioxygen activation to form Pt^{IV}(OOH) species

2.7. The Pt-to-Pt methyl transfer is a minor reaction under these conditions. The *C*$_1$-symmetric (dpms)Pt^{IV}Me(OH)$_2$ is a very poor alkylating agent; the isomerization of **2.5**/dioxygen activation sequence leading to the peroxo-species **2.16** (Scheme 2.34) or its hydroxo-analog **2.3** (Scheme 2.19 **B**) is presumed to be responsible for the formation of *C*$_1$-symmetric (dpms)Pt^{IV}**Me**$_2$(OH).

The redox potentials of peroxo compounds depend on pH: higher pH values correspond to lower potentials. Hence, O-O bond cleavage step **2.7** + **2.1** (or **2.5**) → **2.2** becomes rate limiting at pH ≥ 10, as reflected in the 2nd order dependence in (dpms)Pt^{II}Me(OH)$^-$.

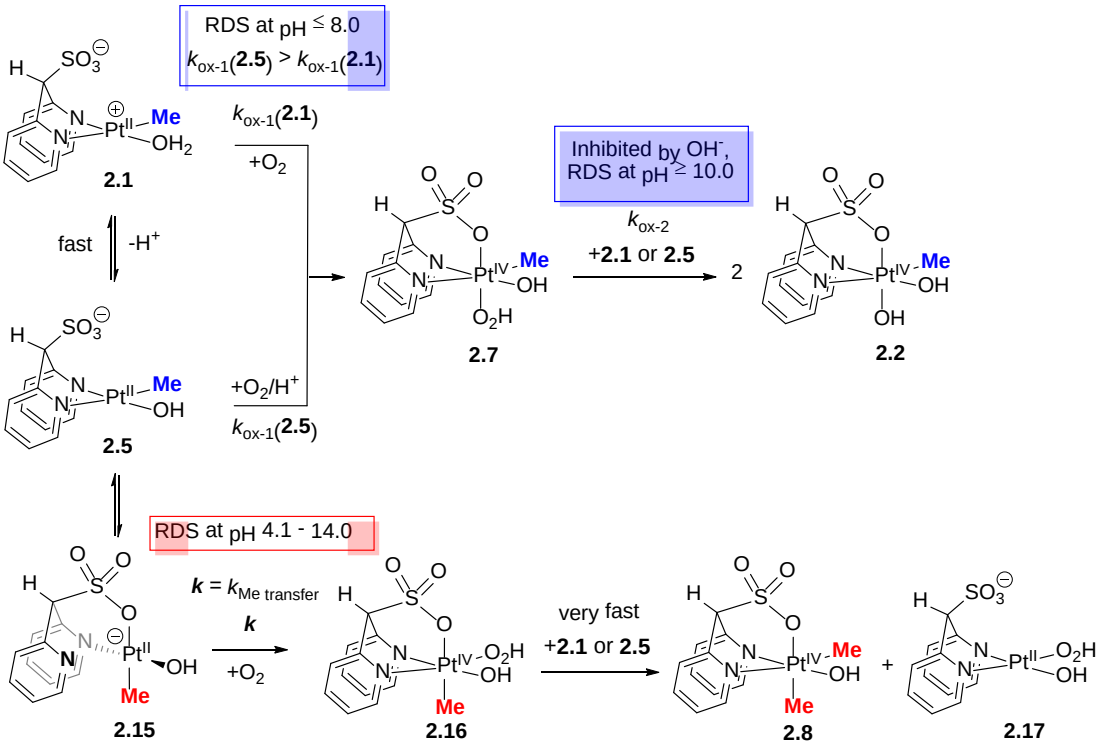

Scheme 2.34 Proposed mechanism of oxidation of K(dpms)Pt^{II}Me(OH) to form *C*$_1$-symmetric-(dpms)Pt^{IV}Me(OH)$_2$, and Pt-to-Pt methyl transfer to form (dpms)Pt^{IV}Me$_2$(OH).

The formation of the proposed Pt^{IV} peroxo-species **2.16** (Scheme 2.34) becomes competitive with the oxidation reaction at pH ≥ 11.9. According to DFT calculations, reaction of O$_2$ with **2.15** (Scheme 2.34 and 2.27) is a rate-limiting step.

Finally, at a relatively low pH the peroxo-species **2.16** may be equally likely to be involved in OH and Me group transfer, whereas at a relatively high solution pH the methyl transfer from **2.16** will be much faster than the OH group transfer, leading to possible accumulation of peroxo-species such as **2.17**.

In conclusion, using experiment and theory we were able to propose a mechanism of oxidation – methyl group transfer pathway. This new reaction direction leading from monomethyl-Pt(II) to dimethyl-Pt(IV) is an important transformation because it might uncover the new avenue for oxidative homocoupling of methane to ethane.

2.10 Experimental Section

Preparation of K(dpms)Pt^{II}Me(OH/OD) (Me = CH_3, CD_3)

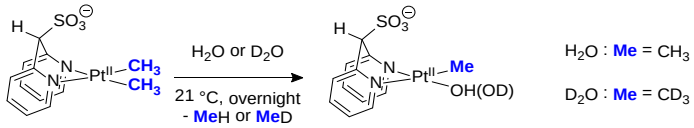

A stock solution of K(dpms)Pt^{II}Me(OH), Me = CH_3[79] or CD_3[98] was prepared under argon atmosphere via hydrolysis of K(dpms)Pt$^{II}(CH_3)_2$[99]. A sample of K(dpms)Pt$^{II}(CH_3)_2$ (10.6 mg, 20.6 µmol) was dissolved in 1.00 mL of degassed H_2O or D_2O, and was left to stir overnight in the glove box at ambient temperature. K(dpms)Pt^{II}Me(OH) (Me = CH_3 when solvent was H_2O, Me = CD_3 when solvent was D_2O) was formed in quantitative yield and was used as an aqueous solution without further purification.

K(dpms)Pt^{II}CD$_3$(OD), 2.5-*d*$_3$ ^{1}H NMR (400 MHz, D_2O) δ: 8.84 (d, ^3J = 5.9 Hz, 1H), 8.79 (d, ^3J = 5.9 Hz, 2H), 8.05 (dt, J = 1.5, 7.9 Hz, 1H), 8.01 (dt, J = 1.5, 7.9 Hz, 1H), 7.80 (d, ^3J = 7.9 Hz, 1H), 7.68 (d, ^3J = 7.9 Hz, 1H), 7.55 (ddd, J = 1.5, 5.9, 7.9 Hz,

1H), 7.27 (ddd, J = 1.5, 5.9, 7.9 Hz, 1H), C*H*-SO_3 peak is not observed due to the H/D exchange, 0.85 (br., residual signal Pt-CH_2D), 0.79 (br., residual signal Pt-CHD$_2$).

Independent Synthesis of *unsym*-(dpms)Pt^{IV}(CH$_3$)(OH)(*axial*-CD$_3$) 2.8-*d*$_{3(ax)}$

Under an argon atmosphere a solution of K(dpms)Pt^{II}CH$_3$(OH) (4.8 µmol) in D_2O was combined with CD_3I (0.30 µL, 4.8 µmol). The mixture was stirred at room temperature for 5 minutes.

^{1}H NMR (400 MHz, D_2O) δ: 8.69 (d, ^3J = 5.8 Hz, 1H), 8.54 (vd, ^3J = 6.4 Hz, $^3J_{Pt-H}$ = 40 Hz, 1H), 8.22 (vt, ^3J = 8.0 Hz, 2H), 8.00 (d, ^3J = 8.0 Hz, 1H), 7.98 (dd, J = 1.1, 8.0 Hz, 1H), 7.81 (ddd, J = 1.1, 5.5, 8.0 Hz, 1H), 7.67 (m, 1H), 6.40 (s, 1H, C*H*-SO_3), 1.66 (s, J_{Pt-H} = 67 Hz, 3H, Pt-CH_3).

Independent Synthesis of *unsym*-(dpms)Pt^{IV}(CD$_3$)(OH)(*axial*-CH$_3$) 2.8-*d*$_{3(eq)}$

Under an argon atmosphere a solution of K(dpms)Pt^{II}CD$_3$(OH) (3.1 µmol) in D_2O was combined with CH_3I (0.20 µL, 3.2 µmol). The mixture was stirred for 5 minutes.

^{1}H NMR (400 MHz, D_2O) δ: 8.69 (d, ^3J = 6.0 Hz, 1H), 8.54 (vd, ^3J = 6.6 Hz, $^3J_{Pt-H}$ = 40 Hz, 1H), 8.22 (m, 2H), 8.02 (d, ^3J = 8.4 Hz, 1H), 7.98 (vd, J = 8.4 Hz, 1H), 7.81 (m, 1H), 7.67 (m, 1H), C*H*-SO_3 peak is not observed due to H/D exchange, 1.97 (s, J_{Pt-H} = 79 Hz, 3H, Pt-CH_3).

Preparation of Buffer Solutions pH 4.1 – 14.0

Solution A: Citric acid 0.64 g (3.33 mmol), H_3PO_4 (85 %) 0.23 mL (3.33 mmol), H_3BO_3 0.35 g (5.7 mmol), NaOH (1 M) 34.3 mL, 65.7 mL H_2O.

Solution B: 0.1 M solution of $HClO_4$.

Ionic strength	$C_{(buffer)}$	pH	Buffer Composition
0.27	0.14 M	4.1	10 mL of Solution A + 25.3 mL of Solution B + 14.7 mL of H_2O
0.36	0.07 M	5.9	88 mL of 0.0667M KH_2PO_4 + 12 mL Na_2HPO_4 of 0.0667M
0.34	0.07 M	8.0	5.5 mL of 0.0667M KH_2PO_4 + 94.5 mL of 0.0667M Na_2HPO_4
0.23	0.11 M	10.0	10 mL of Solution A + 9.0 mL of Solution B + 31 mL of H_2O
0.22	0.09 M	11.9	10 mL of Solution A + 0.2 mL of Solution B + 39.8 mL of H_2O
1.0	1.0 M	14.0	1 M KOH

Table 2.5 Buffer composition, ionic strength and concentration.

Inertness of (dpms)$Pt^{II}Me(OH_n)^{(2-n)-}$ with respect to ligand exchange in buffer solutions. Control experiment

Under an argon atmosphere of the glove box, solution of (dpms)$Pt^{II}Me(OH_2)$[99] (0.35 mL, 60 mM) in D_2O was combined with KH_2PO_4, (2.86 mg, 21.0 μmol) or Na_2HPO_4, (2.98 mg, 21.0 μmol). The reaction mixture was monitored by ^1H NMR spectroscopy. No changes to the (dpms)$Pt^{II}Me(OH_2)$ were observed over 24 hours.

Similar control experiment was performed with pH 4.1, 10.0, 11.9 buffer. A solution of (dpms)$Pt^{II}Me(OH_2)$ (0.1 mL, 60 mM) in D_2O was combined with 0.5 mL of pH 4.1, 10.0, 11.9 buffer. Reaction mixture was monitored for several days by ^1H NMR spectroscopy. No changes to the (dpms)$Pt^{II}Me(OH_2)$ were observed over three days.

Determination of pK_a of (dpms)$Pt^{II}Me(OH_2)$ 2.1

Under an argon atmosphere aqueous K(dpms)$Pt^{II}Me(OH)$ (1.0 mL, 0.01N) was placed in a vial with a stir bar and a rubber septum. The vial was taken out of the glove box and a digital pH meter probe was immersed into the solution. Titration was performed using 0.05 N H_2SO_4 in 10 μL aliquots.

pH	$V(H_2SO_4)$ (µL)
11.00	0
10.66	10
10.03	20
9.47	30
9.20	40
8.97	50
8.76	60
8.63	70
8.50	80
8.38	90
8.24	100
8.12	110
8.01	120
7.89	130
7.77	140
7.64	150
7.46	160
7.27	170
6.90	180
6.21	190
4.94	200
4.27	210
3.93	220
3.66	230
3.48	240
3.32	250

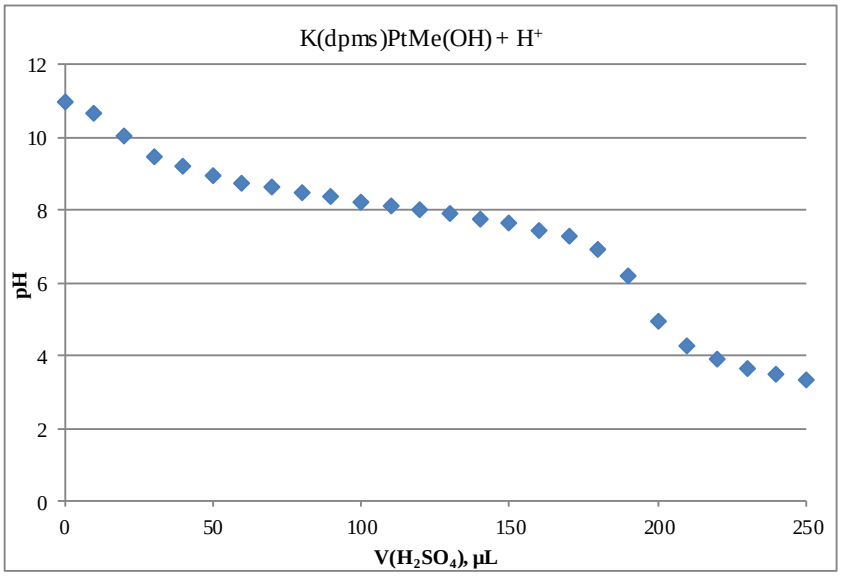

This data was used to calculate the $[LPt^{II}Me(OH_2)]/[LPt^{II}Me(OH)]$ ratio for each *pOH* value. Then using the linear regression of *pOH* – pK_b = $log([LPt^{II}Me(OH_2)]/[LPt^{II}Me(OH)])$ the pK_b value was determined.

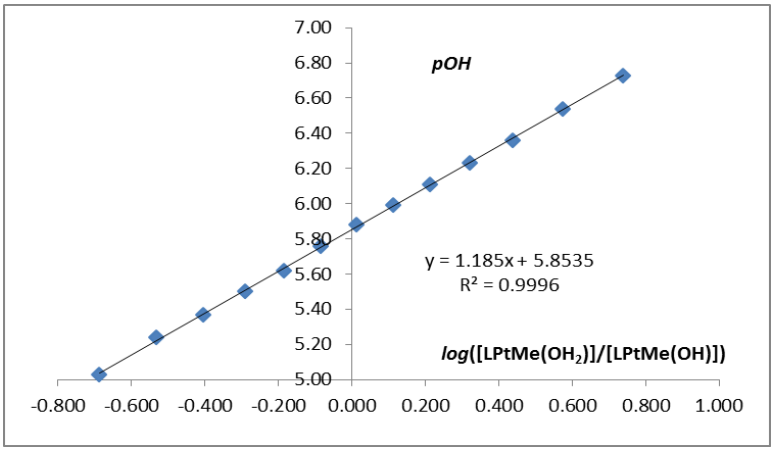

Slope = 1.19±0.01 pK_a = 8.15±0.01

Intercept 5.85±0.01 = pK_b;

Kinetics and product distribution in aerobic oxidation of K(dpms)Pt^{II}Me(OH) at pH 4.1 – 14.0

General procedure. The oxidation of aqueous (dpms)$Pt^{II}Me(OH_n)^{(2-n)-}$ was run under vigorous stirring in a 25 mL round-bottom flask filled with $O_2(g)$ equipped with a stirring bar and an O_2-filled balloon. Reactions under air were performed under vigorous stirring in 25 mL round-bottom flask, equipped with a stir bar and a needle for pressure equilibration. The solution pH was maintained using buffer solutions (pH 4.1, 5.9, 8.0, 10.0, 11.9) or 1.0 M KOH (pH 14.0). First, approximately 2.0 mL of ~3-17 mM stock solution of aqueous K(dpms)Pt^{II}Me(OH) were combined with an appropriate aqueous buffer or 1.0 M KOH under an argon atmosphere. The mixture was temperature-equilibrated and then injected with a syringe into the reaction flask placed in a temperature-controlled water-ethylene glycol bath at 21.0 °C. Vigorous stirring began immediately. Periodically a ~0.2 mL aliquot of the reaction mixture was taken with a syringe, transferred into argon-filled NMR tube, and diluted with 0.3 mL degassed D_2O to stop the reaction. Concentrations of the reactant, *unsym*-(dpms)$Pt^{IV}Me(OH)_2$ and *unsym*-(dpms)$Pt^{IV}Me_2(OH)$ were monitored by ^{1}H NMR spectroscopy with 1,4-dioxane used as an internal standard. Methyl group balance was calculated based on the sum of representative aromatic or aliphatic protons. Minimum of two kinetics runs were performed.

Kinetic plots of disappearance of the (dpms)$Pt^{II}Me(OH_n)^{(2-n)-}$, *n*=1, 2 at pH 4.1 – 14.0 under O_2

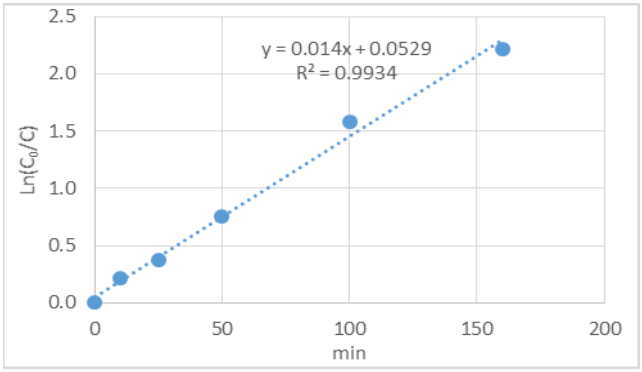

[SM] = 4.4 mM,
conversion = 93%
(dpms)$Pt^{IV}Me(OH)_2$ yield = 91%
(dpms)$Pt^{IV}Me_2(OH)$ yield = 2%
$t_{1/2}$ = 46 min

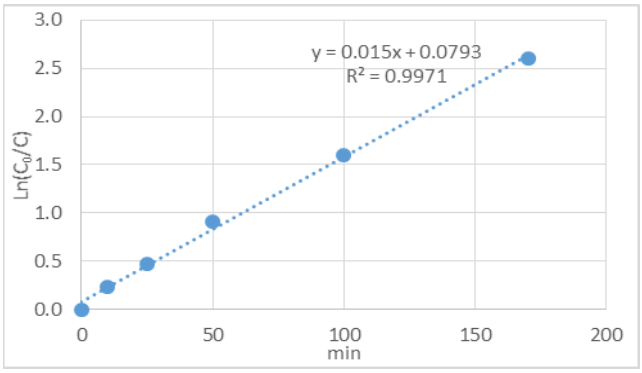

[SM] = 4.1 mM,
conversion = 89%
(dpms)$Pt^{IV}Me(OH)_2$ yield = 87%
(dpms)$Pt^{IV}Me_2(OH)$ yield = 1.6%
$t_{1/2}$ = 50 min

Figure 2.2 First-order kinetics plots for disappearance of (dpms)$Pt^{II}Me(OH_2)$ at **pH 4.1**, at 21.0 °C.

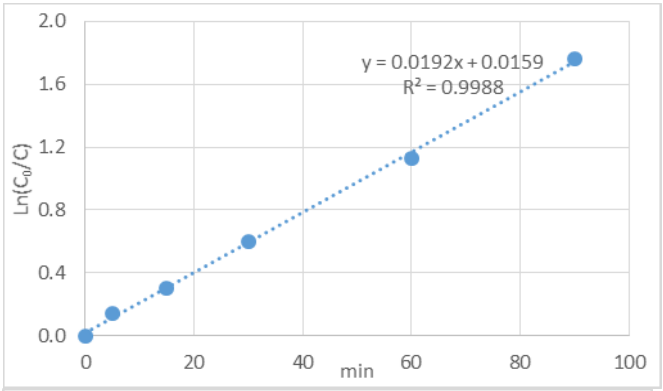

[SM] = 3.5 mM,
conversion = 89%
(dpms)$Pt^{IV}Me(OH)_2$ yield = 88%
(dpms)$Pt^{IV}Me_2(OH)$ yield = 1.4%
$t_{1/2}$ = 33 min

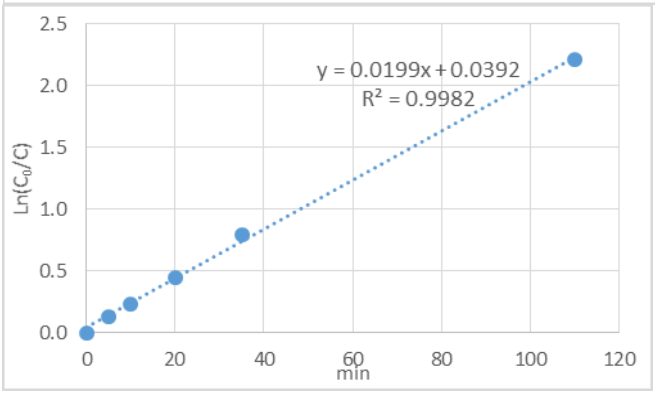

[SM] = 3.6 mM,
conversion = 83%
(dpms)$Pt^{IV}Me(OH)_2$ yield = 82%
(dpms)$Pt^{IV}Me_2(OH)$ yield = 1.0%
$t_{1/2}$ = 36 min

Figure 2.3 First-order kinetics plots for disappearance of (dpms)$Pt^{II}Me(OH_2)$ at **pH 5.9**, at 21.0 °C.

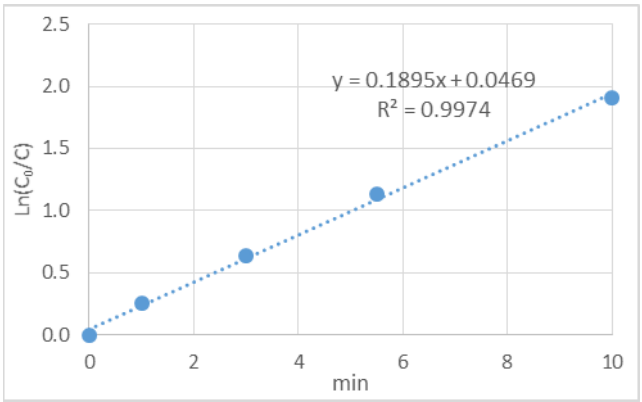

[SM] = 4.9 mM,
conversion = 85%
(dpms)$Pt^{IV}Me(OH)_2$ yield = 85%
(dpms)$Pt^{IV}Me_2(OH)$ yield = 0%
$t_{1/2}$ = 3.7 min

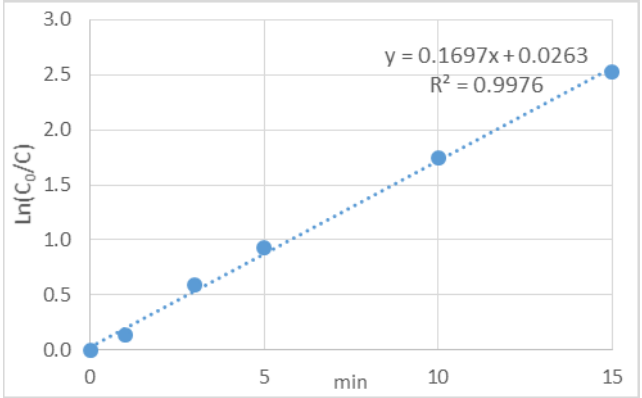

[SM] = 8.9 mM,
conversion = 92%
(dpms)$Pt^{IV}Me(OH)_2$ yield = 92%
(dpms)$Pt^{IV}Me_2(OH)$ yield = 0.4%
$t_{1/2}$ = 4.1 min

Figure 2.4 First-order kinetics plots for disappearance of (dpms)$Pt^{II}Me(OH_2)$ at **pH 8.0**, at 21.0 °C.

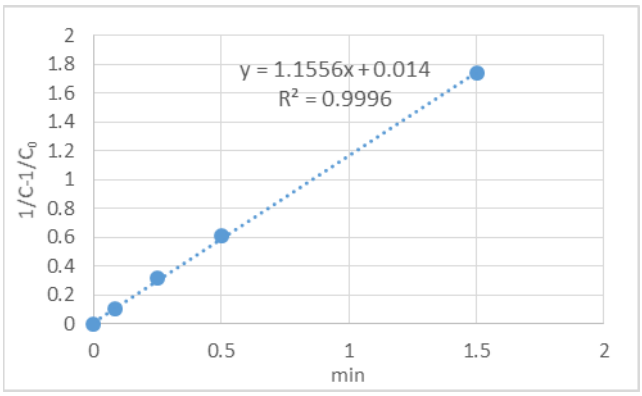

[SM] = 4.2 mM, conversion = 87%
(dpms)$Pt^{IV}Me(OH)_2$ yield = 85%
(dpms)$Pt^{IV}Me_2(OH)$ yield = 2.5%
$t_{1/2}$ = 0.21 h

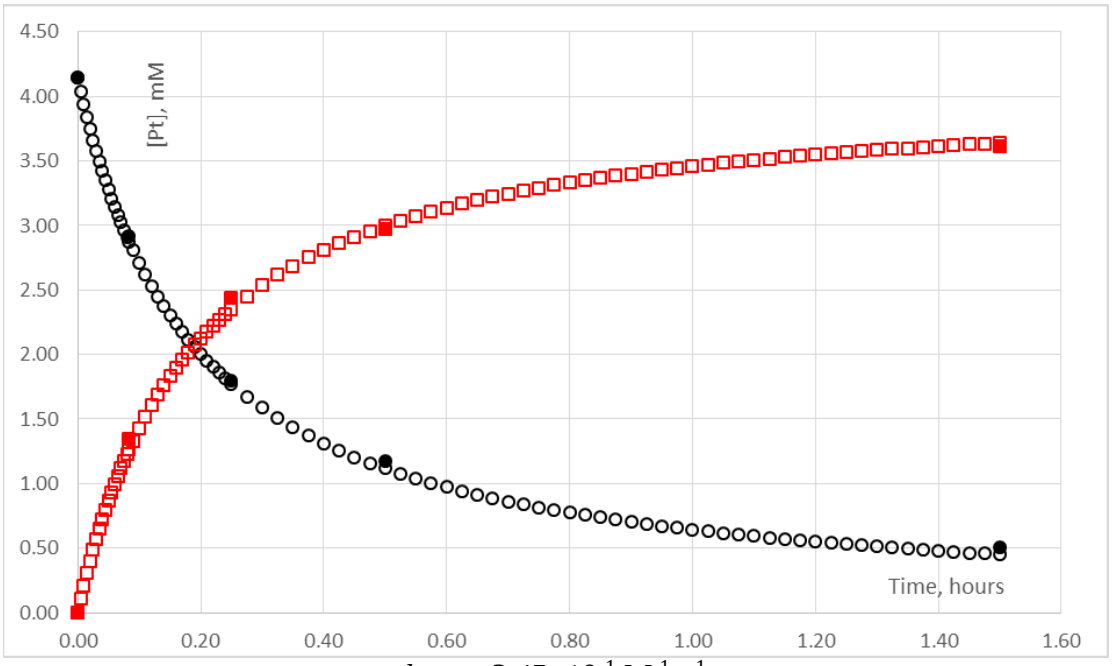

$k_{ox\text{-}2} = 3.45\times10^{-1}\ M^{-1}\ s^{-1}$
$k_{Me\ transfer} = 9.17\times10^{-6}\ s^{-1}$

Figure 2.5 Second-order kinetics plot for disappearance of (dpms)$Pt^{II}Me(OH)$ at **pH 10.0**, at 21.0 °C (top). Best least square fitting of the experimental data for **pH 10.0**: empty circles – [2.5], empty squares – [2.2]. (bottom).

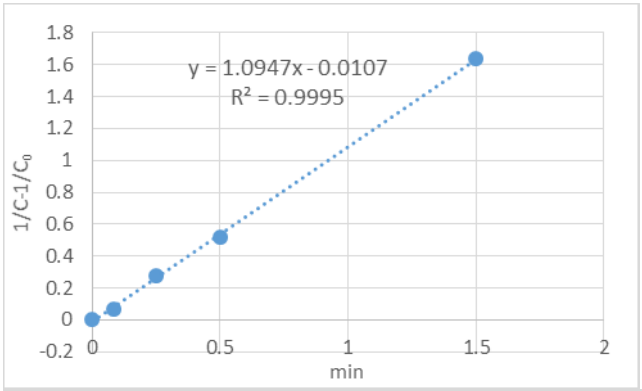

[SM] = 4.0 mM,
conversion = 88%
(dpms)$Pt^{IV}Me(OH)_2$ yield = 86%
(dpms)$Pt^{IV}Me_2(OH)$ yield = 2%
$t_{1/2}$ = 0.23 h

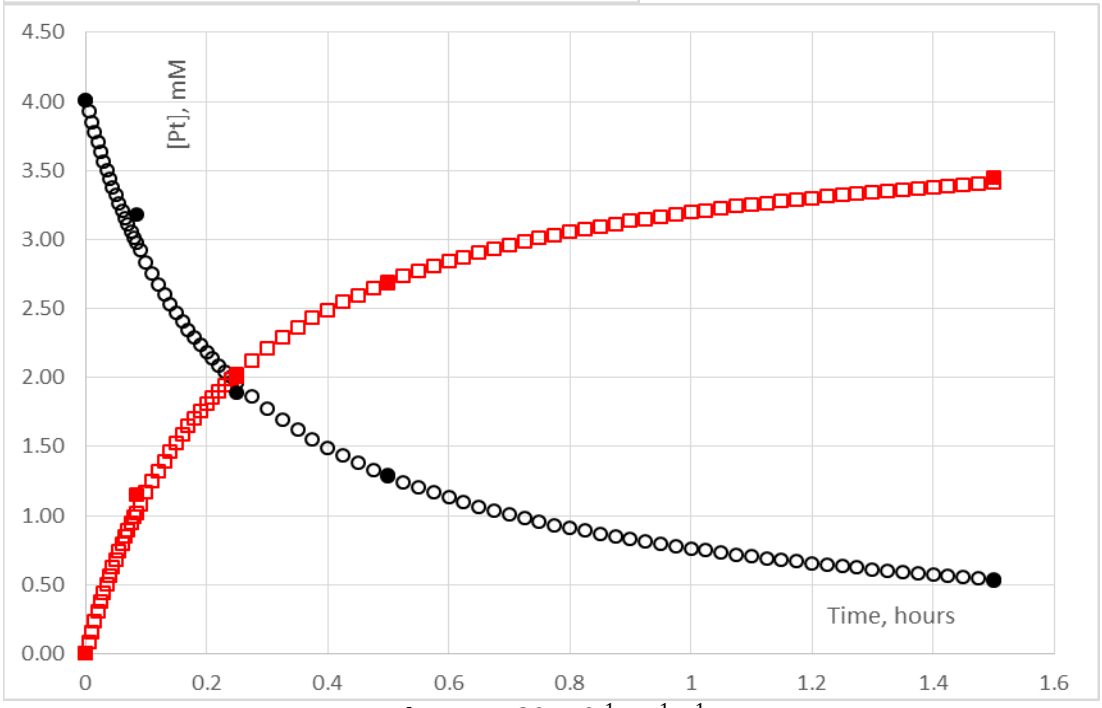

$k_{ox\text{-}2} = 2.80\times10^{-1}\ M^{-1}\ s^{-1}$

$k_{Me\ transfer} = 8.85\times10^{-6}\ s^{-1}$

Figure 2.6 Second-order kinetics plot for disappearance of (dpms)$Pt^{II}Me(OH)$ at **pH 10.0**, at 21.0°C (top). Best least square fitting of the experimental data for **pH 10.0**: empty circles – [2.5], empty squares – [2.2] (bottom).

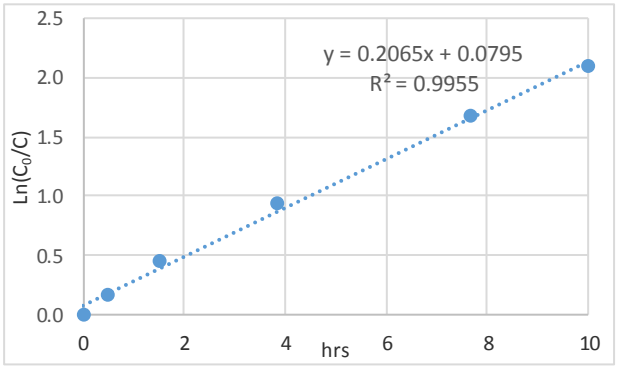

[SM] = 7.1 mM,
conversion = 87%
(dpms)$Pt^{IV}Me(OH)_2$ yield = 43%
(dpms)$Pt^{IV}Me_2(OH)$ yield = 44%
$t_{1/2}$ = 3.4 h

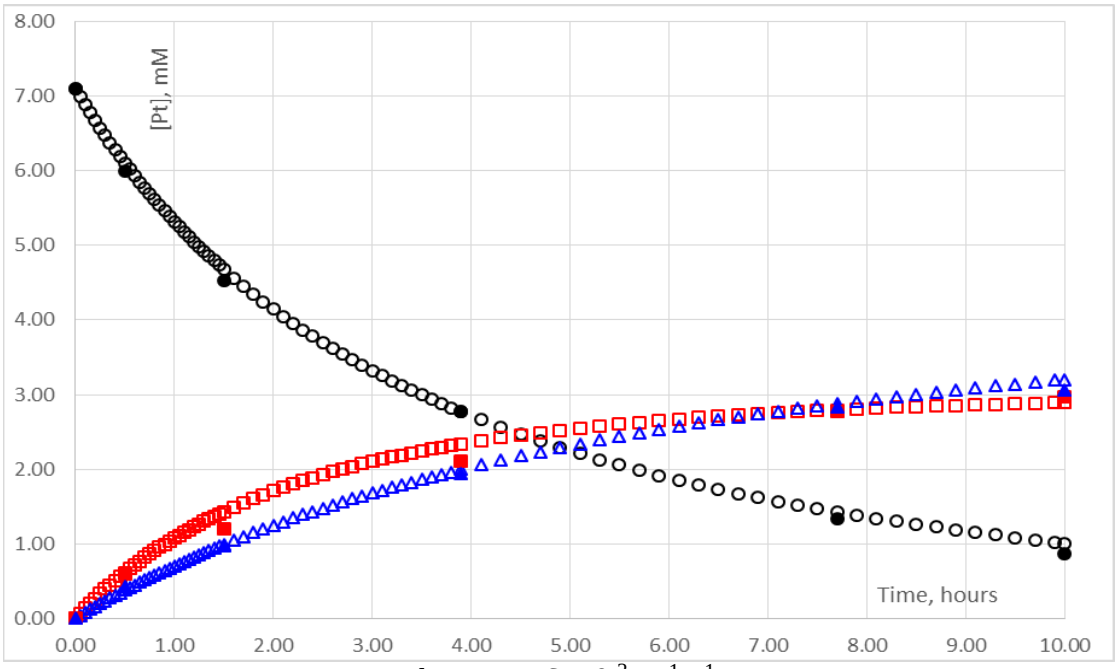

$k_{ox\text{-}2} = 7.76\times10^{-3}\ M^{-1}\ s^{-1}$

$k_{Me\ transfer} = 3.18\times10^{-5}\ s^{-1}$

Figure 2.7 First-order kinetics plots for disappearance of (dpms)$Pt^{II}Me(OH)$ at **pH 11.9**, at 21.0 °C (top). Best least square fitting of the experimental data for **pH 11.9**: empty circles – [2.5], empty squares – [2.2], empty triangles – [2.8] (bottom).

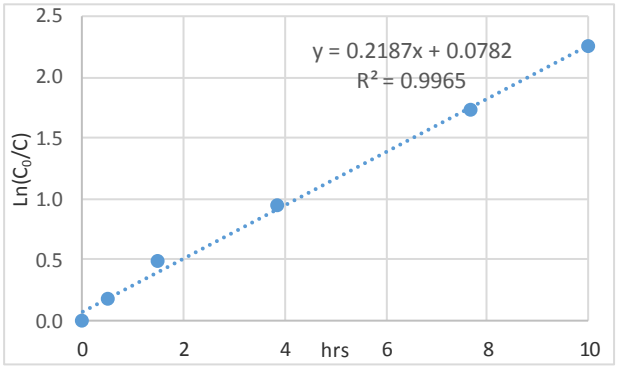

[SM] = 8.0 mM,
conversion = 90%
(dpms)$Pt^{IV}Me(OH)_2$ yield = 46%
(dpms)$Pt^{IV}Me_2(OH)$ yield = 43%
$t_{1/2}$ = 3.2 h

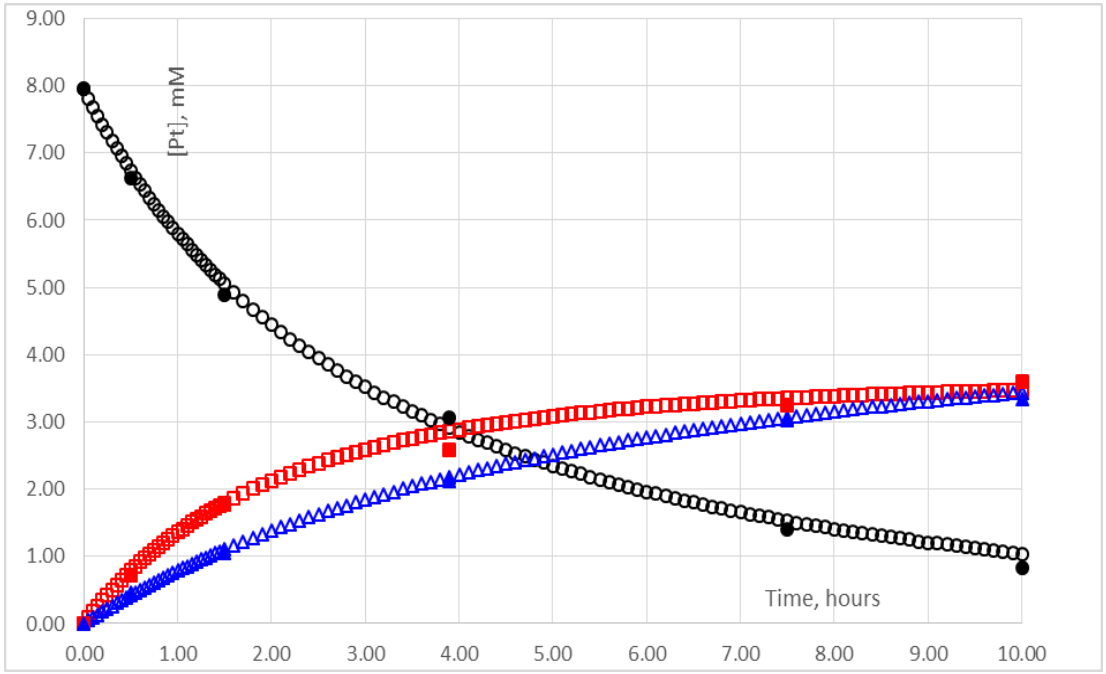

$k_{ox\text{-}2} = 8.02\times10^{-3}\ M^{-1}s^{-1}$
$k_{Me\ transfer} = 3.21\times10^{-5}\ s^{-1}$

Figure 2.8 First-order kinetics plots for disappearance of (dpms)$Pt^{II}Me(OH)$ at **pH 11.9**, at 21.0 °C (top). Best least square fitting of the experimental data for **pH 11.9**: empty circles – [2.5], empty squares – [2.2], empty triangles – [2.8] (bottom).

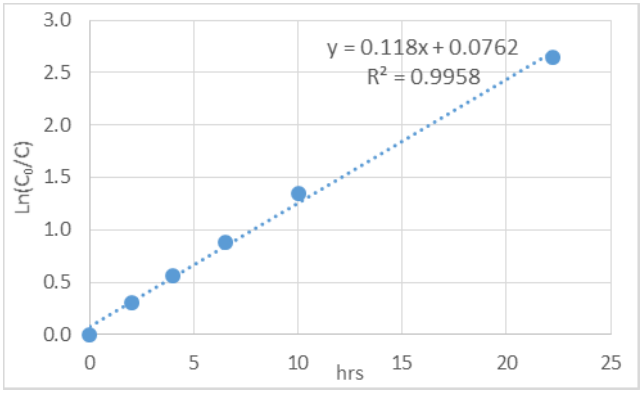

[SM] = 16.7 mM,
conversion = 93%
(dpms)$Pt^{IV}Me(OH)_2$ yield = 27%
(dpms)$Pt^{IV}Me_2(OH)$ yield = 65%
$t_{1/2}$ = 5.9 h

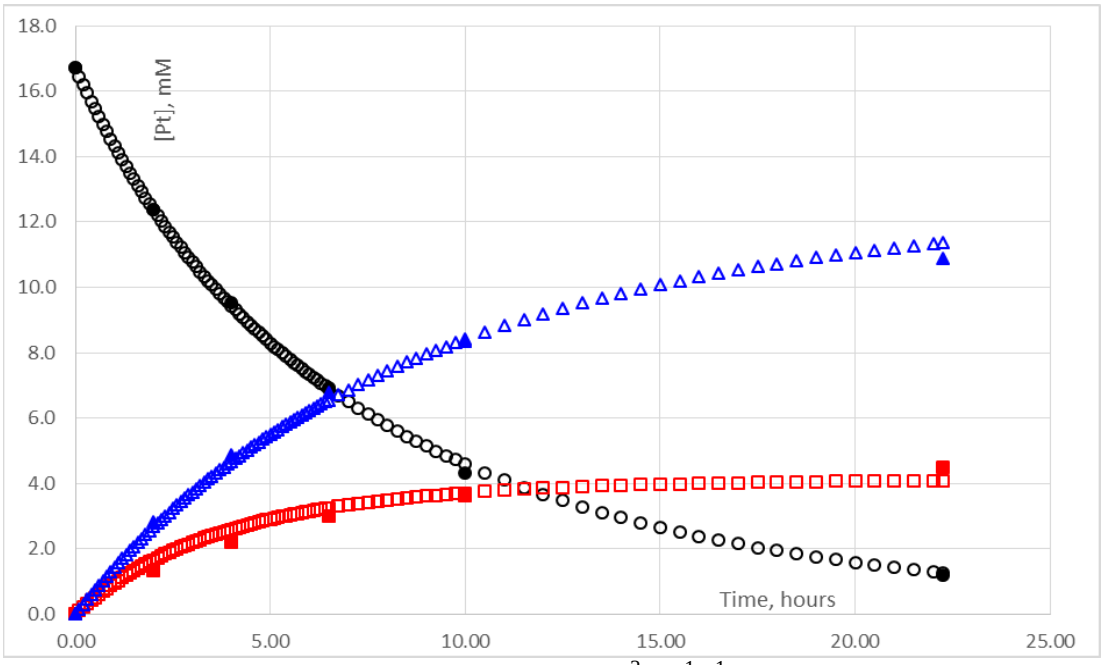

$k_{ox\text{-}2} = 1.09\times10^{-3}\ M^{-1}s^{-1}$
$k_{Me\ transfer} = 2.56\times10^{-5}\ s^{-1}$

Figure 2.9 First-order (top) and second-order (bottom) kinetics plots for disappearance of (dpms)$Pt^{II}Me(OH)$ at **pH 14.0**, at 21.0 °C (top). Best least square fitting of the experimental data for **pH 14.0**: empty circles – [2.5], empty squares – [2.2], empty triangles – [2.8] (bottom).

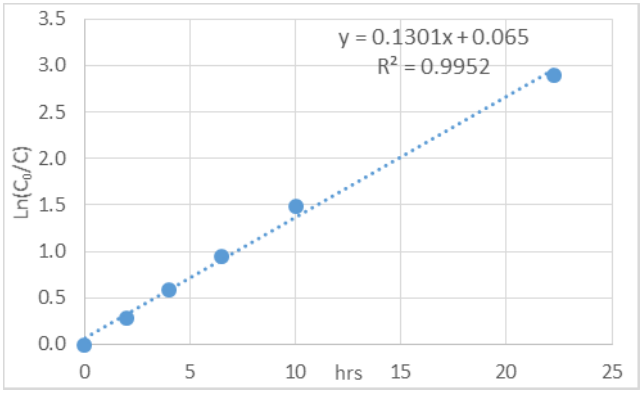

[SM] = 17.1 mM,
conversion = 95%
(dpms)$Pt^{IV}Me(OH)_2$ yield = 29%
(dpms)$Pt^{IV}Me_2(OH)$ yield = 66%
$t_{1/2}$ = 5.3 h

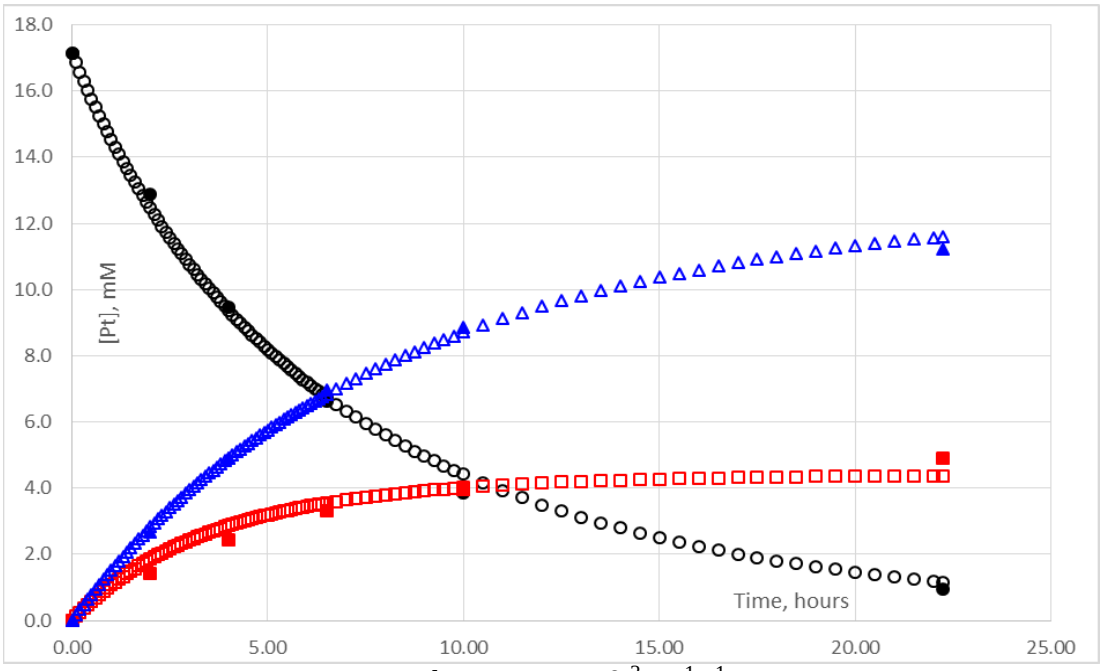

$k_{ox\text{-}2} = 1.17\times10^{-3}\ M^{-1}s^{-1}$

$k_{Me\ transfer} = 2.66\times10^{-5}\ s^{-1}$

Figure 2.10 First-order (top) and second-order (bottom) kinetics plots for disappearance of (dpms)$Pt^{II}Me(OH)$ at **pH 14.0**, at 21.0 °C (top). Best least square fitting of the experimental data for **pH 14.0**: empty circles – [2.5], empty squares – [2.2], empty triangles – [2.8] (bottom)

Kinetic plots of disappearance of the (dpms)$Pt^{II}Me(OH_2)$ at pH 6.5 under air

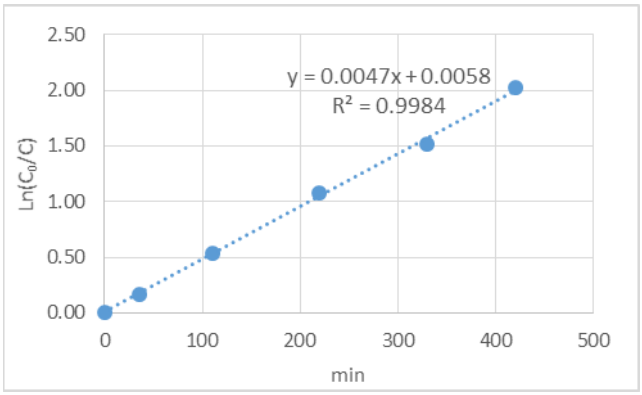

[SM] = 9.8 mM,
conversion = 87%
(dpms)$Pt^{IV}Me(OH)_2$ yield = 84%
(dpms)$Pt^{IV}Me_2(OH)$ yield = 1.7%
$t_{1/2}$ = 147 min

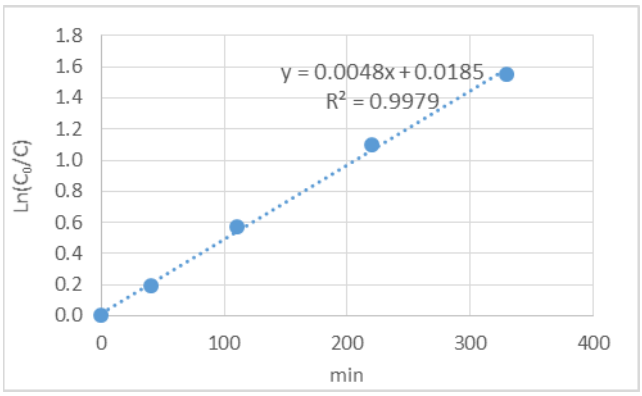

[SM] = 3.8 mM,
conversion = 79%
(dpms)$Pt^{IV}Me(OH)_2$ yield = 76%
(dpms)$Pt^{IV}Me_2(OH)$ yield = 1.7%
$t_{1/2}$ = 144 min

Figure 2.11 First-order kinetics plots for disappearance of (dpms)$Pt^{II}Me(OH)$ at **pH 6.5**, at 21.0 °C.

The secondary deuterium kinetic isotope effect for the Pt-to-Pt methyl group transfer

In the argon-filled glove box two Schlenk flasks, equipped with a magnetic stir bars, were charged with 10.2 mg (20 μmol) of K(dpms)$Pt^{II}(Me)_2$ each. Deoxygenated H_2O (0.62 mL) was added to the first Schenk flask and D_2O (0.64 mL) was added to the second Schenk flask. Schlenk flasks were taken out of the box and were kept in the water bath at 40 °C for 6 h to give K(dpms)$Pt^{II}CH_3(OH)$ and K(dpms)$Pt^{II}CD_3(OH)$ respectively in quantitative yield. Flasks were brought back inside the glove box, their contents were mixed together and combined with 0.20 mL of 1.00 M NaOH. The mixture was taken out of the glove box and purged with O_2. The Schlenk flask was sealed and the mixture was stirred overnight at room

temperature. The secondary kinetic isotope effect was calculated based on integration of the Pt^{IV}-CH_3 peaks in the upfield region of ^1H NMR spectra. Spectra were recorded on 600 MHz NMR spectrometer.

Model Studies of Pt-to-Pt Methyl group Transfer

Model study of Methyl group transfer from *unsym*-(dpms)$Pt^{IV}Me(OH)_2$ to K(dpms)Pt^{II}Me(OH) at pH 14

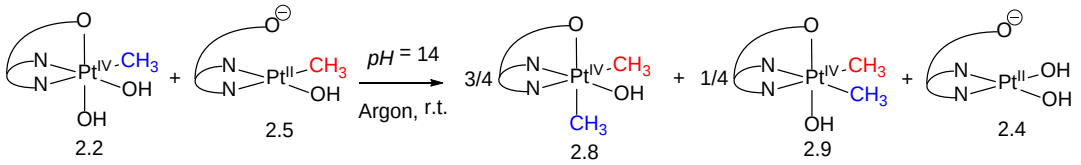

In an argon filled glove box, a solution of *unsym*-(dpms)$Pt^{IV}Me(OH)_2$ (0.40 mL, 11.0 µmol) in H_2O was combined with K(dpms)Pt^{II}Me(OH) (0.45 mL, 12.3 µmol) in D_2O. pH of the reaction mixture (total volume 0.85 mL) was adjusted to pH 14 using 47.6 mg (0.85 mmol) KOH under an argon atmosphere. Reaction was transferred into NMR tube with airtight Teflon valve, and taken out of the glove box. Methyl group transfer was monitored by ^1H NMR spectroscopy over 22 days. Mass balance was calculated based on integration of Pt^{IV}-CH_3 groups relative to 1,4-dioxane.

Time (days)	C_1-unsym-$Pt^{IV}CH_3(OH)_2$	$Pt^{II}CH_3(OH)$	C_1-sym-$Pt^{IV}(CH_3)_2(OH)$	C_s-sym-$Pt^{IV}(CH_3)_2(OH)$	Mass Balance
0	0.81	0.96	0.04	0.05	1.86
1	0.77	0.91	0.10	0.05	1.83
2	0.71	0.87	0.18	0.08	1.84
5	0.63	0.73	0.38	0.12	1.86
8	0.51	0.62	0.55	0.17	1.85
10	0.45	0.58	0.67	0.19	1.89
14	0.34	0.46	0.78	0.25	1.83
18	0.26	0.4	0.88	0.28	1.82
22	0.19	0.33	0.98	0.36	1.86

Table 2.6 Mass balance of the reaction between *unsym*-(dpms)$Pt^{IV}Me(OH)_2$ and K(dpms)Pt^{II}Me(OH) was calculated based on the integration of the methyl protons. Conditions: room temperature, pH 14.0.

Complex	Conversion (%)	Yield (%)
unsym-LPt^{IV}(CH$_3$)(OH)$_2$	77	-
LPt^{II}CH$_3$(OH)	64	-
unsym-LPt^{IV}(CH$_3$)$_2$(OH)	-	53
sym-LPt^{IV}(CH$_3$)$_2$(OH)	-	19

Table 2.7 Summary of product distribution of the reaction between *unsym*-(dpms)Pt^{IV}Me(OH)$_2$ and K(dpms)Pt^{II}Me(OH). Conditions: room temperature, pH 14.0.

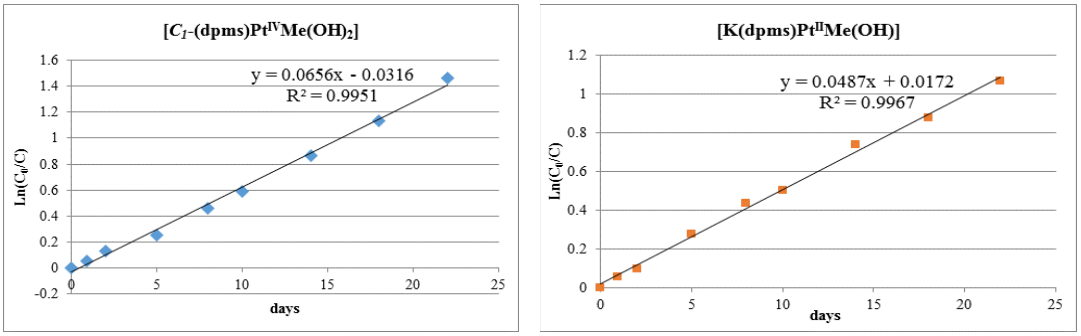

Figure 2.12 First-order kinetics plot for disappearance of *unsym*-(dpms)Pt^{II}Me(OH)$_2$ (blue) and K(dpms)Pt^{II}Me(OH) (red) at pH 14.0, ambient temperature.

The reaction rate constant, $k_{2.5\text{-}2.2}$ (Pt^{IV}) = 7.57×10^{-7} s^{-1}, k (Pt^{II}) = 5.65×10^{-7} s^{-1}

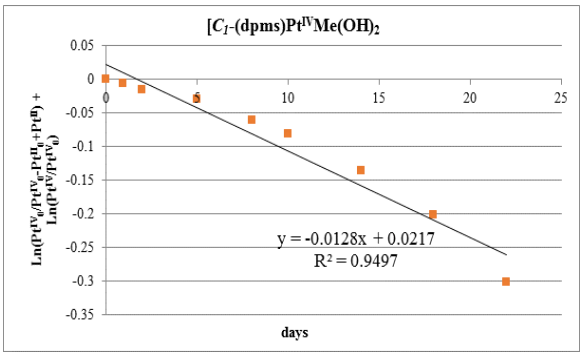

Figure 2.13 A representative second-order kinetics plot for disappearance of *unsym*-(dpms)Pt^{II}Me(OH)$_2$ at pH 14.0, 21 °C.

Based on the average yield of Me group transfer product (70 ± 1%) and half-life of disappearance of the (dpms)Pt^{II}**CH$_3$**(OH) under aerobic conditions ($t_{1/2}$ = 5.6 h), relative rate of accumulation of *unsym*-(dpms)Pt^{IV}(**CH$_3$**)$_2$(OH) and *sym*-(dpms)Pt^{IV}(**CH$_3$**)$_2$(OH) under aerobic conditions is 34 times faster than in the model study (Table 2).

$k_{2.5\text{-}2.2}$, 23 °C, [**2.5**] 23.3 mM	$k_{Me\ transfer}$, 21 °C, [**2.5**] 16.7 mM	Relative Rate of Formation of **2.8** and **2.9**	
		$k_{2.5\text{-}2.2}$	$k_{Me\ transfer}$
7.57×10^{-7} s^{-1}	$(2.61\pm0.05)\times10^{-5}$ s^{-1}	1	34

Model study of Me group transfer from *sym*-(dpms)$Pt^{IV}Me(OH)_2$ to K(dpms)Pt^{II}Me(OH) at pH 14.0

In an argon filled glove box, pH of *sym*-(dpms)$Pt^{IV}Me(OH)_2$ (0.45 mL, 17.1 μmol) in H_2O was adjusted to pH 14 using 18 mg (0.45 mmol) NaOH under an argon atmosphere. In a separate vial, pH of K(dpms)Pt^{II}Me(OH) (0.45 mL, 20.9 μmol) was adjusted to pH 14 using 18 mg (0.45 mmol) NaOH. Solutions of *sym*-(dpms)$Pt^{IV}Me(OH)_2$ and K(dpms)Pt^{II}Me(OH) were combined, immediate color change from colorless to yellow was observed. Analysis of the reaction mixture by ^{1}H NMR spectroscopy after a few minutes showed complete consumption of both *sym*-(dpms)$Pt^{IV}Me(OH)_2$ and K(dpms)Pt^{II}Me(OH). ^{1}H NMR analysis showed presence of K(dpms)Pt^{II}Me(OH) (18% remaining), (dpms)$Pt^{II}(OH)_2^-$ and *unsym*-(dpms)$Pt^{IV}(CH_3)_2$(OH). Yellow color of the solution faded overnight.

Pt-to-Pt Methyl group Transfer in the Presence of Fc^+

A stock solution of (dpms)$Pt^{II}CH_3$(OH) in H_2O (9.4 μmol) was evaporated to dryness and redissolved in CD_3OD. $Cp_2Fe^{III}PF_6$ (3.4 mg, 10.3 μmol) was added and solution turned green within minutes and ferrocene precipitate began to form. ^{1}H NMR spectrum indicated formation of paramagnetic Pt^{III} due to broadening of the signals. After 1 day ^{1}H NMR showed presence of *unsym*-(dpms)$Pt^{IV}(CH_3)_2$(OH) in 23 % yield, 16 % of unreacted (dpms)$Pt^{II}CH_3$(OH) remained in the reaction mixture.

Computational Details

Geometry optimization and frequency calculation were carried out in Prof. William A. Godard lab, Caltech, at the level of B3LYP[100,101]/LACVP** including

solvation by the Poisson–Boltzmann self-consistent polarizable continuum method[102] with dielectric constant = 80.37 and effective radius = 1.4 Å to represent water. Pt was described with the small core (18 explicit electrons) Hay-Wadt[103] angular momentum projected effective core potential.[104,105] Single point energies were refined using a larger 3-□ basis set with diffuse and polarization functions (LACV3P**++ augmented with two f-functions for Pt, 6-311G**++ on other elements and 6-311G**++ augmented with one d-functions for S).

Unless otherwise specified all energies are Gibbs free energies calculated by the following formula: $G_{298K} = E_{singlepoint} + G_{solv} + ZPE + H_{vib} + 6kT - TS_{mod}$, where $S_{mod} = S_{vib} + 0.54(S_{trans} + S_{rot}) + 0.24$ is Wertz's approximation for the entropy fit to the experimental solvation entropy of small molecules.[106] One explicit water molecule per Pt was added to provide a better description of hydrogen bonding between water and OH_n ligands on Pt. The triplet-singlet (T-S) crossing points were located with Harvey's script.[107] If free hydroxide anion is present, three explicit water molecules were placed to provide better description of solvation. All calculations were carried out by Jaguar 7.7.[99,108]

Chapter 3 : Preparation of (dpms)$Pt^{II}Me(X)^-$ complexes and Study of Their Behavior Towards O_2

3.1 Introduction

Oxidation of platinum complexes, discussed in Chapter 2, involves a four electron reduction of O_2 in two consecutive steps. In the first step O_2 is reduced to hydroperoxide HO_2^-, and in the second step the latter is reduced to hydroxide OH^-. The overall reaction stoichiometry is 2 equiv. of Pt^{II} per 1 equiv. of O_2.[75] The first step is rate limiting at pH < 10 due to the spin-forbidden triplet-singlet interconversion.

Spin-forbidden reaction of Pd^0 and O_2 have been studied by DFT calculations, in order to establish the role of one-electron steps in alleviation of spin restrictions. Addition of singlet Pd^0 to triplet O_2 to form singlet (en)Pd(η^2-OO), en = ethylenediamine), was proposed to occur via superoxide adduct (NN)Pd(η^1-OO) (Scheme 3.1). The latter is a triplet diradical, where one unpaired electron occupies the superoxide π* orbital, and the second – the Pd s-d combination. The intersystem crossing from the triplet to singlet reaction surfaces occurs at the minimum energy crossing point, which is uphill by only 0.2 kcal/mol.[34,109]

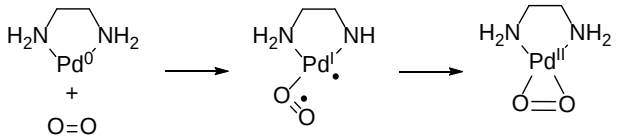

Scheme 3.1 Proposed mechanism for the reaction between (en)Pd^0 and O_2 to generate η^2-peroxo-Pd(II) complex.

In case of dimethyl-Pt(II) complexes, solvent was shown to play an important role in their reaction with O_2. For example, in aprotic solvents, such as THF, DCM,

and toluene, (tmeda)$Pt^{II}Me_2$ complex showed no sign of oxidation to (tmeda)$Pt^{IV}Me_2(OH)(OOH)$. Only a small fraction (<10%) of the starting material was consumed to form blue-colored solution. This solution was EPR active, suggesting the presence of paramagnetic species. The species could be quenched with MeOH to yield a mixture of Pt^{IV} products.[75] These observations indicate the involvement of Pt^{III} intermediates in a stepwise formation of singlet hydroperoxo-Pt^{IV} intermediates. It is interesting to note that in a DFT-study by Wei-Guang Liu (W. A. Goddard III group), of the reaction between (dpms)$Pt^{II}Me(OH_2)$ and O_2, superoxo Pt^{III} species were not found.

Previously Labinger and Bercaw demonstrated that the electron density at the metal center can be correlated directly to the rate of oxidation of Pt^{II} complexes.[75,110] When triplet-singlet interconversion is a rate-limiting step, it can be assumed that the barrier for this interconversion is reduced with higher electron density at the metal center. Our group has demonstrated that electron density of the metal center is not the only factor that affects oxidation of Pt^{II} with O_2. When HX = $PhNH_2$, the rate of oxidation is very slow ($t_{1/2} \approx 30$ h) even though aniline is a better electron donor than water and methanol. The half-life of oxidation of (dpms)$Pt^{II}Me(XH)$ where XH = MeOH, H_2O, $PhNH_2$ is shown in Table 3.1.[111]

	$Pt^{II}Me(MeOH)$	$Pt^{II}Me(H_2O)$	$Pt^{II}Me(NH_2Ph)$
$t_{1/2}$	15 min	15 min	30 h
pK_a (HX)	15.5	15.7	30.6

Table 3.1 Half-life of disappearance of (dpms)$Pt^{II}Me(XH)$ species, and pK_a of the corresponding XH.

Table 3.1 demonstrates that the rate of oxidation increases with increasing Brønsted acidity of ligand HX. This implies that anionic (dpms)$Pt^{II}Me(X)^-$ specie is more reactive towards dioxygen than (dpms)$Pt^{II}Me(XH)$.[80,111]

In Chapter 2 we showed that the rate of oxidation of (dpms)$Pt^{II}Me(OH)^-$ in water is highly dependent on the reaction pH. Among the tested solution pH values, 4.1, 5.9, 8.0, 11.9 and 14.0 the fastest reaction occurs at pH 8.0 with a $t_{1/2}$ = 3.9 ± 0.2 min. This pH appears to be close to the optimal condition for the reduction of dioxygen in this system. Based on the pK_a of (dpms)$Pt^{II}Me(OH_2)$, the ratio of (dpms)$Pt^{II}Me(OH)^-$: (dpms)$Pt^{II}Me(OH_2)$ is 4:6 at pH 8.0. This appears to be close to the most favorable balance of anionic Pt^{II}, needed for dioxygen activation, and concentration of H^+, needed for reduction of hydroperoxide Pt^{IV}-OOH to Pt^{IV}-OH.

We sought to explore the effect of X-type ligands on the rate of aerobic oxidation of (dpms)$Pt^{II}Me(X)^-$ complexes. Varying ligand X^- and comparing the reactivity of the related complexes towards O_2 will allow us to explore the structure-reactivity relationship. Understanding this relationship might bring us closer to the development of faster $Pt^{II} \rightarrow Pt^{IV}$ conversion, which is vital for efficient Pt-catalyzed C-H functionalization with O_2 as a terminal oxidant.

Halide-derived anionic (dpms)$Pt^{II}Me(X)^-$ might be more reactive toward O_2. The effect of basicity of ligand X on the reactivity of $Pt^{II}Me(X)$ might evaluated with the following: $H_2PO_4^-$, AcO^-, HCO_3^- where basicity increases in the order of $H_2PO_4^- < AcO^- < HCO_3^-$. Polyanionic ligands, e.g. HPO_4^{2-}, and CO_3^{2-}, are attractive candidates since they may provide (dpms)$Pt^{II}Me(X)^{2-}$ complex with (2-) negative charge.

3.2 Attempted Generation of (dpms)$Pt^{II}Me(X)^-$ Complexes

In an attempt to find a relationship between reactivity of [(dpms)$Pt^{II}Me(X)]^-$ towards dioxygen and nature of X^-, the following anionic ligands, potential components of systems for C-H functionalization, have been selected: $X^- = F^-$, Cl^-, Br^-

, I^-, OAc^-, $H_2PO_4^-$, HPO_4^{2-}, HCO_3^-, CO_3^{2-}. General scheme for obtaining $(dpms)Pt^{II}Me(X)^-$ is shown in Scheme 3.2.

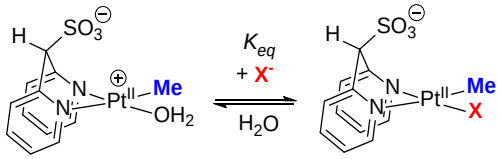

2.1

3.2, X = Cl
3.3, X = Br
3.4, X = I
3.5, X = AcO

Scheme 3.2 Generation of $K(dpms)Pt^{II}Me(X)$.

$$K_{eq} = \frac{[LPtMe(X)]}{[LPtMe(OH_2)][X^-]}$$

X^-	K_{eq}
Cl^-	136
Br^-	213
AcO^-	29

Table 3.2 Equilibrium constant K_{eq} for the reaction between $(L)Pt^{II}Me(OH_2)$ and X^-.

The generation of $(dpms)Pt^{II}Me(X)^-$ complexes was performed at ambient temperature via ligand exchange between equimolar ratios of $(dpms)Pt^{II}Me(OH_2)$ and the corresponding X^- in water. The identity of the new complexes $(dpms)Pt^{II}Me(X)^-$ was confirmed by ^1H NMR and ESI-MS. Ligand exchange was monitored by ^1H NMR spectroscopy at 20 ^oC for several days until no further changes in $(dpms)Pt^{II}Me(OH_2)$: $(dpms)Pt^{II}Me(X)^-$ were observed.

When one equivalent of solid NaX or KX was added to the reaction mixture containing 59.8 mM of $(dpms)Pt^{II}Me(OH_2)$, the equilibrium ratio of $(dpms)Pt^{II}Me(OH_2)$: $(dpms)Pt^{II}Me(X)^-$ was 1 : 0.9 for X = OAc; 1 : 2.4 for X = Cl; and 1 : 3.1 for X = Br. The ^1H NMR of Pt^{II}-CH_3 resonance in $(dpms)Pt^{II}Me(X)^-$ complexes is δ = 0.84, 0.89, and 0.77 ppm for X = Cl, Br, and OAc respectively, compared to $(dpms)Pt^{II}Me(OH)^-$ δ = 0.85 ppm. Table 3.2 shows K_{eq} for the reaction in Scheme 3.2. The reaction equilibrium constants decrease in the following order: X^- = I > Br > Cl > AcO.[112]

In case of X^- = $H_2PO_4^-$, HPO_4^{2-}, HCO_3^-, CO_3^{2-} and F^- no ligand exchange has been observed, with $(dpms)Pt^{II}Me(OH_2)$ being the only complex observed by ^1H NMR spectroscopy. The lack of reactivity might be associated with mismatch of hard

anions with soft Pt^{II} metal center, and/or their high basicity leading to a conversion of (dpms)Pt^{II}Me(OH_2) to a much less reactive (dpms)Pt^{II}Me$(OH)^-$.

3.3 Attempted Aerobic Oxidation of (dpms)Pt^{II}Me$(X)^-$ Complexes in Water, (X = Cl, Br, OAc)

It may be anticipated that aerobic oxidation of (dpms)Pt^{II}Me$(X)^-$ (X = Cl, Br, OAc) complexes would lead to formation of (dpms)Pt^{IV}Me(X)(OH) (Scheme 3.3, **C**). However, when X = Cl and Br analysis of the reaction mixture after reaction with O_2 showed selective formation of (dpms)Pt^{IV}Me$(OH)_2$ (Scheme 3.3, **A**). This indicates that in the equilibrium mixture in Scheme 3.3 oxidation of **2.1** occurs faster than oxidation **3.2** and **3.3** (Scheme 3.3, **A** and **B**).

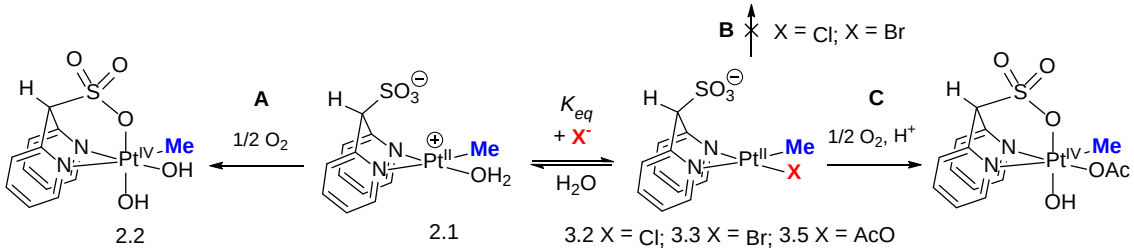

Scheme 3.3. Possible routes of oxidation for K(dpms)Pt^{II}Me(H_2O) and K(dpms)Pt^{II}Me(X).

When X = OAc formation of a minor product was observed in 7% yield (Scheme 3.3, **C**). The new specie was proposed to be (dpms)Pt^{IV}Me(OAc)(OH), due to a more downfield shifted resonance of the Pt^{IV}-CH_3, δ: 2.62, $^2J_{PtH}$ = 64 Hz, compared to (dpms)Pt^{IV}Me$(OH)_2$, δ 2.45, $^2J_{PtH}$ = 66 Hz. When oxidation of (dpms)Pt^{II}Me(OH_2) and K(dpms)Pt^{II}Me(OAc) was performed in methanol, the major product was still (dpms)Pt^{IV}Me(OMe)(OH), resulting from oxidation of (dpms)Pt^{II}Me(MeOH). The minor product, (dpms)Pt^{IV}Me(OAc)(OH), was formed in 22 % yield. Similar to the aqueous solution the new specie has also a more downfield shift of the Pt^{IV}- CH_3 resonance in methanoic solution: δ 2.58 (Pt^{IV}-CH_3, $^3J_{PtH}$ = 68

Hz) for (dpms)Pt^{IV}Me(OAc)(OH), compared to δ 2.38 (Pt^{IV}-C*H*$_3$, $^2J_{PtH}$ = 68 Hz) for (dpms)Pt^{IV}Me(OCH_3)(OH). The relatively small $^2J_{PtH}$ = 64 and 68 Hz for the Pt^{IV}-Me group is an indication of the presence of a ligand *trans* to the methyl with a relatively strong *trans* influence (py rather than SO_3 group). The OOCC*H*$_3$ signal of the (dpms)Pt^{IV}Me(OAc)(OH) could not be located due to the presence of excess NaOAc.

The lack of reactivity of (dpms)Pt^{II}Me$(X)^-$ (X = Cl, Br) with O_2 was attributed to the electronic effects. Halogens are electronegative and have an electron-withdrawing inductive effect, and electron donating resonance effect of the lone pairs. Thus the inductive and resonance effects are counter to each other, but the former is somewhat stronger then the latter.[113]

3.4 Aerobic Oxidation of Unbuffered (dpms)Pt^{II}Me$(I)^-$ in Water and Methanol

Ligand exchange between aqua ligand in (dpms)Pt^{II}Me(OH_2) complex and KI was complete within minutes upon addition of the reagent. The resulting product K(dpms)Pt^{II}Me(I) could be isolated, and was characterized by ^{1}H, ^{13}C NMR spectroscopy, ESI-MS, and elemental analysis. The ^{1}H NMR signal of the Pt^{II}-Me group in K(dpms)Pt^{II}Me(I) is shifted slightly downfield, compared to the K(dpms)Pt^{II}Me(OH) (δ = 0.97 *vs*. 0.85 ppm respectively).

Aerobic oxidation of (dpms)Pt^{II}Me$(I)^-$ in water resulted in formation of white precipitate. When all Pt^{II} complex was consumed, reaction mixture was evaporated and the remaining solid was redissolved in DMSO-d_6. Analysis of the solution by ^{1}H NMR spectroscopy revealed presence of two dimethyl-Pt(IV) species, which were identified as C_1-symmetric (dpms)$Pt^{IV}Me_2$(OH) and C_1-symmetric (dpms)$Pt^{IV}Me_2$(I).

These complexes were present in ~1:1 ratio (40% yield each, based on the methyl group balance.

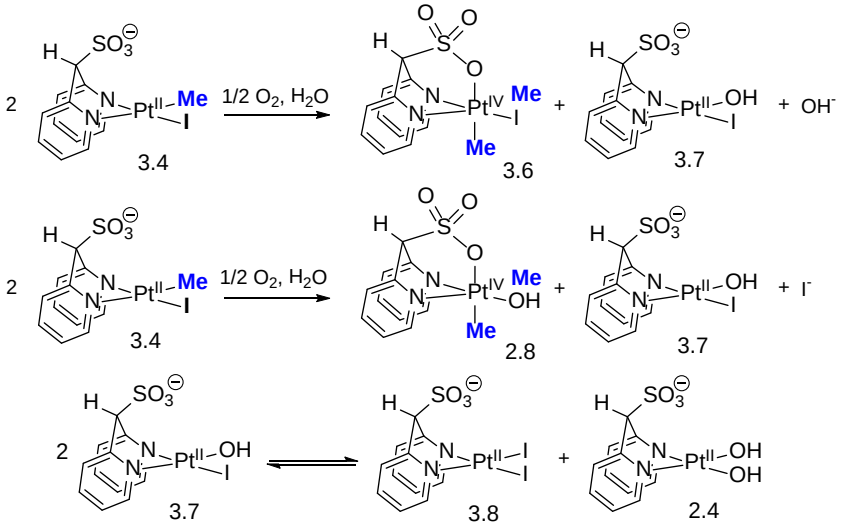

Scheme 3.4. Products of oxidation of K(dpms)Pt^{II}Me(I) in water.

In Chapter 2, Pt-to-Pt methyl group transfer was observed in aerobic oxidation of K(dpms)Pt^{II}Me(OH) at pH $\geq$ 12.0. In addition to *C*$_1$-symmetric (dpms)Pt^{IV}Me$_2$(OH), formation of *C*$_1$-symmetric (dpms)Pt^{IV}Me(OH)$_2$ was also observed under these conditions. Aerobic oxidation of K(dpms)Pt^{II}Me(I) resulted in *C*$_1$-symmetric (dpms)Pt^{IV}**Me$_2$**(X) (X = I, OH) exclusively. This indicates that Pt-to-Pt methyl group transfer is the main reaction direction in K(dpms)Pt^{II}Me(I)/O$_2$ system. The pH of the reaction mixture at the end of oxidation is ~10, consistent with the accumulation of OH$^-$ according to Scheme 3.4.

Identity of *C*$_1$-symmetric (dpms)Pt^{IV}Me$_2$(OH) was confirmed by comparison with the previously reported ^{1}H NMR data, and *C*$_1$-symmetric (dpms)Pt^{IV}(Me)$_2$I was identified by independent synthesis. Reaction of K(dpms)Pt^{II}Me(I) and MeI in water resulted in quantitative formation of *C*$_1$-symmetric (dpms)Pt^{IV}(Me)$_2$I. The product

was isolated by filtration, washed with water, and dried under vacuum to afford analytically pure compound (Scheme 3.5).

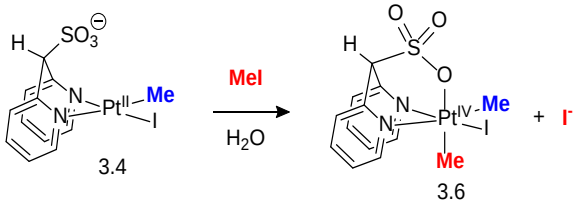

Scheme 3.5 Independent synthesis of *C*$_1$-symmetric (dpms)Pt^{IV}(Me)$_2$I.

Complex **3.6** was characterized by ^{1}H, ^{13}C NMR spectroscopy, ESI-MS, and elemental analysis. In particular, ^{1}H NMR spectrum of this complex shows two distinct Pt^{IV}-CH$_3$ resonances at δ = 1.85 ($^2J_{Pt-H}$ = 66 Hz) and 1.94 ($^2J_{Pt-H}$ = 80 Hz) ppm for equatorial and axial Me group, respectively. The downfield shift of the Pt-methyl groups in (dpms)Pt^{IV}Me$_2$(I) compared to (dpms)Pt^{IV}Me$_2$(OH) (δ DMSO-*d*$_6$: 1.48, $^2J_{PtH}$ = 66 Hz; and 1.64, $^2J_{Pt-H}$ = 80 Hz) is consistent with the presence of the iodide ligand, and its deshielding character. Larger $^2J_{Pt-H}$ coupling constant corresponds to the methyl group *trans* to the sulfonate group.

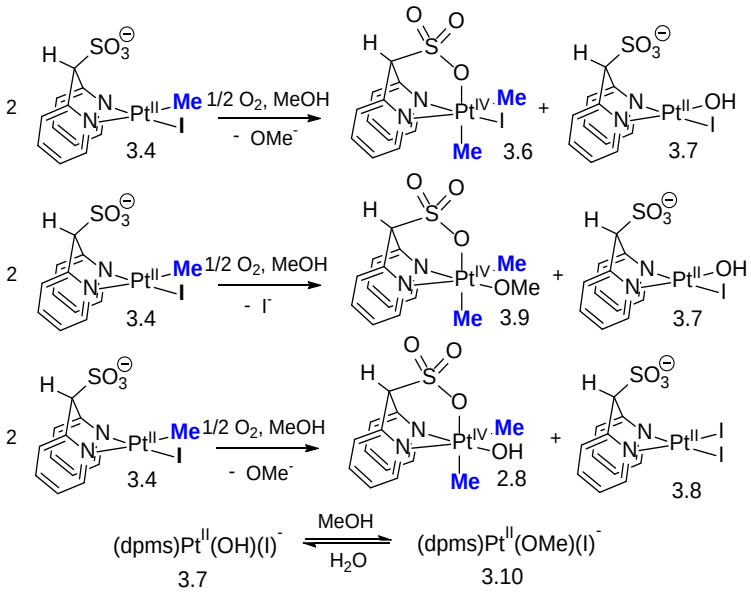

Scheme 3.6 Products of oxidation of K(dpms)Pt^{II}Me(I) in methanol.

Aerobic oxidation of (dpms)$Pt^{II}Me(I)^-$ in MeOH also resulted in formation of Pt-to-Pt methyl group transfer products. The products are accounted for in Scheme 3.6. In addition to *C*$_1$-symmetric (dpms)$Pt^{IV}Me_2(OH)$ and *C*$_1$-symmetric (dpms)$Pt^{IV}Me_2(I)$, *C*$_1$-symmetric (dpms)$Pt^{IV}Me_2(OMe)$ is observed (18, 35, and 26% yield respectively). This observation indicates that (dpms)$Pt^{II}Me(I)^-$ undergoes fast ligand exchange with the solvent (Scheme 3.7) and that Me group transfer is equally fast to either $Pt^{II}Me(I)^-$, $Pt^{II}Me(H_2O)$, or (dpms)$Pt^{II}Me$(MeOH).

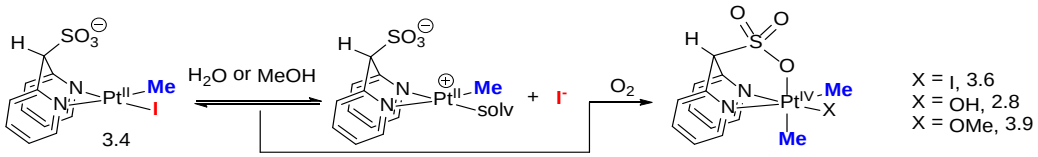

Scheme 3.7 Oxidation of K(dpms)$Pt^{II}Me(I)$ in water and methanol.

When an aqueous or methanoic solution of (dpms)$Pt^{II}Me(I)^-$ was monitored by ^{1}H NMR spectroscopy at room temperature under inert atmosphere, no changes in the ^{1}H NMR spectra were observed over extended period of time. This observation indicates that methyl transfer does not occur between two Pt^{II} species[85], but only under oxidizing conditions.

3.5 Oxidation of K(dpms)$Pt^{II}Me(OH)$ with I_2 and I_3^-

Previously Pt-to-Pt methyl group transfer has been reported in the presence of I_2 as an oxidant.[114,115] In acidic media iodides can be oxidized by O_2 to give I_2 therefore we considered the possibility of I_2 being generated *in situ* according to Eq. 3.1.[116]. Another pathway, leading to I_2 under our reaction conditions might involve oxidation of I^- to I_2 by the hydroperoxo-Pt^{IV} complexes. Oxidation of I^- by hydroperoxo rhodium complexes occurs readily (Eq. 3.2), the rate constants for a variety of MOOH complexes are shown in Table 3.6.[117] According to Scheme 2.34

the reaction pathway leading to *unsym*-(dpms)$Pt^{IV}Me(OH)_2$ involves formation of (dpms)$Pt^{IV}Me(OH)(OOH)$ **2.7**. This intermediate might lead to formation of I_2 followed by Pt-to-Pt methyl group transfer and formation of **2.8** and **3.6**.

$$2\ I^- + O_2 + 4\ H^+ \longrightarrow I_2 + 2\ H_2O$$

Equation 3.1

$$2\ I^- + L(H_2O)RhOOH^{2+} + 3\ H^+ \longrightarrow I_2 + LRh(H_2O)_2{}^{3+} + H_2O$$

Equation 3.2

$LMOOH^{2+}$	k, $M^{-1}\ s^{-1}$
$(H_2O)_5\mathbf{Cr}OOH^{2+}$	988
$(NH_3)_4(H_2O)\mathbf{Co}OOH^{2+}$	100
$(NH_3)_4(H_2O)\mathbf{Rh}OOH^{2+}$	8800

Table 3.3. Aqueous solution, 25 °C, pH ≤ 1.

We investigated the effect of I_2 on the reactivity of (dpms)$Pt^{II}Me(OH_2)$ at pH 5.0. Experiment was performed under an argon, and iodine was dissolved in acetone prior to addition to the reaction mixture to insure homogeneous media. Reaction was complete momentarily upon addition of I_2 and generated C_1-symmetric (dpms)$Pt^{IV}Me_2OH$ in 63 ± 2% yield (Scheme 3.8). In addition presence of (dpms)$Pt^{IV}(Me_{eq})(OH)(I_{ax})$ was observed in ~15% yield, with Pt^{IV}-Me resonance at 2.55 ppm (s, $^2J_{Pt\text{-}H}$ = 62 Hz, 3H).

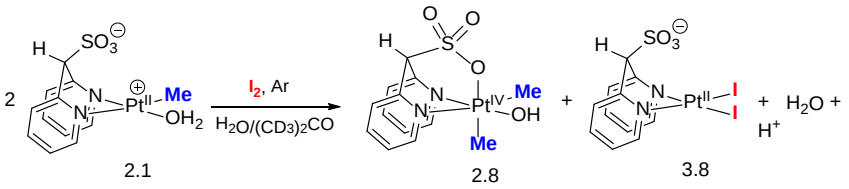

2.1 2.8 3.8

Scheme 3.8 Oxidation of (dpms)$Pt^{II}Me(OH_2)$ with I_2 in water at pH 5.0.

In turn, when I_3^- was used as an oxidant, both C_1-symmetric (dpms)$Pt^{IV}Me_2OH$ and C_1-symmetric (dpms)$Pt^{IV}Me_2I$ were generated in 58 ± 12 and 19 ± 12% yield respectively (Scheme 3.9). These two experiments demonstrate that (L)$Pt^{IV}(Me)_2OH$ is produced due to the methyl group transfer to $Pt^{II}Me$ complex, while (L)$Pt^{IV}(Me)_2I$ is generated due to the presence $Pt^{II}Me(I)^-$. A broad distribution in the yields of dimethyl-Pt(IV) products could be associated with a relatively slow

OH_2/I^- exchange at Pt^{II} center and the different amount of *in situ* generated $(dpms)Pt^{II}Me(I)^-$ (Scheme 3.10).

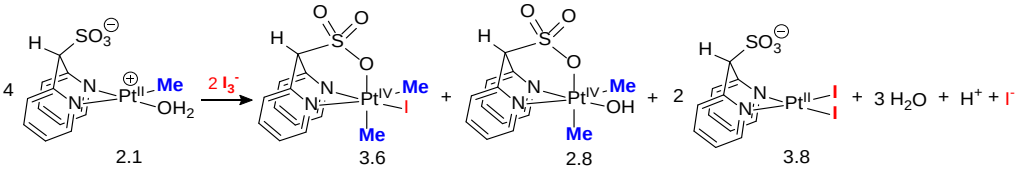

Scheme 3.9 Oxidation of $(dpms)Pt^{II}Me(OH_2)$ with I_3^- in water at pH 5.0.

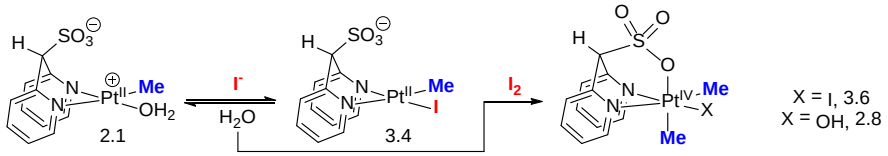

Scheme 3.10 Ligand exchange in oxidation of $(dpms)Pt^{II}Me(OH_2)$ with I_3^- in water at pH 5.0.

Mechanism of reaction of **2.1** with I_2 and I_3^- was studied in more detail. The reaction of **2.1** with I_2 and I_3^- was performed in the presence of TEMPO under ambient light and in the dark. No effect of light was observed and no Me-TEMPO adduct was detected. This indicates that similar to the $(dpms)Pt^{II}Me(OH)^-/O_2$ system at pH 14.0, Me group transfer does not involve radical pathway.

Oxidative addition of I_2, followed by Pt-to-Pt methyl group transfer has been reported in case of bimetallic phosphine supported complexes (P-P = $Me_2PCH_2PMe_2$) (Scheme 3.11). The reaction was proposed to occur via electrophilic attack by iodine at one platinum center, followed by intramolecular Me transfer. Since iodide is a better bridging group, a conformation rearrangement affords the final mixed-valent Pt^{IV}-Pt^{II} complex.[114] This rapid transformation is in contrast to the Me transfer reactions between mononuclear Pt^{IV} and Pt^{II} complexes, which take two days to reach equilibrium.[118] This indicates the unique reactivity of the binuclear system.[114]

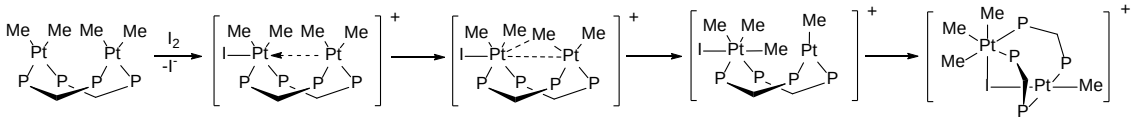

Scheme 3.11 Proposed mechanism for the electrophilic Pt^{IV}-to-Pt^{II} methyl group transfer.

Reaction of diimine-supported Pt^{II} complexes and I_2 leads to formation of the product of oxidative addition, (N-N)$Pt^{IV}Me(X)(I)_2$ (X = Me, Cl). Addition of iodide

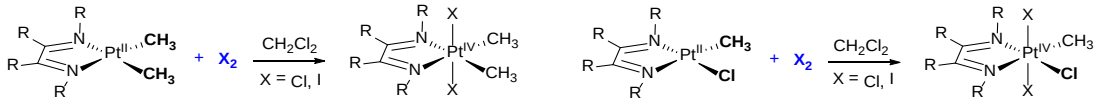

Scheme 3.12 Oxidation of monomethyl- and dimethyl-Pt(II) with Cl_2 and I_2.

ligands *trans* to each other indicates a stepwise process (Scheme 3.12).[115] No methyl group transfer was observed in this system, however, one electron oxidation of (phen)$Pt^{II}Me_2$ by ferrocenium hexafluorophosphate resulted in the presumed formation of Pt^{III}, and disproportionation of the latter via methyl group transfer to form $Pt^{IV}Me_3$ and $Pt^{II}Me$ species.[115]

Based on reaction in Scheme 3.12, formation of (dpms)$Pt^{IV}Me(X)(I)_2^-$, (X = I, OH) **3.14** might be expected in reaction between (dpms)$Pt^{II}Me(X)^-$ and I_2 or I_3^- (Scheme 3.13). Complex **3.14** was never observed under the reaction conditions, possibly due to its high reactivity, however, an analog of **3.14** complex **2.10** have been discussed in Chapter 2 and was detected by ^{1}H NMR spectroscopy.

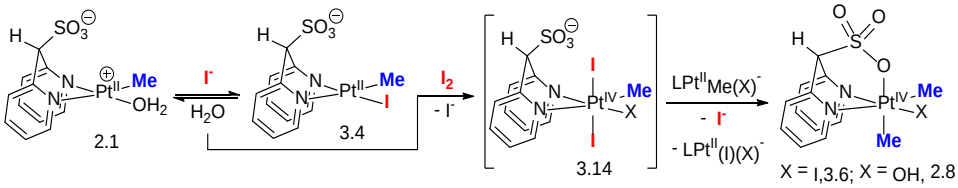

Scheme 3.13 Proposed mechanism for oxidation of (dpms)$Pt^{II}Me(OH_2)$ with I_3^- in water at pH 5.0.

Comparable product distribution in the (dpms)$Pt^{II}Me(I)^-/O_2$ system and (dpms)$Pt^{II}Me(OH_2)/I_3^-$ system indicates that I_2 might act as an oxidant under our reaction conditions. Formation of $Pt^{IV}Me(OH)(OOH)$ has been proposed previously in aerobic oxidation of (dpms)$Pt^{II}Me(OH)^-$, thus, generation of I_2 according to Eq. 3.2 appears to be feasible. Since the rate of oxidation of I^- to I_2 by MOOH is very fast, the

overall rate of reaction in Scheme 3.14 will depend on the rate of formation of (dpms)Pt^{IV}Me(OH)(OOH), and therefore will be similar to the k_{obs} in the presence and in the absence of iodide. This is inconsistent with our experimental observations. In addition, according to the reaction stoichiometry in Eq. 3.2 and Scheme 3.14, formation of *C*$_1$-symmetric-(dpms)Pt^{IV}Me$(OH)_2$ is expected, which is not observed in

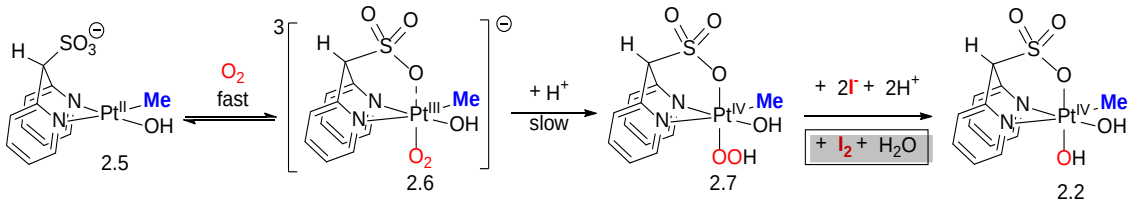

Scheme 3.14 Hypothetic mechanism of formation of I_2 in aerobic oxidation of (dpms)Pt^{II}Me(OH_2).

the unbuffered reaction (Scheme 3.4, 3.6). Formation of I_2 according to Eq. 3.1 is expected to be slower than the time scale of Me transfer reaction, which should result in the formation of *unsym*-(dpms)Pt^{IV}Me$(OH)_2$ as well. Based on our experimental observations, reactivity of (dpms)Pt^{II}Me$(OH_2)/I_3^-(I_2)$ cannot account for the reactivity of (dpms)Pt^{II}Me$(I)^-/O_2$ system.

3.6 Proposed Mechanism of Aerobic Oxidation of Unbuffered (dpms)Pt^{II}Me(I)$^-$

In view of the mechanism of oxidation – methyl group transfer pathway discussed in Chapter 2, we propose that the same mechanism might be responsible for formation of **3.6** and **2.8** in the course of oxidation of **3.4** by O_2. The overall mechanism leading to Pt-to-Pt methyl group transfer product in (dpms)Pt^{II}Me$(I)^-/O_2$ system is shown in Scheme 3.15. The N,O-coordinated isomer (*κN,κO*-dpms)Pt^{II}Me$(I)^-$ reacts with O_2 to form (dpms)Pt^{IV}Me(I)(OOH), where the methyl

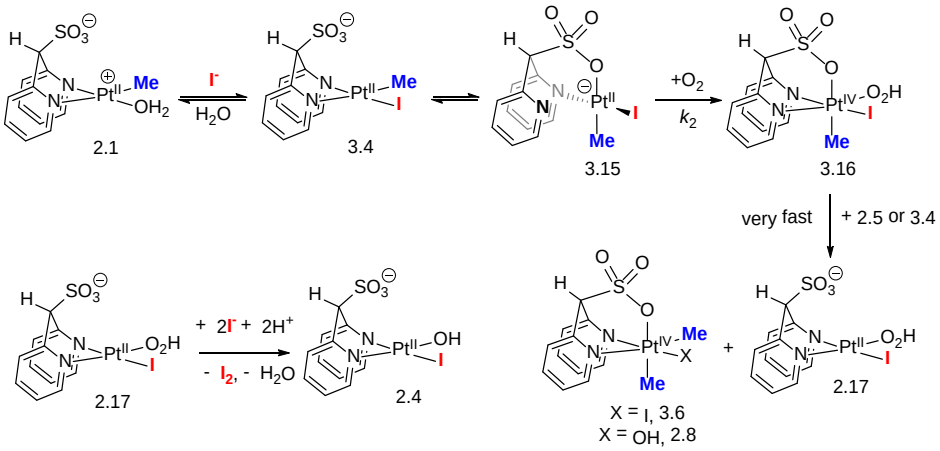

Scheme 3.15 Proposed mechanism for Pt-to-Pt methyl group transfer upon oxidation of K(dpms)Pt^{II}Me(I) with O_2 in unbuffered solution.

group is in the axial position. Methyl group is rapidly transferred from (dpms)Pt^{IV}Me(I)(OOH) to (dpms)Pt^{II}Me(X)$^-$, generating dimethyl-Pt(IV) and Pt^{II}-peroxo complex. The peroxo complex can oxidize I^- to I_2, and the latter could produce more Pt^{IV}Me species. Oxidation of (dpms)Pt^{II}Me(I)$^-$ with O_2 is proposed to be the rate limiting step.

Formation of (dpms)Pt^{IV}Me(I)(OH), followed by isomerization to (dpms)$Pt^{IV}Me_{ax}$(I)(OH), with the Me group in the axial position and Me group transfer to Pt^{II}, is not a likely mechanism. Similar isomerization was considered in case of (dpms)Pt^{IV}Me$(OH)_2$ complex in Chapter 2, but was concluded to be a non-competitive reaction direction.

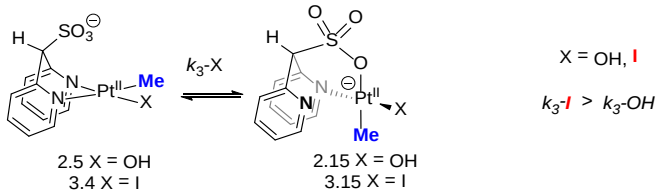

Figure 3.1 Isomerization of K(dpms)Pt^{II}Me(I) and K(dpms)Pt^{II}Me(OH).

The lack of monomethyl-Pt^{IV} complexes in Scheme 3.4 and 3.6 indicates that Pt-to-Pt Me group transfer is a preferred reaction direction in the unbuffered

K(dpms)Pt^{II}Me(I)/O_2 system. As one of the possible explanations to this fact, isomerization of **3.4** to **3.15** may be much faster than an isomerization of **2.5** to **2.15** (Figure 3.1) under analogous conditions. Indeed, both CH_3 and I are stronger *trans*-effect ligands than OH,[119] weakening the Pt-py bond *trans* to I and/or CH_3. This induces greater lability of K(dpms)Pt^{II}Me(I) species (Figure 3.1) and results in selective formation of Me group transfer product.

3.7 Aerobic Oxidation of (dpms)Pt^{II}Me(I)$^-$ in Buffered Solutions

3.7.1 The Effect of [I^-] on Reactivity of K(dpms)Pt^{II}Me(I) at pH 6.5

Since oxidation of K(dpms)Pt^{II}Me(I) and O_2 in H_2O leads to a change of the reaction pH, we also performed oxidation in buffered solutions. Initial mechanistic studies began with the investigation of the effect of [I^-] on the rate of oxidation of K(dpms)Pt^{II}Me(I) with dioxygen in a phosphate buffer ($H_2PO_4^-$/HPO_4^{2-}) at pH 6.5. As was discussed above, these anions are unreactive with (dpms)Pt^{II}Me(OH_2). The kinetic experiments were performed with: 1) 1.0 equiv. of I^-, and 2) 10.0 equiv. of I^-. The reaction mixtures were stirred vigorously under oxygen atmosphere in temperature controlled bath at 21.0 ºC, aliquots of the reaction mixture were collected every 5-15 minutes, and immediately analyzed by ^{1}H NMR spectroscopy. Kinetic monitoring of disappearance of Pt^{II} showed formation of a new short-lived specie (Scheme 3.16). The new complex has a Pt^{IV}-Me resonance at 2.76 ppm (s, $^2J_{Pt\text{-}H}$ = 65 Hz, 3H) with ^{195}Pt satellites. Aromatic region shows eight multiplets, consistent with an unsymmetrical complex. Selective NOE revealed transfer of nuclear spin polarization between resonance at 2.76 ppm, and one of the *ortho*-pyridine hydrogens of the dpms ligand at 8.45 ppm in 3% (Figure 3.2), indicating that the signal at 2.76

ppm corresponds to the equatorial Me group. The proposed structure of the new complex is (dpms)$Pt^{IV}(Me_{eq})(I)(OH)$, **3.11** its identity was confirmed by ESI-MS.

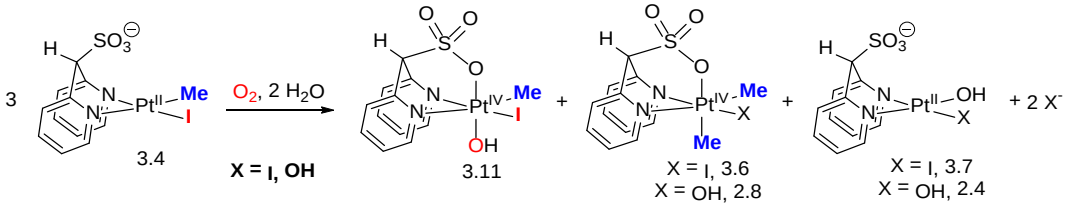

Scheme 3.16 Oxidation of K(dpms)Pt^{II}Me(I) with O_2 in water at pH 6.5.

A control experiment was conducted in order to establish whether $H_2PO_4^-$ /HPO_4^{2-} anions in the buffer are responsible for formation of the new complex, or whether it is an effect of solution pH. When oxidation of K(dpms)Pt^{II}Me(I) was performed in water in the presence of 3 equiv. of acetic acid-d_4, formation of the same (dpms)$Pt^{IV}(Me_{eq})(I)(OH)$ specie was observed in 45% yield. Therefore, the

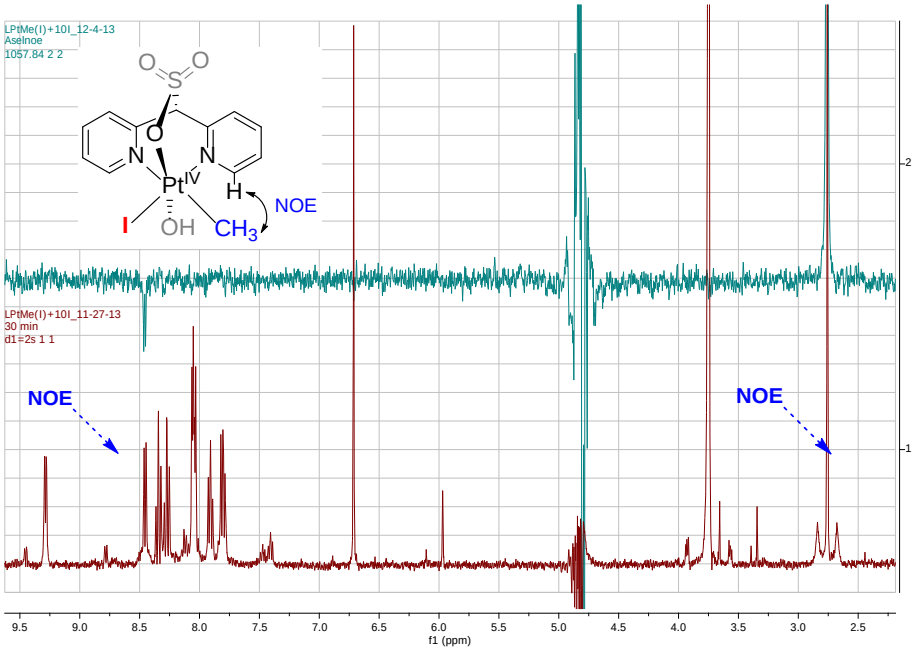

Figure 3.2 Selective NOE of (dpms)Pt^{IV}Me(I)OH in H_2O/D_2O.

difference in the product distribution with and without control of pH can be explained by accumulation of OH^- in the unbuffered solution in the course of oxidation (Scheme 3.4 and 3.6). Higher pH was shown to favor Pt-to-Pt methyl group

transfer reactivity (Chapter 2). In acidic solution, (dpms)$Pt^{IV}(Me_{eq})(I)(OH)$ becomes the major product (Scheme 3.17).

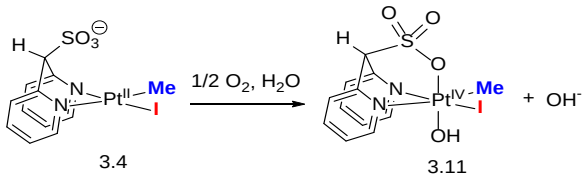

Scheme 3.17 Formation of (dpms)Pt^{II}Me(I)OH in water.

Conversion (%) / Reaction Time	Pt^{IV}**Me**(I)OH (%)	Pt^{IV}**Me**$(OH)_2$ (%)	Pt^{IV}**Me**$_2$(X) (%)	Other Products
67 / 20 min	59	8	0	0
100 / 1 day	9	35	X=OH, 6%; X=I, 25%	2.15 ppm=15%; 1.92 ppm=10%

Table 3.4 Product distribution in reaction between K(dpms)Pt^{II}Me(OH), 1.0 equiv. KI and O_2 in water at pH 6.5, after 20 min, entry 1; and after 1 day, entry 2.

The maximum observed yield of (dpms)$Pt^{IV}(Me_{eq})(I)(OH)$ under kinetic conditions was 84 ±1% after approximately 30 min in reactions with either one or ten equiv. of KI. Further monitoring shows decrease in the amount of (dpms)$Pt^{IV}(Me_{eq})(I)(OH)$, along with formation of precipitate – (dpms)$Pt^{IV}Me_2(I)$ over the course of an hour. When the solution was left overnight, further decrease in the fraction of $LPt^{IV}(Me_{eq})(I)(OH)$, with concomitant formation of LPt^{IV}**Me**$(OH)_2$ and LPt^{IV}**Me**$_2$(X) (Table 3.4). In addition, presence of two new unidentified species at 2.15 ppm (s, $^2J_{PtH}$ = 80 Hz) and 1.92 ppm (s, $^2J_{PtH}$ = 66 Hz) was detected. Formation of LPt^{IV}**Me**$(OH)_2$ and disappearance of (dpms)$Pt^{IV}(Me_{eq})(I)(OH)$ **3.11** implies an iodide ligand exchange.

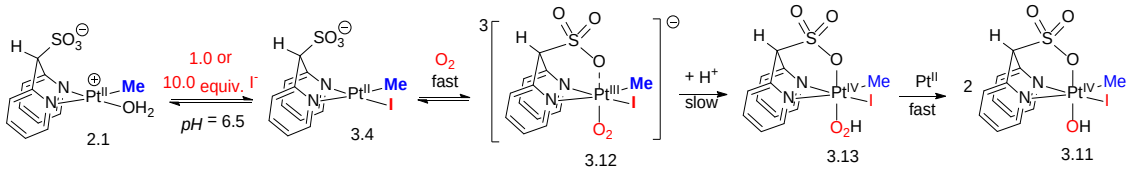

Scheme 3.18 Proposed mechanism for formation of (dpms)Pt^{IV}Me(I)OH at pH 6.5.

Conditions	$LPt^{IV}\mathbf{Me}(OH)_2$: $LPt^{IV}\mathbf{Me}_2(OH)$ Ratio	$t_{1/2}$, min	Reaction Order [SM]
pH 5.9, no I^-	97.0 : 1	34.5 ± 1.5	1
pH 6.5, 1 equiv. I^-	2.2 : 1	12.8 ± 0.4	1
pH 6.5, 10 equiv. I^-	2.3 : 1	12.5 ± 0.1	1

Table 3.5 Half-life and reaction order in oxidation of $(dpms)Pt^{II}Me(OH_2)$ with O_2 in water at pH 6 in the absence and the presence of 1 equiv. and 10 equiv. of KI.

From Chapter 2, the reaction half-life for oxidation of $K(dpmsPt^{II}Me(OH)$ with O_2 at pH 5.9 was determined to be $t_{1/2}$ = 34.5 ± 1.5 min, with $LPt^{IV}\mathbf{Me}(OH)_2$ being the major product. The half-life of oxidation of $K(dpms)Pt^{II}Me(I)$ at pH 6.5 is independent on the concentration of iodide ($t_{1/2}$ = 12.8 ± 0.4 and 12.5 ± 0.1 min with 1 and 10 equiv. of iodide respectively), and is ~2.7 times faster than $K(dpms)Pt^{II}Me(OH)/O_2$/pH 5.9 system (Table 3.4).

Disappearance of $K(dpms)Pt^{II}Me(I)$, follows 1st-order kinetics, with $(dpms)Pt^{IV}(Me_{eq})(I)(OH)$ as the initial product. Therefore, we propose that $LPt^{IV}(Me_{eq})(I)(OH)$ is formed according to the mechanism in Scheme 3.18, analogous to $(dpms)Pt^{IV}\mathbf{Me}(OH)_2$.

Overall, in the absence of a buffer, dimethyl-Pt(IV) complexes are the main products of reaction between $K(dpms)Pt^{II}Me(I)$ and O_2, due to the increase in the reaction pH , while in the presence of weakly acidic buffer, formation of monomethyl-Pt(IV) complex is predominant reaction direction.

3.7.2 Oxidation of $K(dpms)Pt^{II}Me(OH)$ at pH 8.0 – 12.0 with and without KI

The effect of KI additives on the reaction $K(dpms)Pt^{II}Me(I)$ and O_2 in water was studied in the pH range 8.0-12.0. Oxidation of $K(dpms)Pt^{II}Me(OH)$ with air was performed in the buffer solutions at pH 8.0, 10.0, and 12.0 in the absence of stirring (NMR tube). The disappearance of the starting material was monitored by ^1H NMR

spectroscopy over several days. Product summary of the reaction with and without iodide is shown in Table 3.5. With higher pH the fraction of C_1-symmetric (dpms)Pt^{IV}**Me$_2$**(OH) increases both in the presence and in the absence of KI. Formation of (dpms)Pt^{IV}Me(I)OH and (dpms)Pt^{IV}**Me$_2$**(I) was not observed.

C_1-symmetric (dpms)Pt^{IV}**Me$_2$**(OH) complex was produced in slightly higher yield in the presence of I^-. The most significant effect of iodide was observed at pH 8.0. At this pH the (dpms)Pt^{II}Me(OH)$^-$ to (dpms)Pt^{II}Me(OH_2) ratio is ~4:6, based on the pK_a of (dpms)Pt^{II}Me(OH_2), therefore both (dpms)Pt^{II}Me(OH)$^-$ and (dpms)Pt^{II}Me(I)$^-$ are expected in solution. Presence of (dpms)Pt^{II}Me(I)$^-$ is responsible for faster Me transfer reactivity. At pH 10.0, anionic (dpms)Pt^{II}Me(OH)$^-$ is the dominant specie (~99%) that does not produce (dpms)Pt^{II}Me(I)$^-$, which explains small effect of added iodide on the yield of (dpms)Pt^{IV}**Me$_2$**(OH). Finally, the absence of (dpms)Pt^{IV}**Me$_2$**(I) could be explained by lower nucleophilicity of (dpms)Pt^{II}Me(I)$^-$ than (dpms)Pt^{II}Me(OH)$^-$.

Buffer pH	Conversion (%) / Reaction time	LPt^{IV}**Me**$(OH)_2$ (%)	LPt^{IV}**Me$_2$**(OH) (%)
pH 8.0, 1 equiv. I^-	100 / 1 day	84	16
pH 8.0	100 / 1 day	95	5
pH 10.0, 1 equiv. I^-	95 / 2 days	77	18
pH 10.0	99 / 2 days	86	13
pH 12.0, 1 equiv. I^-	97 / 3 days	48	49
pH 12.0	92 / 2 days	51	41

Table 3.6 Oxidation of K(dpms)Pt^{II}Me(I) and O_2 in water at pH 8.0, 10.0, and 12.0 in the presence and in the absence of KI.

Overall, the presence of I^- affects methyl group transfer reactivity at pH 6 – 10. The equilibrium between (dpms)Pt^{II}Me(OH_2) and K(dpms)Pt^{II}Me(I) governs

which pathway becomes predominant: oxidation *vs*. Me-group transfer. When iodide is present, Pt-to-Pt methyl group transfer becomes viable at lower pH values.

3.8 Attempted Hydrocarbyl Group Transfer, R = C_2H_4, Ph, C_2H_4NMe

In order to learn more about the substrate scope of Pt-to-Pt hydrocarbyl group transfer, aerobic oxidations have been attempted with the following complexes: (dpms)$Pt^{II}Ph(OH_2)$, (dpms)$Pt^{II}(\eta^2\text{-}C_2H_4)(OH)$ and (dpms)$Pt^{II}(C_2H_4NHMe\text{-}kC,kN)$. None of these complexes was able to generate the product of R-group transfer. Formation of either air stable halide-derivatives or products of typical aerobic oxidation have occurred. For detailed discussion refer to Experimental Section.

3.9 Summary and Conclusions

Generation of several new anionic (dpms)$Pt^{II}Me(X)^-$ complexes was achieved in water via a reversible ligand exchange reaction between (dpms)$Pt^{II}Me(OH_2)$ and NaX or KX (where X = Cl, Br, I, OAc). The equilibrium constant for aqua ligand exchange decreased in the series: X = I > Br > Cl > AcO. No ligand exchange was observed in case of phosphates and carbonate anions $H_2PO_4^-$, HPO_4^{2-}, HCO_3^-, and CO_3^{2-}. Aerobic oxidation of aqueous solutions of equilibrated mixtures of (dpms)$Pt^{II}Me(OH_2)$ and (dpms)$Pt^{II}Me(X)^-$ involved either oxidation of the former complex in the case of X = Cl, Br, or both (dpms)$Pt^{II}Me(OH_2)$ and (dpms)$Pt^{II}Me(X)^-$ in the case of X = OAc, I. When X = I formation of products resulting from Pt-to-Pt methyl group transfer is the main reaction direction in unbuffered solutions. This reactivity may be important for the development of systems for catalytic methane to ethane conversion.

Oxidation of (dpms)$Pt^{II}MeI^-$ with O_2 in a phosphate buffer at pH 6.5 resulted in initial fast formation of (dpms)Pt^{IV}Me(I)(OH), followed by its slow decomposition. Kinetics of oxidation at pH ~6 showed that the rate of oxidation of (dpms)$Pt^{II}Me(I)^-$ is faster than that of (dpms)$Pt^{II}Me(OH_2)$.

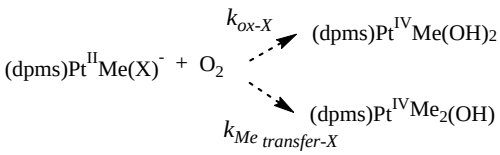

X = OH, **I**	Conditions
$k_{ox\text{-}I} > k_{ox\text{-}OH}$	pH 6.5
$k_{Me\ transfer\text{-}I} > k_{Me\ transfer\text{-}OH}$	No additives

Figure 3.3 Comparison of aerobic reactivity of K(dpms)Pt^{II}Me(I) and K(dpms)Pt^{II}Me(OH).

In conclusion, the structure - reactivity study presented in this chapter revealed that not only solution pH, but also the nature of the ligand X can direct the reactivity of (dpms)$Pt^{II}Me(X)^-$ complexes toward either oxidation or oxidation – methyl group transfer pathway.

3.10 Experimental Section

Preparation of K(dpms)Pt^{II}Me(X) (X^- = F^-, Cl^-, Br^-, I^-, OAc^-, $H_2PO_4^-$, HPO_4^{2-}, HCO_3^-, CO_3^{2-})

General procedure for preparation of K(dpms)Pt^{II}Me(X)

The general Scheme for preparation of monomethylplatinum(II) complexes K(dpms)Pt^{II}Me(X) where X^- = F^-, Cl^-, Br^-, I^-, OAc^-, $H_2PO_4^-$, HPO_4^{2-}, HCO_3^-, CO_3^{2-} is shown in Scheme 3.2.

Method A. Air tight NMR tube was charged in the argon-filled glove box with 59.7 mM stock solution of K(dpms)PtMe(OH_2)[79] in D_2O (20.9 μmol, 0.35 mL) and 1.0 equiv. of appropriate X^-. All solids were allowed to dissolve, and establishment of the equilibrium was monitored by ^1H NMR spectroscopy.

Method B. A Schlenk flask, equipped with a magnetic stir bar, was charged with K(dpms)$Pt(Me)_2$[99] and deoxygenated H_2O in the argon-filled glove box. Schlenk

flask was taken out of the box and the reaction was kept in the water bath at 40 °C overnight to give K(dpms)PtMe(OH) (**2.5**) in quantitative yield. Schlenk flask was brought back into the glove box, phosphate buffer $H_2PO_4^-/HPO_4^{2-}$, (pH 6.0) or citrate/phosphate buffer (pH 2 - 6) was added , followed by addition of 1.0 eq. of the corresponding X^-. All solids were allowed to dissolve and equilibrium was monitored by ^{1}H NMR spectroscopy. Unless otherwise mentioned, K(dpms)Pt^{II}Me(X) complexes were prepared according to method A.

In case of $X^- = F^-$ (2 days in D_2O), $H_2PO_4^-$ (5 days in D_2O, 2 days in CD_3OD), HPO_4^{2-} (1 day in D_2O, 5 days in CD_3OD), HCO_3^- (4 days in D_2O), CO_3^{2-} (3 days in D_2O) no ligand substitution was observed. Time of attempted ligand exchange is shown in parenthesis. For $X^- = Cl^-$, Br^-, I^-, OAc^-, observed rate of substitution is $I^- > Br^- > Cl^- > AcO^-$.

Preparation of K(dpms)Pt^{II}Me(Cl) (3.2)

NaCl (1.2 mg, 20.9 µmol). After three days of reaction equilibrium was established and the starting material to product ratio (dpms)Pt^{II}Me(OH_2): of K(dpms)Pt^{II}Me(Cl) was 1:2.4. ^{1}H NMR (D_2O, 22 °C), δ: 0.84 (s, 3H, Pt-*CH*$_3$, $^2J_{PtH}$ = 70 Hz), 5.90 (s, 1H, C*H*-SO_3), 7.35 (m, 1H), 7.46 (m, 1H), 7.72 (m, 1H), 7.75 (m, 1H), 7.99 (td, *J* = 1.3, 7.7, 8.5 Hz, 1H), 8.04 (td, *J* = 1.3, 7.7, 8.5 Hz, 1H), 8.77 (vd, ^3J = 5.7 Hz, 1H), 8.66 (vd, ^3J = 5.4 Hz, 1H).

ESI-MS analysis for [(dpms-*d*)$Pt^{II}CH_3$(Cl)]$^-$: m/z = 494.989, calculated for $C_{12}H_{11}DClN_2O_3PtS$ 494.99677.

Preparation of K(dpms)Pt^{II}Me(Br) (3.3)

KBr (2.5 mg, 20.9 μmol). Equilibrium was established after five days and the starting material to product ratio K(dpms)PtMe(H_2O): of K(dpms)PtMe(Br) was 1:3.1. ^{1}H NMR (D_2O, 22 ^oC), δ: 0.89 (s, 3H, Pt-*CH*$_3$, $^2J_{PtH}$ = 72 Hz), 5.90 (s, C*H*-SO_3, 1H), 7.37 (ddd, *J* = 1.2, 6.6, 7.7 Hz, 1H), 7.46 (ddd, *J* = 1.2, 6.6, 7.7 Hz, 1H), 7.74 (d, ^3J = 7.7 Hz, 2H), 7.97 (td, *J* = 1.2, 8.0 Hz, 1H), 8.05 (td, *J* = 1.2, 8.0 Hz, 1H), 8.76 (d, ^3J = 6.0 Hz, 1H), 9.15 (dd, *J* = 1.2, 5.6 Hz, 1H).

ESI-MS analysis for [(dpms-*d*)Pt^{II}CH_3(Br)]$^-$: m/z = 538.939, calculated for $C_{12}H_{11}DBrN_2O_3PtS$ 538.94625.

Preparation of K(dpms)Pt^{II}Me(I) (3.4)

Synthesis performed according to the general procedure for preparation of K(dpms)Pt^{II}Me(X) using 1.0 eq. of KI (3.5 mg, 20.9 μmol). Complex K(dpms)PtMe(I) can also be prepared by reaction between anionic monomehtylatinum(II)hydroxide complex K(dpms)PtMe(OH) (**2.5**) and Et_3NI. Schlenk flask was brought back into the glove box and equimolar amount of Et_3NI (2.4 mg, 10.3 μmol) was added. Solvent was evaporated and the solid was dried at 50 ^oC under vacuum for 2 hours to remove residual Et_3N.

^{1}H NMR (D_2O, 22 ^oC), δ: 0.97 (s, 3H, Pt-C*H*$_3$, $^2J_{PtH}$ = 72.5 Hz), 5.93 (s, C*H*-SO_3, 1H), 7.37 (ddd, *J* = 1.4, 5.6, 7.7 Hz, 1H), 7.44 (ddd *J* = 1.4, 5.6, 7.8 Hz, 1H), 7.77 (m, 2H), 7.99 (td, *J* = 1.6, 7.8 Hz, 1H), 8.10 (td, *J* = 1.6, 7.8 Hz, 1H), 8.74 (dd, *J* = 1.2, 5.8 Hz, 1H), 9.41 (dd, *J* = 1.2, 5.7 Hz, 1H).

^{1}H NMR (MeOD, 22 ^oC), δ: 1.12 (s, 3H, Pt-*CH*$_3$, $^2J_{PtH}$ = 74 Hz), 6.85 (s, C*H*-SO_3, 1H), 7.32 (ddd, *J* = 1.2, 5.5, 7.7 Hz, 1H), 7.39 (ddd, *J* = 1.3, 5.7, 8.0 Hz, 1H),

7.95 (td, J = 1.6, 7.9 Hz, 1H), 8.08 (td, J = 1.6, 7.9 Hz, 1H), 8.45 (d, ^3J = 8.1 Hz, 1H), 8.52 (d, ^3J = 8.1 Hz, 1H), 8.69 (d, ^3J = 5.8 Hz, 1H), 9.25 (m, 1H). *Endo* conformer ^{1}H NMR(CD_3OD): δ 1.02 (s, $^2J_{PtH}$ = 72, Pt-CH_3), 5.88 (s, CH), 8.18 (m, 1H, py-H4), 8.76 (d, overlaps with satellites of *exo* diastereomer, py-H3), 8.82 (d, J = 5.9 Hz, py-H3), 8.89 (d, J = 5.9 Hz, py-H6), 9.64 (d, J = 5.9 Hz, py-H6). Second H4 and both H5 overlap with exo diastereomer and (dpms)Pt^{IV}Me(OH)Me.

^{13}C NMR (151 MHz, H_2O/D_2O, 22 ºC) δ: 155.15, 152.46, 151.32, 150.02, 139.58, 139.53, 129.84, 129.01, 126.90, 126.22, 77.24, -21.39 (^{195}PtC satellites were not detected).

ESI-MS analysis [(dpms)$PtCH_3(I)]^-$: m/z = 585.930, calculated for $C_{12}H_{12}IN_2O_3PtS$ 585.92610.

Found: C, 21.89; H, 1.87; N, 4.11. Calculated for $C_{12}H_{12}IKN_2O_3PtS\times1/5KI$: C, 21.89; H, 1.84; N, 4.25.

Preparation of K(dpms)Pt^{II}Me(OAc) (3.5)

CH_3COOK (2.0 mg, 20.9 µmol). After 5 days of reaction time product was present in 1:0.9 ratio with the starting material. ^{1}H NMR (D_2O, 22ºC), δ: 0.77 (s, 3H, Pt-CH_3, $^2J_{PtH}$ = 70 Hz), 5.90 (s, 1H, CH-SO_3), 7.30 (m, 1H), 7.48 (m, 1H), 7.68 (d, ^3J = 7.1 Hz, 1H), 7.78 (d, ^3J = 7.8 Hz, 1H), 7.98-8.09 (overlapping resonances m, 2H), 8.51 (d, ^3J = 5.2 Hz, 1H), 8.81 (d, ^3J = 5.9 Hz, 1H).

Independent Synthesis of (dpms)$Pt^{IV}Me_2$(I) (3.6)

Air tight NMR tube was charged in the argon-filled glove box with a solution of K(dpms)Pt^{II}Me(I) (54 µmol) in acetone, and MeI (7.6 mg, 54 µmol). Formation of the white precipitate occurred immediately, which was collected by filtration, washed with fresh H_2O and dried under vacuum.

^{1}H NMR (dmso-*d*$_6$) (**6**), δ: 1.85 (s, 3H, Pt-*CH*$_3$, $^{2}J_{PtH}$ = 66 Hz), 1.95 (s, 3H, Pt-*CH*$_3$, $^{2}J_{PtH}$ = 80 Hz), 6.64 (s, 1H, C*H*-SO$_3$), 7.76 (m, 1H), 7.83 (ddd, *J* = 1.5, 5.7, 7.9 Hz, 1H), 8.01 (d, ^{3}J = 7.9 Hz, 1H), 8.05 (d, ^{3}J = 7.9 Hz, 1H), 8.27 (td, *J* = 1.5, 8.0 Hz, 1H), 8.34 (td, *J* = 1.5, 8.5 Hz, 1H), 8.55 (d, ^{3}J = 5.7 Hz, $^{3}J_{PtH}$ = 22 Hz, 1H), 9.07 (d, 1H, ^{3}J = 5.6 Hz, $^{3}J_{PtH}$ = 8.0 Hz, 1H). Small admixture of *sym*- and *unsym*-(dpms)Pt^{IV}Me$_2$(OH) are observed as well due to oxidation of K(dpms)Pt^{II}Me$_2$.

^{13}C NMR (151 MHz, DMSO) δ: 151.25, 151.04, 150.78, 148.47, 142.56, 141.46, 128.67, 127.94, 127.49, 126.63, 71.27, -6.12 (s, $^{1}J_{195PtC}$ = 545 Hz), -6.91 (s, $^{1}J_{195PtC}$ = 621 Hz).

Found: H, 2.35; C, 25.75; N, 4.54. Calculated for C$_{13}$H$_{15}$IN$_2$O$_3$PtS, H, 2.52; C, 25.95; N, 4.66.

Identification of (dpms)Pt^{IV}Me(I)OH (3.11)

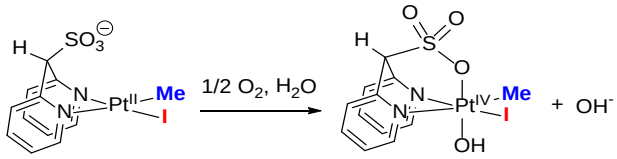

Oxidation of aqueous (dpms)Pt^{II}Me(I)$^{-}$ with O$_2$ in a buffer solutions at pH 6.5, resulted in formation of new specie, which was identified as (dpms)Pt^{IV}Me(I)OH by selective NOE and ESI-MS.

^{1}H NMR (400 MHz, D$_2$O) δ 9.29 (vd, ^{3}J = 5.7 Hz, 1H), 8.45 (vd, ^{3}J = 6.6 Hz, 1H), 8.34 (dt, *J* = 1.5, 8.7 Hz, 1H), 8.27 (dt, *J* = 1.5, 8.7 Hz, 1H), 8.02-8.08 (overlapping d, 2H), 7.91 (m, 1H), 7.80 (m, 1H), 6.71 (s, 1H, C*H*-SO$_3$), 2.76 (s, $^{2}J_{PtH}$ = 65 Hz, 3H, Pt-C*H*$_3$).

ESI-MS analysis showed presence of Pt^{IV} compounds with deuterated bridging CH groups: ((dpms-*d*)Pt^{IV}Me(I)(OH)·H^{+}) (**3.11-*d***·H^{+}) m/z = 604.986,

calculated for $C_{12}H_{13}DIN_2O_4PtS$, 642.94295; ((dpms-*d*)Pt^{IV}Me(I)(OH)·K^+) (**3.11-*d***·K^+) m/z = 642.911, calculated for $C_{12}H_{12}DIKN_2O_4PtS$, 642.89883;

ESI-MS negative mode analysis showed presence of Pt^{IV} compounds: ((dpms)$Pt^{IV}Me_2(OH)(H_2PO_4)^-$) m/z = 587.992, calculated for $C_{13}H_{18}N_2O_8PPtS$, 588.01692; ((dpms)$Pt^{IV}Me_2(I)(H_2PO_4)^-$) m/z = 697.944, calculated for $C_{13}H_{17}IN_2O_7PPtS$, 697.91865.

Calculation of equilibrium constant *Keq*

Concentration of K(dpms)$Pt^{II}Me(OH_2)$ and K(dpms)$Pt^{II}Me(OH)$ was determined by ^{1}H NMR spectroscopy by integration of C_3-*H* or C_6-*H* protons of the dpms ligand.

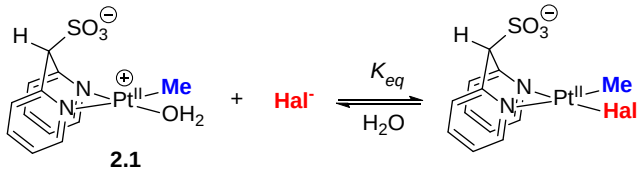

3.2 Hal = Cl
3.3 Hal = Br
3.5 Hal = OAc

Initial concentrtaion	C_0 = 59.8 mM	C_0 = 59.8 mM	C_0 = 0 mM
Concentrtaion at equilibrium	C_{eq} = 59.8 - x mM	C_{eq} = 59.8 - x mM	C_{eq} = x mM

$$K_{eq} = \frac{[LPtMe(X)^-]}{[LPtMe(OH_2)][X^-]} = \frac{x}{(0.0598 - x)^2}$$

Equation 3.3

x	K_{eq}
Cl: 2.4 C_0/3.4	136
Br: 3.1 C_0/4.1	213
AcO: 0.9 C_0/1.9	29

Table 3.7 Calculated K_{eq}.

Attempted Oxidation of K(dpms)Pt^{II}Me(X) (X^- = Cl^-, Br^-, OAc^-)

NMR tubes containing previously prepared solutions of monomethyl-platinum(II) complexes (**3.2**, **3.3** and **3.5**) were exposed to air, capped, and left on the rotator until oxidation was complete. According to the 1H NMR spectra, oxidation of (dpms)$Pt^{II}Me(OH_2)$ occurred instead of oxidation of **3.2**, and **3.3** since the only oxidation product was *unsym*-(dpms)$Pt^{IV}Me(OH)_2$[79].

Oxidation of (**3.5**) generated small amount of (dpms)Pt^{IV}Me(OAc)OH, 7% in D_2O and 22% in CD_3OD. Increasing concentration of OAc^- tenfold did not result in appreciable amount of the desired product (dpms)Pt^{IV}Me(OAc)OH. δ (D_2O): Pt^{IV}-C*H*$_3$, 2.62, $^2J_{PtH}$ = 64 Hz; δ (CD_3OD) 2.58 (Pt^{IV}-C*H*$_3$, $^2J_{PtH}$ = 68 Hz).

Oxidation of Unbuffered K(dpms)Pt^{II}Me(I) in D_2O

NMR tube, containing previously prepared 59.7 mM solution of K(dpms)Pt^{II}Me(I) in D_2O was opened and air was bubbled through the reaction mixture via syringe. NMR tube was capped and placed on the rotator. After approximately three hours, abundant white precipitate began to form. Precipitate was centrifuged from the aqueous phase, washed with H_2O and dried under high vacuum for 30 min. Precipitate has low solubility, but can be dissolved in dmso-*d*$_6$. Product was identified as (dpms)$Pt^{IV}Me_2$(I) (**3.6**), isolated yield 40%. Aqueous phase contained (dpms)$Pt^{IV}Me_2$(OH)[79] (**2.8**, NMR yield 40%) as well as several anionic platinum(II) containing species, which were detected by ESI-MS negative mode (Scheme 3.4).

^{1}H NMR of the reaction mixture after oxidation in DMSO-*d*$_6$ shows presence of two Pt^{IV}Me resonances, which were assigned to (dpms)$Pt^{IV}Me_2$(I), δ: 1.85 (s, 3H, Pt-*CH*$_3$, $^2J_{PtH}$ = 66 Hz), 1.95 (s, 3H, Pt-*CH*$_3$, $^2J_{PtH}$ = 80 Hz), aromatic region very complex.

ESI-MS analysis showed presence of the following Pt^{IV} compounds with deuterated bridging C*D*-SO_3 groups: ((dpms)$Pt^{IV}Me_2$(OH)·K^+) (**2.8**-*d*·K^+) m/z = 531.019, calculated for (**7**-*d*·K^+) $C_{13}H_{15}DKN_2O_4PtS$, 531.01774; ((dpms)$Pt^{IV}Me_2$(I)·K^+) (**3.6**-*d*·K^+) with deuterated bridging CH group m/z = 640.911,

calculated for (**3.6**-*d*·K^+), $C_{13}H_{14}DIKN_2O_3PtS$, 640.91947. In the negative mode, anionic Pt^{II} compounds have been detected with deuterated bridging CH group: ((dpms-*d*)Pt$(OH)_2)^-$, m/z = 479.036, calculated for $C_{11}H_{10}DN_2O_5PtS$ 479.00982; ((dpms-*d*)Pt(OH)I)$^-$, m/z = 589.930, calculated for $C_{11}H_9DIN_2O_4PtS$, 588.91156; ((dpms-*d*)Pt$(I)_2)^-$ m/z = 698.835, calculated for $C_{11}H_8DI_2N_2O_3PtS$, 698.81330.

Oxidation of Unbuffered K(dpms)Pt^{II}Me(I) in MeOD

A 5 mL Schlenk flask equipped with a magnetic stir bar was charged in an argon-filled glove box with 59.8 mM solution of K(dpms)Pt^{II}Me(I) in D_2O. Solvent was removed under vacuum and the remaining solid was dissolved in MeOD-d_4. The solution was transferred into air tight NMR tube and taken out of the box. NMR tube was opened and air was bubbled through the reaction mixture for couple of minutes. Solution was recapped and placed on the rotator overnight. The next day, white precipitate was observed in the reaction mixture. Solution was centrifuged to separate precipitate solid and liquid phase. Solid was washed with H_2O, dried under high vacuum and dissolved in dmso-d_6. Product was identified as (dpms)$Pt^{IV}Me_2$(I), present in 35% yield. According to the ^{1}H NMR spectrum of the aqueous phase, (dpms)$Pt^{IV}Me_2$(OH) (**2.8**) and (dpms)$Pt^{IV}Me_2$(OMe) (**3.9**) were present in 18 and 26 % yield respectively.

^{1}H NMR of the reaction mixture after oxidation (dmso-d_6):

(dpms)$Pt^{IV}Me_2$(OH) (**2.8**) δ: 1.48 (s, 3H, Pt-CH_3, $^2J_{PtH}$ = 66 Hz), 1.52 (s, 3H, Pt-CH_3, satellites overlap with other signals, *sym*-(**2.8**)).

(dpms)$Pt^{IV}Me_2$(OMe) (**3.9**) 1.51 (s, 3H, Pt-CH_3, $^2J_{PtH}$ = 66 Hz), 1.62 (s, 3H, Pt-CH_3, $^2J_{PtH}$ = 80 Hz),

(dpms)$Pt^{IV}Me_2$(I) (**3.6**) 1.85 (s, 3H, Pt-*CH*$_3$, $^2J_{PtH}$ = 66 Hz), 1.95 (s, 3H, Pt-*CH*$_3$, $^2J_{PtH}$ = 80 Hz). Aromatic region very complex.

ESI-MS analysis showed the presence of Pt^{IV} complexes with deuterated bridging CH group: ((dpms)$Pt^{IV}Me_2(OH)\cdot K^+$) (**2.8**-*d*$\cdot K^+$) m/z = 531.039, calculated for (**2.8**-*d*$\cdot K^+$), $C_{13}H_{15}KDN_2O_4PtS$, 531.01774; ((dpms)$Pt^{IV}Me_2(I)\cdot K^+$) (**3.6**-*d*$\cdot K^+$) m/z = 640.897, calculated for (**3.6**-*d*$\cdot K^+$), $C_{13}H_{14}KDIN_2O_3PtS$, 640.91947; ((dpms)$Pt^{IV}Me_2(OCD_3)\cdot K^+$) (**3.9**-*d*$\cdot K^+$) m/z = 548.070, calculated for (**3.9**-*d*$\cdot K^+$), $C_{14}H_{14}D_4KN_2O_4PtS$, 548.05191. In the negative mode, anionic Pt^{II} compounds have also been detected with deuterated bridging CH group: ((dpms-*d*)$Pt(OCD_3)I)^-$, m/z = 605.988, calculated for $C_{12}H_8D_4IN_2O_4PtS$, 605.94573; ((dpms-*d*)$Pt(I)_2)^-$ m/z = 698.857, calculated for $C_{11}H_8DI_2N_2O_3PtS$, 698.81330.

Kinetics of oxidation of K(dpms)Pt^{II}Me(I) in D_2O in a Buffer Solution at pH 6.5

General procedure. The oxidation of aqueous (dpms)$Pt^{II}Me(I)^-$ was run under vigorous stirring in a 25 mL round-bottom flask, filled with O_2(*g*), and equipped with a magnetic stir bar and an O_2-filled balloon. The solution pH was maintained using buffer solutions (pH 6.5). First, approximately 2.0 mL of ~2 mM stock solution of aqueous K(dpms)Pt^{II}Me(OH) were combined with pH 6.5 aqueous buffer under an argon atmosphere, then 1.0 or 10.0 equiv. of KI was added. The mixture was temperature-equilibrated and then injected with a syringe into the reaction flask, placed in a temperature-controlled water-ethylene glycol bath at 21.0 °C. Vigorous stirring began immediately. Periodically a ~0.2 mL aliquot of the reaction mixture was taken with a syringe, transferred into argon-filled NMR tube, and diluted with 0.3 mL degassed D_2O to stop the reaction. Concentrations of the

reactant, (dpms)Pt^{IV}Me(I)(OH) and *C*$_1$-(dpms)$Pt^{IV}Me_2$(OH) were monitored by ^{1}H NMR spectroscopy with 1,4-dioxane used as an internal standard. Methyl group balance was calculated based on the sum of representative $Pt^{IV}CH_3$ protons. Minimum of two kinetics runs were performed, and kinetics were monitored over more than three half-lifes.

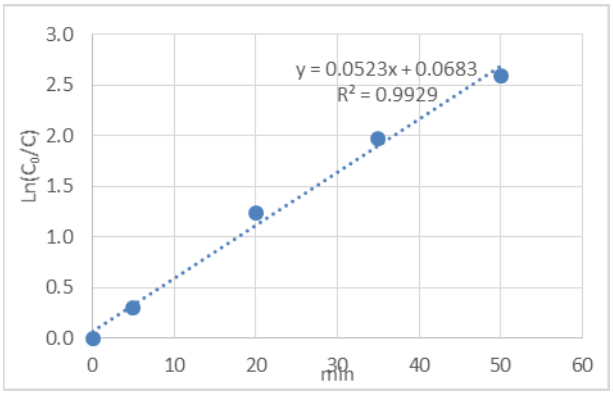

[SM] = 2.3 mM,
conversion = 92%
$t_{1/2}$ = 13.3 min

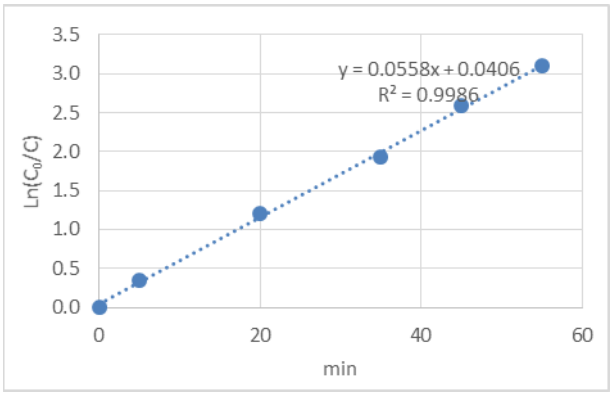

[SM] = 2.2 mM,
conversion = 95%
$t_{1/2}$ = 12.4 min

Figure 3.4 First-order kinetics plot for disappearance of (dpms)Pt^{II}Me(I) at **pH 6.5**, at 21.0 °C with 1 equiv. of KI.

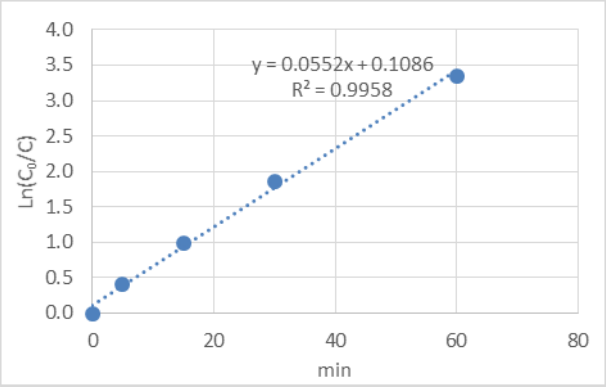

[SM] = 1.8 mM,
conversion = 96%
$t_{1/2}$ = 12.6 min

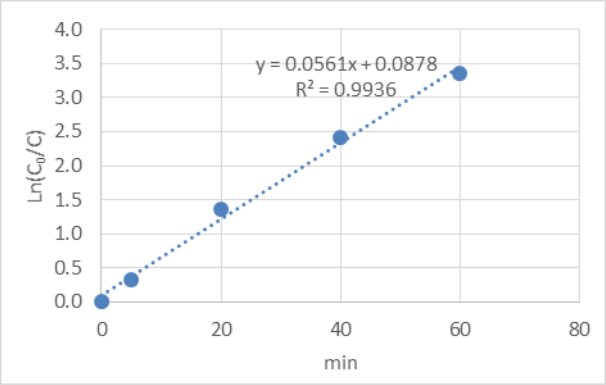

[SM] = 2.5 mM,
conversion = 96%
$t_{1/2}$ = 12.4 min

Figure 3.5 First-order kinetics plot for disappearance of (dpms)Pt^{II}Me(I) at **pH 6.5**, at 21.0 °C with 10 equiv. of KI.

Study of the effect of light on the rate of oxidation of K(dpms)Pt^{II}Me(I) with KI_3

In an argon-filled glove box two vials with stir bars were charged with a solution of K(dpms)Pt^{II}Me(OH) (5.6 µmol each) in 0.2 mL of H_2O, and citrate/phosphate buffer (pH 5.0). One of the vials was wrapped in aluminum foil, and another one was irradiated with incandescent bulb. To the reaction mixture 1.0 equiv. of KI_3 (5.6 µmol) was added as solids, vials were sealed and stirred until no further color changes occurred. Solution changed color from colorless to dark red and formation of precipitate was observed. When no further changes were observed, solvent was evaporated under high vacuum, the remaining residue was died at 30 °C for 40 minutes and dissolved in dmso-d_6 for ^{1}H NMR analysis. The carbon-containing products of the reaction were identified as (dpms)Pt^{II}Me$_2$(OH) and (dpms)Pt^{II}Me$_2$(I).

Conditions	Yield (%) $LPtMe^{IV}(OH)_2$	Yield (%) $LPt^{IV}Me_2(OH)$	Yield (%) $LPt^{IV}Me_2(I)$
hν	none	58 ± 12	19 ± 12
dark	none	55 ± 6	13 ± 8

Table 3.8 Product distribution in the reaction between $K(dpms)Pt^{II}Me(OH)$ and KI_3 at pH 5.0.

Study of the effect of light on the reaction between I_2 and $K(dpms)Pt^{II}Me(I)$

In an argon-filled glove box two NMR tubes with air tight Teflon valves were charged with a solution of $K(dpms)Pt^{II}Me(OH)$ (19.13 μmol and 19.8 μmol) in H_2O/D_2O and citrate/phosphate buffer (pH 5.0). One of the NMR tubes was wrapped in aluminum foil, and another one was exposed to light. A 20.0 μL of a 1.0 M solution of I_2 in acetone was added to each reaction mixture, NMR tubes were shaken and ^1H NMR spectrum was recorded. The rate of oxidation was independent on whether the reaction was kept in the dark or was exposed to light. In both cases, oxidation of $K(dpms)Pt^{II}Me(OH)$ was complete upon addition of iodine. Cooling the reaction mixture to 0 ˚C in an ice-bath prior to addition of I_2 failed to slow down the rate of oxidation. The products of anaerobic oxidation of $K(dpms)Pt^{II}Me(OH)$ with I_2 were identified as $(dpms)Pt^{II}Me_2(OH)$ and $(dpms)Pt^{II}(I)_2$.

ESI-MS analysis showed the presence of Pt^{IV} complexes: $((dpms)Pt^{IV}Me_2(OH)\cdot H^+)$ (**7**$\cdot H^+$) m/z = 492.057, calculated for (**7**$\cdot H^+$), $C_{13}H_{17}N_2O_4PtS$, 492.05568; and Pt^{II} complex: $((dpms)Pt(I)_2)^-$ m/z = 697.809, calculated for $C_{11}H_9I_2N_2O_3PtS$, 697.80710.

Conditions	Yield (%) $LPtMe^{IV}(OH)_2$	Yield (%) $LPt^{IV}Me_2(OH)$	Yield (%) $LPt^{IV}Me_2(I)$
hν	none	61	none
dark	none	63	none

Table 3.9 Product distribution in the reaction between $K(dpms)Pt^{II}Me(OH)$ and I_2 at pH 5.0.

Effect of TEMPO on the reaction between KI_3 and K(dpms)Pt^{II}Me(I)

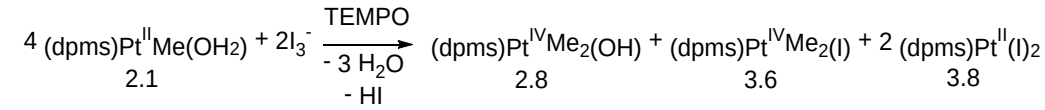

In an argon-filled glove box NMR tube with air tight Teflon valve was charged with a solution of K(dpms)Pt^{II}Me(OH) (18.5 μmol) in H_2O/D_2O, citrate/phosphate buffer (pH 5.0) and (2,2,6,6-tetramethylpiperidin-1-yl)oxidanyl (TEMPO) (2.9 mg, 18.5 μmol). When TEMPO was completely dissolved, KI_3 (7.87 mg, 18.73 μmol) was added to the reaction mixture. NMR tube was shaken and ^{1}H NMR spectrum was recorded. In approximately 20 min. color began to change from faint yellow to orange-brown and solution became cloudy. No more starting complex K(dpms)Pt^{II}Me(OH) was observed by ^{1}H NMR spectroscopy, (dpms)$Pt^{IV}Me_2$(OH) was formed in 76 % yield.

ESI-MS analysis showed the presence of Pt^{IV} complexes: ((dpms)$Pt^{IV}Me_2$(OH)·H^+) (**7**·H^+) m/z = 492.059, calculated for (**7**·H^+), $C_{13}H_{17}N_2O_4PtS$, 492.05568; ((dpms)$Pt^{IV}Me_2$(OH)·K^+) (**7**·K^+) m/z = 530.013, calculated for (**7**-*d*·K^+), $C_{13}H_{16}KN_2O_4PtS$, 530.01156; ((dpms)$Pt^{IV}Me_2$(I)·K^+) (**6**·K^+) m/z = 639.924, calculated for (**6**·K^+), $C_{13}H_{15}KIN_2O_3PtS$, 639.91329. In the negative mode, presence of Pt^{II} complex was observed: ((dpms)$Pt(I)_2)^-$ m/z = 697.870, calculated for $C_{11}H_9I_2N_2O_3PtS$, 697.80710.

Control experiment: oxidation of K(dpms)Pt^{II}Me(OH) (8.8 μmol) in H_2O/D_2O with citrate/phosphate buffer (pH 5.01) in the presence of TEMPO (2.1 mg, 13.4 μmol) in the absence of KI_3, was performed. No inhibition of the reaction and no Pt-to-Pt Me-group transfer product were observed. Product (dpms)$Pt^{II}Me(OH)_2$ was generated in 99% yield.

Dependence of product distribution at pH 8.0, 10.0 and 12.0 in aerobic oxidation of K(dpms)Pt^{II}Me(OH) with and without KI

Stock solution of K(dpms)Pt^{II}Me(OH) was prepared according to method B. In an argon-filled glove box three NMR tubes were charged with a solution of K(dpms)Pt^{II}Me(OH) (4.0 μmol each) in H_2O, and a phosphate buffer $H_2PO_4^-/HPO_4^{2-}$, (pH 8.0 and 10.0), and a citrate/ phosphate buffer pH 12.0. NMR tubes were taken out of the glove box, purged with O_2, and sealed. Upon completion of oxidation, reaction solutions were diluted with D_2O, and ^{1}H NMR spectrum was recorded. 1,4-Dioxane was used as an internal standard. In case of pH 10, 12 some starting material remained after 48 h of exposure to dioxygen. Mass balance was calculated by integration of the Pt^{IV}Me signals.

Same procedure was used for reaction in the presence of iodide. Prior to exposure to O_2, a 0.5 M solution of KI (8.0 μL, 4.0 μmol) in H_2O was added to each reaction mixture.

Attempted R group transfer (R = C_2H_4, Ph, C_2H_4NHMe-*κ*C,*κ*N)

Attempted ethylene group transfer

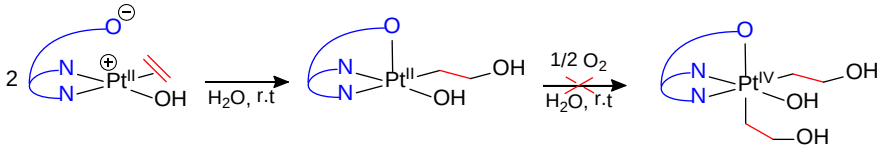

Similar to the reactions between K(dpms)Pt^{II}Me(OH$_2$) and KI, a Schlenk flask, equipped with a magnetic stir bar, was charged with 9.1 mg (18.7 μmol) of K(dpms)Pt^{II}(C_2H_4)OH, 3.1 mg (18.7 μmol) of KI and 0.5 ml of deoxygenated D_2O in the argon-filled glove box. Schlenk flask was taken out of the box and the reaction was exposed to air. After stirring the reaction under air overnight, no Pt-diethylene

containing products have been observed. The major products were K(dpms)Pt^{II}(I)OH, K(dpms)$Pt^{II}(OH)_2$ and K(dpms)$Pt^{II}(I)_2$, which result from decomposition of K(dpms)$Pt^{II}(C_2H_4)$OH. Free C_2H_4 has been observed at 5.41 ppm. Identity of the products has been confirmed by ^{1}NMR and ESI-MS. K(dpms)Pt^{II}(I)OH and K(dpms)$Pt^{II}(OH)_2$ has been characterized before. Complex K(dpms)$Pt^{II}(I)_2$ has been prepared independently.

Attempted phenyl group transfer

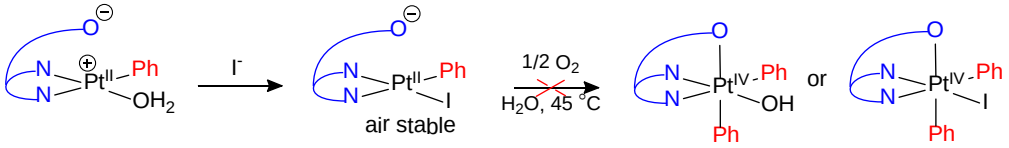

K(dpms)$Pt^{II}Ph(OH_2)$ has been prepared by dissolution of K(dpms)Pt^{II}Ph(MeOH) in H_2O using standard procedure. Schlenk flask equipped with a magnetic stir bar was charged with a solution containing 13.2 mg (24.5 µmol) K(dpms)$Pt^{II}Ph(OH_2)$ in the glove box. 9.2 mg (55.4 µmol) KI was added to the reaction mixture. Schlenk flask was taken out of the glove box and air was introduced into the reaction mixture. After stirring the reaction for seven days open to air, only K(dpms)Pt^{II}(Ph)I was observed by ^{1}NMR spectroscopy.

Addition of 4.8 µl (61.3 µmol) of 30% H_2O_2 resulted in immediate precipitation of yellow K(dpms)Pt^{II}(Ph)I(OH). Product was separated by centrifugation. K(dpms)Pt^{II}(Ph)I(OH) has poor solubility in organic solvents and decomposes when kept in DMSO for more than two weeks.

ESI-MS of calculated for H(dpms)Pt^{II}(Ph)I(OH) $C_{17}H_{16}IN_2O_4PtS$ m+H^+/z = 665.95232, found m+H^+/z = 665.950; calculated for K(dpms)Pt^{II}(Ph)I(OH) $C_{17}H_{15}IKN_2O_4PtS$ m+H^+/z = 703.90820, found m+K^+/z = 703.901.

Attempted phenyl group transfer under basic conditions

A Schlenk flask equipped with a magnetic stir bar was charged with a solution containing 10.3 mg (18.6 µmol) K(dpms)Pt^{II}(Ph)OH_2 in the glove box; 37 µl KOH (0.5M solution) and 23.3 µl of KI_3 (1M solution) were added sequentially. Solvent was partially evaporated, and the product was separated by centrifugation. Diphenyl containing product was not observed, instead isomeric K(dpms)Pt^{II}(Ph)OH(I) was the major product.

Attempted azetidine group transfer

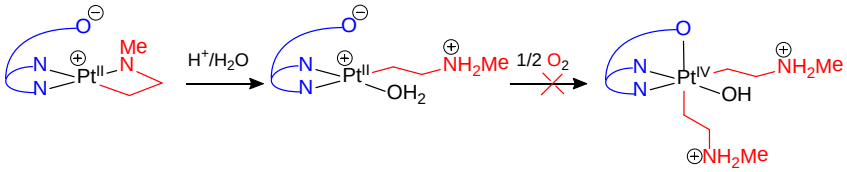

A Schlenk flask equipped with a magnetic stir bar was charged with 4.7 mg (9.4 µmol) of (dpms)Pt^{II}(C_2H_4NHMe-κC,κN), 3.2 mg (19.3 µmol) of KI and 3 ml of phosphate buffer pH = 6.01 ($H_2PO_4^-$/HPO_4^{2-}) in the glove box. The reaction mixture was exposed to air and stirred overnight. ^{1}NMR spectroscopy and ESI-MS analysis showed the absence of diazetidine containing product, instead previously characterized (dpms)Pt^{II}(C_2H_4NHMe-KC,KN)OH[4] was the major Pt containing specie.

Chapter 4 : Effect of the Metal on the Aerobic Reactivity of DPMS-based System. Reactivity of (dpms)$Pd^{II}Me(SMe_2)$ and (dpms)$Pd^{II}Me(X)^-$ (X = I, OH) Complexes

4.1 O_2 as an Oxidant in Pd-mediated Reactions

Aerobic oxidation reactions using palladium have received much attention in the past decade. Examples of these reactions include oxidation of alcohols to ketones, alkenes to carbonyl compounds, intramolecular heterocyclizations of alkenes, and oxidative coupling of alkenes and carbon or heteroatom nucleophiles. These reactions typically proceed via Pd^{II}/Pd^0 pathway and O_2 does not directly participate in the substrate oxidation (Scheme 4.1)[120,68,121]

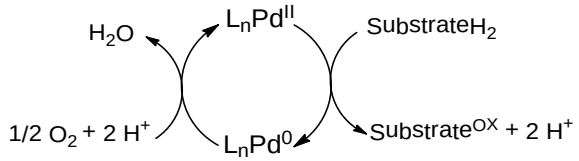

Scheme 4.1. Simplified catalytic cycle for Pd^{II}/Pd^0-catalyzed aerobic oxidation reactions.

Palladium-catalyzed aerobic C-H oxidation reactions have been known since mid-1960s. One of the early precedents for C-H oxidation of this type is homocoupling of arenes. Benzene was shown to react with $Pd^{II}(OAc)_2$ in acetic acid at 100 °C to yield biphenyl.[122] These reactions have not received much attention compared to cross-coupling reactions of aryl halides; however, increased interest in environmentally benign methods for C-H functionalization reactions, provides motivation to reinvestigate these reactions. Palladium mediated oxidation of CH_4 was discussed in Chapter 1. All systems known to date utilize Pd^{II}/Pd^0 couple and require

electron transfer mediators to achieve aerobic turnover. In this chapter we will focus on ligand-supported oxidation of Pd^{II} complexes.

4.1.1 Aerobic Oxidation of Pd Complexes

In Chapter 2 we discussed oxidation of 1,4,7-triazacyclononane (tacn) supported platinum complexes $[(k^2\text{-tacn})_2Pt]^{2+}$ which form $[(k^3\text{-tacn})_2Pt]^{4+}$ at 90 °C.[72] Inspired by this finding, McAuley and *et al.* prepared analogous palladium complex $[(k^2\text{-tacn})_2Pd]^{2+}$ (Scheme 4.2). The ^1H and ^{13}C NMR studies showed fluxional behavior of the latter complex, where Pd atom 'hops' between the three nitrogen atoms of the cyclic ligand. The authors proposed that such fluxional behavior is facilitated by tacn ligand, which has a preference for octahedral (*Oh*) coordination.[87] The same preference for *Oh* geometry was attributed to the ease with which $[(k^2\text{-tacn})_2Pd]^{2+}$ underwent transformation to $[(k^3\text{-tacn})_2Pd]^{3+}$. Formation of Pd^{III} was observed under aerobic and anaerobic conditions. Under anaerobic conditions Pd^{II} disproportionated into Pd^{III} and Pd^0 with the 2nd order rate constant $1.6 \times 10^{-4}\ M^{-1}s^{-1}$. In the presence of O_2, oxidation to Pd^{III} was ~3 fold faster ($4.7 \times 10^{-4}\ M^{-1}s^{-1}$) (Scheme 4.3), indicating that direct aerobic oxidation is now kinetically feasible.[123]

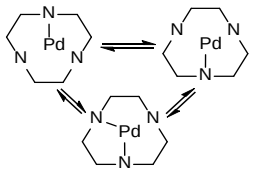

Scheme 4.2 Fluxional behavior of $[(k^2\text{-tacn})_2Pd]^{2+}$.

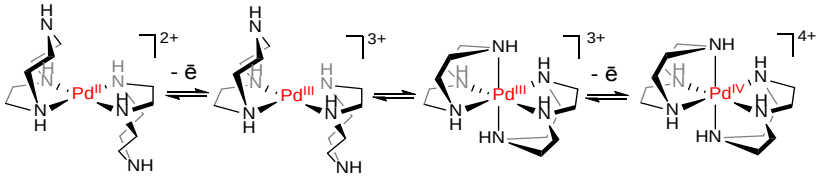

Scheme 4.3 Oxidation of $[(k^2\text{-tacn})_2Pd]^{2+}$ to $[(k^3\text{-tacn})_2Pd]^{3+}$ and $[(k^3\text{-tacn})_2Pd]^{4+}$ with O_2.

The first example of a structurally characterized mononuclear Pd^{III} complex was reported in case of tridentate 1,4,7-trithiacyclononane ligand (Scheme 4.4, **A**) with Pd^{II}/Pd^{III} redox potential $E_{1/2}$ = +0.605 V.[124] Redox chemistry of mixed S- and

N-donor macrocyclic Pd^{II} complexes have also been investigated. Cyclic voltammetry of $[Pd([18]aneN_2S_4)]^{2+}$ [18]$aneN_2S_4$ = 1,4,10,13-tetrathia-7,16-diazacyclooctadecane, showed reversible oxidation at $E_{1/2}$ = +0.57 V *vs.* Fc^0/Fc^+ for Pd^{II}/Pd^{III} redox couple (Scheme 4.4, **B**).[125] And $[Pd([9]aneNS_2)2]^{2+}$ ([9]$aneNS_2$ = 1,4-dithia-7-azacyclononane) has redox potential of $E_{1/2}$ = +0.43 V *vs.* Fc^0/Fc^+ (Scheme 4.4, **C**).[126] Aerobic behavior of these complexes has not been investigated, however redox potentials imply that oxidation by O_2 might be feasible.

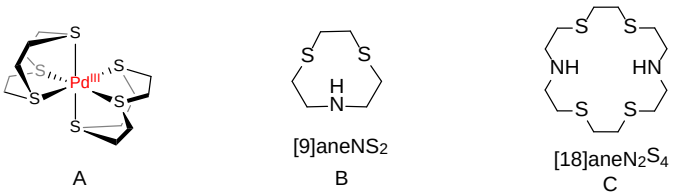

Scheme 4.4 Ligands for stabilization of Pd^{III}.

4.1.2 Pd^{II}/Pd^0 Couple-Mediated Functionalization

The first example of formation of C-O functionalized product was reported by Fujiwara *et al*. in 1987. The authors demonstrated synthesis of phenol from benzene, using Pd^{II} and O_2 in the absence of electron transfer mediators. Reaction proceeds under the conditions of 15 atm of O_2, 15 atm of CO, equimolar amounts of $Pd(OAc)_2$ and 1,10-phenanthroline (phen) ligand in acetic acid at 180 °C. Phenol was formed in 502[127] – 1270%[128] (TON ~5-12) yield based on Pd. Labeling studies with $^{18}O_2$ showed that phenol contained 92% of the oxygen label. Proposed mechanism includes electrophilic C-H activation of benzene to form (phen)Pd^{II}Ph(OAc), followed by insertion of oxygen into Pd^{II}-Ph bond and formation of phenol via reaction with AcOH (Scheme 4.5).[128] Presence of CO and phen ligand is essential for reaction selectivity.[127] The effect of heteropoly acids as electron transfer mediator has also been investigated.[129]

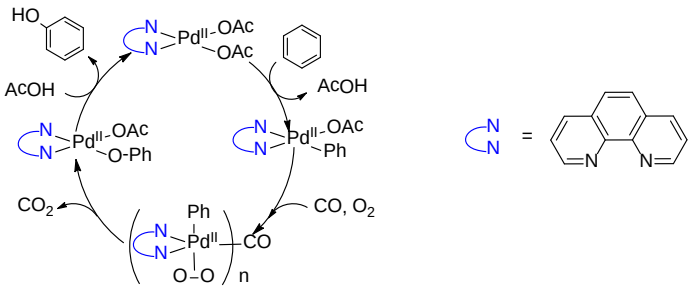

Scheme 4.5 Proposed mechanism for catalytic hydroxylation of benzene in the presence of $Pd(OAc)_2$ and 1,10-phenanthroline (phen).

More recently, Yu *et al*. have reported the *o*-hydroxylation of substituted benzoates with 1 atm of O_2 or air in DMA at 115 °C (Scheme 4.6). Addition of 0.2-1.0 equiv. of *p*-benzoquinone was found to accelerate the reaction, but not essential for reaction to occur. In this system benzoate acts as a ligand and as a substrate, and both electron withdrawing and electron donating functional groups were tolerated.[130] Aerobic hydroxylation of alkenes[131], and α-sp^3 C-H bonds of carbonyl compounds[132] has also been reported.

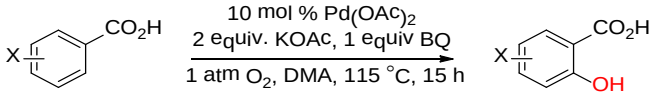

Scheme 4.6 Ligand directed *o*-hydroxylation of substituted benzoates using $Pd(OAc)_2$.

In addition to hydroxylation reactions, significant attention has been given to acetoxylation transformations. Acetoxylation of aromatic compounds has been studied since 1970's. In an early report a mixture of *o*-, *m*-, *p*-acetoxychlorobenzene was formed in reaction of $Pd(OAc)_2/NO_2$ or NO_3^- with O_2 in acetic acid.[133]

The research group led by S. Stahl has been focused on developing a ligand-based strategy that would enable conversion of terminal alkenes to linear allylic acetoxylation products under 1 atm of O_2. Authors speculated that electron-deficient ligands would increase Pd^{II}/Pd^0 reduction potential and would facilitate reductive elimination of C-O functionalized product. However, studies showed that ligand-

promoted reductive elimination is not sufficient to achieve aerobic turnover. For example, 1,10-phenanthroline ligand was almost completely ineffective, only 9% of functionalized product was generated (TON ~2). The most effective ligand appeared to be 4,5-diazafluorenone (Scheme 4.7), acetoxylated product was formed in 81% yield based on starting material (TON ~16). The improved result was assigned to the unique geometry of the ligand.[134]

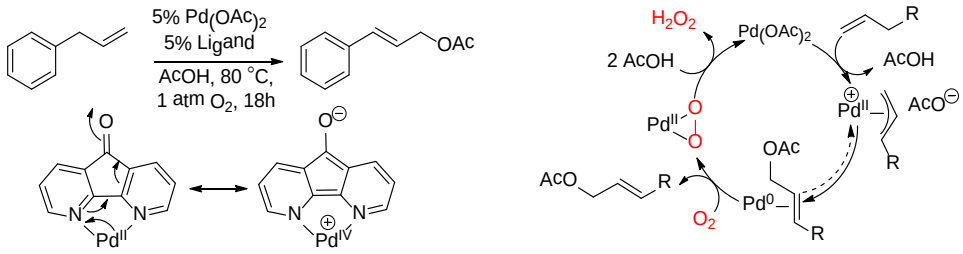

Scheme 4.7. Proposed mechanism for Pd-catalyzed aerobic allylic acetoxylation.

Plausible reaction mechanism for this transformation is shown in Scheme 4.7. C-O bond formation is proposed to occur via nucleophilic attack of AcO^- on $LPd^{II}(\eta^3$-allyl) complex. Authors speculate that nucleophilic attack is promoted by distorted bite angle of the diazafluorenone ligand which leads to destabilitzation of Pd^{II}. [134]

Therefore, in order to achieve partial oxidation of hydrocarbons, ancillary ligands need to satisfy two requirements: 1) facilitate oxidation of Pd by O_2, and 2) facilitate reductive elimination of C-O bonds. Dpms ligand was shown to meet these requirements (*vide infra*).

4.1.3 Pd^{II}/Pd^{IV} Couple Mediated C-H Functionalization

Over the past decade C-H functionalization using high-valent palladium complexes has emerged as a powerful approach to achieve acetoxylation and hydroxylation products.[135] These reactions rely on the ability of the Pd^{IV}-hydrocarbyls to undergo rapid reductive elimination of C-X product (Scheme 4.8).[136]

Oxidation of Pd^{II} to Pd^{IV} requires strong oxidants, such as $PhI(OAc)_2$, IOAc, or $K_2S_2O_8$, which have significant disadvantages of either high cost, and/or poor atom economy.[135] Only few examples of aerobic C-O bond formation via Pd^{II}/Pd^{IV} redox couple have been reported to date.[137-139]

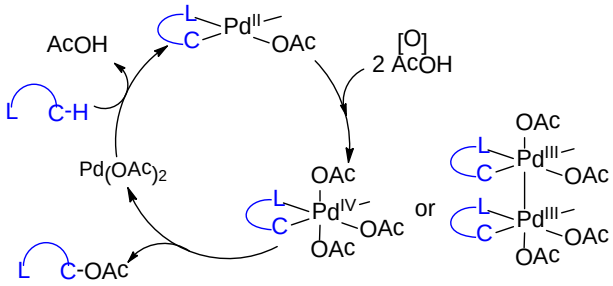

Scheme 4.8. Proposed mechanism for Pd-catalyzed ligand-directed C-H oxidation.

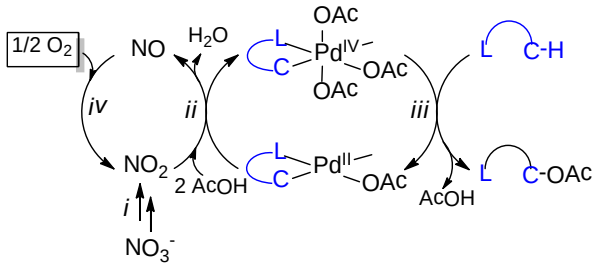

Scheme 4.9. Proposed catalytic cycle for Pd-catalyzed acetoxylation.

The Sanford group achieved aerobic oxidation of sp^3-C-H bonds in pyridine and oxime ether substrates, using nitrates as ETM. Typical reaction conditions were 5 mol% of $Pd(OAc)_2$, 25 mol% of $NaNO_3$, and 1 atm O_2 in $AcOH/Ac_2O$ at 110 °C for 18 h. Proposed catalytic cycle (Scheme 4.9) involves decomposition of NO_3^- to NO_2 (step i), followed by reaction of NO_2 and 2 equiv of AcOH with cyclopalladated Pd^{II} intermediate to generate Pd^{IV} along with NO and H_2O (step ii). Functionalization occurs via reductive elimination step iii, while NO is oxidized to NO_2 by O_2.[137]

Our group has demonstrated that Pd-mediated functionalization of C-H bonds with O_2 or H_2O_2 can be achieved by careful selection of the auxiliary ligand. When cationic monohydrocarbyl Pd^{II} complexes, supported by di-2-pyridyl ketone (dpk)

ligand, were exposed to 2-10 equiv. of H_2O_2, formation of the corresponding Pd^{IV} congener occurred. These Pd^{IV} complexes were shown to form C-O functionalized product in quantitative yield (Scheme 4.10).[139]

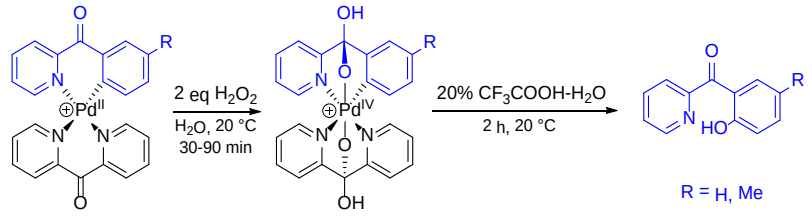

Scheme 4.10 Reductive elimination of $C(sp^2)$-O bond via Pd-mediated oxidation with H_2O_2.

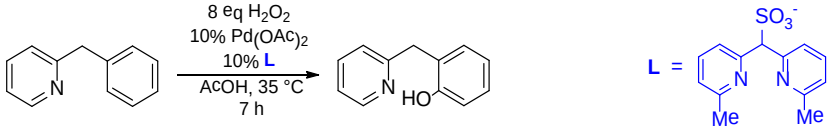

Scheme 4.11. Palladium-catalyzed $C(sp^2)$-H hydroxylation with H_2O_2.

As has been discussed earlier, destabilization of metal center, leads to more efficient reductive elimination. Dpms has a weaker O-donor sulfonate group, compared to dpk, therefore, dpms is expected to provide weaker support for Pd^{IV} metal center, and facilitate product forming step. Indeed, catalytic $C(sp^2)$-H hydroxylation with H_2O_2 was observed with a more bulky auxiliary ligand (Me_2-dpms) (Scheme 4.11). Catalytic hydroxylation of 2-benzylpyridine in acetic acid was observed at 35 °C, and phenol was generated in 95% yield. Reaction is proposed to occur via C-H activation of the substrate at $Pd(OAc)_2$, followed by formation of the ligand-supported palladacycle. Pd^{II} complex undergoes rapid oxidation to Pd^{IV} and the latter forms functionalized product via reductive elimination step.[139,140]

Similar mechanism was proposed for catalytic oxidation of ethylene in H_2O_2/AcOH system. Conversion of ethylene to a mixture of functionalized products was observed in up to 90% yield with high selectivity for glycol acetates (Scheme 4.12).[141]

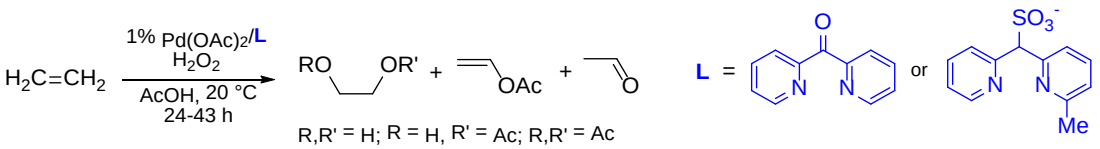

Scheme 4.12. Palladium-catalyzed oxidation of ethylene with H_2O_2 in acetic acid.

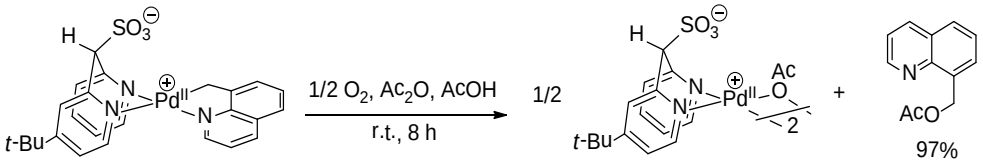

Scheme 4.13 Catalytic aerobic oxidation of 8-methylquinoline.

Finally, aerobic functionalization of benzylic Pd^{II}-C bonds has been observed in 4-^{t}Bu-dpms-supported palladium (II) complexes (Scheme 4.13). Acetoxylated product was formed in 97% yield at 20 °C.[138] Since (dpms)Pd^{II} monohydrocarbyl complexes are able to generate hydroxy- and acetoxy-functionalized products under aerobic conditions[111,140], and (dpms)Pt^{II} monomethyl complexes form MeOH, our goal was to prepare (dpms)Pd^{II} monomethyl complexes and study their behavior in oxidation reactions. In this chapter we describe preparation of neutral (dpms)$Pd^{II}Me(SMe_2)$, and anionic (dpms)$Pd^{II}Me(X)^-$ (X = I, OH) complexes, and probe their reactivity towards O_2 and some other oxidants.

4.2 Preparation and Characterization of (dpms)$Pd^{II}Me(SMe_2)$

Reaction between K(dpms) and $[PdMe(SMe_2)(\mu\text{-}Cl)]_2$[142] precursor in methanol affords (dpms)$Pd^{II}Me(SMe_2)$ complex in up to 97 % yield (Eq. 4.1). At ambient temperature, the ^{1}H NMR spectrum of (dpms)$Pd^{II}Me(SMe_2)$ consists of a four resonances in the aromatic region of the dpms ligand, and a single resonance for methyl groups of the SMe_2 ligand. The symmetrical nature of ^{1}H and ^{13}C NMR spectra is in contrast to the anticipated spectra from the crystal structure of (dpms)$Pd^{II}Me(SMe_2)$ complex (Figure 4.1).

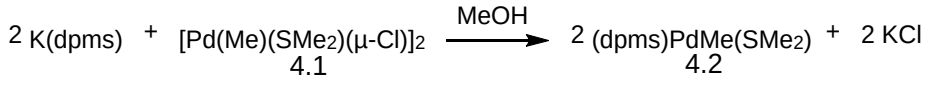

Equation 4.1

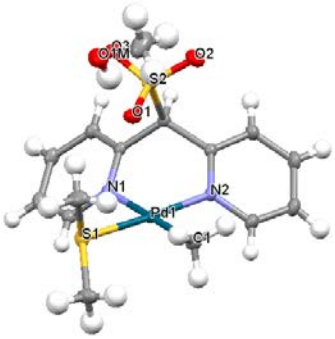

Figure 4.1 ORTEP drawing of complex 4.2. Selected bond distances, Å: Pd1-C1, 2.0314(14); Pd1-S1, 2.2780(4); Pd1-N1, 2.1517(11); Pd1-N2, 2.0718(11).

The apparent C_s symmetry of **4.2** could arise from a dynamic behavior of the Pd^{II} complex.[87,143] Similar behavior was observed in case of tripyrazolylborate complexes of Pd^{II} $[Pd((pz)_3BH)_2]$[144] (Figure 4.2, **A**) which produce a NMR spectra with only one set of signals for the three pyrazolyl groups, as well as for palladium $(py)_3CH$ complex $[Pd((py)_3CH)_2]^{2+}$ (Figure 4.2, **B**). The barrier for interconversion of the latter complex was estimated to be 14.9 kcal/mol at 30 °C.[143]

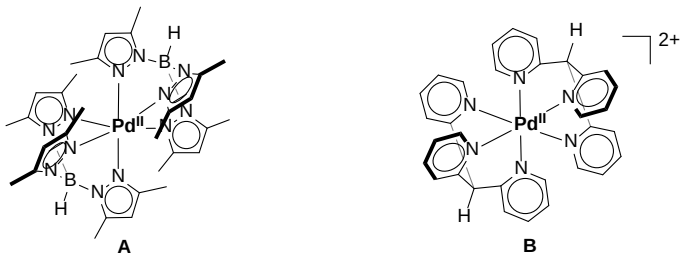

Figure 4.2 A: Tripyrazolylborate-supported palladium(II) $[Pd((pz)_3BH)_2]$. B: tris(pyridin-2-yl)methane $[Pd((py)_3CH)_2]^{2+}$.

Sharp ^1H NMR signals for both aromatic and aliphatic protons of **4.2** indicate that at room temperature the interconversion is very fast on the NMR time scale. Partial resolution into predicted spectrum with non-equivalent pyridine residues was observed in variable temperature ^1H NMR studies in CD_2Cl_2. At -84 °C spectrum displayed two signals of equal intensity for *ortho*-H of the dpms ligand at 8.40 and

8.62 ppm, and two signals of equal intensity for methyl groups of the SMe_2 ligand at 2.25 and 2.31ppm (Figure 4.3).

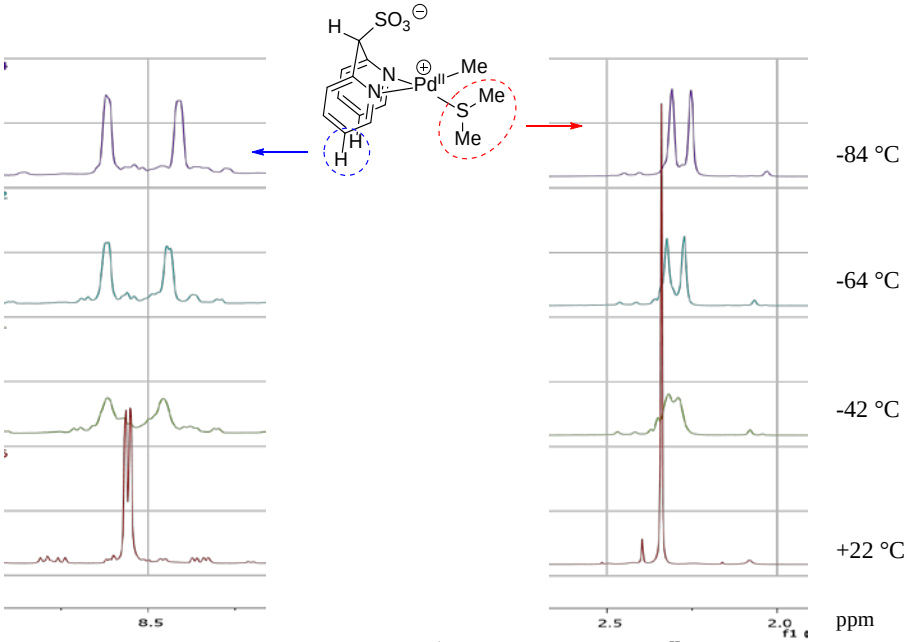

Figure 4.3 Partial variable temperature ^1H NMR of (dpms)$Pd^{II}Me(SMe_2)$ in DCM.

A possible mechanism for the intramolecular isomerization of **4.2**, similar to the one proposed for (dpms)$Pt^{II}Me(OH)^-$ by Wei-Guang Liu, is shown in Scheme 4.14. According to this mechanism one of the nitrogens of the pyridyl ligand *trans* to the Me group dissociates from the metal center due to the strong *trans* effect of the Me ligand. At the same time, O-donor atom of the sulfonate group coordinates to the metal, forming Pd^{II}-OSO_2 bond. According to the X-ray structure of (dpms)$Pd^{II}Me(SMe_2)$, the sulfonate group is oriented toward Pd, (Pd-O1 distance 2.873 Å), which allows for the O atom to donate its electrons to the p_z orbital of the metal. Methyl ligand *trans* to the SO_3 ligand facilitates subsequent dissociation of the sulfonate group. Recoordination of the pyridyl nitrogen with concomitant dissociation of the SO_3^- ligand, completes the isomerization (Scheme 4.14). Dynamic nature of the exchange process is a result of a proximally positioned sulfonate donor group, located

at the axial site of the metal. Another possible mechanism of isomerization of (dpms)$Pd^{II}Me(SMe_2)$ is shown in Scheme 4.15.

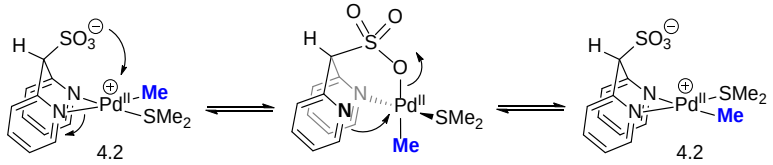

Scheme 4.14 Proposed mechanism of isomerization of (dpms)$Pd^{II}Me(SMe_2)$.

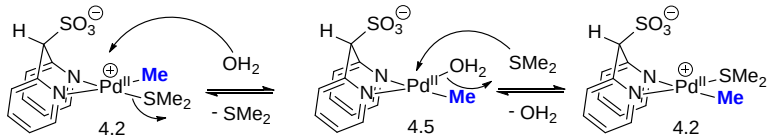

Scheme 4.15 Alternative mechanism of isomerization of (dpms)$Pd^{II}Me(SMe_2)$ in water.

4.2.1 Reactivity of (dpms)$Pd^{II}Me(SMe_2)$ and(dpms)$Pd^{II}Me(OH)^-$ with O_2

Previously, our group has demonstrated that monohydrocarbyl Pt^{II} complexes containing non-ionizable neutral ligands, such as DMSO or SMe_2, do not react with O_2 (Scheme 4.16).[80,145] The lack of reactivity was attributed to the electron poor character of the complex: Pt^{II} is formally cationic, though the overall charge of the complex is zero.

Scheme 4.16 Oxidation of neutral Pt^{II} complexes with O_2.

Similar reactivity could be expected for (dpms)$Pd^{II}Me(SMe_2)$, however, when an aqueous solution of (dpms)$Pd^{II}Me(SMe_2)$ was exposed to O_2 for 6-8 days, formation of MeOH 37 ± 1% yield was observed, along with some other organic products (Scheme 4.17, Table 4.1). Organic products were identified by ^1H NMR spectroscopy by comparison with authentic samples. Complex (dpms)$Pd^{II}(OH)_2^-$ was identified by ^1H NMR and its identity was confirmed by independent synthesis

(Experimental Section). In addition to MeOH, formation of C_2H_6, SMe_2, Me_3S^+, and Me_2SO was observed. Trimethylsulfonium cation Me_3S^+ was detected by ^1H NMR spectroscopy at 2.90 ppm, along with two S-based unknown signals at 2.35 and 2.31

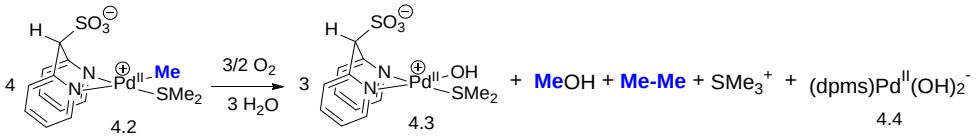

Scheme 4.17 Oxidation of (dpms)$Pd^{II}Me(SMe_2)$ with O_2 at pH 10.6 under ambient conditions.

Conditions	Conversion (%) / Reaction Time	MeOH (%)	C_2H_6 (%)	Me_3S^+ (%)	SMe_2 (%)	Other Products*
pH 7.3, no additives	99 / 7 days	37 ± 1	5 ± 1	26 ± 1	33 ± 1	DMSO 2±1%

Table 4.1 Product distribution in oxidation of (dpms)$Pd^{II}Me(SMe_2)$ with O_2 at pH 10.6 under ambient conditions. *Unidentified SMe_2-based species were present in 16 ± 1% yield.

ppm (16 ± 1% yield). The identity of Me_3S^+ was confirmed by independent synthesis. The cation can be conveniently prepared by reaction between SMe_2 and MeI, to give of Me_3SI as a white solid,[146] reaction between Me_3SI and Ag_2O affords Me_3SOH.[147] The overall mass balance was calculated to be 73%. Methyl group balance was 67±1%. At the end of the reaction, yellow precipitate was formed, which is responsible for non-quantitative mass balance.

In the control experiment aqueous solution of (dpms)$Pd^{II}Me(SMe_2)$ was kept under argon at room temperature for several days (Scheme 4.18, Table 4.2). Slow accumulation of Pd black, C_2H_6, CH_4, CH_3D, and SMe_2 was observed. Methanol and trimethylsulfonium were formed in only 2% yield each, indicating that they result from oxidation of (dpms)$Pd^{II}Me(SMe_2)$.

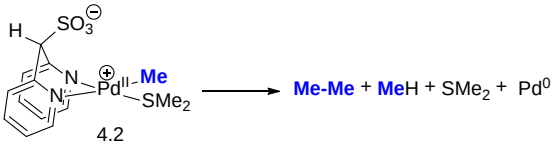

Scheme 4.18 Decomposition of (dpms)$Pd^{II}Me(SMe_2)$ under argon at pH 10.6 under ambient temperature and light.

Conditions	Conversion (%) / Reaction Time	MeOH (%)	C_2H_6 (%)	CH_4 (%)	SMe_2 (%)	Other Products
pH 7.3, no additives	91 / 5 days	2	40	24 (4% CH_3D)	100	Me_3S^+ 2%;

Table 4.2 Product distribution of decomposition of (dpms)$Pd^{II}Me(SMe_2)$ under argon at pH 10.6 under ambient conditions. *Unidentified specie at 2.22 ppm (s) was present in 21 ± 1% yield.

Presence of free SMe_2 (33 ± 1%) in aerobic oxidation of (dpms)$Pd^{II}Me(SMe_2)$ indicates that mechanism, leading to MeOH and Me_3S^+ may involve formation of $LPd^{II}Me(OH_2)$ (Scheme 4.19) which leads to the products of oxidation shown in Table 4.1. In order to assess whether loss of SMe_2 occurs prior to oxidation of (dpms)$Pd^{II}Me(SMe_2)$, oxidation of the latter was performed in the presence of OH^-.

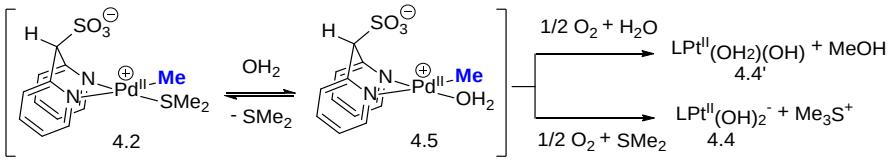

Scheme 4.19 Possible pathways for formation of MeOH and Me_3S^+.

When complex (dpms)$Pd^{II}Me(SMe_2)$ was combined with a solution of aqueous 1.0 M KOH under inert atmosphere formation of a new complex was observed along with free SMe_2 ligand. The new complex was identified as (dpms)$Pd^{II}Me(OH)^-$ by independent synthesis and ESI-MS (Scheme 4.20). Independent synthesis of (dpms)$Pd^{II}Me(OH)^-$ with a *n*-Pr_4N^+ or *n*-Bu_4N^+ as a counterion was performed in two steps. In the first step, (dpms)$Pd^{II}Me(SMe_2)$ was reacted with *n*-Pr_4NI or *n*-Bu_4NI in dichloromethane to give corresponding R_4N(dpms)$Pd^{II}Me(I)$. Product was isolated and fully characterized. In the second step, R_4N(dpms)$Pd^{II}Me(I)$ was reacted with Ag_2O in H_2O to form R_4N(dpms)$Pd^{II}Me(OH)$ (Scheme 4.20). The resulting product is light sensitive and is unstable in solution, therefore, could not be characterized by elemental analysis. The product was characterized by ^1H NMR, ^{13}C NMR, and high resolution ESI-MS.

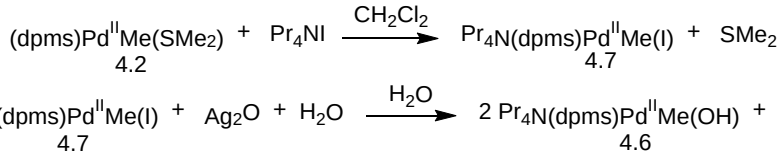

Scheme 4.20 Independent synthesis of $R_4N(dpms)Pd^{II}Me(I)$ and $R_4N(dpms)Pd^{II}Me(OH)$.

In the solution containing **4.2** and 1.0 M KOH the ratio of $(dpms)Pd^{II}Me(OH)^-$ to $(dpms)Pd^{II}Me(SMe_2)$ was 12:1. When the reaction mixture was exposed to O_2, MeOH was produced in 56 ± 5% yield, and $MeOO^-$ in 5 ± 2% yield (Scheme 4.21, Table 4.3, entry 1). Oxidation of independently prepared $R_4N(dpms)Pd^{II}Me(OH)$ with 1 atm O_2 was performed in 1.0 M KOH. Slow conversion of the starting complex resulted in formation of MeOH (49 ± 1%) and $MeOO^-$ (20 ± 1 %) after 6 days (Scheme 4.22, Table 4.3 entry 2). Formation of palladium black and $R_4N(dpms)Pd^{II}(OH)_2$ was observed as well.

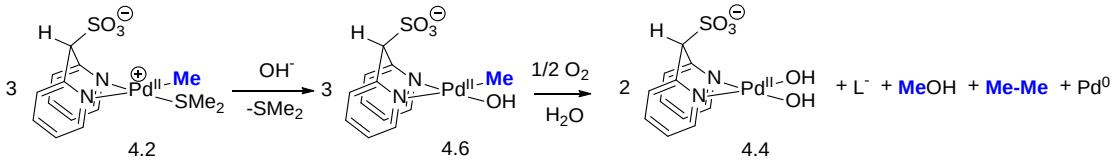

Scheme 4.21 Oxidation of $(dpms)Pd^{II}Me(SMe_2)$ with O_2 at pH 14.0 under ambient conditions.

Entry	Reagent, pH	Conversion / Reaction time	C_2H_6 (%)	MeOH (%)	MeOOH (%)	Other Products (%)
1	$Pd^{II}Me(\mathbf{SMe_2})$, pH 14.0	89 % / 6 days	n.a.	56 ± 5	5 ± 2	$LPd^{II}(OH)_2$ 81 ± 17%
2	$Pd^{II}Me(\mathbf{OH})^-$, pH 14.0	98 % / 6 days	n.a.	49 ± 1	20±1	$LPd^{II}(OH)_2^-$ 71 ± 1%
3	$Pd^{II}Me(\mathbf{OH})^-$, pH 6.3	100 / 3 days	59 ± 6	10 ± 3	0	$LPd^{II}(OH_2)(H_2PO_4)^-$ 58 ± 1%; CH_4 31 ± 7
4	$Pd^{II}Me(\mathbf{SMe_2})$, pH 7.3	99 / 7 days	5 ± 1	37 ± 1	0	DMSO 2±1%; Me_3S^+ 26 ± 1; SMe_2 33 ± 1;*

Table 4.3 Product distribution in oxidation of Pd^{II} with O_2 under ambient conditions; *Unidentified SMe_2-based species (2.35 and 2.31 ppm) were present in 16 ± 1% yield.

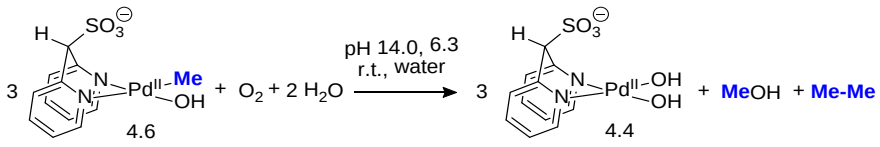

Scheme 4.22 Oxidation of $R_4N(dpms)Pd^{II}Me(OH)$ with O_2 at pH 6.3 and 14.0 under ambient conditions.

Oxidation of $R_4N(dpms)Pd^{II}Me(OH)$ and $(dpms)Pd^{II}Me(SMe_2)$ at pH 14.0 with O_2 under ambient temperature and light resulted in comparable product distribution (Table 4.3 entry 1 and 2). This confirms that $(dpms)Pd^{II}Me(SMe_2)$ is converted to $(dpms)Pd^{II}Me(OH)^-$ at this pH and the latter complex is a reactive intermediate in Scheme 4.21. These observations indicate that the loss of SMe_2 can indeed result in generation of MeOH, however, the yield methanol at pH 14.0 was much higher than in reaction of **4.2** under neutral conditions, in addition presence of Me_3S^+ was not observed. These observations suggest that $(dpms)Pd^{II}Me(OH)^-$ and $(dpms)Pd^{II}Me(SMe_2)$ react via different mechanistic pathways.

4.2.2 Mechanism of Oxidation of $(dpms)Pd^{II}Me(SMe_2)$

In order to elucidate whether **4.2** undergoes ligand exchange with the solvent prior to generation of MeOH (Scheme 4.19), oxidation of **4.6** was performed at pH 6.3. Comparable product distribution would indicate that **4.5** is reactive species leading to methanol.

The amount of methanol which was produced in aerobic oxidation of $R_4N(L)Pd^{II}Me(OH)$ at pH 6.3 (phosphate buffer) was considerably lower, compared to $(dpms)Pd^{II}Me(SMe_2)/O_2$ system (Table 4.3 entry 3 and 4). Therefore complex **4.5** in Scheme 4.19, only partially accounts for the formation of MeOH in Table 4.3 entry 3. It appeared that unlike previously reported complexes in Scheme 4.16, $(dpms)Pd^{II}Me(SMe_2)$ is reactive towards dioxygen. Oxidation of $(dpms)Pd^{II}Me(SMe_2)$ may occur according to Scheme 4.23, similarly, to the mechanism, proposed for oxidation of $R_4N(dpms)Pd^{II}Me(OH)$ (see Chapter 5). Presence of Me_3S^+ as a product of oxidation of **4.2** (Table 4.3 entry 4) implies the

involvement Pd^{IV}, further studies are needed to fully uncover the mechanism of aerobic oxidation of **4.2**.

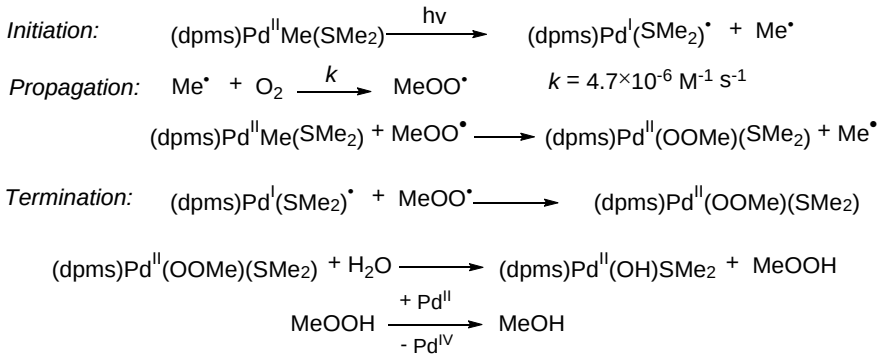

Scheme 4.23 Proposed mechanism for aerobic oxidation of (dpms)$Pd^{II}Me(SMe_2)$ under ambient conditions.

There are very few examples of formation of ethane from monomethyl Pd complexes, one study has been reported recently.[148] Oxidation of $Pd^{II}Me$ complexes to form methanol in the presence of 1 atm O_2 as an oxidant, in aqueous solution and at room temperature, is unprecedented. A detailed mechanistic study of MeOH and C_2H_6 formation in (dpms)$Pd^{II}Me(OH)^-/O_2$ system will be presented in Chapter 5.

4.3 Summary and Conclusions

We have described preparation of (dpms)$Pd^{II}Me(SMe_2)$, R_4N(dpms)$Pd^{II}Me(I)$ and R_4N(dpms)$Pd^{II}Me(OH)$ which react with O_2, I_2, and MeI. We have shown the first example of Pd-mediated formation of MeOH via aerobic oxidation of monomethyl-Pd(II) in water at ambient temperature in the absence of electron transfer mediators. Methanol was generated upon oxidation of neutral (dpms)$Pd^{II}Me(SMe_2)$, and anionic complexes, (R_4N(dpms)$Pd^{II}Me(I)$ and R_4N(dpms)$Pd^{II}Me(OH)$), in the presence light (37, 25, and 16% yield, respectively, in the absence of additives). This reactivity is unprecedented and is a result of

synergistic effect of dpms ligand and a $Pd^{II}Me$ functionality. The highest yield of MeOH (56 ± 5) was obtained in oxidation of (dpms)$Pd^{II}Me(SMe_2)$/1.0 M KOH, where R_4N(dpms)$Pd^{II}Me(OH)$ is the major species.

Generation of C_2H_6 also occurred upon oxidation of (dpms)$Pd^{II}Me(SMe_2)$, R_4N(dpms)$Pd^{II}Me(I)$ and R_4N(dpms)$Pd^{II}Me(OH)$. Methyl iodide was observed in case of R_4N(dpms)$Pd^{II}Me(I)$.

Reactivity of monomethyl-Pd(II) complexes is in sharp contrast to the reactivity of analogous Pt(II) species. Overall, the reactivity of Pd^{II} complexes containing the same auxiliary dpms ligand is more diverse compared to the Pt^{II} analogs. For example, neutral (dpms)$Pt^{II}Ph(DMSO)$ is inert towards O_2, while aqueous (dpms)$Pd^{II}Me(SMe_2)$ undergoes aerobic functionalization to form methanol, among other products, already at room temperature. Oxidation of K(dpms)$Pt^{II}Me(OH)$ with O_2 in water results in formation of (dpms)$Pt^{IV}Me(OH)_2$, or (dpms)$Pt^{IV}Me_2(OH)$, depending on pH . Oxidation of R_4N(dpms)$Pd^{II}Me(OH)$ with O_2, however, does not generate observable Pd^{IV} intermediates; in view of the recent developments in high oxidation palladium chemistry, formation of Pd^{III} transients cannot be excluded.[148,156] Instead, formation of MeOH and C_2H_6 was demonstrated. Similarly oxidation of R_4N(dpms)$Pd^{II}Me(I)$ with O_2 resulted in formation of organic products, while oxidation of K(dpms)$Pt^{II}Me(I)$ resulted in Pt^{IV} species.

In conclusion, the difference in reactivity between dpms-supported monomethyl Pt^{II} and Pd^{II} is related to the stability of the M^n (M = Pd or Pt, n = III or IV) transient species, and the ability of Pd^{II} methyl complexes to undergo photoexcitation to form Me radicals. Generation of MeOH and C_2H_6 occurs under

milder conditions in monomethyl-Pd(II)/O_2 system compared to analogous Pt(II)/O_2 system, but the overall reaction rates are slower.

4.4 Experimental Section

Preparation of (dpms)$Pd^{II}Me(SMe_2)$ (4.2)

In the glove box, K(dpms) ligand (0.1 g, 0.36 mmol) was dissolved in 5 mL of MeOH and 5 drops of H_2O, followed by addition of $[PdMe(SMe_2)(\mu\text{-}Cl)]_2$ precursor (0.076 g, 0.17 mmol). Stirring the reaction mixture for 5 min gave clear yellow solution. Stirring continued for additional 30 min, during that time abundant yellow-white precipitate was formed. Precipitate was filtered off to give the product in 80 % yield. Additional product was obtained by evaporation of the solvent in the glove box over 1 h. The residual solid was dried under vacuum for 30 min. Separation of inorganic salt was achieved by extraction of the product with CH_2Cl_2 and filtration using filter aid Celite. Solvent was removed and the solid was washed with MeOH until the solvent runs clear to give the product as light yellow solid in 97 % yield. The product (dpms)$Pd^{II}Me(SMe_2)$ is easily soluble in H_2O, moderately soluble in CH_2Cl_2 and $CHCl_3$, poorly soluble in MeOH, and insoluble in acetone. The product is stable in the glove box freezer and can be kept for extended periods of time, while decomposes within days when kept at room temperature outside of the glove box. In solution (dpms)$Pd^{II}Me(SMe_2)$ turns brown within 2 h and forms black precipitate within several days when kept in H_2O at room temperature.

^{1}H NMR (400 MHz, D_2O): δ 8.59 (br. s, 2H), 8.00 (td, *J* = 7.8, 1.7 Hz, 2H), 7.74 (d, *J* = 7.8 Hz, 2H), 7.50 (ddd, *J* = 7.3, 5.6, 1.4 Hz, 2H), 5.99 (s, 1H), 2.29 (s, 6H), 0.67 (s, 3H).

^{13}C NMR (126 MHz, D_2O) δ 151.03, 140.63, 129.59, 129.55, 126.03, 74.95 (*C*H-SO_3), 54.52 (S-(*C*H_3)$_2$), 21.12 (Pd-*C*H_3).

^{1}H NMR (500 MHz, $CDCl_3$) δ 8.56 (d, *J* = 5.5 Hz, 2H), 7.93 – 7.82 (m, 4H), 7.35 (td, *J* = 5.8, 2.9 Hz, 2H), 5.94 (s, 1H), 2.39 (s, 6H), 0.77 (s, 3H).

^{13}C NMR (126 MHz, $CDCl_3$) δ 154.38, 150.18, 139.19, 129.36, 123.94, 75.91 (*C*H-SO_3), 53.55 (S-(*C*H_3)$_2$), 21.70 (Pd-*C*H_3).

^{1}H NMR (400 MHz, CD_2Cl_2) δ 8.56 (dd, *J* = 5.6, 1.8 Hz, 2H), 7.88 (td, *J* = 7.6, 1.9 Hz, 2H), 7.74 (d, *J* = 7.8 Hz, 2H), 7.36 (ddd, *J* = 7.1, 5.5, 1.5 Hz, 2H), 5.78 (s, 1H), 2.34 (s, 6H), 0.70 (s, 3H).

ESI-MS: m+H^+/z 432.969, calculated for $C_{14}H_{19}N_2O_3PdS_2$ 432.98719, m+K^+/z 470.928, calculated for $C_{14}H_{18}KN_2O_3PdS_2$ 470.94307

Found: C, 38.57; H, 4.57; N, 5.93. Calculated for $C_{14}H_{18}N_2O_3PdS_2$×CH_3OH: C, 38.75; H, 4.77; N, 6.03.

Crystals suitable for X-ray analysis were obtained by dissolution of (dpms)$Pd^{II}Me(SMe_2)$ in H_2O and addition of CH_3OH in 1:1 ratio. Solvents were gently mixed and resulting solution was placed in the glove box freezer overnight.

In solution (dpms)$Pd^{II}Me(SMe_2)$ appears as a symmetrical complex due to fast rotation. Low temperature NMR showed that at temperatures below -40 °C C_6-H on the pyridine ring splits into two multiplets, and $H^{3,4,5}$ display broadening. In addition singlet corresponding to Pd–S(C*H*$_3$)$_2$ becomes a virtual doublet, consistent with fast rotation around Pd–S(CH_3)$_2$ bond.

Crystal data and structure refinement for (dpms)$Pd^{II}Me(SMe_2)$ (4.2)

Sample and crystal data

Identification code	2340	
Chemical formula	$C_{15}H_{22}N_2O_4PdS_2$	
Formula weight	464.86	
Temperature	150(2) K	
Wavelength	0.71073 Å	
Crystal size	0.17 × 0.23 × 0.27 mm	
Crystal habit	colorless prism	
Crystal system	monoclinic	
Space group	P 1 21/c 1	
Unit cell dimensions	a = 9.2940(8) Å	α = 90°
	b = 11.7682(10) Å	β = 90.1712(12)°
	c = 16.3112(14) Å	γ = 90°
Volume	1784.0(3) $Å^3$	
Z	4	
Density (calculated)	1.731 Mg/cm^3	
Absorption coefficient	1.296 mm^{-1}	
F(000)	944	

Data collection and structure refinement

Diffractometer	Bruker APEX-II CCD
Radiation source	sealed tube, MoKα
Theta range for data collection	2.13 to 30.00°
Index ranges	$-13 \le h \le 13$, $-16 \le k \le 16$, $-22 \le l \le 22$
Reflections collected	29714
Independent reflections	5204 [R(int) = 0.0192]
Coverage of independent reflections	100.0%
Absorption correction	multi-scan
Max. and min. transmission	0.8020 and 0.7110
Structure solution technique	direct methods
Structure solution program	ShelXS-97 (Sheldrick, 2008)
Refinement method	Full-matrix least-squares on F^2
Refinement program	SHELXL-2012 (Sheldrick, 2012)
Function minimized	$\Sigma\, w(F_o^2 - F_c^2)^2$
Data / restraints / parameters	5204 / 0 / 266
Goodness-of-fit on F^2	1.000
Δ/σ_{max}	0.001

Final R indices	4937 data; I>2σ(I) R_1 = 0.0176, wR_2 = 0.0393
	all data R_1 = 0.0189, wR_2 = 0.0398
Weighting scheme	$w=1/[\sigma^2(F_o^2)+(0.0100P)^2+1.8450P]$, $P=(F_o^2+2F_c^2)/3$
Extinction coefficient	0.0008(1)
Largest diff. peak and hole	0.633 and -0.594 eÅ^{-3}
R.M.S. deviation from mean	0.061 eÅ^{-3}

$R_{int} = \Sigma|F_o^2 - F_o^2(\text{mean})| / \Sigma[F_o^2]$
$R_1 = \Sigma||F_o| - |F_c|| / \Sigma|F_o|$
$\text{GOOF} = S = \{\Sigma[w(F_o^2 - F_c^2)^2] / (n - p)\}^{1/2}$
$wR_2 = \{\Sigma[w(F_o^2 - F_c^2)^2] / \Sigma[w(F_o^2)^2]\}^{1/2}$

Preparation of R_4N(dpms)Pd^{II}Me(I) (4.7)

In the glove box, 15.3 mg of (dpms)$Pd^{II}Me(SMe_2)$ (35.3 µmol) was dissolved in 2 mL of $CHCl_3$, to this solution 11.0 mg of Pr_4NI (35.3 µmol) or Bu_4NI was added. Upon addition of Pr_4NI yellow solution turned red indicating the ligand exchange between SMe_2 and I^-. The solution was stirred for few minutes followed by evaporation of the solvent and drying of the product under vacuum to remove SMe_2. The reaction gives the product as a red solid which was used without further purification, yield 97 %. The product is easily soluble in $CHCl_3$ and CH_2Cl_2, and poorly soluble in H_2O. In the solid state Pr_4N(dpms)Pd^{II}Me(I) is very stable in the glove box freezer, and decomposition outside of the glove box at r.t. is slow.

The use of KI or Me_4NI as a source of I^- resulted in rapid decomposition of the starting material.

Major isomer:

^{1}H NMR (600 MHz, $CDCl_3$) δ 9.03 (dt, *J* = 5.0, 1.5 Hz, 1H), 8.78 (d, *J* = 8.1 Hz, 1H), 8.63 (d, *J* = 8.1 Hz, 1H), 8.46 – 8.42 (m, 1H), 7.83 (td, *J* = 7.8, 1.7 Hz, 1H), 7.71 (td, *J* = 7.8, 1.8 Hz, 1H), 7.32 – 7.28 (m, 1H), 7.16 (ddd, *J* = 7.1, 5.5, 1.3 Hz,

1H), 6.62 (s, 1H, C*H*-SO_3), 3.37 – 3.24 (m, 8H, Bu_4N^+), 1.72 – 1.62 (m, 8H, Bu_4N^+), 1.39 (s, *J* = 7.4 Hz, Bu_4N^+), 0.97 (t, *J* = 7.3 Hz, 12H, Bu_4N^+), 0.90 (s, 3H, Pd-CH_3).

^{13}C NMR (126 MHz, $CDCl_3$) δ 156.62, 155.11, 152.49, 150.14, 138.73, 138.15, 124.80, 124.26, 124.11, 123.37, 73.00 (*C*H-SO_3), 61.07 (Pr_4N^+), 16.18 (Pr_4N^+), 11.05 (Pr_4N^+), -8.08 (Pd-CH_3).

Minor isomer

^{1}H NMR (500 MHz, $CDCl_3$) δ 9.23 (d, *J* = 5.5 Hz, 1H), 8.72 (d, *J* = 8.5 Hz, 1H), 8.49 (d, *J* = 5.6 Hz, 1H), 7.67 – 7.62 (m, 2H), 7.25 – 7.19 (m, 2H), 5.66 (s, 1H, C*H*-SO_3), 0.81 (s, 3H, Pd-CH_3).

ESI-MS: m/z 496.84; calculated for $C_{24}H_{40}IN_3O_3PdS$ 496.86481

Found: C, 39.15; H, 5.59; N, 5.72. Calculated for $C_{24}H_{40}IN_3O_3PdS\times CH_2Cl_2$: C, 39.05; H, 5.51; N, 5.46.

Preparation of Pr_4N(dpms)Pd^{II}Me(OH) (4.6)

In the glove box solid Pr_4N(dpms)Pd^{II}Me(I) (35.2 mg, 51.46 μmol), Ag_2O (11.9 mg, 51.46 μmol) and 2 mL of deaerated H_2O were placed in a 5 mL round bottom flask, and the mixture was stirred for 10 min in the dark to form grey slurry. The mixture was filtered and the filter was washed with clean H_2O to collect the product. The resulting clear colorless solution was evaporated to give a yellow product in 90 % yield. The product is air sensitive and was kept in the glove box freezer as a solid or in aqueous solution. Pr_4N(dpms)Pd^{II}Me(OH) has very good solubility in H_2O, and decomposes slowly with formation of Pd black and free ligand upon prolonged standing at r.t. under inert atmosphere. Product decomposes within minutes in DMSO and MeOH via loss of a ligand.

^{1}H NMR (600 MHz, D_2O) δ 8.66 (d, ^{3}J = 6.3 Hz, 1H), 8.62 (d, ^{3}J = 5.7 Hz, 1H), 7.98 (td, J = 1.7, 8.0 Hz, 1H), 7.96 (td, J = 1.7, 8.0 Hz, 1H), 7.74 (d, ^{3}J = 7.8 Hz, 1H), 7.71 (d, ^{3}J = 7.8 Hz, 1H), 7.52 (m, 1H), 7.41 (ddd, J = 1.3, 5.9, 7.4 Hz, 1H), 5.98 (s, 1H, C*H*-SO_3) 3.24 – 3.05 (m, 8H, Pr_4N^+), 1.83 – 1.54 (m, 8H, Pr_4N^+), 0.93 (t, J = 7.6 Hz, 12H, Pr_4N^+), 0.57 (s, 3H, Pd-C*H*$_3$).

1,4-Dioxane was used as an internal standard and a reference peak in ^{13}C NMR.

^{13}C NMR (151 MHz, H_2O/D_2O) δ: 153.85, 152.53, 150.00, 149.72, 139.68, 139.48, 129.91, 128.76, 125.75, 125.38, 75.40 (*C*H-SO_3), 60.48 (Pr_4N^+), 15.41 (Pr_4N^+), 10.45 (Pr_4N^+), -2.45 (Pd-C*H*$_3$).

ESI-MS: m/z 386.970; calculated for $C_{12}H_{13}N_2O_4PdS$, 386.96309 (dpms)$Pd^{II}CH_3(OH)$.

Independent synthesis of $Pr_4N(dpms)Pd^{II}(OH)_2$ (4.4)

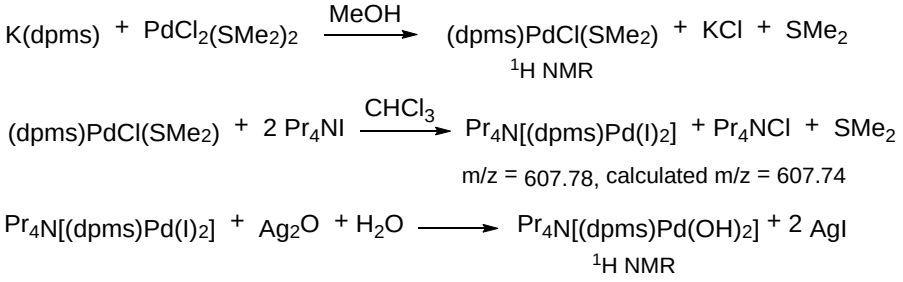

In order to confirm the identity of the products in aerobic oxidation reactions, $Pr_4N(dpms)Pd^{II}(OH)_2$ was independently synthesized using the following procedure: in a vial with stir bar, K(dpms) ligand (28.8 mg, 100 μmol) was dissolved in 1.5 mL of methanol, followed by addition of $Pd^{II}Cl_2(SMe_2)_2$ (30.4 mg, 100 μmol). Light yellow precipitate began to form within 2-3 minutes of stirring. Precipitate was collected by filtration and washed with small amount of methanol (35.2 mg, 80% yeld). Product was identified as (dpms)$Pd^{II}Cl(SMe_2)$ and is poorly soluble in H_2O.

^{1}H NMR (400 MHz, D_2O) δ 8.92 (d, ^{3}J = 6.9 Hz, 1H), 8.78 (d, ^{3}J = 6.6 Hz, 1H), 8.17 (td, J = 1.3, 8.7 Hz, 1H), 8.13 (td, J = 1.3, 8.7 Hz, 1H), 7.92 (d, ^{3}J = 8.6 Hz, 2H), 7.88 (d, ^{3}J = 8.2 Hz, 2H) 7.62 (ddd, J = 1.5, 5.7, 8.1 Hz, 1H), 7.56 (m, 1H), 6.30 (s, 1H, C*H*-SO_3), 1.23 (s, 6H, S(C*H*$_3$)$_2$).

(dpms)$Pd^{II}Cl(SMe_2)$ (35.2 mg, 77.7 μmol) was suspended in 1 mL of dichloromethane and Pr_4NI (24.3 mg, 77.7 μmol) was added, resulting in deep red clear solution. Solution was stirred for 15 minutes, and the solvent was evaporated, giving dark red solid. ^{1}H NMR analysis showed a mixture of products. ESI-MS spectrum showed presence of three species: (dpms)$Pd^{II}(I)_2$ (major), (dpms)$Pd^{II}Cl(I)$, and (dpms)$Pd^{II}(Cl)_2$.

ESI-MS: m/z 608.780; calculated for $C_{11}H_9I_2N_2O_3PdS$, 608.74581 (dpms)$Pd^{II}(I)_2$. m/z 516.890; calculated for $C_{11}H_9ClIN_2O_3PdS$, 516.81019 (dpms)$Pd^{II}Cl(I)$ m/z 424.869; calculated for $C_{11}H_9Cl_2N_2O_3PdS$, 424.87458 (dpms)$Pd^{II}(Cl)_2$.

Residue, which was obtained after evaporation of the solvent in the previous step was used without purification. Solid suspended in 1.5 mL of water, followed by addition of Ag_2O (18.0 mg, 77.7 μmol). Mixture was stirred for 30 minutes or until brown residue disappeared and grey slurry was formed. Slurry was filtered through filter aid Celite to give clear light yellow solution, containing target product (dpms)$Pd^{II}(OH)_2$.

^{1}H NMR (600 MHz, D_2O): δ 8.58 (d, ^{3}J = 5.8 Hz, 2H), 8.05 (t, ^{3}J = 7.8 Hz, 2H), 7.78 (d, ^{3}J = 7.8 Hz, 2H), 7.52 (t, ^{3}J = 6.9 Hz, 2H), 6.12 (s, 1H, C*H*-SO_3), 3.18 – 3.12 (m, 8H, Pr_4N^+), 1.74 – 1.64 (m, 8H, Pr_4N^+), 0.94 (t, J = 7.8 Hz, 12H, Pr_4N^+).

^{13}C NMR (151 MHz, D_2O): δ 151.55, 150.31, 140.68, 129.23, 125.68, 75.41 (*C*H-SO_3), 60.50 (Pr_4N^+), 15.42 (Pr_4N^+), 10.46 (Pr_4N^+).

Attempts to obtain ESI-MS spectrum were unsuccessful.

Determination of Yields of Gaseous Products

For determination of yields of gaseous products, reactions were performed in J. Young NMR tube. Upon full conversion of the starting complex, aqueous and gaseous phase were equilibrated via vigorous shaking. Concentration of gases in the aqueous phase was determined using ^{1}H NMR spectroscopy. Yields of C_2H_6 and CH_4 were then calculated using Henry's Law and the Ideal Gas Law. Henry's constant was determined experimentally for H_2O/D_2O = 1:1, and for 1M KOH solution in H_2O/D_2O = 1:1.

General procedure for determination of Henry's constant

A J. Young NMR tube of known volume was filled with 0.58 mL of H_2O/D_2O = 1:1 open to air and C_2H_6 was bubbled though the solution for one minute. NMR tube was sealed with Teflon valve and shaken. Concentration of C_2H_6 in aqueous phase was determined by integration of peak at 0.81 ppm *vs.* internal standard 1,4-dioxane at ambient temperature. Calculated $k_H = 2.26 \times 10^{-3}$ mol L^{-1} atm^{-1} at 295.0K is in good agreement with literature value $k_H = 2.17 \times 10^{-3}$ mol L^{-1} atm^{-1} (293.15 K).[157]

Henry's constant for C_2H_6 at high pH was determined using aqueous solution of H_2O/D_2O in 1:1 ratio. Solution pH was adjusted to pH 13.3 using 0.1 mL of 1M KOH, resulting in 0.56 mL total volume. Concentration of C_2H_6 in aqueous phase was determined by integration of peak at 0.81 ppm *vs.* internal standard 1,4-dioxane

at ambient temperature. Henry's constant was calculated $k_H = 2.63\times10^{-3}$ mol L^{-1} atm^{-1} at 295.0 K, and is in good agreement with literature value.[157] A literature value for Henry's constant for CH_4 was also used.[157]

Reactivity of (dpms)Pd^{II}Me(SMe_2) towards O_2 in the absence of additives

A solution of (dpms)Pd^{II}Me(SMe_2) (1.6 mg, 3.8 μmol) was prepared in the glove box and was transferred into NMR tube with air tight Teflon valve. The reaction mixture was taken out of the glove box and was purged with pure O_2 for a minute. NMR tube was kept at ambient temperature and light, the reaction of the starting material with O_2 was monitored by ^{1}H NMR spectroscopy. In 6-8 days no more starting material was observed. Yields were determined by integration against internal standard 1,4-dioxane. Products of oxidation included MeOH (37%), C_2H_6 (5%), SMe_2 (33%), Me_3S^+ (26%), and Me_2SO (2%), and unknown signals at 2.35 and 2.31 ppm, corresponding to 16% of methyl group equivalents.

^{1}H NMR (400 MHz, D_2O); **C_2H_6** δ 0.81 (s); **SMe_2** δ 2.11 (s), **Me_2SO** δ 2.71 (s), **Me_3S^+** δ 2.90 (s); **MeOH** δ 3.34 (s).

Reactivity of (dpms)Pd^{II}Me(SMe_2) towards O_2 in 1M KOH

To a solution of (dpms)Pd^{II}Me(SMe_2) (1.6 mg, 3.8 μmol) in 0.5 mL of D_2O, 28 mg (0.5 mmol) of KOH was added. Mixture was prepared in the glove box and was transferred into NMR tube with air tight Teflon valve. The reaction was taken out of the glove box and was purged with pure O_2 for a minute. NMR tube was kept at ambient temperature and light, the reaction of the starting material with O_2 was monitored by ^{1}H NMR spectroscopy. In 6 days no more starting material was observed. Yields were determined by integration against internal standard 1,4-dioxane. Products of oxidation included MeOH (61%), MeOOH (7%).

^{1}H NMR (400 MHz, D_2O): **MeOH** δ 3.34 (s), **MeOOH** δ 3.66 (s) at pH 14.

Reactivity of (dpms)Pd^{II}Me(SMe$_2$) towards Argon

A solution of (dpms)Pd^{II}Me(SMe$_2$) (1.2 mg, 2.7 μmol) was prepared in the glove box and was transferred into NMR tube. The NMR tube was filled to the top with 2.7 mL with D_2O so that no headspace was left to avoid the escape of volatiles into the gas phase. Reaction mixture was sealed with airtight Teflon valve, and was kept at ambient temperature without stirring. Decomposition of the starting material was monitored by ^{1}H NMR. In approximately 5 days abundant black precipitate was formed. Products of decomposition were generated: MeOH (2%), C_2H_6 (40%), CH_4 (24%), CH_3D (4%), SMe_2 (100%), Me_3S^+ (2%), and unknown signal at 2.22 ppm, corresponding to 21% of methyl group equivalents.

Oxidation of Pr$_4$N(dpms)Pd^{II}Me(I) with O$_2$

A solution of Pr$_4$N(dpms)Pd^{II}Me(I) (2.8 mg, 4.09 μmol) was prepared in the glove box and was transferred into NMR tube with air tight Teflon valve. The reaction mixture was taken out of the glove box and was purged with pure O_2 for a minute. NMR tube was kept at ambient temperature and the reaction of the starting material with O_2 was monitored by ^{1}H NMR spectroscopy. In 48 h no more starting material was observed. Yields were determined by integration against internal standard 1,4-dioxane. Products of oxidation included MeI (37%), C_2H_6 (4% in solvent phase) and MeOH (23%).

^{1}H NMR (400 MHz, D_2O); **C_2H_6** δ 0.86 (s); **MeI** δ 2.17 (s); **MeOH** δ 3.49 (s).

Reactivity of Pr$_4$N(dpms)Pd^{II}Me(I) under Ar

A solution of Pr$_4$N(dpms)Pd^{II}Me(I) (3.3 mg, 4.8 μmol) was prepared in the glove box and was transferred into NMR tube. The NMR tube was filled to the top

with 2.7 mL with $CDCl_3$ so that no headspace was left to avoid the escape of volatiles into the gas phase. Reaction mixture was sealed with air tight Teflon valve, and was kept at ambient temperature without stirring. Decomposition of the starting material was monitored by ^1H NMR. In approximately 5 days conversion or the starting complex was 91%. Products of decomposition were generated: C_2H_6 (20%), CH_4 (41%), CH_3D (13%), MeI (15%), CH_3Cl (14%), and unknown signal at 2.66 ppm, corresponding to 6% of methyl group equivalents.

Reactivity of $Pr_4N(dpms)Pd^{II}Me(I)$ under Ar with Pr_4NI

A solution of $Pr_4N(dpms)Pd^{II}Me(I)$ (2.1 mg, 3.1 μmol) and Pr_4NI (1.0 mg, 3.1 μmol) was prepared in the glove box and was transferred into NMR tube. The NMR tube was filled to the top with 2.7 mL with $CDCl_3$ so that no headspace was left to avoid the escape of volatiles into the gas phase. Reaction mixture was sealed with air tight Teflon valve, and was kept at ambient temperature without stirring. Decomposition of the starting material was monitored by ^1H NMR. In approximately 24 h full conversion or the starting complex was observed. Products of decomposition were generated: CH_4 (9%), CH_3D (10%), MeI (33%), CH_3Cl (4%), and unknown signal at 2.66 ppm, corresponding to 25% of methyl group equivalents.

Oxidation of $Bu_4N(dpms)Pd^{II}Me(I)$ with I_2

To a solution of $Bu_4N(dpms)Pd^{II}Me(I)$ (7.9 mg, 10.8 μmol) in $CHCl_3$, 4.7 mg of I_2 was added (18.5 μmol). Within minutes no starting material was detected by ^1H NMR. Analysis of the product mixture showed quantitative formation of MeI and $Bu_4N(dpms)Pd^{II}(I)_2$. Inorganic $Bu_4N(dpms)Pd^{II}(I)_2$ exists in solution as a mixture of

exo and endo isomers with different ratios in $CHCl_3$ and MeOH. Yields were determined by integration against internal standard 1,4-dioxane.

Major isomer:

^{1}H NMR (600 MHz, $CDCl_3$) δ 9.25 (dd, *J* = 5.6, 0.9 Hz, 1H), 8.74 (dd, *J* = 8.0, 0.9 Hz, 1H), 7.84 (td, *J* = 7.8, 1.6 Hz, 2H), 7.23 (ddd, *J* = 7.5, 5.8, 1.5 Hz, 2H), 6.74 (s, 1H), 3.38 – 3.23 (m, 8H), 1.72 – 1.65 (m, 8H), 1.43 (h, *J* = 7.4 Hz, 8H), 0.99 (t, *J* = 7.3 Hz, 12H).

Minor isomer:

^{1}H NMR (600 MHz, $CDCl_3$) δ 9.78 (dd, *J* = 5.8, 1.6 Hz, 2H), 7.81 (dd, *J* = 7.7, 1.8 Hz, 2H), 7.67 (dd, *J* = 7.8, 1.5 Hz, 2H), 7.20 (ddd, *J* = 7.5, 6.3, 1.5 Hz, 2H), 5.74 (s, 1H), 3.38 – 3.23 (m, 8H), 1.72 – 1.65 (m, 8H), 1.43 (h, *J* = 7.4 Hz, 8H), 0.99 (t, *J* = 7.3 Hz, 12H).

ESI-MS: m/z 608.780; calculated 608.74581 for $(dpms)Pd^{II}(I)_2$.

Oxidation of $Bu_4N(dpms)Pd^{II}Me(I)$ with I_2 in the presence of TEMPO

To a solution of $Pr_4N(dpms)Pd^{II}Me(I)$ (1.9 mg, 2.8 μmol) in $CHCl_3$, 0.8 mg (2.8 μmol) of TEMPO, and 0.71 mg (2.8 μmol) of I_2 were added. ^{1}H NMR spectrum was recorded within minutes, and no starting material was detected by ^{1}H NMR. Analysis of the product mixture showed quantitative formation of MeI and $Pr_4N(dpms)Pd^{II}(I)_2$. Yields were determined by integration against internal standard 1,4-dioxane.

Reactivity of $Pr_4N(dpms)Pd^{II}Me(I)$ with MeI

A solution of $Pr_4N(dpms)Pd^{II}Me(I)$ (4.4 mg, 6.4 μmol) and CH_3I (2.7 μL, 43.8 μmol), and a solution of $Pr_4N(dpms)Pd^{II}Me(I)$ (2.0 mg, 2.9 μmol) and CD_3I (1.0 μL,

16.1 μmol) were prepared in the glove box, and were transferred into NMR tube with air tight Teflon valve. The reaction mixture was kept at ambient temperature and light under Ar. After 48 h starting complex was completely consumed. Product distribution was analyzed by ^{1}H NMR spectroscopy.

Chapter 5 : Mechanistic Studies of Methanol and Ethane Formation in Oxidation Reactions of (dpms)$Pd^{II}Me(OH)^-$ in Water

5.1 Introduction

5.1.1 O_2 Insertion into M-R Bond

In Chapter 4 we have discussed aerobic functionalization of C-H bonds mediated by Pd^{II}/Pd^0 and Pd^{IV}/Pd^{II} redox couples. In these systems molecular oxygen acts as an oxidant for the Pd center[138,139,141] or for the cocatalyst[133,137] (electron transfer mediator). Another type of Pd-mediated C-H bonds functionalization does not require change of the metal oxidation state and involves insertion of O_2 into M-R bond. These reactions are rare (M = Pd, Pt; R = H, Me). One of the recent examples was reported by Goldberg and co-workers (Scheme 5.1, **A**). Mechanism of this reaction has not been fully elucidated, but preliminary observations suggest radical chain mechanism.[158]

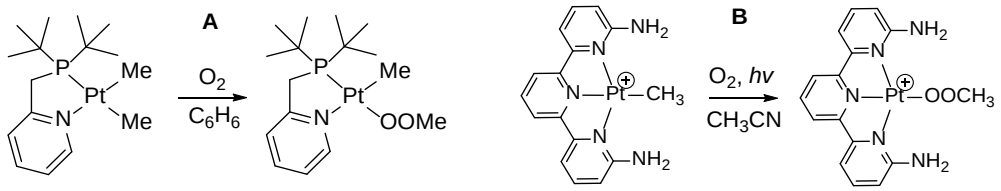

Scheme 5.1 A: Insertion of O_2 into Pt^{II}-Me bond of (PN)$Pt^{II}Me_2$ (PN = 2-(di-*tert*-butylphosphinomethyl)pyridine. B: Insertion of O_2 into Pt^{II}-Me bond of [(^{NH2}terpy)Pt^{II}Me][SbF_6].

Another example of O_2 insertion into Pt^{II}-C bond to form methylperoxo Pt^{II} complex was demonstrated with a diaminoterpyridine ligand (Scheme 5.1, **B**). The reaction was proposed to proceed via formation of singlet oxygen, where

[(^{NH_2}terpy)Pt^{II}Me][SbF_6] acts as a O_2 sensitizer, and not via radical mechanism. This unusual reactivity was attributed to the amino substituents, which have a marked effect on the electronic properties of the complex. Analogous [(terpy)Pt^{II}Me][SbF_6] without the amino group does not result in O_2 insertion reaction.[159]

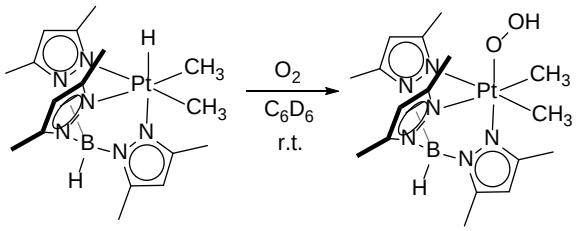

Scheme 5.2 Insertion of O_2 into Pt^{II}-Me bond of Tp^{Me2}PtMe$_2$H (Tp^{Me2} = hydridotris(3,5-dimethylpyrazolyl)borate).

Insertion of O_2 into Pt-H bond has been reported with a Pt^{IV} dimethyl hydride complexes to form hydroperoxo Pt^{IV} species (Scheme 5.2).[160] A detailed mechanistic analysis is strongly suggestive of a radical chain pathway.[161]

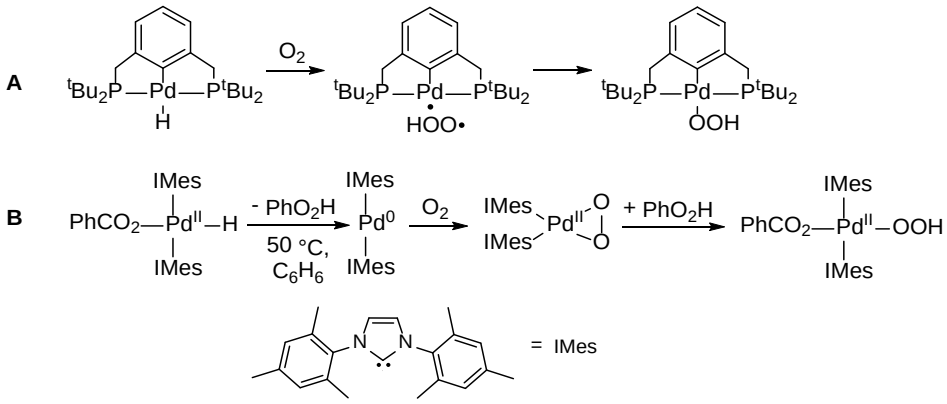

Scheme 5.3 A: Insertion of O_2 into Pd^{II}-H bond of (^{tBu}PCP)Pd^{II}H. B: Insertion of O_2 into Pd^{II}-H bond of *trans*-(IMes)$_2$Pd(H)(O_2CAr).

In 2006 Goldberg *et al.* reported insertion of dioxygen into Pd^{II}-H bond. Formation of relatively stable hydroperoxo intermediate (^{tBu}PCP)Pd^{II}OOH was observed along with hydroxo complex (^{tBu}PCP)Pd^{II}OH (Scheme 5.3, **A**).[162] The mechanism of O_2 insertion into Pd^{II}-H bond was elucidated using DFT calculations. It was determined that the process operates hydrogen atom abstraction mechanism

followed by fast radical recombination.[163] This conclusion is supported by high kinetic isotope effect k_H/k_D = 5.8 (Pd^{II}-H/ Pd^{II}-D).[162]

Non-radical mechanism for the insertion of O_2 into Pd^{II}-H bond was proposed by Stahl *et al*. in N-heterocyclic carbene supported *trans*-$(IMes)_2Pd(H)(O_2CAr)$.[164] When para-substituted benzoates ($ArCO_2^-$ ligand) have electron withdrawing substituents, reductive elimination of $ArCO_2H$ and formation of trans-$(IMes)_2Pd^0$ occurs before O_2 activation. Reductive elimination of $PhCO_2H$ is followed by oxidative addition of O_2, protonolysis of the resulting $Pd(\eta^2\text{-}O_2)$ complex, and recoordination of $PhCO_2^-$ ligand to generate trans-$(IMes)_2Pd(OOH)(O_2CAr)$ (Scheme 5.3, **B**). However, when para-substituents on benzoate ligand were electron donating, mechanism switched from reductive elimination to hydrogen atom abstraction.[164,165]

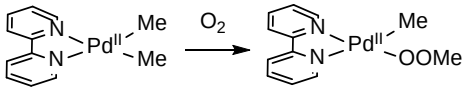

Initiation

AIBN → 2 In•

In• + O_2 → InOO•

Propagation

InOO• + (bpy)$Pd^{II}Me_2$ → (bpy)Pd^{II}Me(OOIn) + Me•

Me• + O_2 → MeOO•

MeOO• + (bpy)$Pd^{II}Me_2$ ⇌ (bpy)$Pd^{III}Me_2$(OOMe)•

(bpy)$Pd^{III}Me_2$(OOMe)• → (bpy)Pd^{II}Me(OOMe) + Me•

Termination

MeOO• + (bpy)$Pd^{III}Me_2$(OOMe)• → non-propagating products

Scheme 5.4 Proposed mechanism for insertion of O_2 into Pd^{II}-Me bond of (bpy)$Pd^{II}Me_2$.

Of particular interest is the example of O_2 insertion into the Pd^{II}-Me bond of the (bpy)$Pd^{II}Me_2$ complex. The effects of light and a radical initiator implicate mechanism involving radical intermediates. Kinetic studies showed reaction rates were fully reproducible in the presence of radical initiator AIBN, half-order dependence on [AIBN] and on the [Pd^{II}] was found. The proposed mechanism is shown in Scheme 5.4 and involves attack of MeOO• at the Pd center. This results in

homolytic displacement of Me group in a stepwise process via formation of pentacoordinate Pd^{III} intermediate. The half-order dependence on [Pd^{II}] was explained in terms of termination step. A termination by homocoupling of two MeOO• radicals would lead to the 1st-order dependence on [Pd^{II}]. The involvement of (bpy)$Pd^{III}Me_2$(OOMe)• was proposed to account for the experimentally observed kinetic behavior.[166]

5.1.2 Palladium Mediated Formation of Ethane

Palladium-mediated formation of C-C bonds is well-known in organometallic chemistry.[167] Two general pathways leading to C_2H_6 from $LPd^{II}Me_2$ intermediates are: 1) direct C-C bond forming reductive elimination; or 2) oxidatively induced C-C coupling. Examples or direct reductive elimination of ethane from dimethyl-Pd(II) complexes dates back to 1980s.[168,169] Factors that control these transformations have been extensively studied.[170] Examples include facile elimination of ethane from strained $Pd^{II}Me_2$ complexes (Scheme 5.5),[171] or by thermal decomposition of bis(phosphine)dimethylpalladium complexes[169,172].

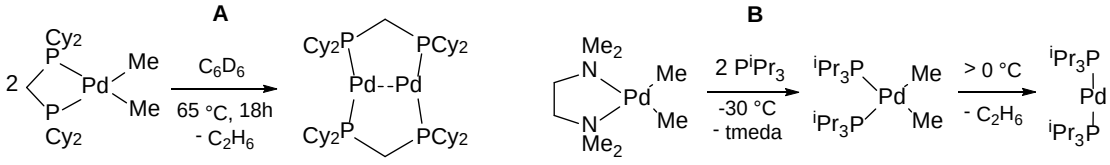

Scheme 5.5 Examples of reductive elimination of ethane from strained $Pd^{II}Me_2$ complexes.

In the pioneering work demonstrating the first isolated Pd^{IV} complex, (bpy)$Pd^{IV}Me_3I$, formation of ethane occurred at 100-110 °C.[173] A detailed study suggested that formation of pentacoordinate specie via dissociation of iodide preceded ethane formation (Scheme 5.6).[174,175]

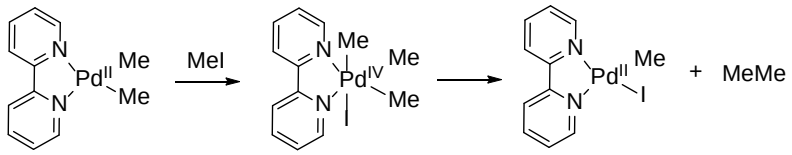

Scheme 5.6 Oxidation of (bpy)$Pd^{II}Me_2$ with MeI, followed by reductive elimination of ethane.

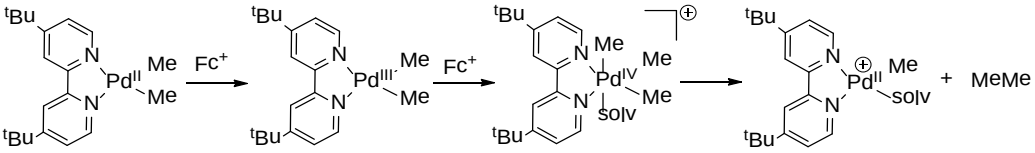

Scheme 5.7 Oxidation of ($^tBu_2$bpy)$Pd^{II}Me_2$ with Fc^+, followed by reductive elimination of ethane.

The mechanism of oxidatively induced coupling of Me-Me was studied by Sanford *et al*. Reaction of (^{t}Bu$_2$bpy)$Pd^{II}Me_2$ with 1.1 equiv. ferrocenium hexafluorophosphate ($Cp_2Fe^+PF_6^-$, Fc^+) in acetone-d_6 at 25 °C was complete within minutes and resulted in quantitative formation of (^{t}Bu$_2$bpy)Pd^{II}Me(acetone)$^+$ and ethane. Mechanistic tests are consistent with the pathway, involving: 1) one electron oxidation to form Pd^{III} intermediate; 2) disproportionation to form $Pd^{IV}Me_3$; and 3) C-C coupling to form ethane (Scheme 5.7).[176]

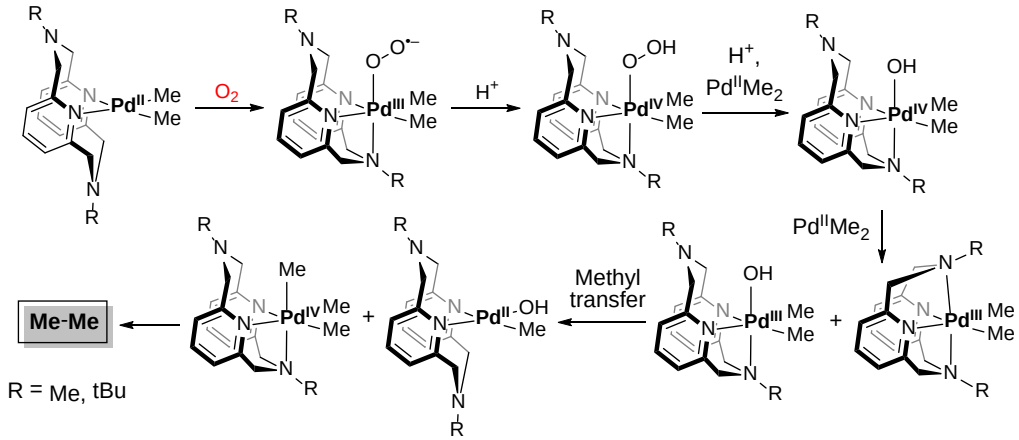

Scheme 5.8 Oxidation of (N4)Pd^{II}Me(OH) with O_2, followed by reductive elimination of ethane.

The first example of ethane formation upon aerobic oxidation of (N4)$Pd^{II}Me_2$ complexes was reported in 2012. Oxidation with O_2 was shown to lead to Pd^{III} species, followed by methyl group transfer to form (N4)$Pd^{IV}Me_3$. Transient formation

of the latter complex is needed for selective elimination of C_2H_6 and monomethyl (N4)Pd^{II}Me(OH). Based on the experimental results, oxidation of Pd^{II} by O_2, generates a transient Pd^{III}-superoxide intermediate (Scheme 5.8). These intermediates have been proposed earlier in aerobic Pt and Pd chemistry.[73-75,77,78] Formation of this intermediate is supported by direct observation of EPR active DMPO adduct (DMPO = 5,5-dimethyl-1-pyrroline-N-oxide). Upon protonation of Pd^{III} superoxide, a Pd^{IV}-hydroperoxide was detected by ESI-MS. The latter was proposed to oxidize another molecule of Pd^{II} to form two equivalents of (N4)$Pd^{IV}Me_2$(OH). The latter species can undergo comproportionation in the presence of Pd^{II} to yield (k^3-N4)$Pd^{III}Me_2$(OH) and $[(N4)Pd^{III}Me_2]^+$. Formation of trimethyl Pd^{IV} species results in elimination of ethane with $t_{1/2}$ = 68 min (N4 = ^{Me}N4).[78,177] Same mechanism was also proposed for aerobic oxidation of (Me_3tacn)$Pd^{II}Me_2$ (Me_3tacn = *N,N',N"*-trimethyl-1,4,7-triazacyclononane).[178]

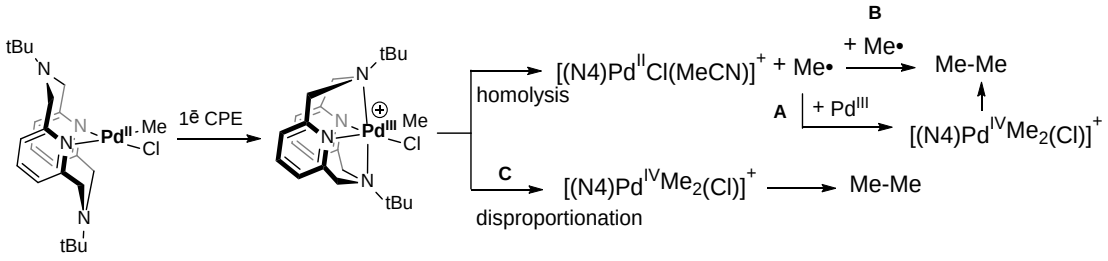

Scheme 5.9 Oxidation of (^{tBu}N4)Pd^{II}Me(Cl) with controlled potential electrolysis, followed by reductive elimination of ethane.

The only example of ethane elimination from monomethyl Pd^{II} complex also came from Mirica group. Controlled potential electrolysis of (^{tBu}N4)Pd^{II}Me(Cl) generated Pd^{III} complex, $[(^{tBu}N4)Pd^{III}Me(Cl)]^+$, which is stable in the absence of light in solid state at -20 °C. When its solution is exposed to light, elimination of ethane (25 ± 1% yield), methyl chloride (8 ± 1%), and methane (9 ± 2%) occurs over 6 h. Mechanistic tests suggest a homolytic cleavage of Pd^{III}-Me bond according to

Scheme 5.9. Three pathways have been considered: **A**) reaction of Me• with (^{tBu}N4)Pd^{II}Me(Cl) to form (^{tBu}N4)Pd^{III}Me$_2$(Cl), followed by reductive elimination; or **B**) homocoupling of Me•. Non-radical pathway, occurring via disproportionation of (^{tBu}N4)Pd^{II}Me(Cl) could not be excluded (Scheme 5.9, **C**).[148]

5.1.3 Possible Mechanisms of MeOH and C_2H_6 Formation in (dpms)Pd^{II}Me(OH)$^-$/O_2 System

In Chapter 4 we described formation of methanol and ethane upon aerobic oxidation of (dpms)Pd^{II}Me(OH)$^-$ complexes in water (Scheme 4.22). In view of the research accounts discussed above, the possible pathways, leading to ethane may include: **A**) homolytic cleavage of Pd^{II}-Me bond to form Me• radicals, the latter can undergo homocoupling, or reaction with (dpms)Pd^{II}Me(OH)$^-$ to form (dpms)Pd^{III}Me$_2$(OH)$^{-\bullet}$; **B**) non-homolytic redox disproportionation of monomethyl (dpms)Pd^{II}Me(OH)$^-$ to form (dpms)Pd^{IV}Me$_2$(OH) and Pd^0; and **C**) non-redox disproportionation to form dimethyl (dpms)Pd^{II}Me$_2^-$ and (dpms)Pd^{II}(OH)$_2^-$ followed by direct reductive elimination of ethane from (dpms)Pd^{II}Me$_2^-$ [151] (Scheme 5.10).

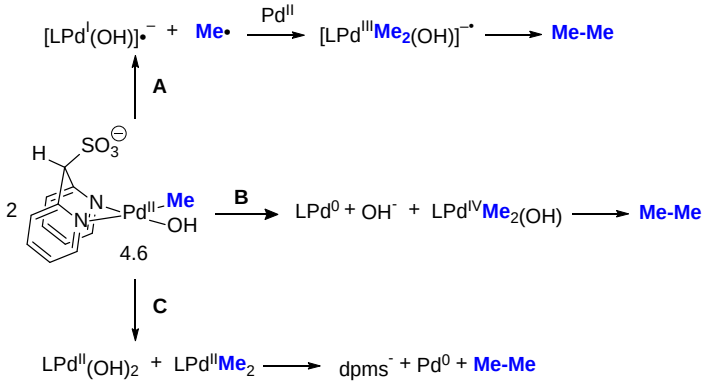

Scheme 5.10 Proposed mechanism for formation of C_2H_6 from (dpms)Pd^{II}Me(OH)$^-$ complex.

Formation of methanol might occur similarly to the (dpms)Pt^{II}Me(OH)$^-$/O_2 system, where oxidation of (dpms)Pt^{II}Me(OH)$^-$ leads to (dpms)Pt^{IV}Me(OH)$_2$. The

latter complex undergoes protonation followed by S_N2-type attack by H_2O molecule at the electrophilic carbon atom of the $Pd^{IV}Me$ group (Scheme 5.11, **A**).[98] Alternatively MeOH can form via direct reductive elimination or via OH^- attack at $Pd^{II}Me$ group (Scheme 5.11, **B**). Finally, insertion of O_2 into Pd^{II}-Me bond could result in formation of $Pd^{II}OOMe$ by radical chain mechanism, analogous to one reported by Goldberg[166], followed by reduction of MeOOH by Pd^{II} to form MeOH (pathway **C**).

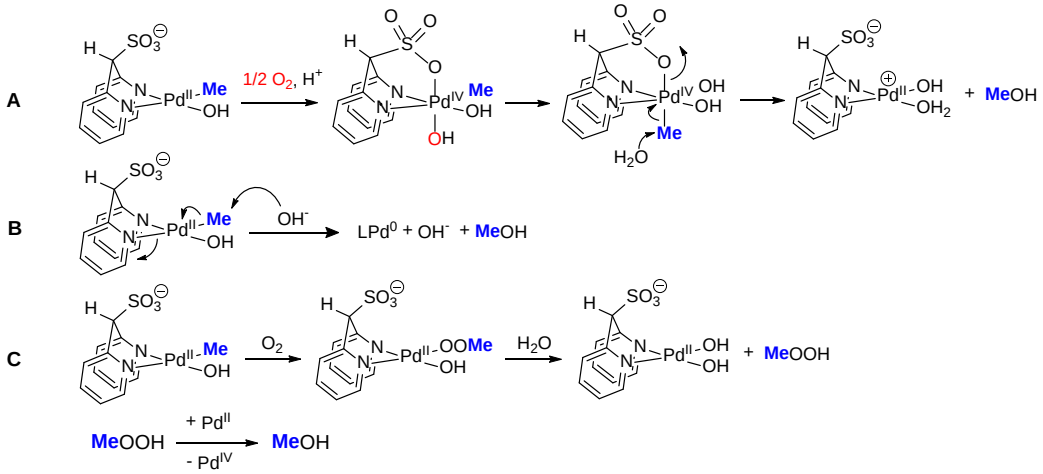

Scheme 5.11 Proposed mechanism for formation of MeOH from $(dpms)Pd^{II}Me(OH)^-$.

In this chapter, we will explore mechanism of aerobic oxidation of $LPd^{II}Me(OH)^-$ via kinetic measurements, analysis of product distribution, and model reactions. These studies are important for the development of catalysts for the aerobic functionalization of alkanes.

5.2 Mass Balance in Aerobic Oxidation of $(dpms)Pd^{II}Me(OH)^-$ in Water at pH 10.6, and 14.0

Oxidation of the aqueous solution of $(dpms)Pd^{II}Me(OH)^-$ with 1 atm O_2 was performed in a J. Young NMR tube. Oxygen was bubbled through the solution for

one minute and the NMR tube was sealed with a Teflon valve. Reaction mixture was kept at ambient temperature and light and ^{1}H NMR spectrum was recorded periodically. The NMR relaxation delay was set to 60 s to accurately quantify the products formed. Yields were determined by integration versus the internal standard 1,4-dioxane, and given as an average of at least two runs. Yield of ethane was calculated using Henry's constant and the Ideal Gas Law. Henry's constant for C_2H_6 was determined experimentally and was in good agreement with the reported value[157].

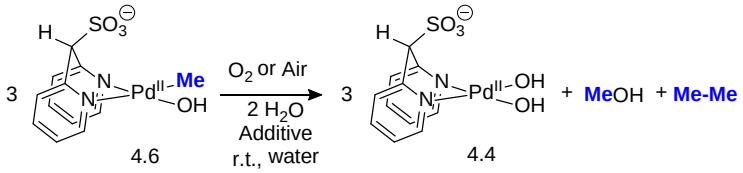

Scheme 5.12 Oxidation of $R_4N(dpms)Pd^{II}Me(OH)$ with O_2 at pH 10.6 under ambient conditions.

Entry	pH , Additive	Conversion (%) / Reaction time	C_2H_6 (%)	MeOH (%)	MeOOH (%)	Other Products (%)
1	O_2, pH 10.6, no additives	98 / 6 days	82 ± 4	16 ± 3	0	$LPd^{II}(OH)_2^-$, 83 ± 5
2	O_2, pH 14.0, 1.0 M KOH	100 / 2 days	n.a.	49 ± 1	20 ± 1	$LPd^{II}(OH)_2^-$, 71 ± 1 $dpms^-$, 21 ± 1
3	Ar, pH 10.6, no additives	99 / 7 days	55 ± 3	0	0	CH_4, 43 ± 1 $dpms^-$, 47 ± 1

Table 5.1 Product distribution in oxidation of $R_4N(dpms)Pd^{II}Me(OH)$ with O_2 at pH 10.6 and 14.0 under ambient conditions. Yields are calculated at 100% conversion.

Slow conversion of the starting complex at pH 10.6 resulted in formation of C_2H_6 (82 ± 4%) and MeOH (16 ± 3 %) (Scheme 5.12, Table 5.1 entry 1), no CH_4 was generated. Formation of palladium black and $(dpms)Pd^{II}(OH)_2^-$ was observed as well. Product distribution shows that MeOH and C_2H_6 are the only organic products of oxidation.

The effect of pH on the product distribution was investigated. When reaction was performed at pH 14.0 the yield of methanol increased to 49 ± 1% (Table 5.1 entry 2). In addition to methanol, a new product was formed in 20 ± 1% yield. The

new specie has a Me group resonance at 3.66 ppm and was identified as methyl hydroperoxide (MeOOH) by independent synthesis. Ethane was not detected by the ^{1}H NMR spectroscopy due to its low concentration in the aqueous phase.

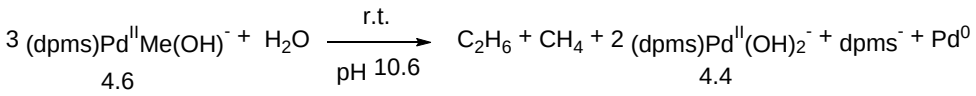

Equation 5.1

In a control experiment reactivity of (dpms)Pd^{II}Me(OH)$^-$ under Ar was monitored by ^{1}H NMR spectroscopy. After 6-8 days under ambient temperature and light the reaction mixture showed formation of C_2H_6 and CH_4 in 55±3%, 43±1% yield respectively (Eq. 5.1 Table 5.1 entry 3). No MeOH was observed. Yield of ethane and methane was calculated using Henry's constant and ideal gas law. A literature value of Henry's constant for CH_4 was used.[157] This reactivity indicates that formation of ethane and methane does not require presence of O_2, methanol, on the other hand, is formed due to the presence of dioxygen. One possible pathway for methane formation is protonolysis of Pd^{II}-Me bond. Protonolyses of several palladium and platinum methyl complexes was studied by Labinger and Bercaw[183] and was observed in case of K(dpms)Pt^{II}Me(OH) complex (Scheme 5.13, **A**). Protonolysis of **4.6** in D_2O would result in CH_3D which was observed in trace amount only (Scheme 5.13, **B**). It can be concluded that protonolysis of Pd^{II}-Me bond does not occur.

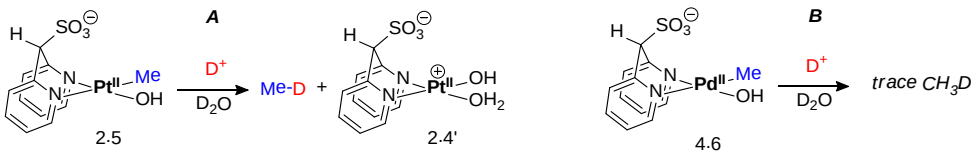

Scheme 5.13 Protonolysis of Pt^{II}-Me and Pd^{II}-Me bond.

When a saturated solution of Pr_4N(dpms)Pd^{II}Me(OH) in D_2O was kept without agitation under argon, presence of CH_4 and CH_3D was observed in 11 and

1% yield respectively. Methyl radical could abstract a hydrogen atom from *n*-Pr_4N^+ counterion. The latter possibility was eliminated when reaction was performed with Na^+ instead of *n*-Pr_4N^+ in D_2O and formation of both CH_4 and CH_3D was still observed. In view of high bond dissociation energy of $D^{16}O$-D (119.7 kcal/mol[184]), formation of methane according to Eq. 5.2 does not occur either.[185]

$$CH_3 + H_2O \longrightarrow CH_4 + OH$$

Equation 5.2

Formation of CH_4 in pure D_2O suggests that abstraction of hydrogen can occur from the ligand. Bridging $(SO_3)C$-*H* group of the dpms ligand could serve as a source of H for CH_4 in D_2O.

Methanol is known to react with some Pd(II) complexes to form formaldehyde, formic acid and CO_2 along with Pd^0 in a stepwise manner.[120,179] In a control experiment, a mixture of $(dpms)Pd^{II}(OH)_2^-$ and Pd black, which were formed in oxidation of $(dpms)Pd^{II}Me(OH)^-$ with O_2 were dried under vacuum, and combined with a aqueous solution, containing a fresh aliquot of MeOH. The intensity of the MeOH peak was monitored by ^1H NMR spectroscopy over 7 days, in order to establish involvement of additional reaction pathways. The intensity of MeOH peak fluctuated within 5%, which is consistent with the integration error. Therefore, methanol is stable under the reaction conditions, and does not undergo further oxidation in the presence of Pd.

5.3 Kinetics of Aerobic Oxidation of (dpms)$Pd^{II}Me(OH)^-$

5.3.1 Effect of TEMPO on the Rate of Oxidation and Product Distribution

Mass balance. The involvement of a radical mechanism was accessed by monitoring oxidation of (dpms)$Pd^{II}Me(OH)^-$ in the presence of radical trap TEMPO (1.3-2.4 equiv.) at the native pH of $Pd^{II}Me$ (pH 10.6). To account for the mass balance, reaction was performed in a sealed NMR tube. Slow reaction between $Pd^{II}Me$ and O_2 occurred over 11 days at room temperature and ambient light, showing 97% conversion. Yield of MeOH was 3 ± 1%, which is lower compared to the similar conditions in the absence of TEMPO (16 ± 3% yield). Formation of Me-TEMPO (7 ± 4% yield, based on Me group balance) as well as C_2H_6 (92%) was observed (Scheme 5.14, Table 5.2). Overall, reaction mass balance is maintained, and formation of ethane is the leading reaction direction.

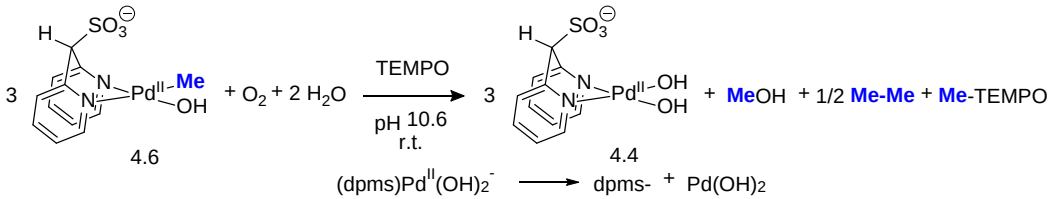

Scheme 5.14 Oxidation of R_4N(dpms)$Pd^{II}Me(OH)$ with O_2 at pH 10.6 in the presence of TEMPO under ambient conditions.

Conditions	Conversion (%) / Reaction time	C_2H_6 (%)	MeOH (%)	Other Products (%)
No additives	98 / 6 days	82 ± 4	16 ± 3	$LPd^{II}(OH)_2^-$, 83 ± 5
TEMPO 1.3, 2.4 equiv.	97 / 11 days	92 ± 1	4 ± 1	$LPd^{II}(OH)_2^-$, 85 ± 1 Me-TEMPO, 7 ± 4

Table 5.2 Product distribution in oxidation of R_4N(dpms)$Pd^{II}Me(OH)$ with O_2 at pH 10.6 in the presence of TEMPO under ambient conditions. Yields are calculated at 100% conversion.

Kinetics. Investigations into the mechanism of aerobic oxidation of (dpms)$Pd^{II}Me(OH)^-$ complexes were pursued via kinetic studies. Kinetic experiments were conducted at 20 °C in a temperature controlled bath under fast stirring, data was

collected over at least three half-lives. Results shown in Table 5.3 are an average of at least two kinetic runs. Presence of Me-TEMPO in entry 2 (Table 5.3) is a direct evidence for the involvement of the radical intermediates. Radical pathways are usually associated with unreliable kinetics, therefore, prior to analysis of the reaction constants reproducibility of the kinetic measurements needs to be verified.

Entry	Conditions	$t_{1/2}$ (h)	MeOH (%)	Other Products (%)	Rxn Order in [Pd^{II}]
1	pH 10.6, no additives	24.7 ± 0.8	14 ± 2	$LPd^{II}(OH)_2^-$, 69 ± 4	1
2	TEMPO 1.3, 2.4 equiv.	38.1 ± 0.6	11 ± 1	$LPd^{II}(OH)_2^-$, 72 ± 4 Me-TEMPO, 7 ± 1	1

Table 5.3. Half-life and reaction order in [Pd^{II}] for the oxidation of $R_4N(dpms)Pd^{II}Me(OH)$ with O_2 at pH 10.6 in the presence of TEMPO under ambient conditions.

To explore the reproducibility of the kinetic measurements two kinetic runs of were performed independently 11 days apart from each other under otherwise identical conditions. Analysis of the reaction half-lifes showed 3.2% variance in the experimental measurements (Table 5.3, entry 1). Second set of reactions were performed in the presence of TEMPO, and reaction half-lifes showed 1.6% discrepancy between two runs (Table 5.3, entry 2). A much smaller percent error was observed for experiments performed simultaneously. For example, when two kinetic runs at pH 6.8 were performed at the same time in the same thermostat bath the experimental error was only 0.2%. For reaction with 1M $NaNO_3$ and with 1M KOH the discrepancy was 0.3% and 0.9% respectively. Due to considerably lower percent error for reactions conducted simultaneously the effect of additives on the rate constants was evaluated in the sets of reactions performed simultaneolusly.

It is expected that presence of a radical trap will have detrimental effect on the reaction rate. Indeed, kinetic monitoring of the reaction revealed that the overall rate of oxidation is 50% slower in the presence of TEMPO, compared to the analogous

conditions in the absence of the radical trap. Me-TEMPO was also observed in 7 ± 1% yield, based on Me group balance, which is in good agreement with reaction in the closed system. Yield of MeOH is the same within experimental error 11 ± 1% *vs*. 14 ± 2% with and without TEMPO respectively (Table 5.3).

Since overall rate constant k_{obs} exhibits 1st-order dependence in [Pd^{II}Me] under various conditions, pathways leading to C_2H_6 and MeOH are proposed to have a 1st-order dependence in [Pd^{II}Me], with a pseudo-1st order rate constants $k_{(Ethane)}$ and $k_{(MeOH)}$, respectively. Assuming that no other organic products are generated except methanol, ethane, and Me-TEMPO at pH 10.6, rate constants for MeOH formation $k_{(MeOH)}$ and ethane formation $k_{(Ethane)}$ can be calculated (Table 5.4).

Conditions	$k_{(MeOH)}$, s^{-1}	$\Delta G^{\ddagger}$ (MeOH)	$k_{(Ethane)}$, s^{-1}	$\Delta G^{\ddagger}$ (Ethane)
pH 10.6, no additives	$(1.1 \pm 0.03)\times10^{-6}$	27.5	$(6.7 \pm 0.2)\times10^{-6}$	26.4
TEMPO 1.3, 2.4 equiv.	$(5.6 \pm 0.09)\times10^{-7}$	27.9	$(4.1 \pm 0.06)\times10^{-6}$	26.7

Table 5.4 Calculated rate constants and Gibbs free energies for MeOH and C_2H_6 formation in oxidation of R_4N(dpms)Pd^{II}Me(OH) with O_2 at pH 10.6 in the presence of TEMPO under ambient conditions.

Pseudo-1st-order rate constant for MeOH formation was calculated from k_{obs} and the product ratio: $k_{(MeOH)}$ is approximately two-fold smaller in the presence of TEMPO compared to the reaction under identical conditions in the absence of the radical trap (Table 5.4). This implicates that Me radicals are involved in generation of methanol, however, the TEMPO additive has negligible effect on the reaction selectivity towards MeOH.

The effect of TEMPO on the rate of ethane formation is less pronounced compared to MeOH; $k_{(Ethane)}$ decreases by 38%. Based on the small amount of Me-TEMPO adduct, and the effect of the radical trap on $k_{(MeOH)}$ and $k_{(Ethane)}$, we propose that both reactions occur via radical chain mechanism.

5.3.2 Effect of Light on the Rate of Oxidation and Product Distribution

Sensitivity to light is very typical for radical reactions. Light-induced scission of Pd-Me bonds to form Me radicals have been reported by Jordan *et al*. Imidazolyl-supported $Pd^{II}Me(Cl)$ complex was shown to undergo fast homolysis of Pd-Me bond at 23 °C in CH_2Cl_2 at ambient light over 68 h. Reaction was proposed to occur via formation of Me• and Pd^{I}• (Scheme 5.15 **A**).[150]

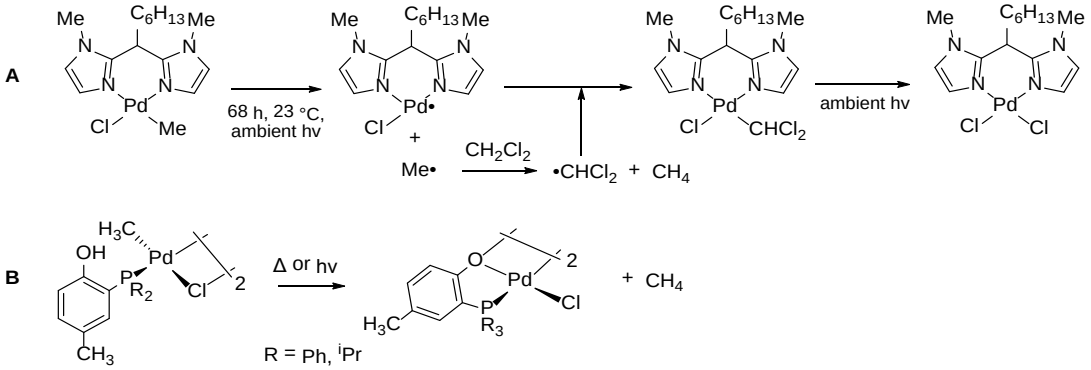

Scheme 5.15 Homolysis of Pd-C bond in $Pd^{II}Me(Cl)$ complexes.

Similar reactivity was observed in case of dinuclear palladium complexes, which undergo photochemical and thermal Pd-Me bond cleavage to produce methane and oxygen-bridged Pd^{II} dimer (Scheme 5.15 **B**). The formation of methyl radicals during the photolysis was suggested by the observation of Me-TEMPO adduct and CH_3D when $CDCl_3$ was used as the solvent.[182]

The effect of irradiation on the reaction selectivity towards MeOH was evaluated at pH 14.0. Experiments were conducted under fast stirring to ensure that concentration of O_2 remains at a stationary level. Reaction under ambient light and under irradiation with 26 W fluorescent lamp were performed at 20 ºC in a temperature controlled bath. Lamp was located 40 cm away from the reaction flask. Reaction in the dark was performed at ambient temperature in an aluminum wrapped

25 mL round bottom flask. Oxidation in the dark was very slow, therefore, experiment was conducted without temperature control.

The effect of light on the rate of oxidation of **4.6** was evaluated for the set of reactions where Rxn #1 was performed simultaneously with Rxn #1 (0.9-2.2% error). Qualitative estimate is presented for reaction in the dark. Results are summarized in Table 5.5.

Entry	Conditions	$t_{1/2}$ (h)	MeOH (%)	Other Products (%)	Rxn Order in [Pd^{II}]
1	Ambient light	16.0 ± 0.15	50 ± 6	$LPd^{II}(OH)_2^-$, 94 ± 5	1
2	26 W lamp	4.4 ± 0.1	42 ± 1	$LPd^{II}(OH)_2^-$, 83 ± 2	1/2
3	Dark	187*	6 ± 1	$dpms^-$, 59 ± 1	1/2

Table 5.5 Half-life and reaction order in [Pd^{II}] for the oxidation of $R_4N(dpms)Pd^{II}Me(OH)$ with O_2 at pH 14.0 at r.t. Yield of MeOH is calculated at 100% conversion. * Qualitative estimate.

The effect of light on the selectivity toward methanol is most significant when oxidation is performed in the dark (Table 5.5, entry 1 and 3). In the absence of light, MeOH was formed in only 6% yield. However, the selectivity in methanol is not affected noticeably by the intensity of irradiation (Table 5.5, entry 1 and 2). Notably, the intensity of irradiation affects the rate of disappearance of the starting complex. Oxidation is fastest under external irradiation, followed by reaction under ambient light; the slowest reaction is in the dark. Reaction in the dark is 42.5 times slower than reaction under irradiation with 26 W lamp, and ~12 times slower than reaction under ambient light.

Irradiation and exclusion of light appear to affect the reaction order, in both cases half-order dependence on [$Pd^{II}Me$] was observed. Half-order and first-order kinetic plots with respect to $R_4N(dpms)Pd^{II}Me(OH)$ (**4.6**) for representative reactions under irradiation are presented in Figures 5.1 and 5.2. More examples of such

comparisons can be found in the Experimental Section. It is clear from examination of these data that the rate of consumption of **4.6** exhibits a well-behaved half-order dependence on [**4.6**].

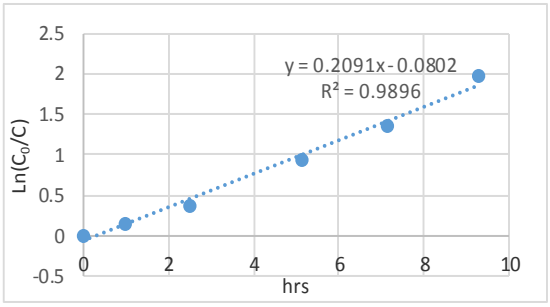

Figure 5.1 First order kinetic plot in [Pd^{II}] for the oxidation of $R_4N(dpms)Pd^{II}Me(OH)$ with O_2 at pH 10.6 under irradiation with 26 W fluorescent lamp.

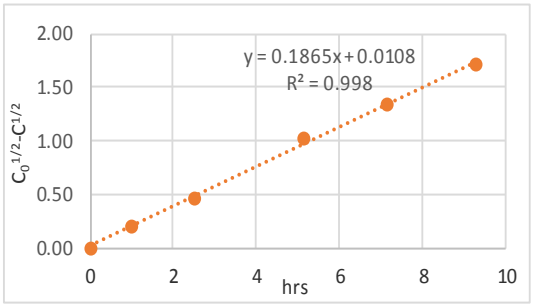

Figure 5.2 Half order kinetic plot in [Pd^{II}] for the oxidation of $R_4N(dpms)Pd^{II}Me(OH)$ with O_2 at pH 10.6 under irradiation with 26 W fluorescent lamp.

Change in the reaction order implicates the change in the reaction mechanism. This could be associated with enhanced radical character in the presence of light, and diminished radical character in the dark. Half-order dependence have been observed previously in the radical chain insertion of O_2 into (bpy)Pd^{II}-Me bond. Reaction order was explained in terms of the termination step. When the termination step involves coupling of two peroxy radicals, reaction is expected to exhibit first order dependence in [Pd^{II}].[180] The rate constant for homocoupling of two MeOO• radicals is diffusion limited, and has a rate constant $k = 1.9 \times 10^8\ M^{-1}\ s^{-1}$ in benzene at 22 °C.[181] In contrast, if termination involves reaction of MeOO• at the Pd metal center, a half-order dependence on [SM] is expected.[166]

Termination: MeOO• + $(bpy)Pd^{III}Me_2(OOMe)$• ⟶ non-propagating products

1/2-order in [SM]

Equation 5.3

Interestingly, both pathways, leading to MeOH and C_2H_6, are both suppressed in the absence of light. Slow reaction in the dark implies that pathway leading to

ethane also involves photoexcitation of Pd^{II}. Formation of MeOH could be a result nucleophilic attack of the methyl group of **4.6** by OH^- and/or due to presence of trace amounts of O_2 in the system.

The ability of the methyl group of Pd^{II}-Me to undergo nucleophilic attack by OH^- to form methanol according to Scheme 5.11 **B** was probed under inert atmosphere. Formation of methanol was not observed when **4.6** was kept at pH 10.6 and 14.0 under ambient light. Therefore, pathway **B** in Scheme 5.11 can be eliminated when Ar atmosphere, ambient temperature and light were used. However, when an aqueous solution of $R_4N(dpms)Pd^{II}Me(OH)$ was monitored under argon in the absence of light at pH 14.0 for 114 days MeOH was produced in 43% based on the reacted starting complex (Table 5.6). This observation indicates that pathway **B** in Scheme 5.10 can be operational but is very slow and has a negligible contribution to the formation of MeOH in the presence of ambient light.

Time (days)	Conversion (%)	MeOH (%)
3	4	2
10	12	3
29	22	10
38	26	14
52	33	14
114	37	16

Table 5.6 Product distribution in decomposition of $R_4N(dpms)Pd^{II}Me(OH)$ under argon at pH 10.6 in the dark at r.t.

Overall it appears that in both pathways, leading to C_2H_6 and MeOH, photoexcitation of Pd^{II} is the key step. The effect of TEMPO and light indicate that generation of methanol and ethane occurs via radical mechanism. Care must be taken in analysis of the rate constants of reactions involving radical intermediates, since they often result in irreproducible kinetics. The rate constants for oxidation of $(dpms)Pd^{II}Me(OH)^-$ with O_2 were shown to be reproducible within 3% error. To

ensure consistency in kinetic measurements, reactions were performed under the same ambient laboratory lighting, and, unless otherwise mentioned, simultaneously in the same temperature controlled bath.

5.3.3 Effect of Pressure of O_2

As demonstrated in Table 5.1 entry 2, MeOOH is observed in considerable amount in aerobic oxidation of **4.6** at pH 14.0. Methyl peroxide can form as a result of reaction between Me radical and O_2, therefore, we explored the effect of concentration of [O_2] on the product distribution and the rate of oxidation. Kinetic studies were conducted at 20 °C in a temperature controlled bath under fast stirring, data was collected over at least three half-lives, and results shown in Table 5.7 are an average of at least two kinetic runs. The effect of partial pressure of O_2 can be elucidated easily by performing oxidation under air and under 1 atm O_2.

In order to ensure consistency in the kinetic tests the effect of p(O_2) on the rate constants was evaluated for the set of reaction where Rxn #1 was performed concurrently with Rxn #2. Overall two sets of reactions were performed (Table 5.8).

Rxn #	Conditions	$t_{1/2}$ (h)	MeOH (%)	Other Products (%)	Rxn Order in [Pd^{II}]
1	0.21 atm (air)	30.7 ± 1.0	6 ± 2	$LPd^{II}(OH)_2^-$, 45 ± 5	1
2	1 atm O_2	24.7 ± 0.8	14 ± 5	$LPd^{II}(OH)_2^-$, 69 ± 4	1

Table 5.7 Half-life and reaction order in [Pd^{II}] for the oxidation of $R_4N(dpms)Pd^{II}Me(OH)$ with air and O_2 at pH 10.6 under ambient conditions. Yield of MeOH is calculated at 100% conversion.

The partial pressure of O_2 in air is 0.21 atm; the yield of methanol is two times lower in Rxn #1 than in Rxn #2, and the overall reaction half-life is 20% greater under air than under 1 atm O_2. Based on these observations and on the behavior of $(dpms)Pd^{II}Me(OH)^-$ under argon, it can be concluded that dioxygen is directly involved in production of MeOH.

Conditions	$k_{(MeOH)}$, s^{-1}	$\Delta G^{\ddagger}$ (MeOH)	$k_{(Ethane)}$, s^{-1}	$\Delta G^{\ddagger}$ (Ethane)
0.21 atm (air)	$(3.8 \pm 0.1)\times10^{-7}$	28.1	$(5.9 \pm 0.2)\times10^{-6}$	26.5
1 atm O_2	$(1.1 \pm 0.02)\times10^{-6}$	27.5	$(6.7 \pm 0.2)\times10^{-6}$	26.4

Table 5.8 Calculated rate constants and Gibbs free energies for MeOH and C_2H_6 formation in oxidation of $R_4N(dpms)Pd^{II}Me(OH)$ with 1 atm and 2 atm O_2 at pH 10.6 under ambient conditions.

Kinetic tests showed 1st-order dependence on [Pd^{II}] in both cases. Pseudo-1st-order rate constants for formation of MeOH and C_2H_6 were calculated, $k_{(MeOH)}$ and $k_{(Ethane)}$. The dependence of $k_{(MeOH)}$ on the partial p(O_2) is nonlinear, a 4.8-fold increase in the p(O_2) results in ~3-fold increase in $k_{(MeOH)}$. A correlation between concentration of [O_2] and the rate constant of MeOH formation $k_{(MeOH)}$, supports the hypothesis that reaction of $(dpms)Pd^{II}Me(OH)^-$ with O_2 occurs before or at the rate limiting step.

Conditions	Conversion (%) / Reaction time	MeOH (%)	MeOOH (%)	Other Products (%)
1 atm O_2, 13.2 mM	98 / 4 days	54 ± 2	4 ± 1	$LPd^{II}(OH)_2^-$, 82 ± 5
2 atm O_2, 12.7 mM	98 / 3 days	56 ± 1	4 ± 1	$LPd^{II}(OH)_2^-$, 78 ± 1 dpms 18 ± 1

Table 5.9 Product distribution in oxidation of $R_4N(dpms)Pd^{II}Me(OH)$ at pH 14.0 under ambient conditions. Yields are calculated at 100% conversion.

The effect of O_2 pressure on the product distribution was investigated at pH 14.0. When oxidation was performed under 2 atm of O_2, no change in the product distribution was observed compared to p(O_2) 1 atm (Table 5.9). Therefore, at pH 14.0 the reaction involving O_2 is not the rate determining step in the pathway leading to MeOH. We propose that at pH 14.0 the rate determining step is homolysis of Pd^{II}-Me bond.

A plausible mechanism for MeOH formation might include photoinitiated cleavage of Pd-Me bond, leading to formation of Me radicals, followed by reaction of Me• with O_2 to form MeOO• (Eq. 5.4). Coupling of R• with O_2 to form ROO• is

essentially diffusion-limited. A value $k = (4.7 \pm 0.7)\times10^6\ M^{-1}\ s^{-1}$ has been determined for (2) Eq. 5.4 in H_2O at 23 °C.[95]

$$2\ [LPd^{II}Me(OH)]^- \xrightarrow{h\nu} 2\ [LPd^{I}(OH)]^{\bullet -} + 2\ Me^{\bullet} \quad (1)$$

$$Me^{\bullet} + O_2 \xrightarrow{k} MeOO^{\bullet} \qquad k = 4.7 \times 10^6\ M^{-1}\ s^{-1} \quad (2)$$

Equation 5.4

So far, we have proposed that ethane is formed via photoinduced process. Pathway leading to MeOH also involves photoexcitation of Pd^{II}, which results in formation of Me radicals. These radicals can then combine with O_2, which was shown to be a very fast process.[95]

Homolytic cleavage of Pd^{II}-Me bonds of the $(bpy)Pd^{II}Me_2$ complex followed by reaction of Me• with O_2, was shown to generate the product of O_2 insertion Pd^{II}-OOMe.[166] Formation of the product of O_2 insertion into Pd-Me bond might also occur in $(dpms)Pt^{II}Me(OH)^-/O_2$ system. Indeed, $MeOO^-$ was observed under certain conditions. Therefore, we next examined reactivity of MeOOH and some other hydroperoxides toward $(dpms)Pd^{II}Me(OH)^-$.

5.4 Reactivity of $(dpms)Pd^{II}Me(OH)^-$ with MeOOH, $NaIO_4$ and I_2

Based on the experimental observations and on the literature precedent[166], formation of methyl hydroperoxide most likely occurs via a sequence of steps shown in Scheme 5.16. In the absence of radical initiators, the initial step involves generation of CH_3 radicals by homolysis of M-CH_3 bond.[186,187] Therefore, we propose that the first step is photoinduced scission of Pd-Me bond leading to Me• and Pd^I. Stable mononuclear Pd^I complexes are rare but their intermediacy has been documented in a variety of radical oxidative addition/reductive elimination processes and in electrochemical studies.[188, 189] Interception of Me• with O_2 gives MeOO•

which can recombine with Pd^{I} in a termination step. Finally, MeOOH is released in a reaction between $(dpms)Pd^{II}(OOMe)(Me)^-$ and water or hydroxide anion.

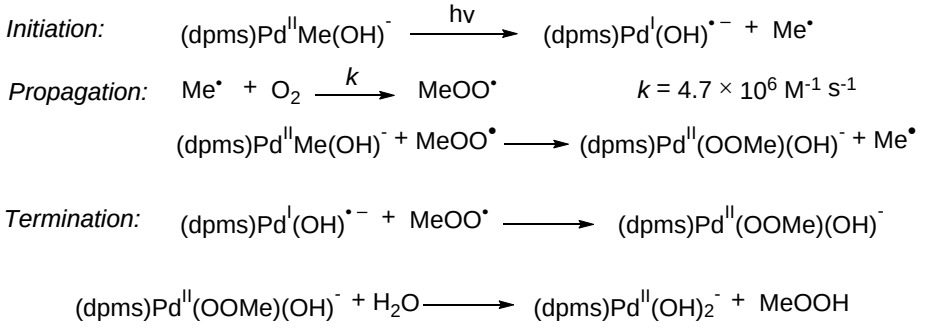

Scheme 5.16 Proposed mechanism for formation of MeOOH in $Pr_4N(dpms)Pd^{II}Me(OH)/O_2$ system.

Once MeOOH or, at high enough pH, $MeOO^-$ is produced it might serve as an oxidant with respect to $Pd^{II}Me$ species and/or undergo decomposition to form MeOH and O_2. Concentration of $MeOO^-$ formed as a result of oxidation of $Pr_4N(dpms)Pd^{II}Me(OH)$ at pH 14.0 was monitored over time (see Experimental section for details). Once all $Pd^{II}Me$ complex was consumed the amount of $MeOO^-$ remained unchanged over 10 days. Therefore, MeOOH is sufficiently stable under these conditions. MeOOH might act as an oxidant for $Pd^{II}Me$ to form MeOH and Pd^{IV} (Scheme 5.17). Peroxides may be powerful oxidants for Pd^{II} and Pt^{II} complexes.[25,78]

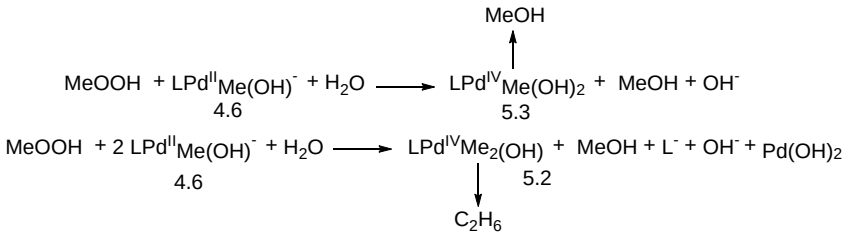

Scheme 5.17 Oxidation of $Pr_4N(dpms)Pd^{II}Me(OH)$ with MeOOH, leading to MeOH and C_2H_6.

This hypothesis was verified in reactions between MeOOH and $(dpms)Pd^{II}Me(OH)^-$ (Scheme 5.18). Methyl hydroperoxide is not commercially available, and its preparation according to the literature procedure results in a significant admixture of H_2O_2, which may also be reactive toward

(dpms)$Pd^{II}Me(OH)^-$. Therefore, MeOOH was prepared in situ, by oxidation of dilute solutions of (dpms)$Pd^{II}Me(OH)^-$. Once all $Pd^{II}Me$ was consumed, pH was adjusted using HBF_4. The yield of MeOOH was determined by NMR integration using an internal standard, and equimolar amount of fresh (dpms)$Pd^{II}Me(OH)^-$ was added. At pH 5.5 and pH 10.6, the reaction was complete within a few minutes to an hour. At pH 14.0, full conversion was achieved overnight (Table 5.10).

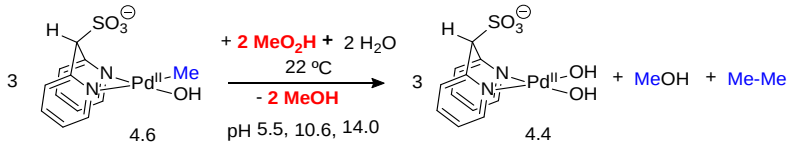

Scheme 5.18 Oxidation of R_4N(dpms)$Pd^{II}Me(OH)$ with MeO_2H under ambient conditions.

Conditions	Conversion (%) / Reaction time	MeOH* (%)	Other Products (%)
pH 10.6, MeOOH (1 eq.) SM = 0.2 mM	100 / 7 min	103 ± 2	$LPd^{IV}Me_2(OH)$, 23 ± 1
pH 5.5, MeOOH (2 eq.) SM = 0.6 mM	100 / 5 h	116 ± 9	$LPd^{IV}Me_2(OH)$, 28 ± 1
pH 14.0, MeOOH (2.5 eq.) SM = 5.6 mM	100 / 16 h	162 ± 5	-

Table 5.10 Product distribution in oxidation of Pd^{II} under ambient conditions
*Yields are based on MeOOH calculated at 100% conversion.

Yield of MeOH was calculated based on the amount of MeOOH reacted at pH 5.5, 10.6, and 14.0, and results are summarized in Table 5.10. Up to 100% yield of MeOH is expected due to formation of 1 equiv. of MeOH per 1 equiv. of MeOOH consumed. The yield of MeOH exceeding 100% means that some MeOH is derived from $Pd^{II}Me$, more specifically, 16 ± 9%, 3 ± 2%, and 62 ± 5% at pH 5.5, 10.6, and 14.0 respectively. The amount of the $Pd^{II}Me$-derived MeOH produced at pH 14.0 and 5.5 is very close to that, observed under typical aerobic oxidation (O_2, ambient temperature and light). This indicates, that MeOOH may indeed be an intermediate in aerobic oxidation of (dpms)$Pd^{II}Me(OH)^-$. At pH 10.6, however, the results are inconsistent. Under typical reaction conditions at pH 10.6, oxidation of

Pr_4N(dpms)Pd^{II}Me(OH) leads to MeOH (14 ± 2%), while when MeOOH was used as an oxidant, the Pd^{II}Me-derived MeOH was formed in only 3 ± 2% based on Pd^{II}. A possible explanation for this discrepancy is that at pH 10.6 the solution is not buffered. A similar trend was observed with other peroxides, such as H_2O_2 and ^{t}BuOOH (see Experimental section for details).

Overall, the experiments with methyl hydroperoxide show that *in situ* generated $MeOO^-$ (or MeOOH) acts as an oxidant for yet unreacted (dpms)Pd^{II}Me$(OH)^-$. This oxidation may lead to Pd^{IV}Me species responsible for the formation of an additional amount of methanol and ethane.

If MeOH is formed via nucleophilic attack of solvent at an electrophilic Pd^{IV}-Me complex then nucleophilic attack of CD_3O^- on the methyl group of (dpms)Pd^{IV}Me will result in formation of CH_3OCD_3. Indeed, oxidation of Pr_4N(dpms)Pd^{II}Me(OH) with O_2 in CD_3OD/1M KOH resulted in CH_3OCD_3 (33 ± 3% yield) along with CH_3OH (26 ± 5% yield).

The role of the oxidant in MeOH production was accessed using a stronger oxidizing agent, $NaIO_4$ (Scheme 5.19, Table 5.11). Sodium periodate can act as one or two electron oxidant.[190] A dramatic change in the product distribution was observed. Presence or exclusion of light had no effect on the reaction rate. This is contrary to the results obtained in the oxidation of (dpms)Pd^{II}Me$(OH)^-$ with O_2, indicating that a different mechanism of oxidation might be operational.

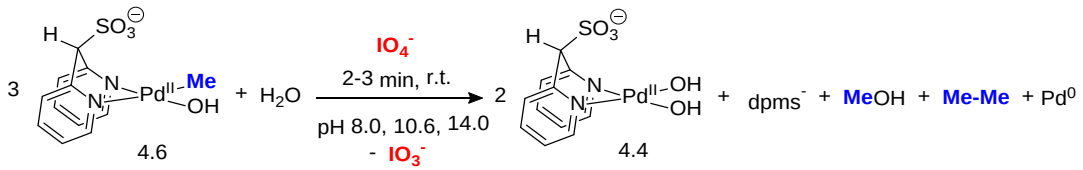

Scheme 5.19 Oxidation of R_4N(dpms)Pd^{II}Me(OH) with IO_4^- under ambient light and in the dark.

Conditions	Conversion (%) / Reaction time	MeOH (%)		Other Products (%)
		Light	**Dark**	
pH 8.0, SM = 1.9 mM	100 / 7 min	60 ± 13	72 ± 5	$LPd^{IV}Me_2(OH)$, 7
pH 10.6, SM = 2.0 mM	100 / 11 min	27	64	$LPd^{IV}Me_2(OH)$, 31
pH 14.0, SM = 2.6 mM	81 / 3 days	28	42	-

Table 5.11 Product distribution in oxidation of $R_4N(dpms)Pd^{II}Me(OH)$ with IO_4^- under ambient light and in the dark. Yields are calculated at 100% conversion.

The increase in the yield of MeOH at lower pH is consistent with the mechanism, where methanol is formed via $(dpms)Pd^{IV}Me(OH)_2$ species, according to Scheme 5.11, **A**. Scheme 5.11, **A**. Some increase of the amount of ethane in the presence of light indicates that C_2H_6 may form via a competing radical pathway.

5.5 Effect of pH on the Reactivity of $Pr_4N(dpms)Pt^{II}Me(OH)$ Toward O_2

In Section 5.2 we have demonstrated that the yield of MeOH increases with increasing pH (from 16 ± 3% at pH 10.6, Table 5.1 entry 1, to 49 ± 1% at pH 14.0, Table 5.1 entry 2). Some MeOH may be generated from $(dpms)Pd^{IV}Me(OH)_2$ via S_N2 mechanism, similar to $(dpms)Pt^{IV}Me(OH)_2$. If so, in basic solutions OH^- should be a preferred nucleophile over H_2O (Scheme 5.20). In addition, OH^- may facilitate release of $MeOO^-$ to a greater extent than H_2O (Eq. 5.5). Notably, formation of MeOOH may also be favored in acidic solutions since MeOOH is a much better leaving group compared to $MeOO^-$.

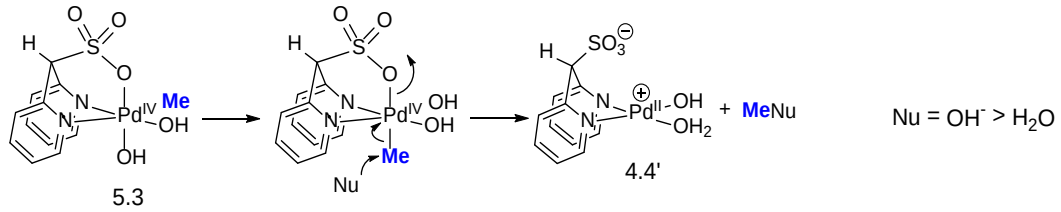

Scheme 5.20 Mechanism of MeOH formation from $(dpms)Pt^{IV}Me(OH)_2$.

$$(dpms)Pd^{II}(OOMe)(OH)^- + Nu \longrightarrow (dpms)Pd^{II}(OH)(Nu)^- + MeOO^- \qquad Nu = OH^- > H_2O$$

Equation 5.5

In order to elucidate the reason behind enhanced selectivity towards MeOH at pH 14.0 we evaluated the rate of disappearance of $Pr_4N(dpms)Pd^{II}Me(OH)$ at pH 10.6 (no additives), 6.8 (phosphate buffer), and 14.0 (1M KOH). We found that at pH 6.8 methanol forms in 10 ± 1% yield, similar to what we observed at pH 10.6.

Kinetics. Kinetic experiments were conducted at 20 °C in a temperature controlled bath under fast stirring, data was collected over at least three half-lives, and results in Table 5.12 are an average of at least two kinetic runs. At pH 10.6, 14.0 and 6.8 reaction exhibits 1st order dependence in $[Pd^{II}Me]$. Reaction at pH 14.0 was performed in the presence of 1.0 M KOH, therefore the effect of the ionic strength on the reaction rate was evaluated using 1M $NaNO_3$. A half-order dependence in $[Pd^{II}Me]$ was observed in this case.

The kinetic runs for Rxn #1-4 (Table 5.12) were performed independently. In view of the photochemical nature of the reaction, inconsistency in the level of ambient irradiation contributes an additional experimental error of 0.7 – 3.2% for each measurement. For this reason quantitative comparison of the $k_{(MeOH)}$ and $k_{(Ethane)}$ cannot be performed, however, general trends can still be evaluated. The reaction $t_{1/2}$ and methanol yields are also summarized in Table 5.12.

Rxn #	Conditions	$t_{1/2}$ (h)	MeOH (%)	Other Products (%)	Rxn Order in $[Pd^{II}]$
1	pH 10.6, no additives	24.7 ± 0.8	14 ± 2	$LPd^{II}(OH)_2^-$, 69 ± 4	1
2	pH 14.0, 1.0 M KOH	16.0 ± 0.15	50 ± 6	$LPd^{II}(OH)_2^-$, 94 ± 5	1
3	pH 6.8, $HPO_4^{2-}/H_2PO_4^-$ buffer	4.8 ± 0.01	10 ± 1	unsym-Pd^{II} complex 58 ± 1	1
4	pH 10.6, 1.0 M NO_3^-	16.1 ± 0.04	9 ± 2	$LPd^{II}(OH)_2^-$, 69 ± 18	1/2

Table 5.12 Half-life and reaction order in $[Pd^{II}]$ for the oxidation of $R_4N(dpms)Pd^{II}Me(OH)$ with O_2 under ambient conditions. Yield of MeOH is calculated at 100% conversion.

The reaction rate is slowest at pH 10.6; it increases approximately five-fold from $t_{1/2}$ ~25 h at pH 10.6 to $t_{1/2}$ ~5 h at pH 6.8, and by ~50% from pH 10.6 to pH 14.0. Interestingly, reaction rate in 1M NO_3^- was the same as in 1M OH^- (Table 5.12), indicating that change in the ionic strength is responsible for the increase in rate of oxidation. The enhanced solution ionic strength does not, however, account for the substantial increase in the yield of MeOH produced at pH 14.0. Change in the reaction order from 1st to half-order indicates a change in mechanism. The origin of this result is unknown at this time.

Conditions	$k_{(MeOH)}$, s^{-1}	$\Delta G^{\#}$ (MeOH)	$k_{(Ethane)}$, s^{-1}	$\Delta G^{\ddagger}$ (Ethane)
pH 10.6, no additives	$(1.1 \pm 0.02)\times10^{-6}$	27.5	$(6.7 \pm 0.2)\times10^{-6}$	26.4
pH 6.8, $HPO_4^{2-}/H_2PO_4^-$ buffer	$(3.8 \pm 0.008)\times10^{-6}$	26.8	$(3.6 \pm 0.008)\times10^{-5}$	25.4

Table 5.13 Calculated rate constants and Gibbs free energies for MeOH and C_2H_6 formation in oxidation of $R_4N(dpms)Pd^{II}Me(OH)$ with O_2 at pH 6.8, and 10.6 under ambient conditions.

Since 1st order dependence on the $[Pd^{II}Me]$ was observed in reactions without NO_3^-, k_{obs} can be determined from the plots of $ln([Pd^{II}Me]_o/[Pd^{II}Me])$ *vs.* time, and the rate constant for methanol formation can be determined from k_{obs} and the observed product ratio. Pseudo first-order rate constants $k_{(MeOH)}$ and Gibbs activation energies $\Delta G^{\#}$ are summarized in Table 5.13.

Rate of MeOH formation at pH 6.8, and 10.6 is on the same order of magnitude, and exhibits a ~3.5-fold increase from pH 10.6 to pH 6.8. Greater $k_{(MeOH)}$ in weakly acidic solution may be a result of faster release of MeOOH from the expected $(dpms)Pd^{II}(OH)(HOOMe)$ intermediate since MeOOH is a much better leaving group compared to $MeOO^-$ that is expected to form in alkaline solutions (eq 5.5). In turn, faster release of MeOOH may lead to a faster formation of MeOH as a result of its oxygen atom transfer to $(dpms)Pd^{II}Me$ species.

Consistent with this explanation, weakly acidic solutions facilitate not only MeOH formation, but also ethane formation. The rate constant $k_{(Ethane)}$ is 5.5-fold greater at pH 6.8 than at pH 10.6, while $k_{(MeOH)}$ shows only ~3.5-fold increase. We propose that pathway leading to C_2H_6 also requires presence of (dpms)$Pd^{IV}Me(OH)_2$ (*vide infra*). In turn, the rate of oxidation of (dpms)$Pd^{II}Me$ species by MeOOH is slower in alkaline solutions (Table 5.10). Correspondingly, presence of $MeOO^-$ among reaction products was observed only at pH 14.0 and the yield of $MeOO^-$ was as high as 20 ± 1%. Finally, the effect of pH on the rate of homolysis of Pd^{II}-Me bond was evaluated using DFT calculations (Eq. 5.6). According to this result, O_2 insertion into Pd^{II}-C bond is noticeably slower at pH 14.0, though the calculations did not consider photochemical reaction.

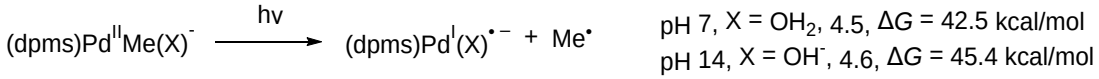

Equation 5.6 Calculated Gibbs free energy for homolytic cleavage of Pd^{II}-Me bond for R_4N(dpms)$Pd^{II}Me(OH)$ and (dpms)$Pd^{II}Me(OH_2)$.

5.6 Model Studies of Ethane Formation

5.6.1 Reductive Elimination of Ethane from (dpms)$Pd^{IV}Me_2(OH)$

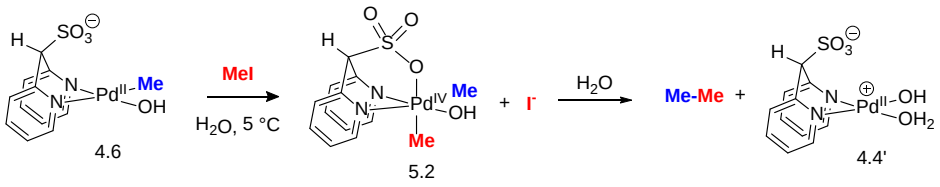

Scheme 5.21 Preparation of (dpms)$Pd^{IV}Me_2(OH)$ as intermediate in ethane elimination.

One possible mechanism for ethane formation is via reductive elimination from (dpms)$Pd^{IV}Me_2(OH)$ which results from an oxidation - methyl group transfer reaction sequence. Such reactivity has been observed by us for (dpms)$Pt^{II}Me(OH_2)$

complex (Chapter 2) and reported by Mirica *et al*. for $Pd^{II}Me$ complexes discussed above (Scheme 5.9).[78,148,177,178]

The viability of *C_1-symmetric* (dpms)$Pd^{IV}Me_2$(OH) as intermediate in ethane elimination was accessed via independent synthesis. Complex was prepared by reaction of MeI with (dpms)$Pd^{II}Me(OH)^-$ in H_2O at 5 °C (Scheme 5.21). The target *C_1-symmetric* (dpms)$Pd^{IV}Me_2$(OH) product was generated in 48% yield in a mixture with unreacted Pd^{II}. This Pd^{IV} complex is very unstable and could not be isolated. Identity of *C_1-symmetric* (dpms)$Pd^{IV}Me_2$(OH) was confirmed by ^1H NMR spectroscopy and selective NOE. Upon irradiation of the signal at 2.91 ppm, which was assigned to the axial methyl group transfer of nuclear spin polarization was observed in 1.2% to the resonance at 2.51 ppm (equatorial Me group) and both *ortho*-pyridine hydrogens in 1.4 ± 1% of the dpms ligand at 8.60 and 8.70 ppm.

Decomposition of *C_1-symmetric* (dpms)$Pd^{IV}Me_2$(OH) leads to exclusive formation of C_2H_6. Disappearance of (dpms)$Pd^{IV}Me_2$(OH) followed the first-order kinetics with the half-life $t_{1/2}$ = 6 min at 21 °C.

These observations indicate that *C_1-symmetric* (dpms)$Pd^{IV}Me_2$(OH) is accessible (see also Table 5.10) and its decomposition to form C_2H_6 is consistent with the proposed mechanism in Scheme 5.10 **B**. In view of the reactivity of (N4)$Pd^{II}Me_2$ complexes with O_2, involvement of Pd^{III} species could not be excluded. The reaction half-live of *C_1-symmetric* (dpms)$Pd^{IV}Me_2$(OH) leading ethane elimination is considerably slower than the half-live of the overall aerobic oxidation reaction of (dpms)$Pd^{II}Me_2(OH)^-$ at pH 10.6. This explains why ~~the presence of~~ (dpms)$Pd^{IV}Me_2$(OH) was never observed in our aerobic oxidation reactions.

5.6.2 Effect of [Pd^{II}] on the Product Distribution

Bimolecular Pd-to-Pd methyl group transfer leading to *C_1-symmetric* (dpms)$Pd^{IV}Me_2$(OH) is expected to be a second order reaction which would be more competitive in concentrated solutions. Therefore, we explored the effect of concentration of (dpms)Pd^{II}Me$(OH)^-$ on the product distribution in its aerobic oxidation at pH 14.0. If C_2H_6 is formed via Me group transfer pathway and intermediacy of (dpms)$Pd^{IV}Me_2$(OH) lower concentration of [Pd^{II}Me] will lead to smaller fraction of (dpms)$Pd^{IV}Me_2$(OH) and, therefore, of ethane among the reaction products. Oxidation with O_2 was performed at three concentrations: ~13.2 mM, 10-fold diluted, and 20-fold diluted solution. Reactions were performed simultaneously in a closed system under ambient light and temperature. Results are summarized in Table 5.14.

Yield of ethane could not be determined directly due to its very low concentration in the aqueous phase. Since reaction mass balance showed quantitative formation of C_2H_6, MeOH, and $MeOO^-$ at pH 14.0 as the only products, yield of ethane can be calculated by:

$$C_2H_6\ (\%) = 100\% - (MeOH\ (\%) + MeOO^-(\%))$$

Entry	Conditions	Conversion / Reaction time	MeOH (%)	MeOOH (%)	Other Products (%)
1	13.2 mM	98 % / 4 days	54 ± 2	4 ± 1	$LPd^{II}(OH)_2^-$, 82 ± 5
2	1.3 mM	100 % / 4 days	44 ± 2	30 ± 1	$LPd^{II}(OH)_2^-$, 92 ± 6
3	0.7 mM	100 % / 4 days	43 ± 1	40 ± 3	$LPd^{II}(OH)_2^-$, 69 ± 2 $dpms^-$, 27 ± 7

Table 5.14 Product distribution in oxidation of R_4N(dpms)Pd^{II}Me(OH) with O_2 at pH 14.0 under ambient conditions. Yields are calculated at 100% conversion.

Therefore, yield of ethane was estimated to be 42%, 26%, and 17% in entries 1-3 in Table 5.14, respectively. Decreasing amount of ethane with decreasing

[$Pd^{II}Me$] is consistent with the proposed oxidation - bimolecular Pd-to-Pd methyl group transfer reaction sequence.

5.6.3 Mechanism of Ethane Formation under Argon

As was shown in Section 5.2 C_2H_6 is generated in the presence of O_2 and under inert atmosphere. Formation of ethane under argon can occur via realization of several pathways (Scheme 5.10 **A**, **B** and **C**). In order to establish whether radical intermediates are involved, complex **4.6** was monitored under argon in the presence of a radical trap. When $R_4N(dpms)Pd^{II}Me(OH)$ was combined with 1.3 equiv. of TEMPO, formation of Me-TEMPO adduct was observed in 7 ± 2% yield along with ethane and methane (Table 5.15, entry 3). Presence of Me-TEMPO implies formation of methyl radicals. Addition of H-atom donor 1,4-cyclohexadiene (CHD), however, did not result in the increase of the amount methane. Instead, oxidation (or disproportionation) of CHD to benzene (detected by ^1H NMR) was observed.

Entry	Conditions	Conversion (%) / Reaction Time	C_2H_6 (%)	CH_4 (%)	MeOH (%)	Other Products (%)
1	pH 10.6, no additives	99 / 7 days	55 ± 3	43 ± 1	0	$dpms^-$, 47
2	pH 14.0 1.0 M KOH, dark	37 / 114 days	n.a.	n.a.	16	$LPd^{II}(OH)_2^-$, 2% $dpms^-$, 15
3	TEMPO 1.3 equiv.	99 / 13 days	63 ± 9	27 ± 8	1	Me-TEMPO, 7 ± 2

Table 5.15 Product distribution in decomposition of $R_4N(dpms)Pd^{II}Me(OH)$ under argon under ambient conditions. Yields are calculated at 100% conversion.

Formation of cyclohexane is also expected as a result of disproportionation of CHD but it was not detected. Lack of effect TEMPO and CHD on the yield of C_2H_6 suggests that formation of ethane does not involve methyl radicals.

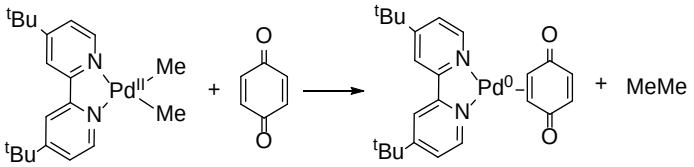

Scheme 5.22 Reductive elimination of ethane from (^{t}Bu$_2$bpy)Pd^{II}Me$_2$ in the presence of benzoquinone.

Scheme 5.10 **C** involves disproportionation of (dpms)Pd^{II}Me(OH)$^-$ to form (dpms)Pd^{II}Me$_2^-$ and (dpms)Pd^{II}(OH)$_2^-$, followed by reductive elimination of C_2H_6 from Pd^{II}Me$_2$. Preparation of (dpms)Pd^{II}Me$_2^-$ was attempted by undergraduate student Yearin Byun. The complex could never be detected by ^{1}H NMR spectroscopy even at -60 ºC. Instead, formation of (dpms)Pd^{IV}Me$_3$ and Pd^0 was observed. Based on this result, direct reductive elimination of C_2H_6 from (dpms)Pd^{II}Me$_2^-$, as it was shown by Sanford *et al*. (Scheme 5.22) is unlikely. Therefore pathway **B** in Scheme 5.10 appears to be most probable mechanism leading to C_2H_6.

5.7 Proposed Mechanism of MeOH and C_2H_6 Formation under O_2

Based on mehanistic studies reported in this chapter, the mechanism of aerobic oxidation of (dpms)Pd^{II}Me(OH)$^-$ involves: 1) photo-excitation of (dpms)Pd^{II}Me(OH)$^-$ followed by scission of Pd-Me bond, leading to Pd^I and Me• that can be trapped by TEMPO and O_2; 2) fast reaction between Me• with O_2 gives MeOO• which can recombine with Pd^I to form the product of O_2 insertion into Pd^{II}-Me bond, (dpms)Pd^{II}(OOMe)(OH)$^-$, analogous to the report by Goldberg *et al*; 3) H_2O or OH$^-$ - assisted release of MeOO$^-$ (alkaline solutions) with its subsequent protonation (Scheme 5.23) or H$^+$ - assisted release of MeOOH (acidic solutions); 4) methyl hydroperoxide, in turn, oxidizes another equivalent of (dpms)Pd^{II}Me(OH)$^-$ to form MeOH and *C_1-symmetric* (dpms)Pd^{IV}Me(OH)$_2$. 5) The latter Pd^{IV} complex

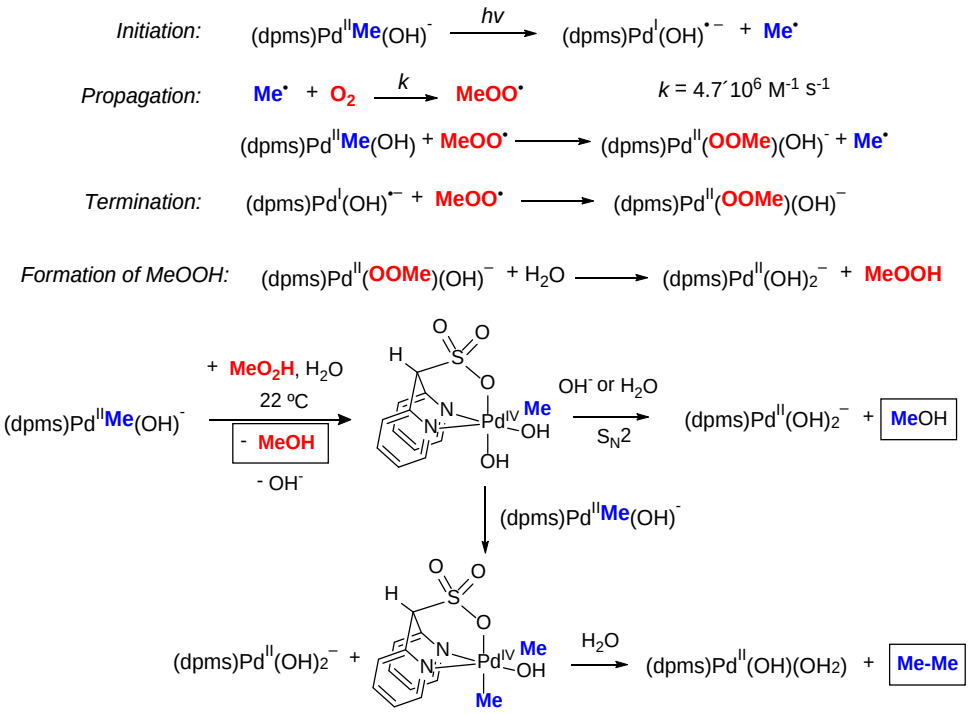

Scheme 5.23 Proposed mechanism for MeOH and C_2H_6 formation in aerobic oxidation of $R_4N(dpms)Pd^{II}Me(OH)$ under ambient temperature and light.

undergoes S_N2-type attack by OH^- at the electrophilic Me ligand and releases a second equivalent of MeOH. In a competing, parallel pathway, $(dpms)Pd^{IV}Me(OH)_2$ undergoes methyl group transfer in a bimolecular reaction with $(dpms)Pd^{II}Me(OH)^-$ to form $(dpms)Pd^{IV}Me_2(OH)$. 6) the *C_1-symmetric* $(dpms)Pd^{IV}Me_2(OH)$ $(dpms)Pd^{IV}Me_2(OH)$ transient reductively eliminates ethane (Scheme 5.23). The dependence of $k_{(MeOH)}$ and $k_{(Ethane)}$ on the presence of radical traps and $[O_2]$, and high yield of MeOH with MeOOH used as an oxidant (except pH 10.6) is consistent with the proposed mechanism.

Formation of ethane can also occur via photochemical methyl group transfer (Scheme 5.24). In this case, methyl radicals and O_2 are not involved, which is consistent with the kinetics studies. Greater fraction of C_2H_6 was observed at lower

pH, where neutral Pd^{II}-Me complex is present, (dpms)$Pd^{II}Me(OH_2)$. Methyl group transfer was shown to be faster from cationic and neutral complexes.[81]

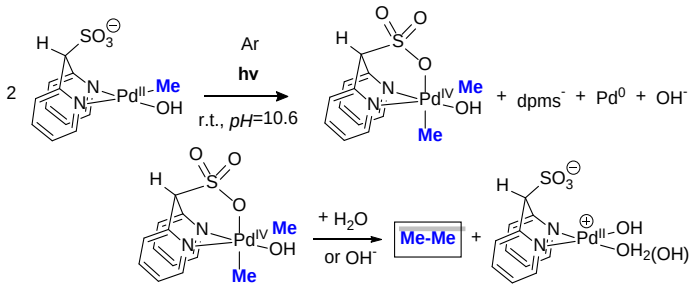

Scheme 5.24 Proposed mechanism for C_2H_6 formation from R_4N(dpms)$Pd^{II}Me(OH)$ under argon, ambient temperature and light.

5.8 Summary and Conclusions

It is interesting to compare aerobic functionalization of two analogous complexes (dpms)$M^{II}Me(OH_2)$, M = Pd and Pt. In the Pd system formation of MeOH occurs at room temperature and the reaction selectivity toward methanol, which is low in acidic media, increases at high pH. In Pt system, however, selectivity towards methanol is very high in acidic solutions and decreases at high pH; elevated temperatures and acidic or basic conditions are needed for MeOH elimination here. Unlike oxidation of K(dpms)$Pt^{II}Me(OH)$, for the Pd analog second reaction direction involving methyl group transfer and leading to (dpms)$M^{IV}Me_2(OH)$ and ethane in the case of M = Pd is highly competitive in the whole range of pH 6 - 14. Both methyl transfer reactions appear to be bimolecular and could be suppressed in dilute solution. Though *C_1-symmetric* (dpms)$Pd^{IV}Me_2(OH)$ is unstable and highly reactive, its intermediacy was confirmed by independent synthesis and model studies. Attempts to detect *C_1-symmetric* (dpms)$Pd^{IV}Me(OH)_2$ intermediate which is presumed to be responsible for formation of some MeOH were unsuccessful.

The marked difference between aerobic oxidation of Pt^{II} and Pd^{II} complexes is that oxidation of the latter requires photochemical homolytic cleavage of the Pd^{II}-CH_3 bond followed by the series of steps that eventually lead to MeOOH. Methyl hydroperoxide is an active oxidant of $Pd^{II}Me$ species generating one mol of MeOH per each mole of MeOOH and some additional amount of MeOH via proposed *C_1-symmetric* $LPd^{IV}Me(OH)_2$. The latter complex is also involved in a concurrent methyl group transfer to $(dpms)Pd^{II}Me(OH)^-$ to form *C_1-symmetric* $(dpms)Pd^{IV}Me_2(OH)$ and, eventually, C_2H_6. Although O_2 does not seem to be directly involved in oxidation of Pd^{II} to Pd^{IV} (or Pd^{III}), this is the first example of aerobic Pd^{II}-Me bond functionalization to form MeOH.

5.9 Experimental Section

Reactivity of $Pr_4N(dpms)Pd^{II}Me(OH)$ Under Argon at pH 10.6

A solution of $Pr_4N(dpms)Pd^{II}Me(OH)$ (4.3 μmol, 8.8 mM) was prepared in the glove box and was transferred into NMR tube with air tight Teflon valve. The reaction mixture was kept at ambient temperature without stirring, and decomposition of the starting material was monitored by ^1H NMR. In approximately 24 h abundant black precipitate was formed giving black-grey slurry. Upon full consumption of the starting complex (6-8 days), C_2H_6, CH_4 and free $(dpms)^-$ ligand were formed in 55±3%, 43±1% and 47 % yield respectively. No MeOH was generated.

^1H NMR (400 MHz, D_2O): **C_2H_6** δ 0.81 (s); **CH_4** δ 0.17 (s).

Reactivity of $Pr_4N(dpms)Pd^{II}Me(OH)$ Under Argon at pH 14.0

$$3\ (dpms)Pd^{II}Me(OH)^- + H_2O \xrightarrow[pH\ 14.0]{r.t.} C_2H_6 + CH_4 + \underset{44\%}{2\ (dpms)^-} + Pd(OH)_2 + Pd^0 + \underset{16\%}{(dpms)Pd(OH)_2^-}$$

A solution of $Pr_4N(dpms)Pd^{II}Me(OH)$ (3.2 µmol, 6.4 mM) was prepared in the glove box and was transferred into NMR tube with air tight Teflon valve. The reaction mixture was kept at ambient temperature and light, and decomposition of the starting material was monitored by ^1H NMR spectroscopy. At 98% conversion (14 days), $(dpms)Pd^{II}(OH)_2^-$ and free ligand $(dpms)^-$ were formed in 16% and 44 % yield respectively. Yields of C_2H_6 and CH_4 could not be determined. No MeOH was generated.

Reactivity of $Pr_4N(dpms)Pd^{II}Me(OH)$ Under Argon at pH 14.0 in the Dark

$$3\ (dpms)Pd^{II}Me(OH)^- + H_2O \xrightarrow[pH\ 14.0]{Dark,\ r.t.} C_2H_6 + CH_4 + 2\ (dpms)^- + Pd(OH)_2 + Pd^0 + (dpms)Pd(OH)_2^-$$

A solution of $Pr_4N(dpms)Pd^{II}Me(OH)$ (19.2 µmol, 48.0 mM) was prepared in the glove box and was transferred into J. Young NMR tube. NMR tube was wrapped in aluminum foil and was kept at ambient temperature for 114 days. Disappearance of the starting complex was monitored by ^1H NMR spectroscopy. Small amount of precipitate was observed after 29 days at 23% conversion. Slow accumulation of MeOH was observed.

Reactivity of $Pr_4N(dpms)Pd^{II}Me(OH)$ Under Argon at pH 10.6 in the presence of TEMPO

$$2\ (dpms)Pd^{II}Me(OH)^- + H_2O \xrightarrow[pH\ 10.6]{TEMPO,\ r.t.} 1/2\ C_2H_6 + CH_4 + (dpms)^- + Pd(OH)_2 + 1/2\ [(dpms)Pd(\mu\text{-}OH)]_2^{2-}$$

In an argon filled glove box, to a solution of $Pr_4N(dpms)Pd^{II}Me(OH)$ (13.0 µmol, 21.7 mM) in H_2O/D_2O, 2.6 mg (16.5 µmol) of (2,2,6,6-Tetramethylpiperidin-1-yl)oxyl (TEMPO) was added to give clear yellow solution. The reaction mixture was transferred into NMR tube with airtight Teflon valve and was kept at ambient temperature and light. ^1H NMR spectrum was recorded periodically. After 4 days conversion was 99 %, C_2H_6 and CH_4 were generated in 63 ± 9% and 27 ± 8% yield

respectively. Me-TEMPO was formed in 7 ± 2% yield and MeOH was generated in 1% yield. Trace amount of free ligand was observed.

^{1}H NMR (600 MHz, D_2O) **Me-TEMPO** δ 3.63 (s, 3H), 1.53 (s, 6H), 1.41 (s, 6H), 1.31 – 1.07 (overlapping signals, 6H).

Reaction mixture was analyzed by ESI-MS spectroscopy. In the positive mode (50/50 = MeOH/H_2O + 1% TFA), presence of H^+Me-TEMPO was observed.

ESI-MS (+): calculated for $C_{10}H_{22}NO$ 172.17014, observed 172.16758.

Conditions	Conversion (%) / Reaction Time	C_2H_6 (%)	CH_4 (%)	MeOH (%)	Other Products (%)
pH 10.6, no additives	99 / 7 days	55 ± 3	43 ± 1	0	$dpms^-$, 47
pH 14.0, 1.0 M KOH	98 / 14 days	n.a.	n.a.	0	$LPd^{II}(OH)_2^-$, 16 $dpms^-$, 44
pH 14.0, 1.0 M KOH, dark	37 / 114 days	n.a.	n.a.	16	$LPd^{II}(OH)_2^-$, 21 $dpms^-$, 15
pH 10.6, TEMPO (1.3 equiv.)	99 / 13 days	63 ± 9	27 ± 8	1	Me-TEMPO, 7 ± 2

Table 5.16 Summary of product distribution in reaction of $(dpms)Pd^{II}Me(OH)^-$ under argon.

Product Distribution in Aerobic oxidation of $Pr_4N(dpms)Pd^{II}Me(OH)$ in Closed System

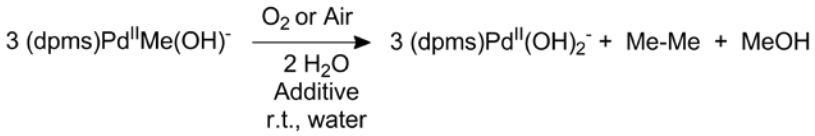

General procedure: The oxidation of aqueous $Pr_4N(dpms)Pd^{II}Me(OH)$ was performed without stirring in J. Young NMR tube. The solution pH was maintained using buffer solution pH 5.9 or 1.0 M KOH (pH 14.0). First, approximately 0.5 mL of ~4-72 mM stock solution of aqueous $Pr_4N(dpms)Pd^{II}Me(OH)$ was combined with an aqueous buffer or 1.0 M KOH under an argon atmosphere. After ^{1}H NMR spectrum of the starting complex was recorded, reaction mixture was purged with pure O_2(g) or air and sealed with a Teflon valve. All reactions were kept at ambient temperature and light. Formation of black precipitate was observed over time. Concentrations of reactant, MeOH and ethane were monitored by ^{1}H NMR spectroscopy with 1,4-

dioxane used as an internal standard. Aqueous and gaseous phase were equilibrated before each ^{1}H NMR spectrum was recorded. The identity of MeOH and ethane was confirmed by addition of the authentic sample to the reaction mixture and comparison of the chemical shifts. C_2H_6 yield was determined using Henry's constant, Ideal Gas Law and integration of C_2H_6 peak in the aqueous phase.

Rxn #	Conditions	Conversion / Reaction time	C_2H_6 (%)	MeOH (%)	Other Products (%)
1	No KOH, SM 5.4 μmol, 9.8 mM	98 % / 6 days	86	13	$LPd^{II}(OH)_2^-$, 78
2	No KOH, SM 4.2 μmol, 7.2 mM	77 % / 3 days	78	19	$LPd^{II}(OH)_2^-$, 88

Table 5.17 Product distribution in oxidation reaction under O_2 at pH 10.6.

Rxn #	Conditions	Conversion / Reaction time	C_2H_6 (%)	MeOH (%)	Other Products (%)
1	KOH 0.2 M, SM 6.5 μmol, 13.3 mM	99 % / 6 days	66	33	$LPd^{II}(OH)_2^-$, 98
2	KOH 0.16 M, SM 5.4 μmol, 9.0 mM	98 % / 7 days	87	13	$LPd^{II}(OH)_2^-$, 86

Table 5.18 Product distribution in oxidation reaction under O_2 at pH 13.2.

Rxn #	Conditions	Conversion / Reaction time	C_2H_6 (%)	MeOH (%)	Other Products (%)
1	KOH 1.0 M, SM 9.6 μmol, 24.0 mM	100 % / 2 days	n.a.	47	$LPd^{II}(OH)_2^-$, 71 MeO_2H, 19
2	KOH 1.0 M, SM 9.7 μmol, 24.0 mM	100 % / 4 days	n.a.	47	$LPd^{II}(OH)_2^-$, 66 MeO_2H, 21

Table 5.19 Product distribution in oxidation reaction under O_2 at pH 14.0.

Rxn #	Conditions	Conversion / Reaction time	C_2H_6 (%)	MeOH (%)	Other Products (%)
1	SM 3.0 μmol, 4.2 mM	65 % / 1 day	50	7	CH_4, 38%
2	SM 3.4 μmol, 4.4 mM	60 % / 1 day	68	10	CH_4, 24%

Table 5.20 Product distribution in oxidation reaction under O_2 at pH 6.3.

Rxn #	Conditions	Conversion / Reaction time	C_2H_6 (%)	MeOH (%)	Other Products (%)
1	No KOH, SM 3.4 μmol, 7.6 mM	99 % / 5 days	88	11	$LPd^{II}(OH)_2^-$, 78
2	No KOH, SM 17.0 μmol, 34.0 mM	98 % / 5 days	94	7	$LPd^{II}(OH)_2^-$, 64

Table 5.21 Product distribution in oxidation reaction under air at pH 10.6.

Rxn #	Conditions	Conversion / Reaction time	C_2H_6 (%)	MeOH (%)	Other Products (%)
1	KOH 0.33 M, SM 20.7 μmol, 46.0 mM	78 % / 3 days	n.a.	41	$LPd^{II}(OH)_2^-$, 91
2	KOH 0.3 M, SM 23.4 μmol, 46.8 mM	80 % / 5 days	n.a.	40	$LPd^{II}(OH)_2^-$, 93

Table 5.22 Product distribution in oxidation reaction under air at pH 13.5.

Rxn #	Conditions	Conversion / Reaction time	C_2H_6 (%)	MeOH (%)	Other Products (%)
1	KOH 1.0 M, SM 5.1 μmol, 9.6 mM	80 % / 3 days	n.a.	45	$LPd^{II}(OH)_2^-$, 77
2	KOH 1.0 M, SM 26.6 μmol, 53.2 mM	95 % / 9 days	n.a.	38	$LPd^{II}(OH)_2^-$, 76
3	KOH 3.6 M, SM 29.1 μmol, 72.7 mM	68 % / 2 days	n.a.	51	$LPd^{II}(OH)_2^-$, 67

Table 5.23 Product distribution in oxidation reaction under air at pH 14.0.

Stability of MeOOH at pH 14.0

When aqueous $Pr_4N(dpms)Pd^{II}Me(OH)$ was kept under O_2 at pH 14.0 formaiton of MeOH and MeOOH was observed (Table 5.19). Monitoring of the reaction mixture after complete disappearance of the Pd^{II} complex revealed slow decomposition of MeOOH over 28 days.

Rxn #	4 days	7 days	15 days	21 days	28 days
1	19%	17%	13%	13%	12%
2	21%	18%	15%	14%	14%

Reactivity of $Pr_4N(dpms)Pd^{II}Me(OH)$ under 2 atm O_2

The oxidation of aqueous $Pr_4N(dpms)Pd^{II}Me(OH)$ (6.4 μmol) was performed without stirring in J. Young NMR tube. The solution pH was maintained using 1.0 M KOH (pH 14.0). After ^1H NMR spectrum of the starting complex was recorded, reaction mixture was pressurized with 2 atm of O_2(g) and sealed with a Teflon valve. All reactions were kept at ambient temperature and light. Concentrations of reactant, MeOH and ethane were monitored by ^1H NMR spectroscopy with 1,4-dioxane used

as an internal standard. Aqueous and gaseous phase were equilibrated before each ^{1}H NMR spectrum was recorded.

Rxn #	Conditions	Conversion / Reaction time	C_2H_6 (%)	MeOH (%)	MeO_2H (%)	Other Products (%)
1	pH 14.0, SM 12.8 mM	98 % / 3 days	n.a.	56	4	$LPd^{II}(OH)_2^-$, 78 $dpms^-$, 18
2	pH 14.0, SM 12.6 mM	98 % / 3 days	n.a.	56	4	$LPd^{II}(OH)_2^-$, 79 $dpms^-$, 17

Effect of Concentration of $Pr_4N(dpms)Pd^{II}Me(OH)$ on the Yield of MeOH in Closed System

General procedure: The oxidation of aqueous $Pr_4N(dpms)Pd^{II}Me(OH)$ was performed without stirring in J. Young NMR tube. The solution pH was maintained using 1.0 M KOH (pH 14.0). First, 0.5 mL of 12.6 and 13.8 mM stock solution of aqueous $Pr_4N(dpms)Pd^{II}Me(OH)$ was combined with 28.0 mg of KOH (0.5 mmol) each under an argon atmosphere. Then, 50 μL of each stock solution was taken and a solution of 1.0 M KOH in D_2O was added up to 0.5 mL mark. The resulting solutions have concentrations of 1.26 and 1.38 mM respectively. Similarly, 20-fold diluted solution was prepared by combining 25 μL of stock solution with 1.0 M KOH in D_2O to give solutions of 0.63 and 0.69 mM respectively.

After ^{1}H NMR spectrum of the starting complexes was recorded, reaction mixtures were purged with O_2(g) and sealed with a Teflon valve. All reactions were kept at ambient temperature and light. Disappearance of the starting complex, and formation of organic products was monitored by ^{1}H NMR spectroscopy with 1,4-dioxane used as an internal standard. Over four days, formation of MeOH and MeO_2^- was observed. Yield of ethane could not be determined due to its low concentration in the aqueous phase. Yields in Table 5.24-5.26 are calculated at 100% conversion.

Rxn #	Conditions	Conversion / Reaction time	MeOH (%)	MeO_2H (%)	Other Products (%)
1	SM 6.3 μmol, 12.6 mM	98 % / 4 days	56	5	$LPd^{II}(OH)_2^-$, 78
2	SM 6.9 μmol, 13.8 mM	98 % / 4 days	53	4	$LPd^{II}(OH)_2^-$, 88

Table 5.24 Product distribution in oxidation reaction under O_2 at pH 14.0.

Rxn #	Conditions	Conversion / Reaction time	MeOH (%)	MeO_2H (%)	Other Products (%)
1	SM 0.63 μmol, 1.26 mM	100 % / 4 days	46	30	$LPd^{II}(OH)_2^-$, 98
2	SM 0.69 μmol, 1.38 mM	100 % / 4 days	41	31	$LPd^{II}(OH)_2^-$, 86

Table 5.25 Product distribution in oxidation reaction under O_2 at pH 14.0. Stock solution diluted 10 fold.

Rxn #	Conditions	Conversion / Reaction time	MeOH (%)	MeO_2H (%)	Other Products (%)
1	SM 0.32 μmol, 0.63 mM	100 % / 4 days	42	43	$LPd^{II}(OH)_2^-$, 71 $dpms^-$, 21
2	SM 0.35 μmol, 0.69 mM	100 % / 4 days	43	37	$LPd^{II}(OH)_2^-$, 66 $dpms^-$, 34

Table 5.26 Product distribution in oxidation reaction under O_2 at pH 14.0. Stock solution diluted 20 fold.

Oxidation with O_2 using radical trap Tempo

In an argon filled glove box, to a solution of $Pr_4N(dpms)Pd^{II}Me(OH)$ (16.5 μmol) in H_2O/D_2O, 2.6 mg (16.5 μmol) of (2,2,6,6-Tetramethylpiperidin-1-yl)oxyl (TEMPO) was added to give clear yellow solution. Reaction mixture was transferred into J. Young NMR. The reaction mixture was taken out of the glove box and O_2 was bubbled through the solution. NMR tube was sealed and was kept at ambient temperature and light until full conversion. Concentrations of reactant, MeOH and ethane were monitored by ^1H NMR spectroscopy with 1,4-dioxane used as an internal standard. Aqueous and gaseous phase were equilibrated before each ^1H NMR spectrum was recorded. Yield of MeOH was calculated based in the integration, and C_2H_6 yield was determined using Henry's constant, Ideal Gas Law and integration of C_2H_6 peak in the aqueous phase.

Followed by ^{1}H NMR analysis, reaction was analyzed with ESI-MS spectroscopy. In the positive mode (50/50 = MeOH/H_2O + 1% TFA), presence of H^+ - Me-TEMPO was observed.

ESI-MS (+): calculated for $C_{10}H_{22}NO$ 172.17014, observed 172.19746.

Rxn #	Conditions	Conversion / Reaction time	C_2H_6 (%)	MeOH (%)	Other Products (%)
1	pH 10.6, SM 13.0 µmol, 21.6 mM, TEMPO, 16.5 µmol	97 % / 11 days	92	4	$LPd^{II}(OH)_2^-$, 85 Me-TEMPO, 3
2	pH 10.6, SM 20.3 µmol, 40.6 mM, TEMPO, 12.6 µmol	96 % / 10 days	n.a.*	2	$LPd^{II}(OH)_2^-$, 75 Me-TEMPO, 1%

*Yield of C_2H_6 could not be calculated due to broadening of peaks

Aerobic Oxidation of (dpms)$Pd^{II}CH_3$(OH) in Methanol in the presence of 1.0 M KOH

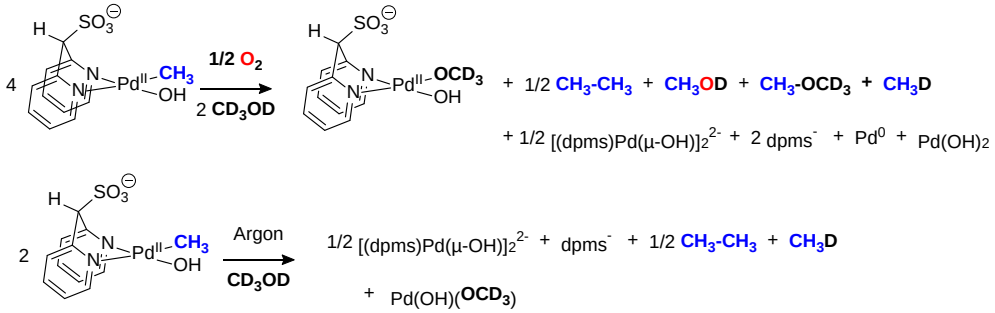

In an argon filled glove box, Pr_4N(dpms)$Pd^{II}CH_3$(OH) (11.7 µmol) was dissolved in a 1.0 M solution of KOH (120 mg, 2.1 mmol) in methanol-d_4. The resulting mixture was divided into two portions and each portion was transferred into air tight NMR tube. Both NMR tubes were taken out of the glove box. Tube #1 was flushed with O_2 for 30 seconds, tube #2 was kept sealed under argon as a control experiment. Both reactions were kept at ambient light and temperature (21 °C) and formation of black precipitate was observed in both cases. ^{1}H NMRs of both reaction mixtures were taken periodically. Reaction #1 showed formation of MeOH (16 ± 5% yield), $MeOCD_3$ (36 ± 3% yield), C_2H_6 and CH_3D. Identity of Me_2O was confirmed with authentic sample.

Rxn #	Conditions	Conversion / Reaction time	C_2H_6 (%)	MeOH (%)	Other Products (%)
1	SM 6.4 μmol, 6.7 mM, 1.0 M KOH	98 % / 4 days	n.a.	21	*$MeOCD_3$, 33
2	SM 11.7 μmol, 21.6 mM, 1.0 M KOH	98 % / 6 days	n.a.	11	*$MeOCD_3$, 39

*Yield of CH_3D and C_2H_6 could not be determined

Rxn #2 showed gradual decomposition of $Pr_4N(dpms)Pd^{II}CH_3(OH)$ over two days with formation of C_2H_6, CH_3D, CH_4. Formation of CH_3OD and CH_3OCD_3 was not observed in the absence of dioxygen.

Kinetics of Aerobic Oxidation of $(dpms)Pd^{II}Me(OH)^-$

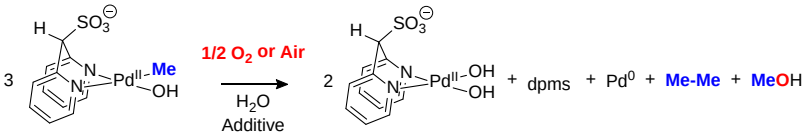

General procedure. The oxidation of aqueous $(dpms)Pd^{II}Me(OH_n)^{(2-n)-}$ was run under vigorous stirring in a 25 mL round-bottom flask filled with $O_2(g)$, equipped with a stirring bar and an O_2-filled balloon. Reactions under air were performed under vigorous stirring in 25 mL round-bottom flask, equipped with a stir bar and a needle for pressure equilibration. The solution pH was maintained using buffer solution (pH 6.8) or 1.0 M KOH (pH 14.0). First, approximately 2.0 mL of ~4-10 mM stock solution of aqueous $(dpms)Pd^{II}Me(OH)^-$ were combined with an appropriate aqueous buffer or 1.0 M KOH under argon atmosphere. The mixture was temperature-equilibrated and then injected with a syringe into the reaction flask placed in a temperature-controlled water-ethylene glycol bath at 20.0 °C. Vigorous stirring began immediately. Periodically a ~0.2 mL aliquot of the reaction mixture was taken with a syringe, transferred into argon-filled NMR tube, and diluted with 0.3 mL degassed D_2O to stop the reaction. Concentrations of the reactant, $(dpms)Pd^{II}(OH)_2^-$ and MeOH were monitored by ^1H NMR spectroscopy with 1,4-dioxane used as an internal

standard. Yield of C_2H_6 could not be determined since reaction was performed in open system. Starting complex is presumed to undergo full conversion to generate MeOH, C_2H_6 and $(dpms)Pd^{II}(OH)_2^-$ as has been showed in reactions in closed system (vide supra). Minimum of two kinetics runs were performed. Unless otherwise mentioned, kinetic runs were performed under ambient laboratory light in Pyrex® glassware. In order to test the effect of ionic strength on the rate of oxidation, experiment was performed in 1M KNO_3 solution.

Kinetic plots of oxidation of the $(dpms)Pd^{II}Me(OH)$ under air

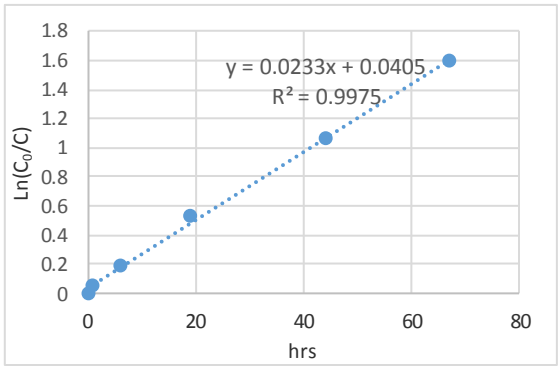

[SM] = 8.4 mM,
conversion = 80%
MeOH yield = 5%
$(dpms)Pd^{II}(OH)_2^-$ yield = 40%
$t_{1/2}$ = 30 h

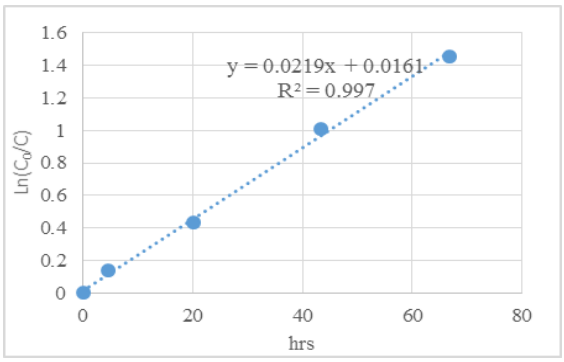

[SM] = 5.2 mM,
conversion = 90%
MeOH yield = 8%
$(dpms)Pd^{II}(OH)_2^-$ yield = 50%
$t_{1/2}$ = 32 h

Figure 5.3 First-order kinetics plots for oxidation of $(L)Pd^{II}Me(OH)$ under air at **pH 10.6**, 20.0 °C.

Kinetic plots of oxidation of the (dpms)Pd^{II}Me(OH) under O_2

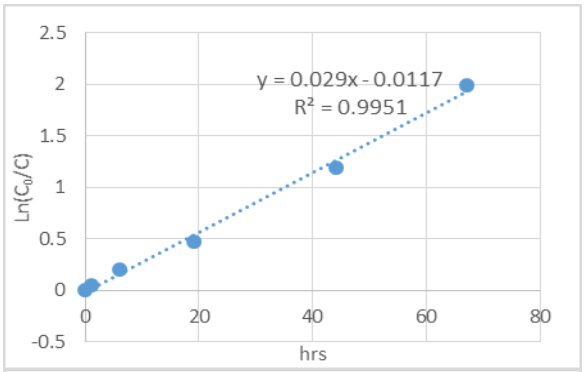

[SM] = 8.8 mM,
conversion = 86%
MeOH yield = 9%
(dpms)$Pd^{II}(OH)_2^-$ yield = 65%
$t_{1/2}$ = 23.9 h

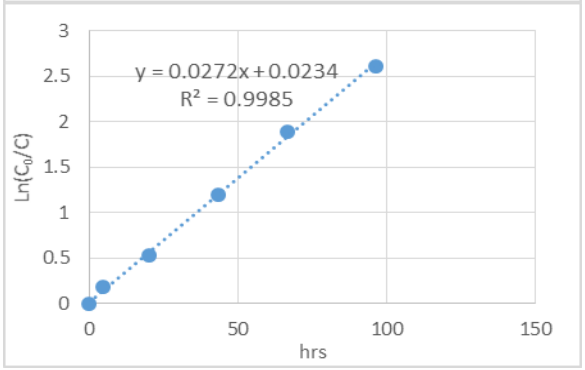

[SM] = 9.9 mM,
conversion = 93%
MeOH yield = 19%
(dpms)$Pd^{II}(OH)_2^-$ yield = 72%
$t_{1/2}$ = 25.5 h

Figure 5.4 First-order kinetics plots for oxidation of (L)Pd^{II}Me(OH) under **O_2** at **pH 10.6**, 20.0 °C.

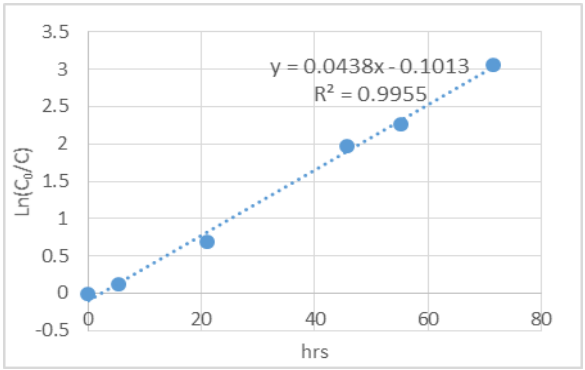

[SM] = 6.3 mM,
conversion = 95%
MeOH yield = 46%
(dpms)$Pd^{II}(OH)_2^-$ yield = 99%
$t_{1/2}$ = 15.8 h

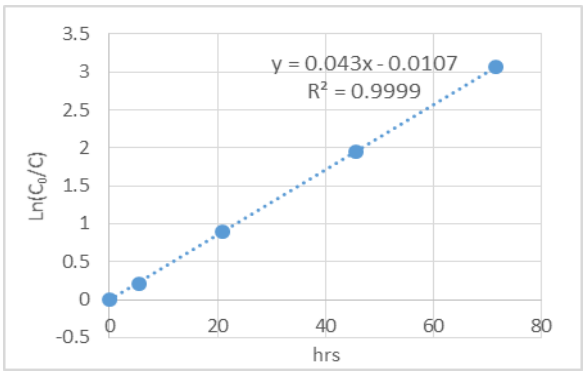

[SM] = 6.3 mM,
conversion = 95%
MeOH yield = 55%
(dpms)$Pd^{II}(OH)_2^-$ yield = 89%
$t_{1/2}$ = 16.1 h

Figure 5.5 First-order kinetics plots for oxidation of (L)Pd^{II}Me(OH) under **O_2** at **pH 14.0**, 20.0 °C.

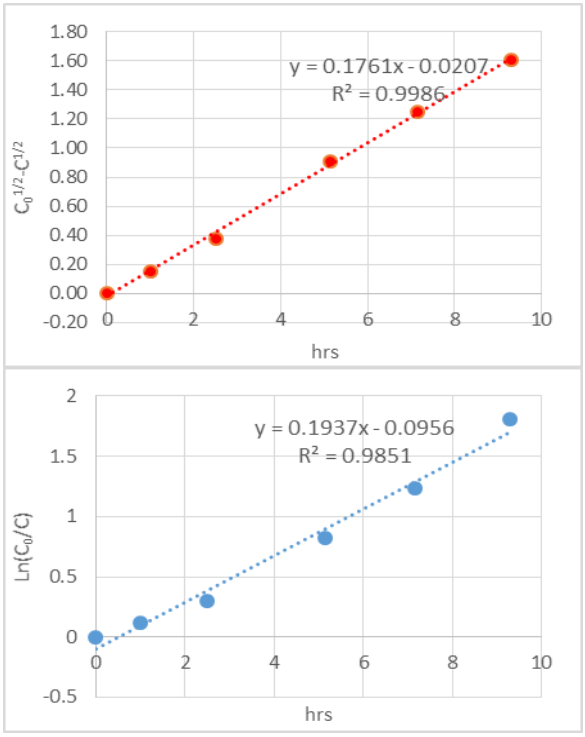

[SM] = 7.3 mM,
conversion = 96%
MeOH yield = 42%
(dpms)$Pd^{II}(OH)_2^-$ yield = 81%
$t_{1/2}$ = 4.5 h

Figure 5.6 Half-order (**top**) and first-order (**bottom**) kinetics plots for oxidation of (L)Pd^{II}Me(OH) under **O_2** at **pH 14.0**, 20.0 °C. Reaction mixture was irradiated with 26 W fluorescent lamp.

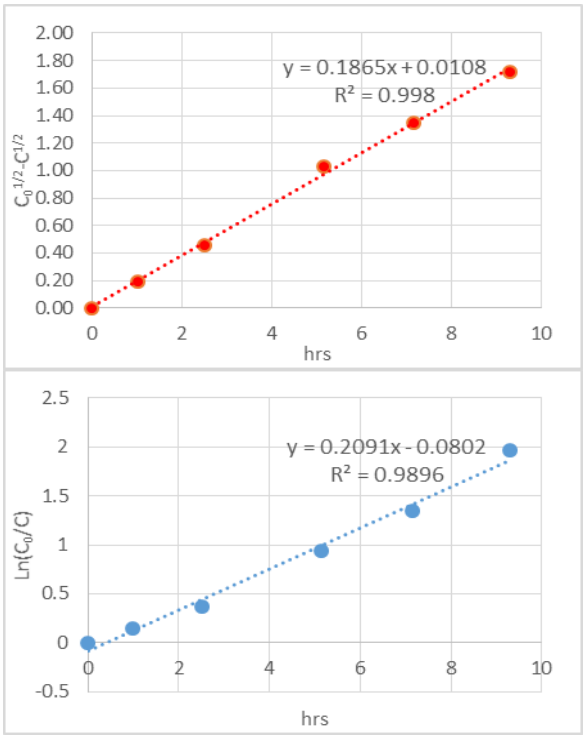

[SM] = 7.5 mM,
conversion = 86%
MeOH yield = 41%
(dpms)$Pd^{II}(OH)_2^-$ yield = 85%
$t_{1/2}$ = 4.3 h

Figure 5.7 Half-order (**top**) and first-order (**bottom**) kinetics plots for oxidation of (L)Pd^{II}Me(OH) under **O_2** at **pH 14.0**, 20.0 °C. Reaction mixture was irradiated with 26W fluorescent lamp.

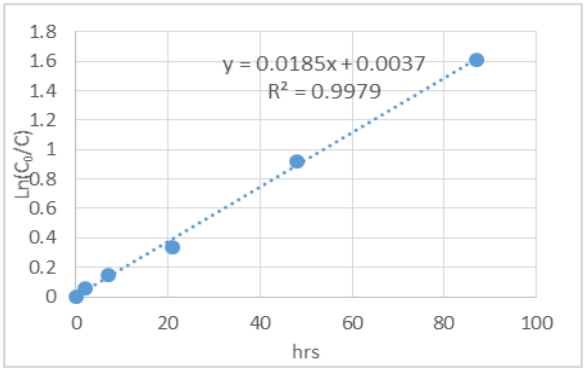

[SM] = 4.0 mM,
conversion = 80%
MeOH yield = 10 %
(dpms)$Pd^{II}(OH)_2^-$ yield = 68 %
$t_{1/2}$ = 37.5 h
TEMPO = 2.7 mg, 17.3 µmol, 2.4 equiv.
Me-TEMPO = 8 %

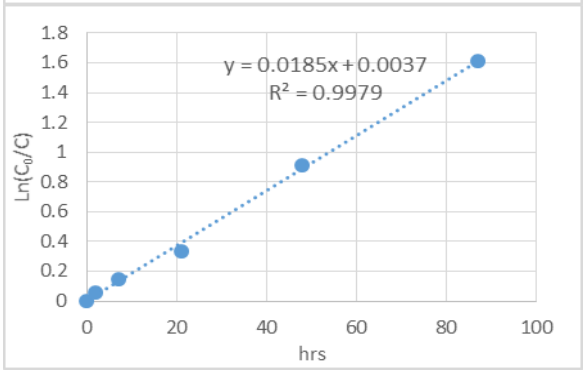

[SM] = 5.9 mM,
conversion = 82%
MeOH yield = 12 %
(dpms)$Pd^{II}(OH)_2^-$ yield = 76 %
$t_{1/2}$ = 38.7 h
TEMPO = 2.2 mg, 14.1 µmol, 1.3 equiv.
Me-TEMPO = 6 %

Figure 5.8 First-order kinetics plots for oxidation of (L)Pd^{II}Me(OH) under **O_2** at **pH 10.6** with **TEMPO**, 20.0 °C.

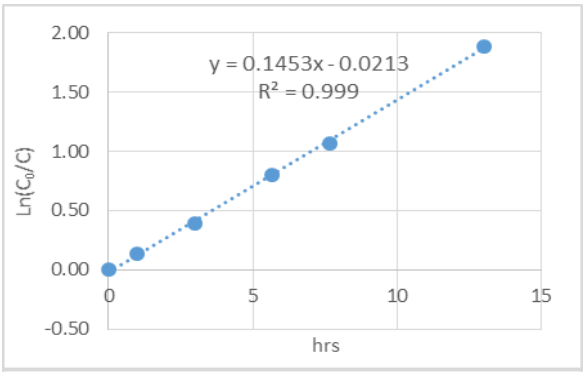

[SM] = 3.9 mM,
conversion = 83%
MeOH yield = 9%
$t_{1/2}$ = 4.8 h

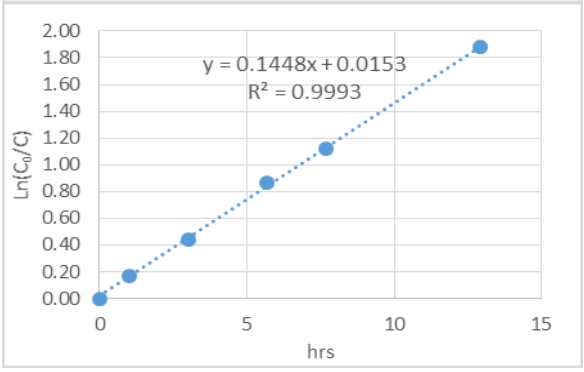

[SM] = 4.0 mM,
conversion = 88%
MeOH yield = 10%
$t_{1/2}$ = 4.8 h

Figure 5.9 First-order kinetics plots for oxidation of (L)Pd^{II}Me(OH) under **O_2** at **pH 6.8**, 20.0 °C.

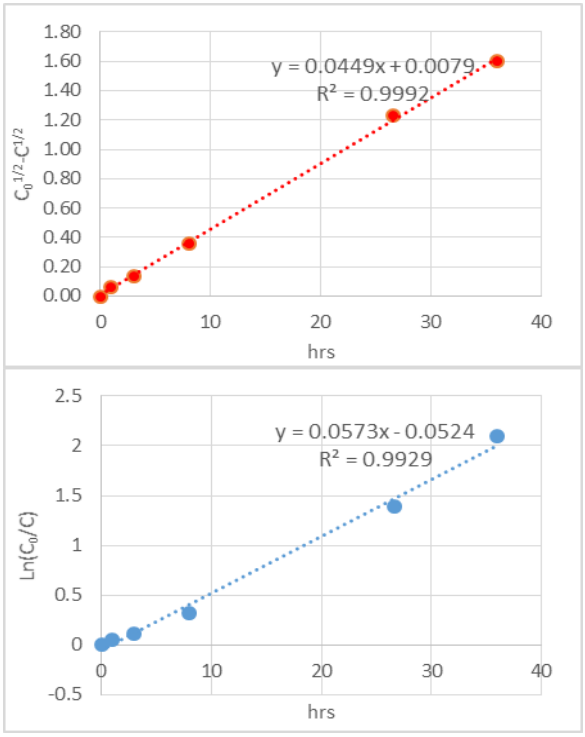

[SM] = 6.1 mM,
conversion = 87%
MeOH yield = 7%
$(dpms)Pd^{II}(OH)_2^-$ yield = 51%
$t_{1/2}$ = 16.1 h
KNO_3 = 180.3 mg, 1.78 mmol

Figure 5.10 Half-order (**top**) and first-order (**bottom**) kinetics plots for oxidation of $(dpms)Pd^{II}Me(OH)$ under $\mathbf{O_2}$ at **pH 10.6**, in 1M KNO_3, 20.0 °C.

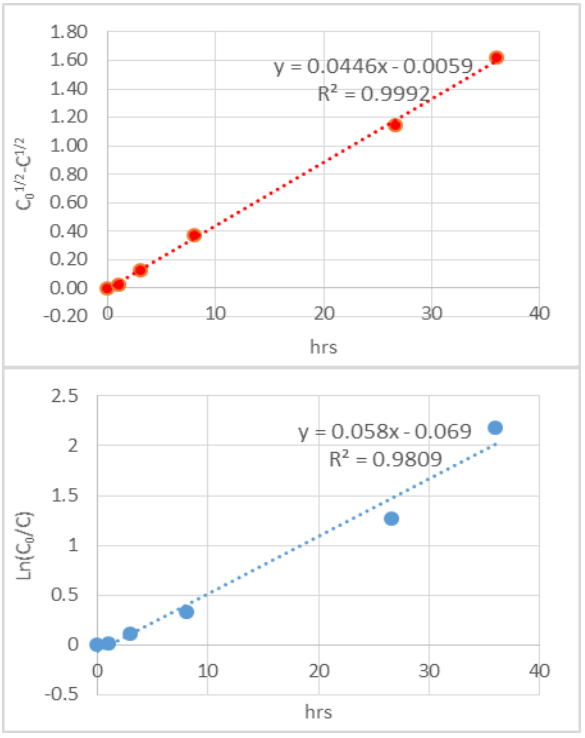

[SM] = 5.9 mM,
conversion = 89%
MeOH yield = 11%
$(dpms)Pd^{II}(OH)_2^-$ yield = 87%
$t_{1/2}$ = 15.5 h
KNO_3 = 182.8 mg, 1.80 mmol

Figure 5.11 Half-order (**top**) and first-order (**bottom**) kinetics plots for oxidation of $(dpms)Pd^{II}Me(OH)$ under $\mathbf{O_2}$ at **pH 10.6**, in 1M KNO_3, 20.0 °C.

Qualitative Estimate of the Rate of Oxidation of (dpms)$Pd^{II}Me(OH)$ under O_2 in the Dark

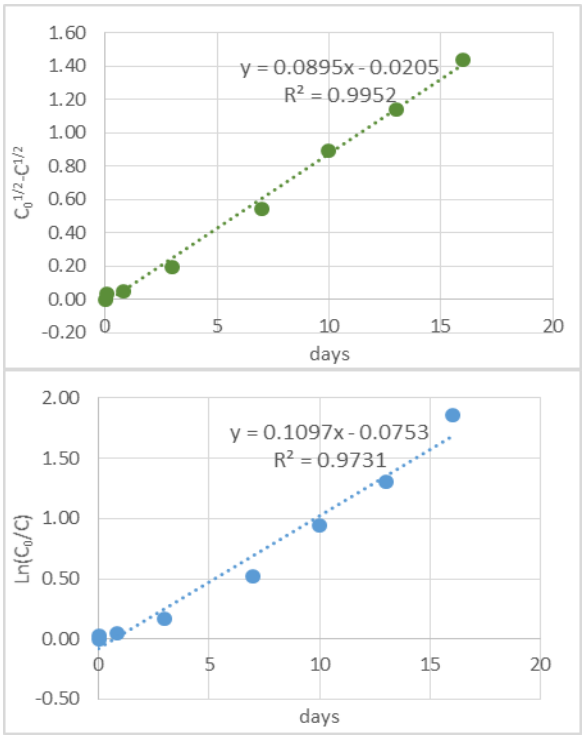

[SM] = 5.7 mM,
conversion = 84%
MeOH yield = 6%
$(dpms)^-$ yield = 59 %
$t_{1/2}$ = 7.8 days, 187.2 h

Figure 5.12 Half-order (**top**) and first-order (**bottom**) kinetics plots for oxidation of (dpms)Pd^{II}Me(OH) under **O_2** at **pH 14.0**, in the dark, room temperature.

Conditions	Conversion (%)	$t_{1/2}$ (h)	MeOH (%)	Other Products (%)	Rxn Order
Air, pH 10.6	85 ± 5	30.7 ± 1	6 ± 2	$LPd^{II}(OH)_2^-$, 45 ± 5	1
O_2, pH 10.6	90 ± 4	24.7 ± 0.8	14 ± 5	$LPd^{II}(OH)_2^-$, 69 ± 4	1
O_2, pH 14.0	95 ± 1	16.0 ± 0.15	50 ± 6	$LPd^{II}(OH)_2^-$, 94 ± 5	1
O_2, pH 14.0, Light	91 ± 5	4.4 ± 0.1	42 ± 1	$LPd^{II}(OH)_2^-$, 83 ± 2	1/2
O_2, pH 10.6, TEMPO	81 ± 1	38.1 ± 0.6	11 ± 1	$LPd^{II}(OH)_2^-$, 72 ± 4 Me-TEMPO, 7 ± 1	1
O_2, pH 6.8	86 ± 3	4.8 ± 0.01	10 ± 1	Pd^{II} complex, 58 ± 1	1
O_2, pH 10.6, 1M NO_3^-	89 ± 1	15.8 ± 0.3	9 ± 2	$LPd^{II}(OH)_2^-$, 69 ± 18	1/2
O_2, pH 14.0, Dark*	84	187.2	6	$dpms^-$, 59	1/2

Table 5.27 Summary of product distribution in kinetics of oxidation of (dpms)$Pd^{II}Me(OH_n)^{(2-n)-}$ under various conditions. Yields are determined at 100% conversion.

Conditions	$k_{(MeOH)}$, s^{-1}	$\Delta G^{\ddagger}$ (MeOH)	$k_{(Ethane)}$, s^{-1}	$\Delta G^{\ddagger}$ (Ethane)
Air, pH 10.6	$(3.8 \pm 0.1)\times10^{-7}$	28.1	$(5.9 \pm 0.2)\times10^{-6}$	26.5
O_2, pH 10.6	$(1.1 \pm 0.02)\times10^{-6}$	27.5	$(6.7 \pm 0.2)\times10^{-6}$	26.4
O_2, pH 10.6, TEMPO	$(5.6 \pm 0.09)\times10^{-7}$	27.9	$(4.1 \pm 0.01)\times10^{-6}$	26.7
O_2, pH 14.0	$(6.0 \pm 0.04)\times10^{-6}$	26.5	$(3.7 \pm 0.02)\times10^{-6}$	26.8
O_2, pH 6.8	$(3.8 \pm 0.008)\times10^{-6}$	26.8	$(3.6 \pm 0.008)\times10^{-5}$	25.4

Table 5.28 Summary of k_{MeOH} and k_{Ethane} under various conditions.

Oxidation of $Pr_4N(dpms)Pd^{II}Me(OH)$ with I_2

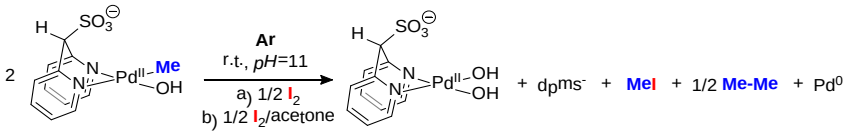

In the glove box, to an aqueous solution of $Pr_4N(dpms)Pd^{II}Me(OH)$ (2.70 µmol) I_2 was added (4.8 mg, 18.9 µmol). The reaction mixture was transferred into NMR tube with air tight Teflon valve. NMR tube was taken out of the glove box and was kept at ambient temperature without stirring. The reaction of the starting material with I_2 under Ar was monitored by ^1H NMR spectroscopy. In approximately one hour the solution started to turn darker and formation of precipitate was observed. At 100 % conversion, MeI (δ 2.16, s), C_2H_6 (δ 0.81, s,) and $Pr_4N(dpms)Pd^{II}(OH)_2$ were observed by ^1H NMR spectroscopy.

Conditions	Conversion / Reaction time	C_2H_6 (%)	MeI (%)	Other Products (%)
SM 2.7 µmol, 3.9 mM	87 % / 9 days	92	8 ± 2	$LPd^{II}(OH)_2^-$, 50

Table 5.29 Product distribution in oxidation reaction with I_2 at pH 10.6.

When I_2 was dissolved in acetone-d_6 and then combined with the aqueous solution of $Pr_4N(dpms)Pd^{II}Me(OH)$, complete conversion was observed with minutes after addition of I_2.

Conditions	Conversion / Reaction time	MeI (%)	Other Products (%)
SM 4.2 μmol, 5.8 mM	100 % / 22 min	43 ± 7	$LPd^{II}(OH)_2^-$, 52 ± 9

Table 5.30 Product distribution in oxidation reaction with I_2/acetone-d_6, at pH 10.6.

Formation of trace amounts of MeOH (1-2 %) and (dpms)$Pd^{II}Me_2(OH)$ (1 %) was observed in the reaction mixture.

Oxidation of Pr_4N(dpms)Pd^{II}Me(OH) with peroxides

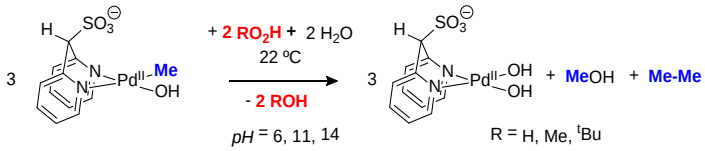

General procedure. Under an argon atmosphere, pH of aqueous $LPd^{II}Me(OH)^-$ was adjusted using buffer solution (pH 6.7) or 1.0 M KOH (pH 14.0). ^{1}H NMR spectrum of the starting material was recorded, followed by addition of H_2O_2 (2-6 equiv.), MeOOH (2-6 equiv.) or ^{t}BuOOH (1-6 equiv.). ^{1}H NMR spectrum was recorded again immediately after addition of peroxide. In all cases except with MeOOH, presence of *unsym* -$LPd^{IV}Me_2(OH)$ was observed and ethane was the major methyl-containing product. Formation of *unsym* -$LPd^{IV}Me_2(OH)$ was observed in reactions with tBuOOH and H_2O_2 in acidic and basic pH. Structure of *unsym*-$LPd^{IV}Me_2(OH)$ was confirmed by independent synthesis. At 5 °C slow decomposition of *unsym*-$LPd^{IV}Me_2(OH)$ occurs over 1-2 hours, which allows for observation of selective NOE. Yields are calculated at 100% conversion

Conditions	Conversion / Reaction time	C_2H_6 (%)	MeOH (%)	Other Products (%)
pH 10.6, 15 mM, 22 °C	74 % / 3 days	81	7 ± 3	$LPd^{IV}Me_2(OH)$, 11
pH 6.0, 16 mM, 5 °C	100 % / 7 min	78	14	$LPd^{IV}Me_2(OH)$, 47 MeOOH, 19
pH 14.0, 26 mM, 22 °C	59 % / 1 hr	n.a.	32	MeOOH, 26

Table 5.31 Product distribution in oxidation reaction with H_2O_2.

Conditions	Conversion / Reaction time	C_2H_6 (%)	MeOH (%), ^{t}BuOH (%)	Other Products (%)
pH 10.6, ^{t}BuOOH (1.1 eq.) SM = 18 mM	100 % / 9 min	51	MeOH, 3 ± 2 ^{t}BuOH, 80	$LPd^{IV}Me_2(OH)$, 72 MeOOH, 7
pH 6.0, ^{t}BuOOH (5.9 eq.) SM = 17 mM	100 % / 6 min	93	MeOH, 5 ^{t}BuOH, 94	$LPd^{IV}Me_2(OH)$, 50 MeOOH, 2
pH 14.0, ^{t}BuOOH (2.2 eq.), SM = 26 mM	100 % / 3 h	30	MeOH, 55 ^{t}BuOH, 99	$LPd^{IV}Me_2(OH)$, 15 MeOOH, 14

Yield of ^{t}BuOOH was calculated based on Pd^{II}

Table 5.32 Product distribution in oxidation reaction with ^{t}BuOOH.

Oxidation of $Na(dpms)Pd^{II}CH_3(OH)$ with $NaIO_4$

General procedure. Under an argon atmosphere, pH of aqueous $LPd^{II}Me(OH)^-$ was adjusted using buffer solution (pH 6.7) or 1.0 M KOH (pH 14.0). ^{1}H NMR spectrum of the starting material was recorded, followed by addition of H_2O_2 (2-6 equiv.), MeOOH (2-6 equiv.) or ^{t}BuOOH (1-6 equiv.). ^{1}H NMR spectrum was recorded again immediately after addition of peroxide. In all cases except with MeOOH, presence of *unsym* -$LPd^{IV}Me_2(OH)$ was observed and ethane was the major methyl-containing product. Formation of *unsym* -$LPd^{IV}Me_2(OH)$ was observed in reactions with tBuOOH and H_2O_2 in acidic and basic pH. Structure of *unsym*-$LPd^{IV}Me_2(OH)$ was confirmed by independent synthesis. At 5 °C slow decomposition of *unsym*-$LPd^{IV}Me_2(OH)$ occurs over 1-2 hours, which allows for observation of selective NOE.

Conditions	Conversion (%)/ Reaction time	Yield MeOH (%)		Other Products (%)
		Light	**Dark**	
pH 8.0, SM = 1.9 mM	100 / 7 min	36 ± 3	49 ± 2	$LPd^{IV}Me_2(OH)$, 12
pH 10.6, SM = 1.1 mM	100 / 7 min	22 ± 4	47	$LPd^{IV}Me_2(OH)$, 43 ± 10

Table 5.33 Product distribution in oxidation reaction with 1.0 equiv. of $NaIO_4$.

Conditions	Conversion (%)/ Reaction time	Yield MeOH (%)		Other Products (%)
		Light	**Dark**	
pH 8.0, SM = 1.9 mM	100 / 7 min	60 ± 13	72 ± 5	$LPd^{IV}Me_2(OH)$, 7
pH 10.6, SM = 2.0 mM	100 / 11 min	27	64	$LPd^{IV}Me_2$ (OH), 31
pH 14.0, SM = 2.6 mM	81 / 3 days	28	42	-

Table 5.34 Product distribution in oxidation reaction with 3.0 equiv. of $NaIO_4$.

Preparation of $Pr_4N(dpms)Pd^{II}Me_2(OH)$

Under atmosphere of Argon in the glove box, MeI (1.0µL, 16.0 µmol) was added to a stock solution of $Pr_4N(dpms)Pd^{II}Me(OH)$ in D_2O (8.9 µmol) via microliter syringe. Slow formation of $(dpms)Pd^{IV}Me_2(OH)$ was monitored by ^1H NMR spectroscopy at +5 °C. Maximum observed yield of $(dpms)Pd^{IV}Me_2(OH)$ was 48 % after 47 minutes of reaction time. When mixture was left at ambient temperature for 12 h, $(dpms)Pd^{IV}Me_2(OH)$ decomposes with formation of C_2H_6, Pd black and $(dpms)Pd(OH)_2$. ^1H NMR showed a signal corresponding to C_2H_6, at 0.81 ppm. MeOH was present in 2% yield and $(dpms)Pd^{II}(OH)_2$ yield was formed in 45% yield.

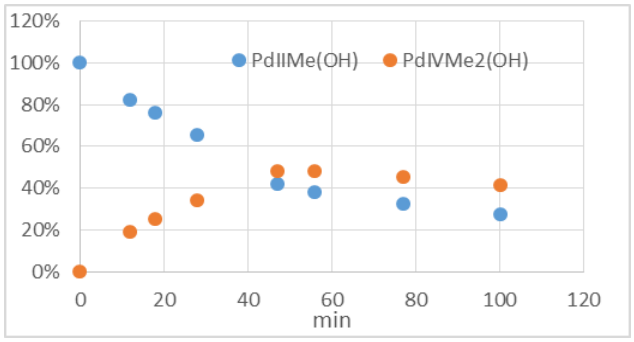

Figure 5.13 Disappearance of $(dpms)Pd^{II}Me(OH)$ in reaction with MeI *vs.* time, and formation of $(dpms)Pd^{IV}Me_2(OH)$.

Time (min)	Pd^{II}**Me**(OH) (%)	Pd^{IV}**Me**$_2$(OH) (%)
0	100	0
12	82	19
18	76	25
28	66	34
47	42	48
56	38	48
77	32	45
100	27	41

Table 5.35 Disappearance of $(dpms)Pd^{II}Me(OH)$ in reaction with MeI.

^1H NMR (400 MHz, D_2O) δ 8.70 (dd, *J* = 5.2, 0.7 Hz, 1H), 8.59 (dd, *J* = 6.3, 0.8 Hz, 1H), 8.19 (m, overlapping td, 2H), 7.98 – 7.91 (m, overlapping dd, 2H), 7.75 – 7.69 (m, 1H), 7.51 (td, *J* = 6.9, 1.2 Hz, 1H), 2.90 (s, 3H), 2.50 (s, 3H). Bridging C*H*-SO_3 was not observed due to H/D exchange.

^{13}C NMR spectrum could not be obtained since product exists in the mixture of $(dpms)Pd^{II}Me(OH)$ and $(dpms)Pd^{II}(OH)_2$.

ESI-MS: m+Na^+/z 424.94; calculated for $C_{13}H_{16}N_2NaO_4PdS$, 424.97633 Na^+(dpms)$Pd(CH_3)_2(OH)$; m+Na^+/z 425.94; calculated for $C_{13}H_{15}DN_2NaO_4PdS$, 425.98261 Na^+(dpms-d)$Pd(CH_3)_2(OH)$.

Selective NOE of (dpms)$Pd^{IV}Me_2(OH)$: Irradiation of signal at 2.91 ppm (Pd-CH_3 axial) shows negative NOE with a singlet at 2.51 ppm (Pd-CH_3 equatorial, 1.2%) and a negative NOE with a dd at 8.60 (H6-dpms ligand, 1.5%) and a dd at 8.70 ppm (H6-dpms ligand, 1.3%).

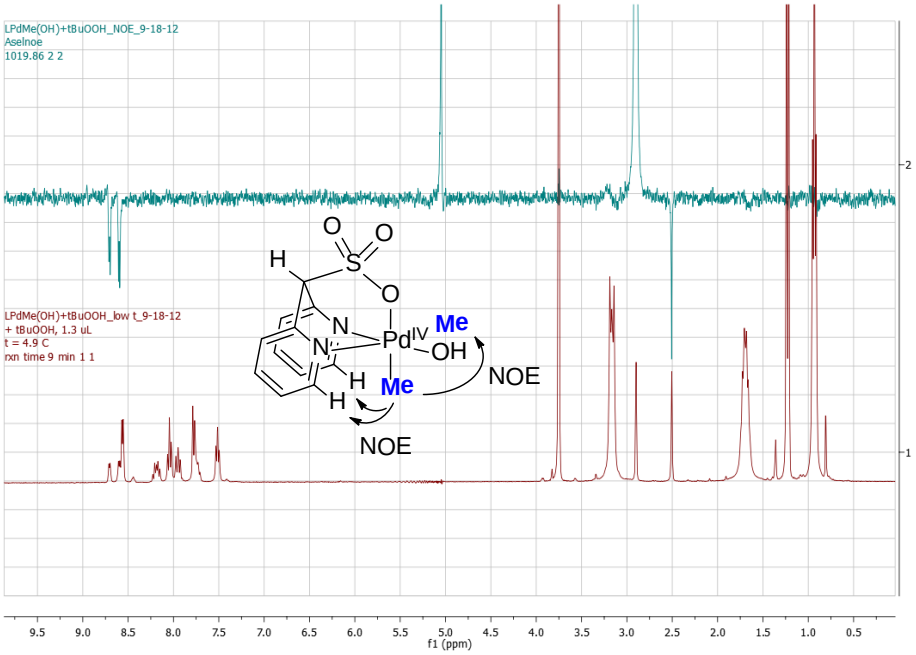

Figure 5.14 Selective NOE of (dpms)$Pd^{IV}Me_2(OH)$.

Attempt to Observe (dpms)$Pd^{IV}CH_3(OH)_2$ Intermediate

Oxidation with *m*-CPBA in D_2O and CD_3CN

General procedure. Under an argon atmosphere, solution of (dpms)$Pd^{II}Me(OH)^-$ in D_2O or CD_3CN was prepared. Reagent in D_2O was cooled to 5 °C, and in CD_3CN to -14 °C. Lower temperature resulted in broadening of the lines, complicating analysis. ^1H NMR spectrum of the starting material was recorded, followed by addition of stock solution of *m*-CPBA in CD_3OD or CD_3CN (1-2 equiv.).

^{1}H NMR spectrum was recorded again immediately after addition of the oxidant. Reaction in D_2O/CD_3OD showed formation of transient *unsym* -$LPd^{IV}Me_2(OH)$. No other intermediated were detected. Products of oxidation include MeOH (δ 3.35, s), Me_2O (δ 3.33, s), and C_2H_6 (δ 0.82, s).

In CD_3CN at -14 °C, no intermediates were observed. The only product of oxidation, observed by ^{1}H NMR spectroscopy is proposed to be MeOOH (δ 3.88, s). Formation of C_2H_6 was not detected.

^{1}H NMR (400 MHz, CD_3CN, 22 °C), (dpms)$Pd^{II}Me(OH)^-$: δ 8.59 (s, 2H), 7.96 (t, *J* = 7.7 Hz, 2H), 7.70 (d, *J* = 7.6 Hz, 2H), 7.41 (s, 2H), 5.73 (s, 1H), 2.11 (s, 1H), 0.77 (s, 3H).

^{1}H NMR (400 MHz, CD_3CN, -14 °C), (dpms)$Pd^{II}Me(OH)^-$: δ 8.59 (d, *J* = 4.3 Hz, 1H), 8.54 (d, *J* = 5.1 Hz, 1H), 7.97 (d, *J* = 4.7 Hz, 2H), 7.73 (d, *J* = 8.2 Hz, 2H), 7.45 (d, *J* = 6.9 Hz, 2H), 5.87 (s, 1H), 0.76 (s, 3H).

Conditions	Conversion (%)/ Reaction time	Other Products (%)
Pd^{II} = 6.5 μmol, *m*-CPBA = 7.2 μmol, 5 °C, D_2O/CD_3OD	100 / 12 min	*$LPd^{IV}Me_2(OH)$, 66; MeOH, 16; Me_2O, 11
Pd^{II} = 1.2 μmol, *m*-CPBA = 2.9 μmol, -14 °C, CD_3CN	100 / 5 min	MeOOH, 82

*Yield of C_2H_6 cannot be determined

Table 5.36 Product distribution in oxidation reaction with 1-2 equiv. of *m*-CPBA.

Oxidation with $NaIO_4$ in D_2O/CD_3OD at -60 °C

A sample of Na(dpms)$Pd^{II}CH_3(OH)$ (7.9 μmol) was dissolved in a 0.12 mL of D_2O and 0.34 mL of methanol-d4 and transferred into NMR tube. NMR tube was placed into dry ice/acetone bath at -60 °C. A sample of $NaIO_4$ (9.0 mg, 42.0 μmol) was dissolved in a fresh portion of 0.12 mL of D_2O and 0.34 mL of methanol-d4 and was slowly added to the cold solution of Na(dpms)$Pd^{II}CH_3(OH)$ in D_2O/CD_3OD.

Two layers were mixed at -60 °C until homogeneous reaction mixture was obtained. Within 5-10 minutes after addition of the oxidant, no more starting material was observed by ^{1}H NMR spectroscopy. Formation of three Pd^{IV} complexes was detected: (dpms)$Pd^{IV}(CH_3)_2(OH)$ 23%, (dpms)$Pd^{IV}(CH_3)_2(OCD_3)$ 18 %, and unknown (dpms)$Pd^{IV}(CH_3)_2(X)$ 13% yield. The rate of disappearance of these complexes at 0 °C was monitored over time.

Upon completion of the reaction MeOH was generated in 32% yield, Me_2O was generated in 32% yield as well. Exact yield of C_2H_6 was not determined. According to ^{1}H NMR, C_2H_6 was present in solution in 25% yield. It is expected that C_2H_6 yield could be up to 36 % due to decomposition of (dpms)$Pd^{IV}(CH_3)_2(OH)$ and (dpms)$Pd^{IV}(CH_3)_2(OCD_3)$.

Rate of disappearance of Pr_4N(dpms)$Pd^{II}Me_2(OH)$ at +5 °C at pH 6.0

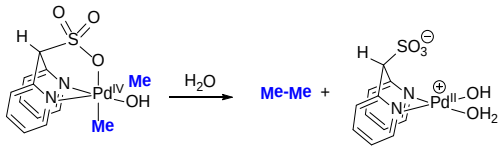

The pH of a stock solution of Pr_4N(dpms)$Pd^{II}Me(OH)$ in D_2O was adjusted with $HPO_4^{2-}/H_2PO_4^-$ buffer to generate a solution of (dpms)$Pd^{II}Me(OH_2)$ (8.1 µmol, 16.2 mM) with pH 6.0. Solution was removed from the glove box and ^{1}H NMR of the starting material was recorded. 1,4-Dioxane was used as internal standard. To the solution of (dpms)$Pd^{II}Me(OH_2)$ in H_2O/D_2O H_2O_2 (4.0 µL, 30wt%) was added open in air via microliter syringe. NMR tube was capped promptly and the reaction mixture was shaken for one minute. Formation of O_2 bubbles was observed. Analysis of the reaction solution by ^{1}H NMR showed complete consumption of the (dpms)$Pd^{II}Me(OH_2)$ and formation of MeOH (15%), C_2H_6 and (dpms)$Pd^{IV}Me_2(OH)$ in 49% yield. Yield of (dpms)$Pd^{IV}Me_2(OH)$ was determined by integration of

characteristic signals of Pd-CH_3 (equatorial) δ 2.51 ppm and of Pd-CH_3 (axial) δ 2.91 ppm. At the end of reaction aromatic region contains unsymmetric non-methyl containing complex (dpms)Pd in 80% yield.

Time (min)	LPd^{IV}**Me_2**(OH), (%)
0	49
8	43
18	31
36	19
60	13
71	9

Table 5.37 Decomposition of $LPd^{IV}Me_2(OH)$ over time.

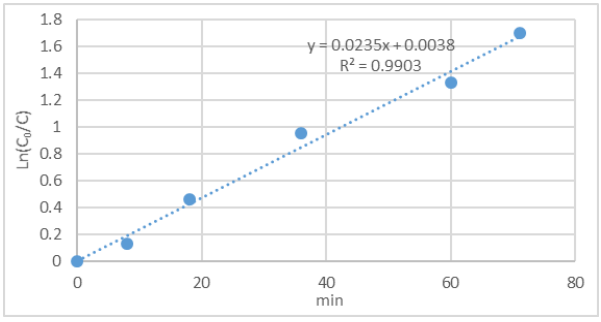

Figure 5.15 First order kinetics plot of decomposition of $LPd^{IV}Me_2(OH)$ over time.

The rate of disappearance of (dpms)$Pd^{IV}Me_2(OH)$ follows first-order kinetics. Calculated half-life of (dpms)$Pd^{IV}Me_2(OH)$ in D_2O from $Ln(C_0/C)$ is $t_{1/2}$ =29 min at +5°C.

Rate of decomposition of Pr_4N(dpms)$Pd^{II}Me_2(OH)$ at 21 °C at pH 10.6

Solution of (dpms)$Pd^{II}Me(OH)$ was removed from the glove box and ^1H NMR of the starting material was recorded. 1,4-Dioxane was used as internal standard. To the solution of (dpms)$Pd^{II}Me(OH_2)$ in H_2O/D_2O (3.1 μmol), $NaIO_4$ (6.8 μL, 0.465 M solution) in D_2O was added. NMR tube was capped promptly and the reaction mixture was shaken for one minute. Starting material was completely consumed within one minute. Analysis of the reaction solution by ^1H NMR showed complete consumption of the (dpms)$Pd^{II}Me(OH_2)$ and formation of MeOH (18%), C_2H_6 and (dpms)$Pd^{IV}Me_2(OH)$ in 52% yield. Yield of (dpms)$Pd^{IV}Me_2(OH)$ was determined by integration of characteristic signals of Pd-CH_3 (equatorial) δ 2.51 ppm and of Pd-CH_3 (axial) δ 2.91 ppm. Disappearance of (dpms)$Pd^{IV}Me_2(OH)$ was monitored *vs.* time. At

the end of reaction ar17omatic region contains complex mixture of non-methyl containing (dpms)Pd complexes.

Time (min)	$LPd^{IV}Me_2(OH)$, (%)
0	52
8	25
14	12
18	8
21	5

Table 5.38 Decomposition of $LPd^{IV}Me_2(OH)$ over time.

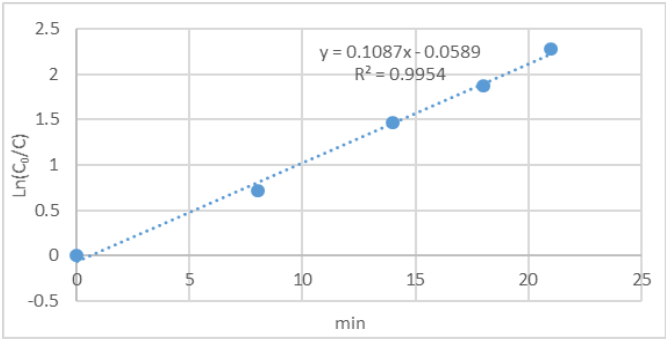

Figure 5.16 First order kinetics plot of decomposition of$LPd^{IV}Me_2(OH)$ over time.

The rate of disappearance of $(dpms)Pd^{IV}Me_2(OH)$ follows first-order kinetics. Calculated half-life of $(dpms)Pd^{IV}Me_2(OH)$ in D_2O from $Ln(C_0/C)$ plot is $t_{1/2}$ =6 min.

Stability of MeOH under reaction conditions

After aerobic oxidation of $Pr_4N(dpms)Pd^{II}Me(OH)$ was complete, solvent was removed and the remaining solid was dried under high vacuum for 20 min to remove the residual volatile products of oxidation. The solid was redissolved in D_2O and 1.0 µL of dioxane was added for calibration. To the solution containing $Pr_4N(dpms)Pd^{II}(OH)_2$ (2.7 µmol) 1.0 µL of MeOH was added and the mixture was kept at ambient temperature in the NMR tube. The solution was checked periodically by ^1H NMR to monitor changes in the integration of added MeOH and observed formation of new peaks. Table below shows the integration values of MeOH over 7 day period.

Time (days)	Integration of MeOH
0	6.93
1	6.72
4	6.61
7	6.70

As seen in the table the integration value of MeOH drops approximately 5 % within the first 24 h, and remains the same for the remaining period of time. It can be concluded that MeOH is stable as a product under oxidation conditions of $LPd^{II}Me(OH)$ with various oxidants.

Oxidation of $LPd^{II}Me(OH)$ with O_2 in the presence of CHD

In an argon filled glove box, a solution of $Pr_4N(dpms)Pd^{II}Me(OH)$ (34.0 µmol) in H_2O/D_2O was prepared. Reaction mixture was transferred into NMR tube with air tight Teflon valve. NMR tube was taken out of the glove box and 3.2 µL (34.0 µmol) of 1,4-cyclohexadiene (CHD) was added, followed by bubbling O_2 though the solution via a long needle. Reaction was kept at ambient temperature and monitored by ^1H NMR over 9 days resulting in 99 % conversion. Formation of C_2H_6, MeOH (11%), Pd black and $(dpms)Pd(OH)_2^-$ was observed. Formation of CH_4 was expected in the presence of CHD since it is a good $H^\bullet$ donor, however, no methane was observed by ^1H NMR. Presence of CHD doesn't affect oxidation of LPdMe(OH) with O_2.

Reactivity of $LPd^{II}Me(OH)$ under Argon in the presence of CHD

In an argon filled glove box, a solution of $Pr_4N(dpms)Pd^{II}Me(OH)$ (16.8, 5.2 µmol) in H_2O/D_2O was prepared. Reaction mixture was transferred into NMR tube with air tight Teflon valve. NMR tube was taken out of the glove box and 1.6 and 4.9 µL (16.8 and 52.0 µmol) of 1,4-cyclohexadiene (CHD) was added respectively. Reaction was kept at ambient temperature and monitored by ^1H NMR over several days. Formation of C_2H_6, CH_4, C_6H_6 and Pd black and was observed. In reaction with 10 equiv. of CHD, another unidentified product was formed.

Conditions	Conversion (%) / Reaction time	C_2H_6 (%)	CH_4 (%)	Total yield*
Ar, no CHD	100 / 6-8 days	55	44	99 ± 2
Ar, 1 eq. CHD	100 / 1 day	41	57	98
Ar, 10 eq. CHD	100 / 1 day	54	44	98

Table 5.39 Product distribution in decomposition of R4N(dpms)Pd^{I}Me(OH) in the presence of 1,4-cyclohexadiene.

Bibliography

(1) Khodakov, A. Y.; Chu, W.; Fongarland, P. *Chem. Rev.* **2007**, *107*, 1692.

(2) Maitra, A. M. *Applied Catalysis a-General* **1993**, *104*, 11.

(3) Krylov, O. V. *Catalysis Today* **1993**, *18*, 209.

(4) Raja, R.; Ratnasamy, P. *Applied Catalysis a-General* **1997**, *158*, L7.

(5) Baik, M. H.; Newcomb, M.; Friesner, R. A.; Lippard, S. J. *Chem. Rev.* **2003**, *103*, 2385.

(6) Lieberman, R. L.; Rosenzweig, A. C. *Nature* **2005**, *434*, 177.

(7) Himes, R. A.; Barnese, K.; Karlin, K. D. *Angew. Chem., Int. Ed.* **2010**, *49*, 6714.

(8) Lucas, H. R.; Li, L.; Sarjeant, A. A. N.; Vance, M. A.; Solomon, E. I.; Karlin, K. D. *J. Am. Chem. Soc.* **2009**, *131*, 3230.

(9) Wang, D.; Farquhar, E. R.; Stubna, A.; Munck, E.; Que, L., Jr. *Nature Chemistry* **2009**, *1*, 145.

(10) Que, L., Jr.; Tolman, W. B. *Nature* **2008**, *455*, 333.

(11) Liu, W.; Groves, J. T. *J. Am. Chem. Soc.* **2010**, *132*, 12847.

(12) Goldshle.Nf; Shteinma.Aa; Shilov, A. E.; Eskova, V. V. *Zhurnal Fizicheskoi Khimii* **1972**, *46*, 1353.

(13) Shilov, A. E.; Shul'pin, G. B. *Chem. Rev.* **1997**, *97*, 2879.

(14) Luinstra, G. A.; Wang, L.; Stahl, S. S.; Labinger, J. A.; Bercaw, J. E. *J. Organomet. Chem.* **1995**, *504*, 75.

(15) Luinstra, G. A.; Labinger, J. A.; Bercaw, J. E. *J. Am. Chem. Soc.* **1993**, *115*, 3004.

(16) Labinger, J. A.; Bercaw, J. E. *Higher Oxidation State Organopalladium and Platinum Chemistry* **2011**, *35*, 29.

(17) Hutson, A. C.; Lin, M. R.; Basickes, N.; Sen, A. *J. Organomet. Chem.* **1995**, *504*, 69.

(18) Sen, A. *Acc. Chem. Res.* **1998**, *31*, 550.

(19) Labinger, J. A.; Herring, A. M.; Lyon, D. K.; Luinstra, G. A.; Bercaw, J. E.; Horvath, I. T.; Eller, K. *Organometallics* **1993**, *12*, 895.

(20) Labinger, J. A.; Herring, A. M.; Bercaw, J. E. *J. Am. Chem. Soc.* **1990**, *112*, 5628.

(21) Labinger, J. A.; Bercaw, J. E. *Nature* **2002**, *417*, 507.

(22) Sen, A.; Lin, M. R.; Kao, L. C.; Hutson, A. C. *J. Am. Chem. Soc.* **1992**, *114*, 6385.

(23) Luinstra, G. A.; Wang, L.; Stahl, S. S.; Labinger, J. A.; Bercaw, J. E. *Organometallics* **1994**, *13*, 755.

(24) Horvath, I. T.; Cook, R. A.; Millar, J. M.; Kiss, G. *Organometallics* **1993**, *12*, 8.

(25) DeVries, N.; Roe, D. C.; Thorn, D. L. *Journal of Molecular Catalysis a-Chemical* **2002**, *189*, 17.

(26) Periana, R. A.; Taube, D. J.; Evitt, E. R.; Loffler, D. G.; Wentrcek, P. R.; Voss, G.; Masuda, T. *Science* **1993**, *259*, 340.

(27) Basickes, N.; Hogan, T. E.; Sen, A. *J. Am. Chem. Soc.* **1996**, *118*, 13111.

(28) Periana, R. A.; Taube, D. J.; Gamble, S.; Taube, H.; Satoh, T.; Fujii, H. *Science* **1998**, *280*, 560.

(29) Jones, C. J.; Taube, D.; Ziatdinov, V. R.; Periana, R. A.; Nielsen, R. J.; Oxgaard, J.; Goddard, W. A. *Angew. Chem., Int. Ed.* **2004**, *43*, 4626.

(30) Periana, R. A.; Mironov, O.; Taube, D.; Bhalla, G.; Jones, C. J. *Science* **2003**, *301*, 814.

(31) Ackerman, L. J.; Sadighi, J. P.; Kurtz, D. M.; Labinger, J. A.; Bercaw, J. E. *Organometallics* **2003**, *22*, 3884.

(32) Wilke, G.; Schott, H.; Heimbach, P. *Angew. Chem., Int. Ed.* **1967**, *6*, 92.

(33) Stahl, S. S.; Thorman, J. L.; Nelson, R. C.; Kozee, M. A. *J. Am. Chem. Soc.* **2001**, *123*, 7188.

(34) Landis, C. R.; Morales, C. M.; Stahl, S. S. *J. Am. Chem. Soc.* **2004**, *126*, 16302.

(35) Gretz, E.; Oliver, T. F.; Sen, A. *J. Am. Chem. Soc.* **1987**, *109*, 8109.

(36) An, Z.; Pan, X.; Liu, X.; Han, X.; Bao, X. *J. Am. Chem. Soc.* **2006**, *128*, 16028.

(37) Fan, Y.; An, Z.; Pan, X.; Liu, X.; Bao, X. *Chem. Comm.* **2009**, 7488.

(38) Park, E. D.; Choi, S. H.; Lee, J. S. *Journal of Catalysis* **2000**, *194*, 33.

(39) Lin, M. R.; Hogan, T.; Sen, A. *J. Am. Chem. Soc.* **1997**, *119*, 6048.

(40) Shen, C. Y.; Garcia-Zayas, E. A.; Sen, A. *J. Am. Chem. Soc.* **2000**, *122*, 4029.

(41) Yuan, J.; Liu, L.; Wang, L.; Hao, C. *Catalysis Letters* **2013**, *143*, 126.

(42) Webb, J. R.; Bolano, T.; Gunnoe, T. B. *Chemsuschem* **2011**, *4*, 37.

(43) Conley, B. L.; Ganesh, S. K.; Gonzales, J. M.; Tenn, W. J., III; Young, K. J. H.; Oxgaard, J.; Goddard, W. A., III; Periana, R. A. *J. Am. Chem. Soc.* **2006**, *128*, 9018.

(44) Tenn, W. J.; Young, K. J. H.; Bhalla, G.; Oxgaard, J.; Goddard, W. A.; Periana, R. A. *J. Am. Chem. Soc.* **2005**, *127*, 14172.

(45) Kloek, S. M.; Heinekey, D. M.; Goldberg, K. L. *Angew. Chem., Int. Ed.* **2007**, *46*, 4736.

(46) Hanson, S. K.; Heinekey, D. M.; Goldberg, K. I. *Organometallics* **2008**, *27*, 1454.

(47) Owens, G. S.; Aries, J.; Abu-Omar, M. M. *Catalysis Today* **2000**, *55*, 317.

(48) AbuOmar, M. M.; Hansen, P. J.; Espenson, J. H. *J. Am. Chem. Soc.* **1996**, *118*, 4966.

(49) Bischof, S. M.; Cheng, M.-J.; Nielsen, R. J.; Gunnoe, T. B.; Goddard, W. A., III; Periana, R. A. *Organometallics* **2011**, *30*, 2079.

(50) Figg, T. M.; Webb, J. R.; Cundari, T. R.; Gunnoe, T. B. *J. Am. Chem. Soc.* **2012**, *134*, 2332.

(51) Pouy, M. J.; Milczek, E. M.; Figg, T. M.; Otten, B. M.; Prince, B. M.; Gunnoe, T. B.; Cundari, T. R.; Groves, J. T. *J. Am. Chem. Soc.* **2012**, *134*, 12920.

(52) Groves, J. T.; McClusky, G. A. *J. Am. Chem. Soc.* **1976**, *98*, 859.

(53) Bell, S. R.; Groves, J. T. *J. Am. Chem. Soc.* **2009**, *131*, 9640.

(54) Zhou, M.; Balcells, D.; Parent, A. R.; Crabtree, R. H.; Eisenstein, O. *Acs Catalysis* **2012**, *2*, 208.

(55) Zhou, M.; Schley, N. D.; Crabtree, R. H. *J. Am. Chem. Soc.* **2010**, *132*, 12550.

(56) Zhou, M.; Hintermair, U.; Hashiguchi, B. G.; Parent, A. R.; Hashmi, S. M.; Elimelech, M.; Periana, R. A.; Brudvig, G. W.; Crabtree, R. H. *Organometallics* **2013**, *32*, 957.

(57) Sen, A.; Benvenuto, M. A.; Lin, M. R.; Hutson, A. C.; Basickes, N. *J. Am. Chem. Soc.* **1994**, *116*, 998.

(58) Hogan, T.; Sen, A. *J. Am. Chem. Soc.* **1997**, *119*, 2642.

(59) Muehlhofer, M.; Strassner, T.; Herrmann, W. A. *Angew. Chem., Int. Ed.* **2002**, *41*, 1745.

(60) Vargaftik, M. N.; Stolarov, I. P.; Moiseev, II *Journal of the Chemical Society-Chem. Comm.* **1990**, 1049.

(61) Lin, M.; Sen, A. *Nature* **1994**, *368*, 613.

(62) Chen, H. Y.; Hartwig, J. F. *Angew. Chem., Int. Ed.* **1999**, *38*, 3391.

(63) Chen, H. Y.; Schlecht, S.; Semple, T. C.; Hartwig, J. F. *Science* **2000**, *287*, 1995.

(64) Neumann, R.; Khenkin, A. M. *Chem. Comm.* **2006**, 2529.

(65) Geletii, Y. V.; Shilov, A. E. *Kinetics and Catalysis* **1983**, *24*, 413.

(66) Valentin.Js *Chem. Rev.* **1973**, *73*, 235.

(67) Selke, M.; Karney, W. L.; Khan, S. I.; Foote, C. S. *Inorg. Chem.* **1995**, *34*, 5715.

(68) Piera, J.; Backvall, J.-E. *Angew. Chem., Int. Ed.* **2008**, *47*, 3506.

(69) Lin, M. R.; Shen, C. Y.; Garcia-Zayas, E. A.; Sen, A. *J. Am. Chem. Soc.* **2001**, *123*, 1000.

(70) Weinberg, D. R.; Labinger, J. A.; Bercaw, J. E. *Organometallics* **2007**, *26*, 167.

(71) Sarneski, J. E.; McPhail, A. T.; Onan, K. D.; Erickson, L. E.; Reilley, C. N. *J. Am. Chem. Soc.* **1977**, *99*, 7376.

(72) Wieghardt, K.; Koppen, M.; Swiridoff, W.; Weiss, J. *J. Chem. Soc., Dalton Trans.* **1983**, 1869.

(73) Davies, M. S.; Hambley, T. W. *Inorg. Chem.* **1998**, *37*, 5408.

(74) Prokopchuk, E. M.; Jenkins, H. A.; Puddephatt, R. J. *Organometallics* **1999**, *18*, 2861.

(75) Rostovtsev, V. V.; Henling, L. M.; Labinger, J. A.; Bercaw, J. E. *Inorg. Chem.* **2002**, *41*, 3608.

(76) Monaghan, P. K.; Puddephatt, R. J. *Organometallics* **1984**, *3*, 444.

(77) Rostovtsev, V. V.; Labinger, J. A.; Bercaw, J. E.; Lasseter, T. L.; Goldberg, K. I. *Organometallics* **1998**, *17*, 4530.

(78) Khusnutdinova, J. R.; Rath, N. P.; Mirica, L. M. *J. Am. Chem. Soc.* **2012**, *134*, 2414.

(79) Vedernikov, A. N.; Binfield, S. A.; Zavalij, P. Y.; Khusnutdinova, J. R. *J. Am. Chem. Soc.* **2006**, *128*, 82.

(80) Khusnutdinova, J. R.; Zavalij, P. Y.; Vedernikov, A. N. *Canadian Journal of Chemistry-Revue Canadienne De Chimie* **2009**, *87*, 110.

(81) Hill, G. S.; Yap, G. P. A.; Puddephatt, R. J. *Organometallics* **1999**, *18*, 1408.

(82) Puddephatt, R. J.; Thompson, P. J. *J. Chem. Soc., Dalton Trans.* **1976**, 2091.

(83) Aye, K. T.; Canty, A. J.; Crespo, M.; Puddephatt, R. J.; Scott, J. D.; Watson, A. A. *Organometallics* **1989**, *8*, 1518.

(84) Nabavizadeh, S. M.; Habibzadeh, S.; Rashidi, M.; Puddephatt, R. J. *Organometallics* **2010**, *29*, 6359.

(85) Scott, J. D.; Puddephatt, R. J. *Organometallics* **1983**, *2*, 1643.

(86) Browning, J.; Beveridge, K. A.; Bushnell, G. W.; Dixon, K. R. *Inorg. Chem.* **1986**, *25*, 1987.

(87) Hunter, G.; McAuley, A.; Whitcombe, T. W. *Inorg. Chem.* **1988**, *27*, 2634.

(88) Rivada-Wheelaghan, O.; Ortuno, M. A.; Diez, J.; Garcia-Garrido, S. E.; Maya, C.; Lledos, A.; Conejero, S. *J. Am. Chem. Soc.* **2012**, *134*, 15261.

(89) Johansson, L.; Ryan, O. B.; Romming, C.; Tilset, M. *Organometallics* **1998**, *17*, 3957.

(90) Wardman, P. *J. Phys. Chem. Ref. Data* **1989**, *18*, 1637.

(91) Chen, J. Y.; Kochi, J. K. *J. Am. Chem. Soc.* **1977**, *99*, 1450.

(92) Amaudrut, J.; Wiest, O. *J. Am. Chem. Soc.* **2000**, *122*, 3367.

(93) Rashidi, M.; Nabavizadeh, S. M.; Akbari, A.; Habibzadeh, S. *Organometallics* **2005**, *24*, 2528.

(94) Habibzadeh, S.; Rashidi, M.; Nabavizadeh, S. M.; Mahmoodi, L.; Hosseini, F. N.; Puddephatt, R. J. *Organometallics* **2010**, *29*, 82.

(95) Thomas, J. K. *Journal of Physical Chemistry* **1967**, *71*, 1919.

(96) Neta, P.; Grodkowski, J.; Ross, A. B. *Journal of Physical and Chemical Reference Data* **1996**, *25*, 709.

(97) Olah, G. A. *Acc. Chem. Res.* **1987**, *20*, 422.

(98) Khusnutdinova, J. R.; Zavalij, P. Y.; Vedernikov, A. N. *Organometallics* **2007**, *26*, 3466.

(99) Vedernikov, A. N.; Fettinger, J. C.; Mohr, F. *J. Am. Chem. Soc.* **2004**, *126*, 11160.

(100) Becke, A. D. *J. Chem. Phys.* **1993**, *98*, 5648.

(101) Lee, C. T.; Yang, W. T.; Parr, R. G. *Phys. Rev. B* **1988**, *37*, 785.

(102) Tannor, D. J.; Marten, B.; Murphy, R.; Friesner, R. A.; Sitkoff, D.; Nicholls, A.; Ringnalda, M.; Goddard, W. A.; Honig, B. *J. Am. Chem. Soc.* **1994**, *116*, 11875.

(103) Hay, P. J.; Wadt, W. R. *J. Chem. Phys.* **1985**, *82*, 299.

(104) Kahn, L. R.; Goddard, W. A. *J. Chem. Phys.* **1972**, *56*, 2685.

(105) Melius, C. F.; Goddard, W. A. *Phys. Rev. A* **1974**, *10*, 1528.

(106) Wertz, D. H. *J. Am. Chem. Soc.* **1980**, *102*, 5316.

(107) Harvey, J. N.; Aschi, M.; Schwarz, H.; Koch, W. *Theor. Chem. Acc.* **1998**, *99*, 95.

(108) Jaguar *Schrodinger, LLC, New York, NY* **2010**.

(109) Popp, B. V.; Morales, C. M.; Landis, C. R.; Stahl, S. S. *Inorg. Chem.* **2010**, *49*, 8200.

(110) Zhong, H. A.; Labinger, J. A.; Bercaw, J. E. *J. Am. Chem. Soc.* **2002**, *124*, 1378.

(111) Vedernikov, A. N. *Chem. Comm.* **2009**, 4781.

(112) Puddephatt, R. J.; Thompson, P. J. *J. Chem. Soc., Dalton Trans.* **1975**, 1810.

(113) Brown, W. H. *Organic chemistry*; Brooks/Cole Cengage Learning: Belmont, CA, 2009.

(114) Ling, S. S. M.; Payne, N. C.; Puddephatt, R. J. *Organometallics* **1985**, *4*, 1546.

(115) Scollard, J. D.; Day, M.; Labinger, J. A.; Bercaw, J. E. *Helvetica Chimica Acta* **2001**, *84*, 3247.

(116) Greenwood, N. N. E. A. *Chemistry of the elements*; Pergamon Press: Oxford [Oxfordshire]; New York, 1984.

(117) Bakac, A. *Coordination Chemistry Reviews* **2006**, *250*, 2046.

(118) Puddephatt, R. J.; Thompson, P. J. *J. Organomet. Chem.* **1979**, *166*, 251.

(119) Hartwig, J. F. *Organotransition metal chemistry : from bonding to catalysis*; University Science Books: Sausalito, Calif., 2010.

(120) Stahl, S. S. *Angew. Chem., Int. Ed.* **2004**, *43*, 3400.

(121) Campbell, A. N.; Stahl, S. S. *Acc. Chem. Res.* **2012**, *45*, 851.

(122) Davidson, J. M.; Triggs, C. *Journal of the Chemical Society a - Inorganic Physical Theoretical* **1968**, 1324.

(123) McAuley, A.; Whitcombe, T. W. *Inorg. Chem.* **1988**, *27*, 3090.

(124) Blake, A. J.; Holder, A. J.; Hyde, T. I.; Schroder, M. *Journal of the Chemical Society-Chem. Comm.* **1987**, 987.

(125) Blake, A. J.; Reid, G.; Schroder, M. *J. Chem. Soc., Dalton Trans.* **1990**, 3363.

(126) Blake, A. J.; Crofts, R. D.; Degroot, B.; Schroder, M. *J. Chem. Soc., Dalton Trans.* **1993**, 485.

(127) Jintoku, T.; Taniguchi, H.; Fujiwara, Y. *Chemistry Letters* **1987**, 1865.

(128) Jintoku, T.; Takaki, K.; Fujiwara, Y.; Fuchita, Y.; Hiraki, K. *Bulletin of the Chemical Society of Japan* **1990**, *63*, 438.

(129) Passoni, L. C.; Cruz, A. T.; Buffon, R.; Schuchardt, U. *Journal of Molecular Catalysis a-Chemical* **1997**, *120*, 117.

(130) Zhang, Y. H.; Yu, J. Q. *J. Am. Chem. Soc.* **2009**, *131*, 14654.

(131) Zhu, M.-K.; Zhao, J.-F.; Loh, T.-P. *J. Am. Chem. Soc.* **2010**, *132*, 6284.

(132) Chuang, G. J.; Wang, W.; Lee, E.; Ritter, T. *J. Am. Chem. Soc.* **2011**, *133*, 1760.

(133) Eberson, L.; Jonsson, E. *Acta Chemica Scandinavica Series B-Organic Chemistry and Biochemistry* **1974**, *B 28*, 771.

(134) Campbell, A. N.; White, P. B.; Guzei, I. A.; Stahl, S. S. *J. Am. Chem. Soc.* **2010**, *132*, 15116.

(135) Lyons, T. W.; Sanford, M. S. *Chem. Rev.* **2010**, *110*, 1147.

(136) Powers, D. C.; Geibel, M. A. L.; Klein, J.; Ritter, T. *J. Am. Chem. Soc.* **2009**, *131*, 17050.

(137) Stowers, K. J.; Kubota, A.; Sanford, M. S. *Chemical Science* **2012**, *3*, 3192.

(138) Zhang, J.; Khaskin, E.; Anderson, N. P.; Zavalij, P. Y.; Vedernikov, A. N. *Chem. Comm.* **2008**, 3625.

(139) Oloo, W.; Zavalij, P. Y.; Zhang, J.; Khaskin, E.; Vedernikov, A. N. *J. Am. Chem. Soc.* **2010**, *132*, 14400.

(140) Vedernikov, A. N. *Acc. Chem. Res.* **2012**, *45*, 803.

(141) Khusnutdinova, J. R.; Newman, L. L.; Vedernikov, A. N. *J. Organomet. Chem.* **2011**, *696*, 3998.

(142) Kukushkin, V. Y.; Oskarsson, A.; Elding, L. I.; Farrell, N.; Vicente, J.; Chicote, M. T.; Kauffman, G. B.; Houghten, R. A.; Likins, R. E.; Posson, P. L.; Ray, R. K.; Tkachuk, V. M.; Vorobiov-Desiatovsky, N. V.; Hill, G. S.; Irwin, M. J.; Levy, C. J.; Rendina, L. M.; Puddephatt, R. J.; Romeo, R.; Monsu'scolaro, L.; Ruffo, F.; De Renzi, A.; Panunzi, A.; Byers, P. K.; Canty, A. J.; Jin, H.; Kruis, D.; Markies, B. A.; Boersma, J.; van Koten, G.; Nazeeruddin, K.; Kalyanasundaram, R.; Gratzel, M.; Bessel, C. A.; Leising, R. A.; Szczepura, L. F.; Perez, W. J.; Huyhn, M. H. V.; Takeuchi, K. J.; Poli, R.; Krueger, S. T.; Mattamana, S. P.; Jacobsen, C. J. H.; Klinke, K. K.; Hyldtoft, J.; Villadsen, J.; Abernethy, C. D.; Botommley, F.; Chen, J.; Kemp, M. F.; Mallais, T. C.; Womiloju, O. O.; Morris, R. J.; Shaw, S. L.; Jefferis, J. M.; Storhoff, J. J.; Goedde, D. M.; Hakanson, M. *Inorganic Syntheses, Vol 32* **1998**, *32*, 141.

(143) Canty, A. J.; Minchin, N. J.; Engelhardt, L. M.; Skelton, B. W.; White, A. H. *J. Chem. Soc., Dalton Trans.* **1986**, 645.

(144) Canty, A. J.; Jin, H.; Roberts, A. S.; Skelton, B. W.; White, A. H. *Organometallics* **1996**, *15*, 5713.

(145) Pal, S.; Vedernikov, A. N. *Dalton Transactions* **2012**, *41*, 8116.

(146) Risley, J. M.; Kuo, F.; Vanetten, R. L. *J. Am. Chem. Soc.* **1983**, *105*, 1647.

(147) Yamauchi, K.; Tanabe, T.; Kinoshita, M. *Journal of Organic Chemistry* **1979**, *44*, 638.

(148) Khusnutdinova, J. R.; Rath, N. P.; Mirica, L. M. *J. Am. Chem. Soc.* **2010**, *132*, 7303.

(149) Vedernikov, A. N. *C-X Bond Formation* **2010**, *31*, 101.

(150) Burns, C. T.; Shen, H.; Jordan, R. F. *J. Organomet. Chem.* **2003**, *683*, 240.

(151) Remy, M. S.; Cundari, T. R.; Sanford, M. S. *Organometallics* **2010**, *29*, 1522.

(152) Canty, A. J.; Denney, M. C.; Skelton, B. W.; White, A. H. *Organometallics* **2004**, *23*.

(153) van Asselt, R.; Rijnberg, E.; Elsevier, C. J. *Organometallics* **1994**, *13*, 706.

(154) Cámpora, J.; Palma, P.; del Río, D.; López, J. A.; Álvarez, E.; Connelly, N. G. *Organometallics* **2005**, *24*, 3624.

(155) Luo, J.; Rath, N. P.; Mirica, L. M. *Organometallics* **2013**, *32*, 3343.

(156) Luo, J.; Khusnutdinova, J. R.; Rath, N. P.; Mirica, L. M. *Chem. Comm.* **2012**.

(157) Rettich, T. R.; Handa, Y. P.; Battino, R.; Wilhelm, E. *Journal of Physical Chemistry* **1981**, *85*, 3230.

(158) Grice, K. A.; Goldberg, K. I. *Organometallics* **2009**, *28*, 953.

(159) Taylor, R. A.; Law, D. J.; Sunley, G. J.; White, A. J. P.; Britovsek, G. J. P. *Angew. Chem., Int. Ed.* **2009**, *48*, 5900.

(160) Wick, D. D.; Goldberg, K. I. *J. Am. Chem. Soc.* **1999**, *121*, 11900.

(161) Look, J. L.; Wick, D. D.; Mayer, J. M.; Goldberg, K. I. *Inorg. Chem.* **2009**, *48*, 1356.

(162) Denney, M. C.; Smythe, N. A.; Cetto, K. L.; Kemp, R. A.; Goldberg, K. I. *J. Am. Chem. Soc.* **2006**, *128*, 2508.

(163) Keith, J. M.; Muller, R. P.; Kemp, R. A.; Goldberg, K. I.; Goddard, W. A., III; Oxgaard, J. *Inorg. Chem.* **2006**, *45*, 9631.

(164) Konnick, M. M.; Decharin, N.; Popp, B. V.; Stahl, S. S. *Chemical Science* **2011**, *2*, 326.

(165) Popp, B. V.; Stahl, S. S. *J. Am. Chem. Soc.* **2007**, *129*, 4410.

(166) Boisvert, L.; Denney, M. C.; Hanson, S. K.; Goldberg, K. I. *J. Am. Chem. Soc.* **2009**, *131*, 15802.

(167) Chen, X.; Engle, K. M.; Wang, D. H.; Yu, J. Q. *Angew. Chem., Int. Ed.* **2009**, *48*, 5094.

(168) Kim, Y. J.; Osakada, K.; Sugita, K.; Yamamoto, T.; Yamamoto, A. *Organometallics* **1988**, *7*.

(169) Gillie, A.; Stille, J. K. *J. Am. Chem. Soc.* **1980**, *102*.

(170) Hartwig, J. F. *Inorg. Chem.* **2007**, *46*, 1936.

(171) Reid, S. M.; Mague, J. T.; Fink, M. J. *J. Am. Chem. Soc.* **2001**, *123*.

(172) Krause, J.; Cestaric, G.; Haack, K. J.; Seevogel, K.; Storm, W.; Porschke, K. R. *J. Am. Chem. Soc.* **1999**, *121*, 9807.

(173) Byers, P. K.; Canty, A. J.; Skelton, B. W.; White, A. H. *Journal of the Chemical Society-Chem. Comm.* **1986**.

(174) Canty, A. J. *Acc. Chem. Res.* **1992**, *25*, 83.

(175) Byers, P. K.; Canty, A. J.; Crespo, M.; Puddephatt, R. J.; Scott, J. D. *Organometallics* **1988**, *7*, 1363.

(176) Lanci, M. P.; Remy, M. S.; Kaminsky, W.; Mayer, J. M.; Sanford, M. S. *J. Am. Chem. Soc.* **2009**, *131*, 15618.

(177) Tang, F.; Zhang, Y.; Rath, N. P.; Mirica, L. M. *Organometallics* **2012**, *31*, 6690.

(178) Khusnutdinova, J. R.; Qu, F.; Zhang, Y.; Rath, N. P.; Mirica, L. M. *Organometallics* **2012**, *31*, 4627.

(179) Remias, J. E.; Sen, A. *Journal of Molecular Catalysis a-Chemical* **2002**, *189*, 33.

(180) Betts, J. *Quarterly Reviews, Chemical Society* **1971**, *25*, 265.

(181) Khursan, S. L.; Safiullin, R. L.; Martemianov, V. S.; Nikolayev, A. V.; Urozhai, I. A. *Reaction Kinetics and Catalysis Letters* **1989**, *39*, 261.

(182) Kim, J. S.; Sen, A.; Guzei, I. A.; Siable-Sand, L. M.; Rheingold, A. L. *J. Chem. Soc., Dalton Trans.* **2002**.

(183) Scott, V. J.; Labinger, J. A.; Bercaw, J. E. *Organometallics* **2011**, *30*, 4374.

(184) Boyarkin, O. V.; Koshelev, M. A.; Aseev, O.; Maksyutenko, P.; Rizzo, T. R.; Zobov, N. F.; Lodi, L.; Tennyson, J.; Polyansky, O. L. *Chemical Physics Letters* **2013**, *568*, 14.

(185) Pieck, R.; Steacie, E. W. R. *Canadian Journal of Chemistry-Revue Canadienne De Chimie* **1955**, *33*, 1304.

(186) Hogenkam.Hp *Biochemistry* **1966**, *5*, 417.

(187) Gabrielsson, A.; Blanco-Rodriguez, A. M.; Matousek, P.; Towrie, M.; Vlcek, A. *Organometallics* **2006**, *25*, 2148.

(188) Pieri, G.; Pasquali, M.; Leoni, P.; Englert, U. *J. Organomet. Chem.* **1995**, *491*, 27.

(189) Huacuja, R.; Graham, D. J.; Fafard, C. M.; Chen, C.-H.; Foxman, B. M.; Herbert, D. E.; Alliger, G.; Thomas, C. M.; Ozerov, O. V. *J. Am. Chem. Soc.* **2011**, *133*, 3820.

(190) Eleziri, F. R.; Sulfab, Y. *Inorganica Chimica Acta* **1977**, *25*, 15.